TOWARDS THE DEVELOPMENT OF SELECTIVE HYDROCARBON OXYGENATION CATALYSTS

Gregorio Guisado Barrios

A Thesis Submitted for the Degree of PhD
at the
University of St. Andrews

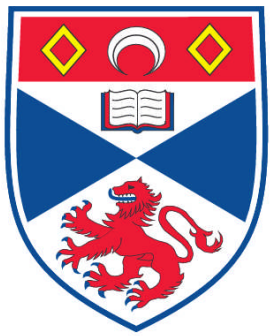

2010

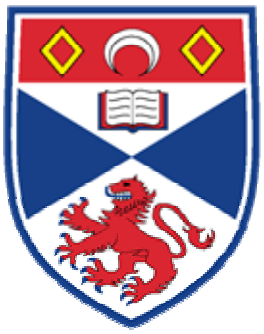

University
of
St Andrews

Towards the Development of Selective Hydrocarbon Oxygenation Catalysts

A thesis presented by Gregorio Guisado Barrios
to the University of St Andrews in application for the
Degree of Doctor in Philosophy.

April 2009

Declarations

I, Gregorio Guisado Barrios, hereby certify that this thesis, which is approximately 49,584 words in length, has been written by me, that it is the record of work carried out by me and has not been submitted in a previous application for a higher degree.

I was admitted as a research student in January 2005 as a candidate for the degree of PhD in Chemistry in February 2006; the higher study for which this is a record was carried out in the University of St Andrews between January 2005 and February 2008.

Signature of candidate Date

I hereby certify that the candidate has fulfilled the conditions of the Resolution and Regulations appropriate for the degree of PhD in the University of St Andrews and that the candidate is qualified to submit this thesis for that degree.

Signature of Supervisor Date

In submitting this thesis to the University of St Andrews I understand that we are giving permission for it to be made available for the use in accordance with the regulations of the University Library for the time being in force, subject to any copyright vested in the work not being affected thereby. We also understand that the title and abstract will be published, and that a copy of the work may be made and supplied to any *bona fide* library or research worker, that my thesis will be electronically accessible for personal or research use unless exempt by award of an embargo as requested below, and that the library has the right to migrate my thesis into new electronic forms as required to ensure continued access to the thesis. We have obtained any third party copyright permission that may be required in order to allow such access and migration, or have requested the appropriate embargo below.

The following is an agreed request by candidate and supervisor regarding the electronic publication of this thesis:

Access to printed copy and electronic publication of thesis through the University of St Andrews.

Signature of candidate Date

Signature of supervisor Date

Dedication

To my parents,

Thank you for all the support.

Acknowledgments

I would firstly like to thank my family, especially my parents and my sister and brother in law who have provided me with much needed support throughout.

I am hugely indebted to Dr David T. Richens for providing me with such a challenging project. Dr Arnald Grabulosa, Dr Bianca Karelia Muñoz, Dr Mª del Carmen Carrión, Dr Carmen Concelló, Dr. Vicente del Amo, Dr. José A. Fuentes, Dr. Wouter Laan and Professor David Cole-Hamilton who have stood at the end of the tunnel with the all-alluring light.

I would like to thank Professor Alex Slawin and Yang Li for help with the X-ray crystal structure determinations, Ms. M. Smith and Dr. T. Lebl for their help with recording NMR spectra, Professor John Walton for help with the EPR experiments, Dr Roberto Sanz for help with the organic chemistry, Professor George Britovsek for help with the catalysis and Peter Pogorzelec for help with the GC analysis. I am also thankful to the EPRSC and Unilever for providing me with funding.

Finally, I would like to thank to all my friends, especially, Christina Müller danke sehr, Rodrigo Arauzo, Sara Ayuso, Gonzalo Jimenez, Oscar Ortega, Daniel Alcalde, David Delgado, Yoland Abad, Beatriz Benito, Adolfo Cabrales, Laura Vázquez, Ana Marroquin, Cristina Perez, Elsa Briones, Laura Vazquez, Veronica Contreras, for encouraging me to go beyond my limits, for being always there, Jacorien Coeetze (chelas!), Jan Hendrik, Helena Escuin por esos cafés y risas and for the tremendous support and being there in the most difficult and the best moments. Simon, Nick, Carmen and for all what I learn from them as chemists and as friends, to al my colleagues specially those of Kamer and Cole-Hamilton´s

group for creating a wonderful atmosphere, leaving space only for fond memories in years to come.

Abstract

The synthesis of pure tris(6-hydroxymethyl-2-pyridylmethyl)amine (**H_3L_{11}**) is reported for the first time. New complexes of **H_3L_{11}** with copper(II), manganese(II) and iron(III) have been characterised by X-ray crystallography. Linear $[Fe_3(\mathbf{L_{11}})_2](ClO_4)_3$ reveals the tightest Fe-O-Fe angle (87.6^o) and shortest Fe…Fe distance (2.834 Å) presently found for a weakly antiferromagnetically-coupled high spin alkoxide-bridged polyiron(III) system.

H_3L_{11} provides a route to various hydrophobic peralkylated TPA ligand derivatives for creating a hydrophobic pocket for the assembly of iron catalysts for the novel 1-hydroxylation of n-alkanes. New 6-py substituted TPA ligands containing methyl (**L_{15}**) and n-octyl (**L_{16}**) ether linkages were synthesised via alkylation. Two further novel 6-py substituted ligands were synthesized incorporating n-hexyl substituents on one (**L_{21}**) and two (**L_{22}**) of the py moieties. Here a urea spacer group was used to promote hydrogen–bond assisted heterolytic O-O cleavage (generation of the potent Fe^V=O oxidant) within the hydroxoperoxoiron(III) precursor. High spin $[Fe^{II}(\mathbf{L})(CH_3CN)_x](CF_3SO_3)_2$ complexes (x = 0–2, **L** = **$L_{15,16,21,22}$**) were characterised in solution by ^{1}H NMR. The structure of $[Fe(\mathbf{L_{22}})](CF_3SO_3)_2$ reveals a distorted iron(II) centre bound to four N atoms and two urea carbonyls.

Iron(II) complexes of **H_3L_{11}, $L_{15,16,21,22}$** and tris(6-Br)-TPA (**L_{24}**), were investigated for catalysis of the oxygenation of cyclohexane by H_2O_2. Reaction of the iron(II) complexes with H_2O_2 and ^{t}BuOOH was followed by time-resolved EPR and UV-VIS spectrophotometry. A correlation between the observed catalytic activity and the nature of the Fe^{III}(L)-OOR intermediates generated is apparent.

A convenient ‘one-pot’ synthesis of benzene-1,3,5-triamido-tris(l-histidine methyl ester) is reported along with attempts at preparing N,N’-bis(pyridylmethyl)-1,3-diaminopropane-2-carboxylic acid (**L_{25}**), a new water soluble pyridine-amine ligand. The final demetallation step resulted in ligand hydrolysis to the novel amino acid; 1,3-diaminopropane-2-carboxylic acid which was characterised as its HCl salt by X-ray crystallography.

List of Contents

Chapter 2: Synthesis of tris(6-hydroxymethyl-2-pyridylmethyl)amine (H_3L_{11}) and a study of its coordination chemistry with Cu^{II}, Mn^{II} and Fe^{III}.

Chapter 3 Synthesis and Characterisation of a Hydrophobic TPA ligand via O-alkylation(R = n-octyl or methyl) of tris(6-hydroxymethyl-2-pyridylmethyl) amine. Characterisation of iron(II) complexes by paramagnetic ^{1}H NMR.

Abbreviations

Å	Angstrom unit, 10^{-10} m
A/K	alcohol/ ketone ratio
BIPBMP	[bis(imino)pyridine] N-(2-methoxyethyl)-N,N-bis(pyridin-2-yl-methyl)amine)
BISP	bis(amine)tetrakis(pyridine)
BPPA	bis(6-pivaloylamido-2-pyridylmethyl)-2'-pyridylmethylamine
BLM	Bleomycin
Bn-tpen	*N*-benzyl-*N'N''N'''*-tris(2-pyridylmethyl)ethane-1,2-diamine
Bpmen	N'-dimethyl-N,N'-bis(2-pyridylmethyl)ethane-1,2-diamine
Bpy	bipyridine
^{t}Bu	*t*-butyl,-C(CH_2)$_3$
cm^{-1}	wavenumber
DBE	dissociation bond energy
DNA	dexoxynucleotic acid
dimest	*trans*-6,13-bis(methoxycarbonyl)-1,4,8,11-tetraazacyclotetradecane
DMF	*N*,*N´*-dimethylformamide, Me_2NCHO
dapsox	H_2dapsox = 2,6-diacetylpyridine-bis(semioxamazide)
EI MS	electron impact mass spectrometry
en	ethane-1,2-diamine
ES MS	electrospray mass spectrometry
FBC	fluorous biphasic catalysis
FT	Fourier Transform (NMR spectrospcopy)
CG	gas chromatography
HBPClNOL	(N-(2-hydroxybenzyl)-N-(2-pyridylmethyl)[(3-chloro)
H_4CDTA	trans-1,2-cyclohexanediamminetetraacetic acid
H_3L_{11}	tris(6-hydroxymethyl-2-pyridylmethyl)amine

Hpic	pyridine-2-carboxylic acid (picolinic acid)
Hz	Hertz
J	coupling constant, Hz
k	rate constant
KIE	kinetic isotopic effect
L_{11}	tris(6-hydroxymethyl-2-pyridylmethyl)amine
L_{15}	tris(6-octanoxymethyl-2-pyridylmethyl)amine
L_{16}	tris(6-methoxymethyl-2-pyridylmethyl)amine
L_{21}	[6-(hexylureyl)-2-pyridylmethyl)-bis-(2-pyridylmethyl)]amine
L_{22}	[Bis-(6-(hexylureyl)-2-pyridylmethyl)-2-pyridylmethyl]amine,
L_{23}	tris-(6-(hexylureyl)-2-pyridylmethyl)amine
L_{24}	tris(6-bromo-2-pyridylmethyl)amine
L_{25}	benzene-1,3,5-tricarboxamide of L-histidine methyl ester
mCPBA	m-chloroperbenzoic acid
Me	methyl,-CH_3
3-Me_3TPA	tris(3-methyl-2-pyridylmethyl)amine
5-Me_2TPA	[bis(5-mehyl-2-pyridylmethyl)(2-pyridylmethyl)]amine
5-Me_3TPA	tris(5-methyl-2-pyridylmethyl)amine
6-Me_2TPA	[bis(6-mehyl-2-pyridylmethyl)(2-pyridylmethyl)]amine
6-Me_3TPA	tris(6-methyl-2-pyridylmethyl)amine
MMO	monooxygenases
MPPH	2-methyl-1-methyl-1-phenyl-2-propylhydroperoxide
MPZPBY	6-(N-3,5-dimethylpyrazolyl)-2,2'-bipyridine
N4Py	N,N-bis(2-pyridylmethyl)-N-[bis(2-pyridyl)methyl]amine
NBS	N-bromo succinamide
m/z	mass-to-charge ratio

OAc	acetate -O_2CCH_3
Oct	Octyl, -$(CH_2)_7CH_3$
$OPPh_3$	triphenylphosphine oxide
PCP	pentachlorophenol
PEO	poly(ethylene oxide)
PPO	poly(propylene oxide)
Ph	phenyl,-C_6H_5
PHIO	Iodosobenzene
ppm	parts per million
POMs	polyoxometalate
Por	porphyrin
py	pyridine
pyO	pyridine N-Oxide
salen	H_2salen = *N,N'*–bis(salicylidene) ethanediamine
TAML	tetraamido macrocyclic ligands
TBUA	tris(t-butylureylethyl)amine
TEPA	tris[2-(2-pyridyl)ethyl]amine
THF	tetrahydrofuran, C_4H_8O
TMC	1,4,8,11-tetramethyl-1,4,8,11-tetraazacyclotetradecane
TNPA	tris(6-neopentylamino-2-pyridylmethyl)amine
tren	tris(aminoethyl)amine
TPA	tris(2-pyridylmethyl)amine
TPOEN	N-(2-pyridylmethoxyethyl)-N,N-bis(2-pyridylmethyl)amine
TON	turnover number
χ_M	magnetic susceptibility

NMR: s = singlet, d = doublet, t = triplet, q =quartet, m = multiplet, br = broad.

General Experimetal conditions

Materials

All commercially available solvents and reagents were purchased from Aldrich or Across and used as received unless stated otherwise, in which case standard schlenk line techniques were employed under argon or dinitrogen atmosphere using glassware which had been pre-dried in an oven at 100 ºC overnight. Pyridine was dried and distilled from CaH_2, THF and diethyl ether were dried and distilled from sodium-benzophenone ketyl. Hexane was dried and distilled from sodium. Dichloromethane and acetonitrile were dried and distilled from calcium hydride respectively

Physical Measurements

^{1}H (400.0 and 300.0 MHz) 13C {^{1}H}(75.4 MHz) ^{19}F NMR (282.0 MHz) NMR spectra were recorded on 400 Advance and 300 Advance Bruker NMR spectrometers. Chemical shifts are refered to internal tetramethylsilane (δ 0)using the high frecuency positive convention.GC analysis was carried out on Agilent 6890A chromatograph with HP-5 column (30 m x 0.25 mm, film thickness 0.25 µm) Toluene was used as a standard for quantitative analysis. UV-vis spectra were recorded at 25 ºC in acetonitrile solution on a Perkin-Elmer Lambda 2 spectrometer. EPR experiments were recorded on Bruker EMX 10/12 spectrometer operating at 9.5 GHz with 100 kHz modulation. The sample was transferred to a quartz EPR tube, (12cm length x 0.4cm i.d.) which was then immersed in a Dewar of liquid nitrogen, and transferred to a cooled sample holder within the EPR spectrometer whose cavity was maintained at 110 K. X-ray crystallography was carried out at 93(2)K using Mo Kα radiation from a Rigaku MM007 rotating anode diffractometer operating with a low temperature.Mass

spectra were acquired on a Water's 2795 HPLC with Micromass LCT equipped with a "lock spray" for accurate mass measurements. Elemental analysis for C, H and N were determined on dried samples using a Carlo Erba CHNS analyser. Variable-temperature, solid-state direct current (dc) magnetic susceptibility data down to 5 K were collected on a powdered microcrystalline sample using a Quantum Design MPMS-XL SQUID magnetometer in an applied field of 0.1 T. Diamagnetic corrections were applied to the observed paramagnetic susceptibilities using Pascal's constants. Electrochemical measurements were carried out on a 3.15×10^{-4} M solution in CH_3CN containing 0.1M $[^nBu_4N][BF_4]$. A standard three electrode system was used comprising a Metrohm 6.1241.060 Pt working electrode, Metrohm 6.0726.100 Ag/AgCl reference electrode and a Pt wire reference electrode. Data were captured on a DELL Pentium III desktop PC with General Purpose Electrochemistry system (GPES) version 4.8 connected to an Autolab PGSTAT30 potentiostat. Quoted data were recorded using a scan rate $\nu = 0.1$ Vs^{-1} and are displayed in the form $(E_{pa} + E_{pc})$ /2 V $(E_{pa} - E_{pc})$. Potentals are vs Ag/AgCl referenced to the ferrocinium/ferrocene couple taken as +0.55 V. *In situ* UV/Vis/NIR spectroelectrochemistry was performed using an optically transparent thin layer electrode (OTTLE) cell using a Perkin-Elmer Lambda 9 spectrophotometer. The spectra were captured on a Datalink Pentium desktop PC running UV Winlab software, version 2.70.01. A platinum gauze working electrode (transparency = 40 %) was used in the quartz cell (path length = 0.5 mm). The platinum wire counter and Ag/AgCl reference electrodes were separated from the test solution by sintered frits in a quartz reservoir above the flat cell. A tight fitting PTFE lid prevented the oxygen-purged solutions being exposed to the atmosphere. The assembly was then placed in a PTFE block fitted with two pairs of quartz windows, inside the spectrometer. Dry, pre-cooled N_2 was passed between the cell and the inner pair of quartz windows to cool the solution. Dry, room temperature N_2 was passed between the outer and inner quartz windows of the PTFE block to prevent frosting of the cell and windows. The spectrometer cavity was kept under N_2. The temperature was monitored

using a thermocouple connected to a digital thermometer and could be controlled by careful adjustment of the N_2 flow rate. Potential was applied and bulk electrolysis performed with UV/Vis/NIR spectra measured every ten minutes. Conversion of the electroactive species was deemed complete when the spectrum became constant and current flow ceased. The potential was then set back to re-generate the original species to ensure reversibility of the redox process.

Chapter 1

Biomimetic Catalysis of Selective Hydrocarbon Oxidation

1.1 Introduction:

One of the most relevant transformations carried out by the chemical industry is the catalytic and selective oxidation of the unactivated alkane molecules such as methane (to methanol) and cyclohexane (to cyclohexanol).[1, 2] The alkane raw materials utilized in these chemical processes come from natural gas such (methane), or from crude oil (cyclohexane). Alkanes are by nature relatively cheap and although the process is thermodynamically favoured they remain difficult to activate for selective reaction. This is largely because (i) the C-H bond energy is high (~ 400 kJ mol^{-1}) and moreover higher than that of its oxidation products resulting in over oxidation to mixtures of alcohol, ketone/aldehyde, and carboxylic acid products, and (ii) there are no activating functional groups available to direct selective reaction. As a result, finding effective routes for the selective functionalization of alkane feedstocks remains one of the most important contemporary goals in academia and industry.[3] In the past, expensive and relatively non-selective stoichiometric oxidants such as chromates and permanganates have been utilized. They have since been replaced by cheaper and more environmentally friendly oxidants such as air or peroxides under metal catalysis. However these processes remain relatively inefficient requiring constant recycling of the substrates. For instance, the oxidation of cyclohexane to a mixture of cyclohexanol and cyclohexanone is maintained below 5% to avoid further oxidation of the products, hence the substrate has to be separated from the reaction mixture and recycled. The latter constitutes a part of the DuPont process where every year 10^6 tonnes of nylon-6 and nylon-6´6 are produced.[4] Increasing the net efficiency of these processes is a key research objective for industry and academia.

In nature, the activation and selective oxygenation of C-H substrates is carried out routinely by a number of metalloenzymes.[5, 6, 7, 8] Some examples are cytochrome P450, methane monooxygenase, and bleomycin. All three contain an iron centre and carry out important selective oxidations. For instance, as well as its role in the water solubilizing of toxic and waste molecules in the body (via C-H hydroxylation) cytochrome P450 plays a crucial role in the biosynthesis of the female hormone progesterone via catalysis of the selective oxidation of aliphatic long chain C-H bonds of cholesterol.[9] Methane is oxidized to methanol by methane monooxygenase during the metabolic process of methanotrops,[6] and the 4´-hydrogen of the rings of ribose on DNA are abstracted by bleomycin in its role as an antitumour drug.[10] All these processes are accomplished under mild conditions, which could be hugely advantageous for the chemical industry. However, the use of biological catalysts in industry is not far advanced because of the need for harsh conditions. There have been some advances in terms of alcohol production from renewable carbon sources, where non fermentative pathways have been utilized to obtain branched chain alcohol which can be used as biofuels. By means of this method it has been possible to synthesise phenylethanol, isobutanol, 2 methyl-1 butanol and butanol.[11] Liao and co-workers reported that alcohols with longer chains would be obtained, via a new synthetic approach in E.coli, (a bacterium with metabolic ability), combined with the last two steps of the Erhlich pathway, where a large variety of substrates containing 2-ketoacid are degraded from different organisms. The 2-keto acid decarboxylases (KDCS) can reduce substrates to aldehydes which are then reduced by alcohol dehydrogenases (ADHs) to alcohols.[11] However, the production, via the C_8 petroleum fraction, of high value long chain alcohols such as 1-octanol, a precursor of some PVC plasticizers and detergent additives, still requires expensive hydroformylation of the long chain C_8 alkene followed by hydrogenation of the corresponding aldehyde. Inspired by the iron based alkane metallooxygenases, the development of a number of biomimetic heme and

non-heme catalysts has raised a huge interest within the chemical community over the past thirty years.

Progress in the understanding of the mechanism of action of heme oxygenase enzymes has led to the development of a range of biomimetic heme catalysts.[12] The corresponding family of non-heme iron catalysts consists of two different groups; dinuclear systems, mirroring alkane monooxygenases such as methane monooxygenase, and mononuclear systems analogous to bleomycin. The availability of X-ray structural data on many of the biocatalysts has led to vast insights into the possible design of effective biomimetic analogues for alkane functionalization.

1.2 Biological Alkane Monooxygenases

Enzymes such as Cytochrome P450, which contains a porphyrin ligand, methane monooxygenase and bleomycin all use iron to catalyse the oxidation (by dioxygen) of C-H bonds in substrates. The respective active sites are shown in figure 1.1, 1.3 and 1.4. A few enzymes like NO synthase,[13, 14] peroxidases[15, 16] and prostaglandin synthase,[17, 18] have a similar heme active site to that of cytochrome P450. The non-heme enzyme methane monooxygenase however has a binuclear carboxylate-bridged diiron centre. This centre is also present in fatty acid desaturase and also in ribonucleotide reductase which uses the diiron centre to generate a tyrosyl radical which is an integral part of the catalytic process.[6]

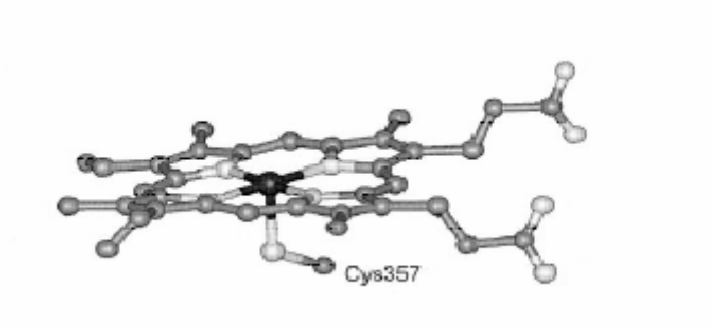

Figure 1.1 Schematic representation of the iron-containing enzymatic centre of cytochrome P450[1]

Finally bleomycin is a mononuclear non-heme iron enzyme wherein five nitrogen containing ligands are coordinated to the iron centre; two amines, a pyrimidine, an amidate and an imidazole.[10] Great strides in understanding how these catalysts perform have been accomplished although much remains to be understood such as the role of endogeneous radicals.

1.2.1 The active site and mechanism of Cytochrome P450

Intensive studies have been carried out during the past 30 years to elucidate how hydrocarbons are oxidized by heme iron-containing enzymes such as cytochrome P450.[19] The generally agreed reaction mechanism is shown in figure 1.2.

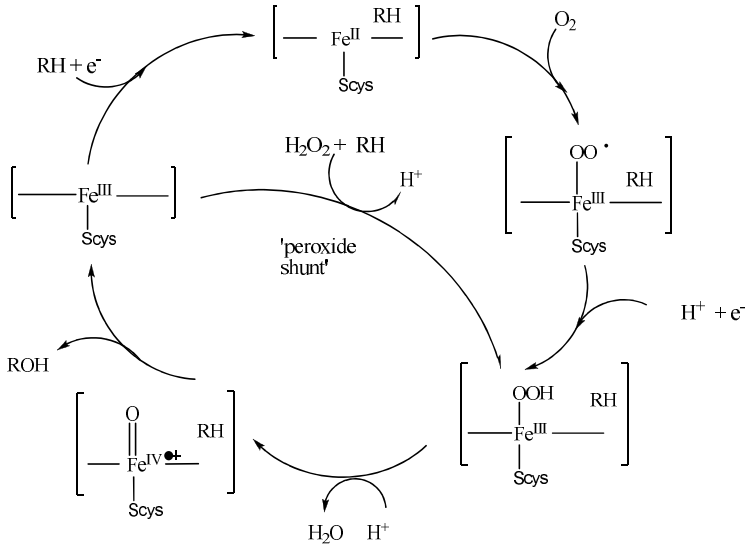

Figure 1.2 Schematic representation of the proposed alkane hydroxylation reaction mechanism for cytochrome P450.[1]

Que et al have reviewed and summarised the various steps taking place during the oxidation process.[1] First of all, the alkane (RH) is bound to the catalytic centre, this step induces the reduction of Fe^{III} to Fe^{II}. In the next step, O_2 is bound to the reduced active site, forming adduct which is equivalent to that in oxy-hemoglobin. Subsequent transfer of a proton and

electron then results in an iron-hydroperoxo intermediate species; (Por)Fe^{III}OOH, which has been characterised with spectroscopic techniques such as EPR, and ENDO.[20] According to DFT calculations[21] this intermediate clearly takes part in the catalytic process. The heterolytic cleavage of the O-O bond of the hydroperoxide then produces formally ($Por^{\cdot+}$)Fe^{IV}=O (or (Por)Fe^{V}=O), the active species responsible for substrate oxidation. The [($Por^{\cdot+}$)Fe^{IV}=O] formulation is preferred from comparisons with heme peroxide compound I. [($Por^{\cdot+}$)Fe^{IV}=O] can also be obtained when the inactive (resting) P450Fe^{III} form reacts with hydrogen peroxide (the peroxide shunt).[15,16] Here H_2O_2 effectively supplies the two electrons and a proton required to get to the hydroperoxide directly. Oxygen transfer agents such as PhIO can also be used to transfer a single atom of oxygen to the resting P450Fe^{III} form.[19] In each case the enzyme works via insertion of the oxygen of [($Por^{\cdot+}$)Fe^{IV}=O] into the C-H bond of the substrate. P450 dependant enzymes will also epoxidise alkenes again via 'addition' of the O atom.

1.2.2 The active site and mechanism of Methane Monooxygenase (MMO)

MMO belongs to a class of non-heme iron containing enzymes which lack the porphyrin group. Its active site, figure 1.3, consists of a carboxylate-bridged diiron centre. However the overall catalytic mechanism is very similar to P450.[22, 23] During the oxidation process, several intermediates, P (or peroxo) and Q, have been characterized following the

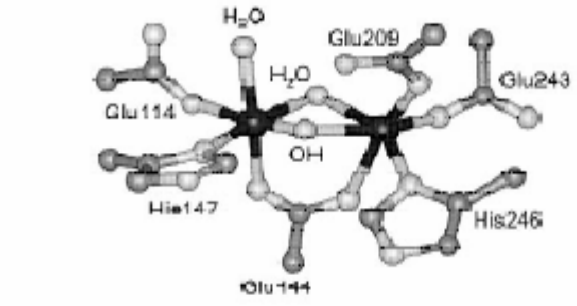

Figure 1.3 Schematic representation of active diiron site of methane monoxygenase in its oxidized form.[1]

binding of oxygen to the diiron(II) centre. Spectroscopic data suggests that P is a μ-1,2-peroxodiiron(III) complex[24, 25] and Q is a diiron(IV) species with a $Fe_2(\mu\text{-}O)_2$ core.[26, 27] DFT calculations are in agreement with the proposed structures.[28, 29, 30, 31] Close comparison between the cytochrome P450 and methane monooxygenase reaction intermediates, figure 1.5, shows that an analogy is observed between the mechanisms of the two enzymes. Intermediate P (MMO) directly corresponds to the heme $Fe^{III}OOH$ (hydroperoxo) intermediate for P450 wherein a proton has been replaced by the second iron(III). Species Q (MMO) then corresponds to the high valent species $[(Por^{\cdot+})Fe^{IV}=O]$ with the porphyrin radical cation replaced by the second iron(IV). Kinetic studies indicated that intermediate Q carries out the C-H bond oxidation step. However, exactly how oxygen is incorporated into the substrate is still the subject of intensive debate.[32 33-35]

Soluble fatty acid desaturase also contains a dinuclear iron centre identical to MMO as shown by its X-ray structure.[36] A similar intermediate P has been characterized by Raman and Mössbauer spectroscopy.[37] However no diiron(IV) intermediate similar to Q has so far been detected. Like MMO, the coordination around the two irons in FD is carboxylate-rich. It is believed that in both cases the activation of oxygen and incorporation into the C-H bond is carried out by a high valent iron species.

1.2.3 The active site and mechanism of Bleomycin.

Bleomycin, figure 1.4, is a non-heme iron enzyme with a high antitumour activity.[10, 38] This property is believed to originate from its capacity to induce DNA cleavage in the presence of dioxygen. Many studies indicate that an Fe^{II} species initially reacts with dioxygen in the presence of proton source forming a hydroperoxo intermediate similar to P450.[39] The activated BLM intermediate[40] generated after the one electron reduction and incorporation of a proton generates a low spin $Fe^{III}OOH$ intermediate[41] as indicated by spectroscopic studies. The DNA C-H bond oxidation is believed to relate to O-O bond cleavage of the hydroperoxo

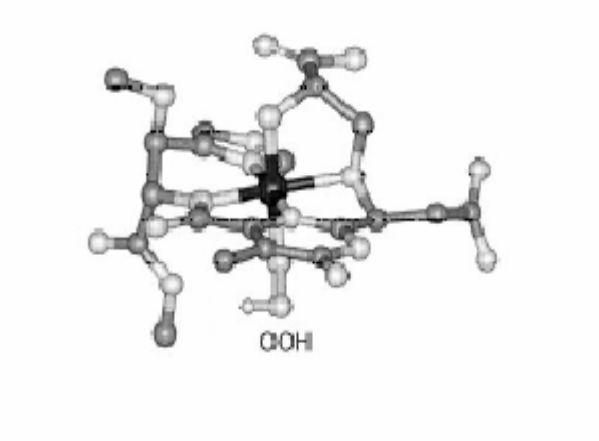

Figure 1.4 Schematic representation of the active centre of bleomycin (shown here as its cobalt hydroperoxo form). [1]

species. However, since DNA cleavage has been observed in the presence and absence of dioxygen, it is still not entirely clear which intermediate species is responsible for the C-H bond activation step.[10, 38] Finally, the Rieske dioxygenase family of enzymes form another group of non-heme iron dependent oxygenases that have been recently characterised. Here both atoms of dioxygen are transferred to the substrate.

Que et al[1] have commented that the various iron dependent oxygenase enzymes, heme or non-heme, share many common features within their catalytic reaction mechanism. In all three enzymes an O_2 adduct is formed initially, called (superoxo), which is converted to a metal peroxide (peroxo), and finally to a high valent oxo-iron form after cleavage of the O-O bond.[42] Once the high valent intermediate is formed, it may follow one of several pathways. Amongst the different possibilities is a direct reaction with the alkane. Here the difference between each enzyme lies in where the oxidizing equivalents are located. For example, in cytochrome P450 they are located on both the iron centre and the heme group, whereas in MMO they are located in electron deficient bridging oxygen atoms between the two irons. Finally in the Rieske Dioxygenase family the oxidizing equivalents are believed to be located solely on the iron centre in the form of a perferryl Fe^{V}=O(OH) species.[42]

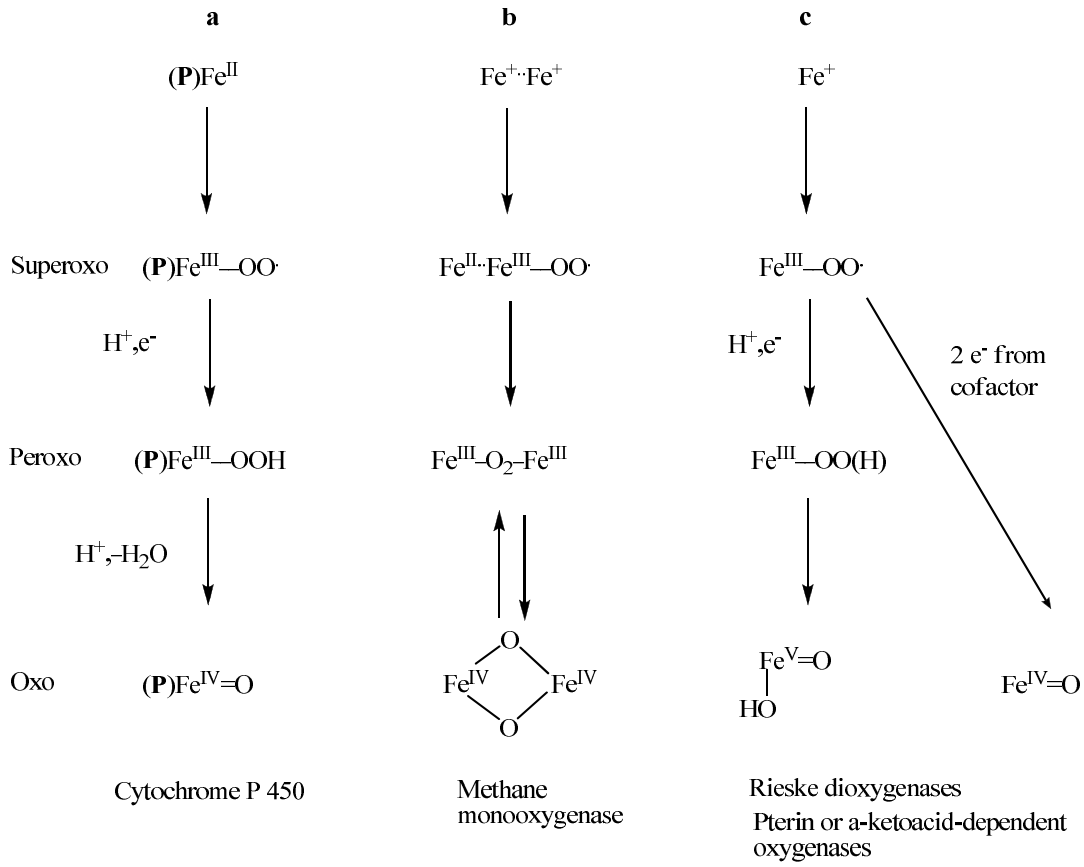

Figure 1.5 Analogies in the reaction mechanism of metallooxygenases (the heme paradigm) (a) mechanism proposed for O_2 activation by heme iron monooxygenases, (b) mechanism proposed for O_2 activation by non-heme diiron alkane monooxygenases and (c) that for mononuclear non-heme iron monooxygenases (e^- = electron; P = porphyrin).

The intensive study of metalloporphyrin-catalysed oxidations during the 80's has contributed much to our present understanding of the mechanism of heme enzymes such as P450. With the study of the non-heme iron enzymes following at a similar pace during the 90´s, a huge body of work is now available concerning a wide range of putative biomimetic heme and non-heme iron catalysts for C-H bond substrates. Because of its relevance to the studies described in this thesis the remainder of the chapter now focuses on the area of biomimetic non-heme iron catalyst for oxidation, its reaction mechanism and its development.

1.3 The development of biomimetic non-heme iron oxidation catalysts.

When iron(II,III) ions react with aqueous solutions of hydrogen peroxide, they generate a flux of hydroxyl radicals, the Fenton-Haber-Weiss reaction. Although known for almost a century, and commonly represented by figure 1.6, the precise nature of the steps involved and the intermediates generated therein are still the subject of much intense debate and disagreement.[43 44-46]

$$Fe^{III} + ROOH \longrightarrow Fe^{II} + ROO^{\bullet} + H^{+} \qquad (1)$$

$$Fe^{II} + ROOH \longrightarrow Fe^{III} + RO^{\bullet} + HO^{-} \qquad (2)$$

Figure 1.6 Schematic representation of the Fenton-Haber-Weiss reaction

Intense debate surrounds whether short lived but highly reactive $Fe^{IV}=O_{aq}$ (or even $Fe^{V}=O_{aq}$) species are generated in significant quantities in addition to ROO· and RO· radicals via the initially formed hydroperoxoiron(II,III) species. Aqueous Fenton reagents based on H_2O_2 are generally non-selective and show little preference for the type of C-H bond, 1^o, 2^o or 3^o indicating that the dominant reactant is the hydroxyl radical. Product profiles stemming from controlled reaction with diffusively free hydroxyl radicals (e.g. generated from aqueous H_2O_2/UV) mirror those obtained from Fenton reagents and have been used as a benchmark for deciding between the involvement of diffusively free hydroxyl radical-based or metal-oxo based processes. In this context a range of biomimetic iron analogues of non-heme iron oxygenase enzymes have been investigated. Tables 1.1 and 1.2 summarize the results from recent investigations of catalytic peroxide (^{t}BuOOH and H_2O_2) oxygenation, respectively, on a series of alkane substrates under a number of standardised conditions including reaction with free $OH^{\cdot}$ radicals.[1] In most of the studies cyclohexane is the chosen substrate since the ketone and/or the secondary alcohol are the only products normally formed and these can be easily identified by GC. Moreover such studies have direct relevance to the development of

more efficient high throughput routes to the production of Nylon-6 and Nylon-6'6 via cyclohexanone.

Tables 1.1 and 1.2 summarise the different efficiencies observed in product distribution. Conversion of alkane solely to alcohol is only observed in a few cases. Because of the variation in product distribution it might be concluded that the mechanism for alkane oxygenation varies somewhat between the different catalysts. However detailed studies have now shown that care is needed when defining the conditions of the experiment. It has been found that product distributions vary with a number of definable parameters, namely the catalyst, the particular peroxy oxidant employed, the oxidant / catalyst ratio, temperature, solvent, time of reaction, presence / absence of dioxygen, presence / absence of a reducing quenching agent, e.g. PPh_3, (probe for the alkylhydroperoxide) and the way the peroxy reagent is administered either as one batch at the start or by slow incremental addition e.g. using a syringe pump. The widely varying conditions employed globally by various research groups have meant that a detailed comparison between different systems is often difficult. However in the data summarized in tables 1.1 and 1.2 some degree of standardisation of the conditions of the experiment has been achieved.

1.3.1 General consideration of the mechanism.

The oxygenation of alkanes catalyzed by high valent iron oxo species has a mechanism which can be separated into two steps. The first is the rupture (activation) of the C-H bond. The second is the creation of the new C-O bond.

$$\text{R-H} + \text{Fe}^{n+}\text{=O} \xrightarrow{\text{C-H abstraction}} \text{R}\bullet + \text{Fe}^{(n-1)+}\text{-OH} \xrightarrow{\text{rebound}} \text{R-OH} + \text{Fe}^{(n-2)+} \qquad (3)$$

The time elapsed between these two steps can explain the differences of the products obtained. If the two steps are synchronised in a concerted fashion, the oxygen atom will be efficiently incorporated into the C-H bond. Alternatively the alkyl radical formed after the

rupture of the C-H bond could be trapped very quickly to form the C-O bond, termed short lived. These two mechanisms are difficult to distinguish but are believed to operate for P450 and MMO, where the stereospecific hydroxylation of alkanes occurs with partial retention of the configuration when chiral alkanes are used as substrates.[47, 48] Another possibility is the formation of long lived alkyl radicals occurring when both steps are not synchronized. These radicals are then available for trapping by other radicals including dioxygen. This is believed to be the case for the antitumour drug bleomycin wherein different products are obtained depending on the presence of absence of oxygen.[10, 49, 50] Thus the reaction mechanism that takes place depends on the lifetime of the new emerging radical and its following reactions. All the biomimetic catalysts employed in tables 1.1 and 1.2 imply the formation of iron peroxoalkyl intermediates obtained from the reaction between the iron catalyst and the peroxide. These intermediates have been characterised spectroscopically. [3, 51-58]

Figure 1.7 shows the four different decomposition pathways of the transient species Fe^{III}-OOR, and the five distinct oxidants which are derived from it.

(a) Pathway (i) corresponds to the Haber-Weiss reaction, wherein the peroxo radical ROO· and Fe^{II} are generated from Fe-O bond homolysis. The peroxo radical (ΔH_{BD}(^{t}BuOO-H) = 372.4 kJ mol^{-1}, ΔH_{BDE} (HOO-H) = 368.2 kJ mol^{-1})[52] is capable of abstracting H only from those alkanes where C-H bond are not strong (e.g. Ph(Me)CH-H, ΔH_{BDE} = 364 kJ mol^{-1}.[59] On the other hand, when two ROO· radical react, the powerful oxoradical RO· is generated (ΔH_{DBE} (^{t}BuO-H) = 439.3 kJ mol^{-1} (ΔH_{BDE} (HO-H) = 497.9 kJ mol^{-1}),[58] which is capable of abstracting H from stronger C-H bonds such as in cyclohexane (ΔH_{BDE} = 399.6 kJ mol^{-1}). [59]

Table 1.1: Alkane oxidation with ^{t}BuOOH using biomimetic catalysts.[a] [1]

Entry	Catalyst	Time	Eff.(%)[b]	A:K	KIE	3°:2°	Ref.
1	$[Fe(OPPh_3)_4]^{2+}$	4-6 h	24	0.2	5.2		[60]
2	$[Fe(CH_3CN)_4]^{2+}$	4-6 h	22	0.1	5.6		[60]
3	$[Fe(bipy)_2]^{2+}$	4-6 h	20	0.1	4.8		[60]
4	$[Fe_2(OH)(Mac16)]^{3+}$	5 min					[61]
	100 equiv. ^{t}BuOOH		28	0.8			
	10 equiv. ^{t}BuOOH (sp)	60 min	34	14			
5	$FeCl_3$	4-6 h	34	0.6	4.3		[60]
6	$[Fe(PMA)]^{2+}$	30 min	40	1.0	6.5	6	[62]
7	$[Fe(PMC)]^{2+}$	30 min	22	1.1			[62]
8	$[FeCl_2(NTB)]$ (ClO_4)	2 h	23	1.3	5.4	7	[63, 64]
9	$[FeCl_2(NTB)]$ (BF_4)	2 h	12	1.5			[65]
10	$[FeBr_2(TPA)](ClO_4)$	1 h	21	0.7		7	[63, 64]
11	$[FeBr_2(NTB)](ClO_4)$	36 h	5	1			[63, 64]
12	$[Fe_2O(bpy)_4(H_2O)](ClO_4)_4$	3-5 min	31	0.9	7.1[f]	10	[66, 67]
13	$[Fe_2O(OAc)(bpy)_4](ClO_4)_3$	2 h	28	1.2	6.1[f]	11	[67]
14	$[Fe_2O(OAc)_2(bpy)_2(H_2O)_2](ClO_4)_2$	10 h	31	1.2			[67]
15	$[Fe_2O(OAc)_2Cl(bpy)_2]$ $(ClO_4)_2$	72 h	54	1.5			[67]
16	$[Fe_2O(tmima)_2(H_2O)_2](ClO_4)_4$ [g]		5%/h	1.0		10	[68]
17	$[Fe_2O(OAc)(tmima)_2]$ $(ClO_4)_3$ [g]	24 h	26	0.9			[68, 69]
18	$[Fe_2O(OAc)(bMimen)_2](ClO_4)_3$ [h]	1 h	6	0.8	4		[70]
19	$[Fe_2O(OAc)(bpmen)_2](ClO_4)_3$ [h]	1 h	21	0.9	3.7		[70]
20	$[Fe_2O(OAc)(bpia)_2(H_2O)](ClO_4)_3$ [h,i]	1h	24	0.8			[71]
21	$[Fe_2O(OBz)_2(BPA)_2](ClO_4)_2$	16 h	25	1.2	6.1		[72]
22	$[Fe_2O(OAc)(NTB)_2](ClO_4)_3$	16 h	10	1.1	7.1		[72]
23	$[Fe_2O(OAc)(TPA)_2](ClO_4)_3$	15 min	24	0.8	4.6		[72]
24	$[Fe_2O(Obz)(TPA)_2](ClO_4)_3$	15 min	23	0.9	4.4		[72]
25	$[Fe_2O(CO_3)(TPA)_2](ClO_4)_2$	4 h	15	1.0	4.6		[72]
26	$[Fe_2O(Obz)(TPA)_2](ClO_4)_3$	10 min					[73]
	150 equiv. ^{t}BuOOH		27	0.7	6 [f]		
	150 equiv. ^{t}BuOOH (sp)		32	2.0			
	10 equiv. ^{t}BuOOH (sp)		40	>100	7-8		

[a] all reactions were performed at r.t in acetonitrile under argon or N_2 unless noted. [b] Eff= Σ(oxidized products)/ ^{t}BuOOH x 100.[c] A/K = cyclohexanol/ cyclohexanone in the oxidation of cyclohexane. [d]KIE =Kinetic Isotopic effect for cyclohexanol formation in the oxidation of cyclohexane and cyclohexane-d_{12}. [e] 3°/2° = 1-adamantanol/(2-adamantanol+2-adamantanone) in the oxidation of adamantane multiplied by 3 (to correct for the threefold higher number of 2° C–H bond). [f] KIE value based on both alcohol and ketone. [g] Under O_2. [h] Under air. [i] carried out in aqueous micelles

Table 1.2: Cyclohexane oxidation with H_2O_2 using biomimetic non-heme catalysts.[a] [1]

Entry	Catalyst	Eff.(%)[b]	A:K	KIE	3°:2° [e]	RC (cis) (%)[f]	RC (trans) (%)[f]	Ref.
1	$HO^{\cdot}$		~1	1~2	2	9	8	[43, 53, 74, 75]
2	$(Por)Fe^{III}$ [g]		5~15	13	6~48	96	78	[57, 76-78]
3	$Fe(ClO_4)_3$	37	1.9	1.5	3.3			[79]
4	$[Fe(OPPh_3)_4]^{2+}$	13	1.2	1.9				[60]
5	$[Fe(CH_3CN)_4]^{2+}$	10	1.0	1.8				[60]
6	$[Fe(bipy)_2]^{2+}$	9	0.8	1.4				[60]
7	$[Fe(PMA)]^{2+}$ [h]	10	0.9					53
8	$[FeCl_2(HDP)]^{+}$	3	1.2					[80]
9	$[FeOCl_2(epy)_2]^{2+}$	2	1.4					[81]
10	$[Fe_2O(OAc)(bpmen)_2]^{3+}$	2.5	0.8					[82]
11	$[Fe_2O(OAc)_2Cl(bpy)_2]$ $(ClO_4)_2$	~8	~ 1	1.4	3.6			[72]
12	$[Fe_2O(OAc)(tmima)_2](ClO_4)_3$	~9	< 1	1.6	3.4			[72]
13	$[Fe_2OCl(tfpy)_2]^{2+}$	3	2.0					[81]
14	$[Fe(DPA)_2]^{2-}$	16	2.3					[83]
15	$[Fe_2O(5\text{-}NO_2Phen)_4(H_2O)]^{4+}$			2.0	3.5 (1.6[h])		72	[84]
16	$[Fe_2O(bpy)(H_2O)]^{4+}$ [h]	6~9	1.3		12			[67, 85]
17	$[Fe_2O(bpy)(H_2O)]^{4+}$			2.4	4.5 (3.3[h])			[84]
18	$[Fe_2O(4,4'\text{-}Me_2bpy)_4(H_2O)_2]^{4+}$			3.1	6.2 (5.0[h])		48	[84]
19	$[Fe_2O(pb)_4(H_2O)_2]^{4+}$ [h]	30	2.0					[86]
20	$[Fe_2O(N4py)(CH_3CN)_2]^{2+}$	31	1.4	1.5	3.3	27 (31[i])	16 (30[i])	[87]
21	$[Fe_2O(TPA)(CH_3CN)_2]^{2+}$	37	4.3	3.5	17	100	100	[88]
22	$[Fe_2O(bpmen)(CH_3CN)_2]^{2+}$	63	8	3.2	15	100	100	[88, 76]

[a] all reactions were performed at r.t in acetonitrile under argon or N_2 unless noted. [b] Eff= Σ(oxidized products)/ ^{t}BuOOH x 100.[c] A/K = cyclohexanol/ cyclohexanone in the oxidation of cyclohexane. [d]KIE =Kinetic Isotopic effect for cyclohexanol formation in the oxidation of cyclohexane and cyclohexane-d_{12}. [e] 3°/2° = 1-adamantanol/(2-adamantanol+2-adamantanone) in the oxidation of adamantane multiplied by 3 (to correct for the threefold higher number of 2° C–H bond). [f] KIE value based on both alcohol and ketone. [g] Under O_2. [h] Under air. [i] In acetone

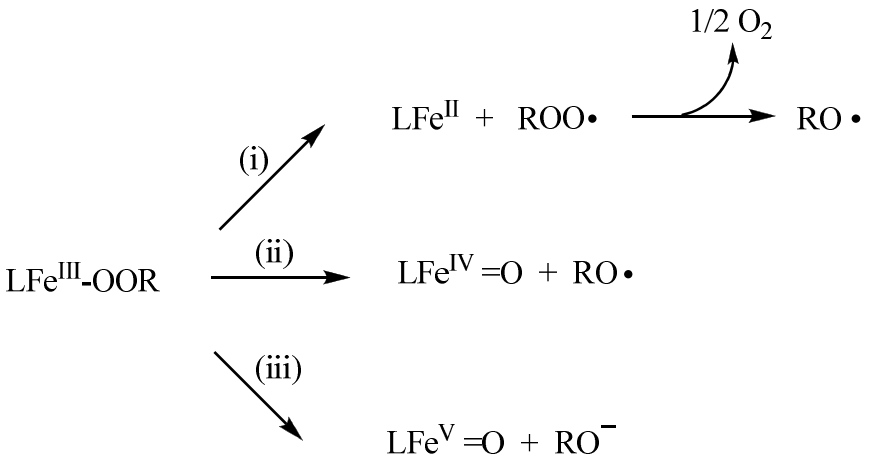

Figure 1.7: Representation of the probable four decomposition routes of Fe^{III}-OOR species[1]

(b) Direct attack of the Fe^{III}-OOR transient species to the alkane similar to the behaviour of early transition metal peroxo complexes.[3]

(c) Homolytic cleavage of the O-O bond from Fe^{III}-OOR transient species to generate two powerful oxidants capable of oxidizing the alkane; the high valent iron oxo Fe^{IV}=O and the oxo-radical RO· corresponding to pathway (ii).

(d) Heterolytic cleavage of the O-O bond from Fe^{III}-OOR, path (iii) to generate an Fe^{V}=O intermediate which oxidizes the alkane, this species is comparable to the [($Por^{\cdot+}$)Fe^{IV}=O] P450 oxidant Q, Rieske dioxygenase and peroxidase compound I.

The answer to elucidating the reaction mechanism for the oxidation of alkanes is to prove the lifetime of the generated radical, since the oxidant species can be metal based such LFe^{III}-OOH, LFe^{IV}=O, or LFe^{V}=O, or radical based such as HO· or RO·. Two types of mechanisms are relevant depending on the lifetime of the radicals generated in the oxidation of alkanes, whether the alkyl radicals are short or long lived. The heme-enzyme cytochrome P450 and non- heme MMO generates a high valent iron oxidant and a short–lived alkyl radical, which is

generated close to the iron and thus being rapidly trapped producing the alcohol, path (iii). However, if Fenton/Haber-Weiss reactions take place this generates HO· or RO· free radicals which produce long-lived R· radicals which are non-selective. When the reaction is carried out under air, the oxygen present will initiate a radical chain autoxidation process, which is responsible for the products formation. Much of the efforts invested in this field are focused towards obtaining a biomimetic catalyst capable of producing a high-valent iron oxidant similar to that believed to operate in cytochrome P450 and MMO.

1.3.2 Mechanistic evidence.

In order to obtain insight into the nature of the species responsible for hydrogen atom abstraction from the substrate C-H bond and the lifetime of the radical R· generated, indirect evidence can be helpful in elucidating the mechanism since it is often very difficult to monitor the key intermediates responsible of the oxidation.

1.3.2.1 Alcohol / ketone ratio (A/K) (cyclohexane)

A powerful indicator of the nature of the oxidant is to measure the A/K ratio in the reaction with cyclohexane which is a measure of the lifetime of the nascent radical. Long lived alkyl radicals may be generated with substrates like cyclohexane which contains only secondary C-H bonds. When the reaction is carried out under air, such alkyl radicals are trappable by dioxygen generating alkylperoxo radicals (4).[58] These species can participate in a Russell-type termination step, figure 1.8 generating the alcohol and ketone with an A/K ratio of near unity (5).[59] Furthermore, the yield of alcohol and ketone will diminish considerably in the absence of O_2 (when reaction is carried out under inert atmosphere), since the radical chain reaction will not propagate. Short-lived alkyl radicals can be generated by high valent metal species, wherein the radical and a high valent M-OH species, formed by H-abstraction from C-H, react rapidly generating the hydroxylated alcohol product (3). This step is termed

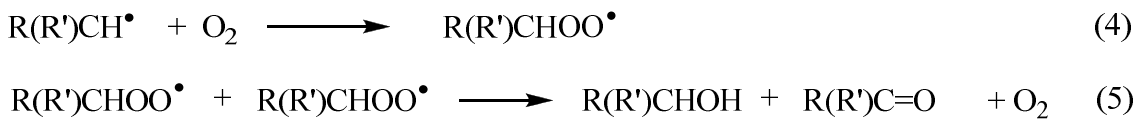

Figure 1.8: A Russell-type termination step.

the oxygen 'rebound' reaction[89] and has a typical rate constant in the range ~ 10^{10} ~10^{13} s^{-1}.[90, 91] Here cyclohexanol would be the only product. However, amounts of cyclohexanone are also typically seen due to over-oxidation of the alcohol or via competition from O_2 with the high valent M-OH species for the nascent alkyl radical leading to participation from (4) and (5).

1.3.2.2 Kinetic isotopic effects (KIE)

The kinetic isotope effect is indicative of the selectivity of the oxidant measured by using standard alkane substrates and their deuterated analogues, which have ~7.14 kJ mol^{-1} energy difference in the C-H/D bond strength. Depending on the substrate utilized it is possible to determine an intermolecular KIE (e.g. using cyclohexane/cyclohexane-d_{12}) or an intramolecular KIE (using CH_nD_{4-n}). For hydroxyl radicals as the oxidant species the typical kinetic isotopic values obtained are ~1-2[53] which indicates a strong but non-selective oxidant with little or no selectivity for C-H vs C-D bonds. Other oxygen radicals are more selective however. When $^tBuO\cdot$ is the active species, the KIE value is significantly higher, 4~5.[54] Since the hydroxyl radical is more reactive than the alkoxyl radical, ((ΔH_{DBE} (HO-H) = 500 kJ mol^{-1} vs ΔH_{DBE} (RO-H) = 441 kJ mol^{-1}), its lower KIE compared to $^tBuO\cdot$, is a direct reflection of its stronger oxidising power which corresponds to a lower selectivity.[58] Metal-based oxidants can give even higher KIE values indicative of a higher discriminatory behaviour. For example KIE values higher than 7 are commonly found in metalloenzyme reactions,[55] where the selectivity can be enhanced by changes to the geometry of the active centre, favouring the

entrance of the substrate to the active centre. Examples are Cytochrome P450 with a KIE higher that 11[16] and MMO with a reported KIE of 50-100.[92]

1.3.2.3 Substrate-based probes of alkyl radical lifetime.

In order to establish, whether short or long-lived alkyl radicals are generated, decalin and the *cis* and *trans* isomers of 1,2-dimethylcyclohexane have been used as substrates in alkane hydroxylation reactions which take advantage of the competition between alcohol formation and epimerization of the presumed formed tertiary alkyl radical species, generating *cis* and *trans* 3º-hydroxylated products. It is known from literature that epimerization of a tertiary carbon has a first order rate constant of 10^9 s^{-1}.[76, 93] When long lived radicals are present, both *cis* and *trans* hydroxylated products are obtained with a *cis/trans* value of 1.2.[74] However, when short-lived radicals are generated, the oxygen-rebound step takes place with a rate constant of 10^{10}~10^{13} s^{-1} (for examples wherein a porphyrin group is present) and retention of the original configuration is maintained. These catalysts hydroxylate substrates with much greater stereospecifically.[16, 62]

1.3.2.4 Regioselectivity

Another method of probing the nature of the oxidant is by studying the competitive oxidation of secondary and tertiary C-H bonds in the same molecule (intramolecular). For this purpose the hydrocarbon adamantane is often employed as it contains only 3º and 2º C-H bonds. Here the regioselectivity factor is measured from the 3º/2º ratio (mols of 1-adamantanol / mols of 2-adamantanol/one) multiplied by 3 to correct for the larger number of 2º C-H bonds. Powerful but unselective oxidants such as HO· typically give regioselective factors of ~2 whereas values ≥10 can indicate more selective oxidants such ^{t}BuO·.[56] For heme oxygenases like cytochrome P450 the regioselectivity factor for adamantane can reach values as high as 48.[94]

1.3.3 Reactions with Alkylperoxides

As shown in table 1.2, regardless which iron complexes are utilized as catalyst, all reactions where alkyl hydroperoxides is used as the oxygen source have a series of common characteristics, figure 1.9. In most cases the A/K ratio is ~ 1 when ROOH reagents are used as

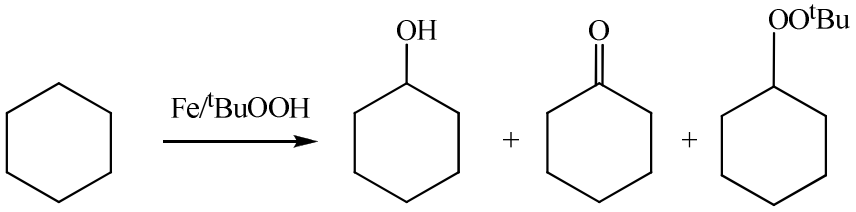

Figure 1.9: Products derived from the catalytic oxidation of cyclohexane by an iron complex with ^{t}BuOOH[1]

the oxygen source in the oxidation of alkanes indicating that long lived radicals are generated. When O_2 is present, the long lived alkyl radicals are trapped giving alkylperoxyl radicals which then take part in Russell-type termination steps giving A/K ratios near unity, figure.1.8. In the absence of O_2 similar A/K ratios are observed since O_2 is generated *in-situ* from the decomposition of ROOH via ROO· (Haber-Weiss reaction). When reactions are carried out under argon, ^{t}BuOOC$_6$H$_{11}$ is obtained from the reaction between ^{t}BuOO· and C$_6$H$_{11}$·. On the other hand its generation is significantly reduced and even completely suppressed when the reaction is carried out under O_2. At the same time, KIE values of ~5 and regioselectivity factors (for adamantane) near 10 indicate that RO· radicals are probably generated from the homolytic cleavage of the O-O bond of ^{t}BuOOC$_6$H$_{11}$.

With the help of the data presented in table 1.1, Que et al have attempted to explain how catalytic performance is directly affected by the catalyst structure, especially the reaction rate in which ROOH is decomposed. There are three important features which are found to increase the reaction rate.

(i) The activity of the metal complex catalyst is found to correlate with a high overall cationic charge on the complex (only a few active catalysts have anionic ligands) (entries **12-15** and **19-26** in table 1.1). This may be due to the Lewis acidity of the iron centre.[95]

(ii) Among all nitrogen-containing heterocycles, the catalytic activity of pyridine-containing ligands is higher (see **10** and **11, 18** and **19**, **22** and **23**, and **16** and **26**).

(iii) When weak ligands are present, which are rapidly exchangeable with H_2O, the catalytic activity is higher (see **12** and **13**, **14** and **15**, **16** and **17**, and **23** and **26** with 10 equivalents of ^{t}BuOOH). When weak ligands are bound, ^{t}BuOOH can easily react with the metal centre. A number of the metal complexes which contain aqua ligands, generate Fe^{III}-OOR transient species which can be detected at low temperature.[3, 52, 53]

1.3.3.1 'Gif' Oxidants (utilizing O_2!)

In 1980 Tabushi et al. described the first dioxygen-dependent system for the oxidation of adamantane mediated by [{Fe(salen)}$_2$(μ-O)}] [H_2salen = *N,N'*–bis(salicylidene) ethanediamine] in the presence of 2-mercaptoethanol in pyridine.[96] 1-adamantanol and 2-adamantanone were the products. A few years later this system was re-investigated by Barton who showed that the reaction to be far from reproducible. The addition of iron powder and acetic acid yielded better results. Barton's first system used dioxygen and iron powder in a 10:1 pyridine acetic acid mixture in the presence of hydrogen sulphide to catalyse the oxygenation of adamantane.[97] This led the development of what are called Gif systems[98] (after the town of Gif-sur-Yvette in France where Barton at the time was director of the Institut de Chimie des Substances Naturelles). The Gif systems were of much interest early on due to the employment of simple reagents, and in several cases, the use of atmospheric dioxygen as oxidant. The Gif^{IV} and GoAgg systems (the latter named after Gif-Orsay-Aggieland (Texas A&M University) - the

various locations for the studies), table 1.3, have proven the most viable for practical use and mechanistic studies. To achieve efficient Gif oxygenations both oxidising and reducing equivalents are necessary; either dioxygen, combined with a reducing agent, or via a reduced form of dioxygen. A heterogeneous mixture of iron(II), dioxygen, acetic acid as the proton source and zinc dust as a reducing agent (Gif^{IV}) supports the most effective oxygenation system in the former category, turnovers number can routinely exceed 2000 under certain conditions. The latter category is best represented

Table 1.3: The various 'Gif'-catalytic systems.

System	Catalyst	Electron Source	Oxidant
Gif^{III}	Fe(II)	Fe^{o}	O_2
$GifI^{V}$	Fe(II)	Zn^{o}	O_2
GO	Fe(II)	Hg/cathode	O_2
$GoAgg^{I}$	Fe(II)	KO_2	
$GoAgg^{II}$	Fe(III)	H_2O_2	
$GoAgg^{III}$	Fe(III)/Hpic	H_2O_2	

Hpic – pyridine-2-carboxylic acid (picolinic acid)

by the $GoAgg^{III}$ system which is a homogeneous combination of iron(III) chloride and picolinic acid (pyridine-2-carboxylic acid) and H_2O_2 which behaves like a shunt "agent". The presence of picolinic acid increases the rate of Gif oxygenations by 50 fold over acetic acid.[99] The presence of a carboxylic acid source is necessary for hydrocarbon oxidation; otherwise only disproportionation of hydrogen peroxide is observed.[100] Gif/GoAgg systems are notable for their high selectivity to the cycloalkanone – in some cases it is the exclusive product. Key to this high selectivity is the presence of pyridine as solvent. A continual source of dioxygen and iron(II) is also essential. In the absence of O_2 the major products are various

cycloalkylpyridines. Richens et al, have proposed a scheme, figure 1.10, for the oxidation of cyclohexane by the various Gif/GoAgg systems.[101] It is believed that pyridine stabilizes (increases the lifetime of) the cycloalkyl radical through a reversible outer-sphere redox reaction with its protonated form (path (b)). This effectively increases the lifetime of the nascent cycloalkyl radical allowing effective trapping by O_2 (path (a)) followed by reaction of the cycloalkylperoxyl radical with iron(II) to generate a cycloalkylperoxoiron(III) species.

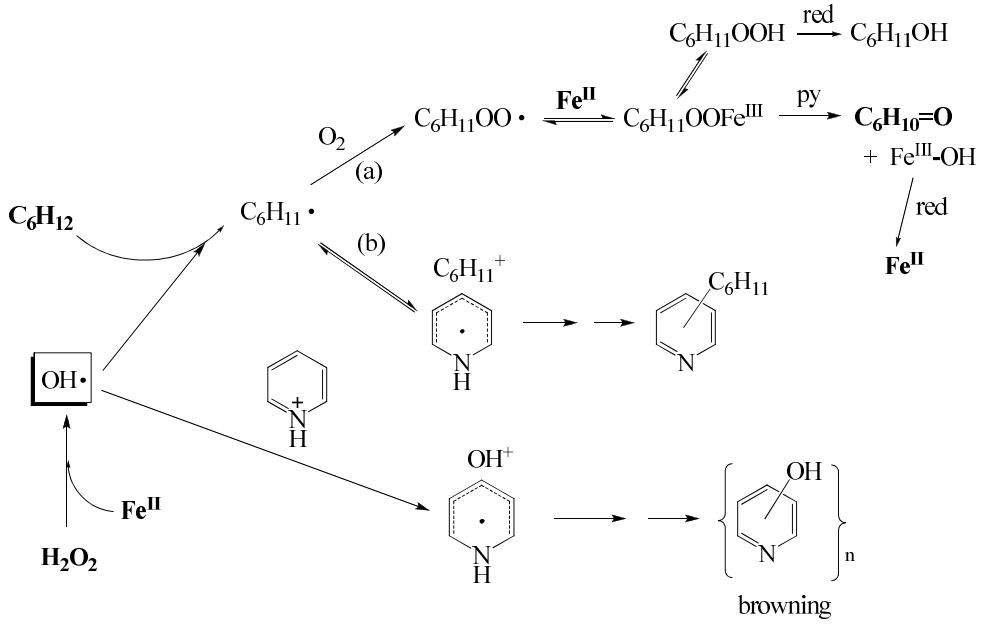

Figure 1.10: Mechanism of Gif catalytic oxygenation on cyclohexane.[101]

This complex then effectively dehydrates in the pyridine solvent to give the cycloalkanone. In the GoAgg systems it is possible to monitor the build up and subsequent decay of the cycloalkylhydroperoxide in presumed equilibrium with its iron(III) complex as the precursor to the ketone product. Amounts of cycloalkanol are also observed although here the timescale of appearance suggests formation, as a result of competitive reduction (e.g. by zinc) of the cycloalkylhydroperoxide or its iron(III) complex precursor.[101] Pyridine is decisive for obtaining good turnover numbers and unusually high K/A ratios (~ 3-10) observed in Gif oxygenations, but its toxicity and potential corrosive properties make the Gif family of reactions presently non-viable for industrial scale oxidation processes. Furthermore solutions

turn brown and oily with time due to polypyridine and hydroxy(poly)pyridine side products, figure 1.10. Although other solvents such as acetonitrile or even the hydrocarbon itself can be used, a minimum amount of a co-ordinatively unhindered pyridine (≥ 10 equivalents over catalyst) is essential for turnover.[102, 103]

1.3.4. Catalysts based on iron complexes of tris(2-pyridylmethyl)amine (TPA).

Much interest has surrounded the effective catalysis of alkane oxidation carried out by biomimetic iron(III) complexes. One such family that have received detailed study are complexes containing the tetradentate ligand (L_1) tris(2-pyridylmethyl)amine (TPA). Que and co-workers have shown that alkanes are catalytically oxidized by peroxides with high efficiency using iron-TPA complexes in the absence of O_2. Using ^{t}BuOOH as a oxygen source, 150 equivalents are consumed efficiently overtime with a variation from min to hours depending on the ancillary ligand.[102, 64, 73] Using the aqua complex $[Fe_2O(TPA)(H_2O)]^{4+}$ a transient blue intermediate was observed to persist for a short time at room temperature. This intermediate was characterized by MAS, EPR, Raman spectroscopy[104] as the low spin t-butylperoxoiron(III) species $[Fe(TPA)(OOBu^t)(H_2O)]^{2+}$. Based on indirect evidence such as the kinetic isotopic effect, regioselectivity factor (adamantine) and reaction time variations, it was concluded that the active species was either the t-butylperoxoiron(III) species or a high valent iron oxo species derived from it via homolysis of the O-O bond.[102]

Subsequently a different mechanistic conclusion was proposed by Ingold and co-workers,[105, 106] after they re-examined Que's work. According to them Que's experiments could not explain the A/K ratios near unity and that the yield of products was considerably modified by the presence of O_2. These two observations were used by Ingold to propose that long-lived alkyl radicals were formed. He proposed that ^{t}BuO· radicals were generated via homolytic cleavage of ^{t}BuOOH and that this radical was responsible for abstracting hydrogen from the alkane C-H bond. Thereafter the products obtained could be rationalised by a

standard a radical autooxidation process. They argued that it was not necessary and indeed incorrect to propose a reactive high valent iron species.

To further confirm whether a specific alkoxyl radical was formed from the alkylperoxide, Ingold and co-workers performed studies using 2-methyl-1-methyl-1-phenyl-2-propylhydroperoxide (MPPH).[105] MPPH was employed because it generates a very unstable alkoxyl radical which undergoes rapid β-scission ($k \sim 2.2 \times 10^8\ s^{-1}$) forming acetone and benzyl radical, Fig 1.11. The resulting benzyl radical is much less reactive than e.g. ^{t}BuO· since the single electron is delocalized over the aromatic ring and as a consequence cannot abstract hydrogen from cyclohexane.

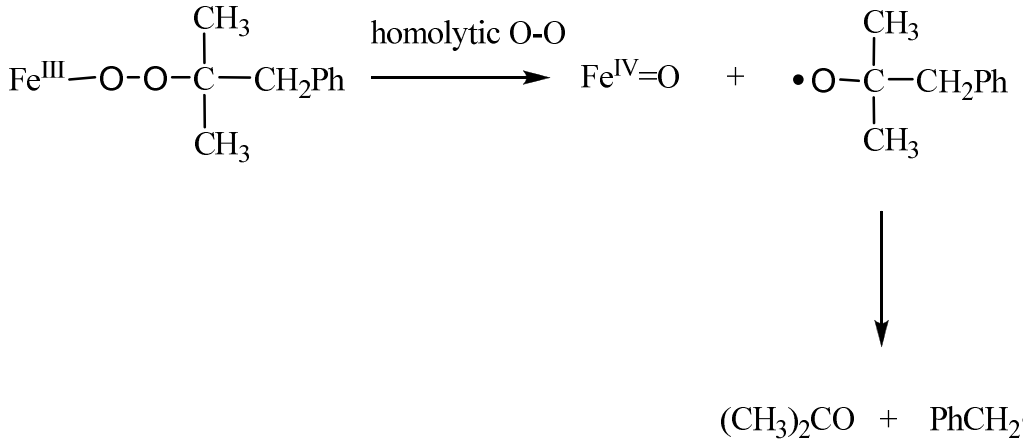

Fig 1.11 Generation of benzyl radical from the synchronised homolysis of Fe^{III}/ MMP

If however the oxidant species was a peroxo iron or oxo iron species in a high oxidation state, the yield of the product should not be affected by the use of MPPH instead of ^{t}BuOOH. At the same time it was claimed that if the oxidant species was the alkoxyl radical this would decrease the yield of the product. This was shown when using MPPH wherein no cyclohexane oxidation could be observed. Finally, the likelihood that MPPH behaves like a special peroxide undergoing a concerted fragmentation to form the benzyl radical directly was also refuted by the observation that MPPH is a more superior oxidant than ^{t}BuOOH in "genuine" $2e^-$ oxidative processes such as Ti^{IV}- catalyzed alkene epoxidation.[107] In later work Que et al.

demonstrated the importance of using diluted solutions of ^{t}BuOOH added to the reaction mixture via syringe pump,[73] in order to reduce the amount of O_2 generated from ^{t}BuOO· decomposition. For example, the addition of 150 equiv of ^{t}BuOOH over 10 min injected to a solution of acetonitrile containing the substrate and the iron complex increased the A/K ratio from 0.7 to 2, table 1.1. When the number of equivalents of ^{t}BuOOH was reduced to only 10, cyclohexanol was observed as the sole product and in a 40% yield based on ^{t}BuOOH as oxidant, table 1.1. Thus it was concluded that it was possible to compromise the radical chain autoxidation under these conditions, such as to encourage the more selective metal-based catalysed reaction. Despite the use of syringe pump and ^{t}BuOOH to avoid the radical chain autooxidation process, RO· radical is still considered to be the principal oxidant since cyclohexanol on its own is obtained when the reaction is carried out under an inert Ar atmosphere. In the presence of O_2 the A/K ratio was unity. Moreover when deuterated substrates such as C_6D_{12} or C_8D_{14} are used the kinetic isotopic effect (KIE) values are the same as that seen using RO·. The key experiment was the replacement of ^{t}BuOOH by MPPH, adding diluted solutions via syringe pump wherein no cyclohexanol was obtained. Based on the results from Ingold and Que, a hybrid mechanism was proposed which could explain all the experimental observations when $[Fe_2(TPA)_2(H_2O)]^{4+}$ is reacted with ROOH. Homolytic O-O bond rupture of the intermediate $[Fe^{III}\text{-}OOH]^{2+}$ generates the high valent iron(IV) oxo species; Fe^{IV}=O along with the oxyl radical RO·. The alkyl radical is formed from the reaction between the alkane and the oxyl RO· radical. When the reaction is carried out under Ar with no O_2 present R· can then react with the high valent iron(IV) oxo species to generate the hydroxylated product via an alkoxide. These ideas were supported by labelling studies using ^{t}BuO^{18}OH wherein the alcohol product was obtained with labelled oxygen.[91] Homolytic O-O cleavage as above would generate a high valent iron(IV) oxo species with labelled oxygen which ultimately traps the alkyl radical forming a bound alkoxide complex which hydrolyses to alcohol. When the reaction is carried out under air (O_2), R· can be intercepted by triplet

dioxygen, generating the alkylperoxyl radical initiating the radical chain autooxidation process. It has been demonstrated that the chemistry of the Fe(TPA)/^{t}BuOOH combinations is not limited to reactions involving only hydrogen abstraction from an alkane by the alkoxyl radical. Lange et al. have taken advantage of homolytic O-O cleavage of the Fe^{III}O-O^{t}Bu bond to show that a high valent iron(IV) oxo complex itself can hydroxylate an arene moiety, figure 1.12.[108] Here a 6-phenyl substituted

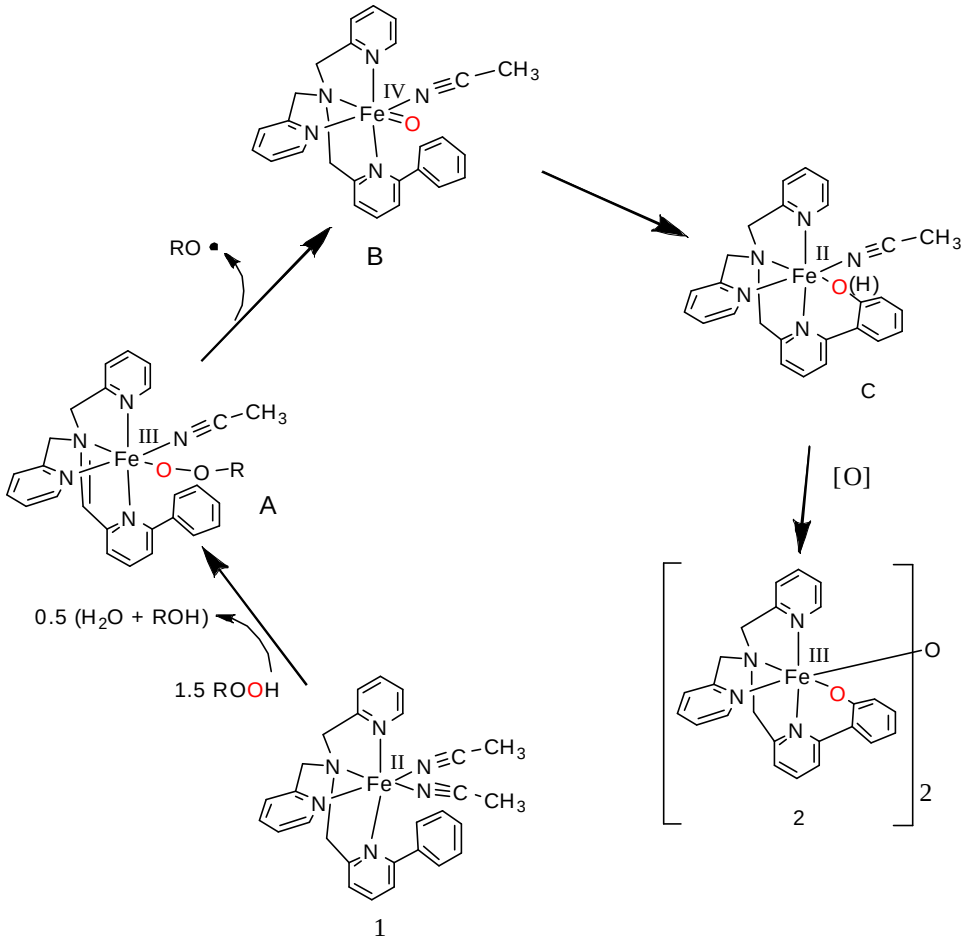

Figure 1.12 Schematic representation of proposed reaction mechanism when [Fe(6-Ph-TPA)] is reacted with ^{t}BuOOH.

TPA derivative ligand was employed. They showed that in the presence of ^{t}BuOOH they could isolate a derivative wherein the phenyl substituent of (L_2) 6-Ph-TPA became hydroxylated at the ortho position (deprotonated and coordinated to iron via the inserted O).

This could only have resulted via direct reaction of a high valent iron oxo species on the arene group. Experiments carried out using labelled $^{t}BuO^{18}OH$ showed that the oxidized product contained the labelled oxygen of the $^{t}BuO^{18}OH$. The intermediate $Fe^{III}OOR$ (A) was characterised at very low temperature (-40°) before reacting on to generate the high valent iron oxo reactant.

Further proof supporting involvement of the high valent iron oxo species resulted from the reaction in the presence of $H_2{}^{18}O$ in solution resulting in the hydroxylated phenyl ring contained ^{18}O. The high valent iron oxo species is the only intermediate which could exchange an atom of oxygen with water.[109] These studies proved that high valent iron oxo species can be generated from the reaction of Fe(TPA) complexes with ROOH reagents and moreover such species possessed the capability themselves of hydroxylating C-H bonds.

1.3.5 Oxidations with Hydrogen peroxide

Table 1.2 shows that hydrogen peroxide can be used as the oxygen source for catalytic oxidation of alkanes by biomimetic non-heme iron complexes. However in most cases the hydroxyl radical is the predominant species generated via metal promoted decomposition of H_2O_2, Fenton-Haber-Weiss chemistry. A/K values <2 were obtained for cyclohexane was used as substrate. This value moreover decreases further in the presence of O_2 indicating the presence of long live alkyl radicals. The generation and isolation of cyclohexyl hydroperoxide via cyclohexyl radical was first reported by Fish and co-workers as a product of radical chain autooxidation.[79] Further evidence for the involvement of hydroxyl radicals came from observations of KIE values < 2 (C_6D_{12}) indicating the presence of a strong but non-selective oxidant. This was further confirmed by a regioselectivity 3º/2º factor for adamantane of ~ 3. Hydroxyl radicals react by hydrogen abstraction generating long lived alkyl radicals from alkane which are then trapped by dioxygen initiating a radical chain autoxidation. However in the case of some of the biomimetic iron complexes e.g. with tetradentate pyridine-based TPA

and BPMEN-type ligands, table 1.2, the results indicate involvement of the more selective oxidant – possibly a high valent iron oxo species. There is evidence that short lived alkyl radicals can be formed giving preferential formation of alcohol over the ketone.[79, 84] Iron complexes such as $[Fe(BPMEN)(CH_3CN)_2]^{2+}$ and $[Fe(TPA)(CH_3CN)]^{2+}$ are very efficient catalysts[54] converting 40-70% of hydrogen peroxide into products. Here A/K ratios (cyclohexane) are between 4-8 in the presence and absence of oxygen indicating the absence of long lived alkyl radicals. When deuterated cycloalkanes are used, KIE values of ~3 are obtained with correspondingly higher 3º/2º regioselectivity factors for adamantane of ~15-17 indicating the presence of a very selective oxidant different from hydroxyl or even alkoxyl radicals. Alkane substrates such as *cis* or *trans* 1,2-dimethylcyclohexane have also been used to provide powerful insights into the nature of the oxidant involved. Using $[Fe(BPMEN)(CH_3CN)_2]^{2+}$ and $[Fe(TPA)(CH_3CN)]^{2+}$ as catalysts the tertiary bonds are hydroxylated stereospecifically. On this basis it has been concluded that short lived alkyl radicals are generated which are immediately trapped by the metal oxo oxidant. A major challenge in this field is to promote heterolytic O-O cleavage within the initially formed hydroperoxoiron(III) species since hydroxyl radicals are generated when the O-O bond is cleaved homolytically. Heterolytic O-O cleavage is desirable since it generates a potentially more powerful putative perferryl metal oxo species ($LFe^{V}=O$ or $L^{+\cdot}Fe^{IV}=O$ (LFe^{IV}-$O^{\cdot -}$) (cf. cyt P450, peroxidase compound 1) as the oxidant while avoiding the co-formation of free oxygen radicals. The contemporary objective is to produce a high valent iron complex which can oxidise alkanes with high chemo-regio and stereoselectivity.[42]

1.3.6 The nature of the high valent iron oxidizing intermediate.

Analysis of products coupled with KIE values and regioselectivity factors has provided the strongest evidence yet that reaction between $[Fe(TPA)(CH_3CN)]^{2+}$ or $[Fe(BPMEN)(CH_3CN)_2]^{2+}$ and H_2O_2 generates a high-valent iron oxo complex which is

largely responsible for the hydroxylation of the alkane substrate. This has prompted further studies to investigate the nature of the putative reactive high valent intermediate and the conditions required to maximise its formation. In section 1.3.3 it was noted that the presence of weak ligands such H_2O enhance the catalytic activity of the complex. At the same time folded tetradentate pyridine based N-donor ligands such as TPA (L_1) and BPMEN (L_3) which facilitate the coordination of peroxide *cis* to a labile coordination site appear to generate the most active catalysts. When the reaction between $[Fe(TPA)(CH_3CN)]^{2+}$ and ^tBuOOH is carried out at low temperatures ($\leq -40^oC$), an intermediate blue species can be detected.[54, 55] This species has been formulated as $[Fe(TPA)(OO^tBu)(S)]^{2+}$ (S = CH_3CN or H_2O). Similar reaction with H_2O_2 yields a similar blue species formulated as $[Fe(TPA)(OOH)(S)]^{2+}$ (S = CH_3CN or H_2O) as indicated by ES-MS. Both of these species have been characterized by EPR and Raman spectroscopy as low spin Fe^{III} complexes with a terminal $OOH(Bu^t)$ bound to the iron. When low spin $[Fe(TPA)(OOH)(S)]^{2+}$ is compared to other iron peroxo complexes the terminally bound OOH^- ligand is found to possess a much lower O-O stretching vibration frequency consistent with its tendency to cleave.[55] The pentadentate iron complex $[Fe(N4Py)(CH_3CN)]^{2+}$ reported by Feringa and co-workers forms a hydroperoxoiron(III) species $[Fe(N4Py)(CH_3CN)]^{2+}$ with a similarly low O-O stretching frequency but here its catalytic behaviour towards alkane oxidation by H_2O_2 is significantly different from that of $[Fe(TPA)(CH_3CN)]^{2+}$. $[Fe(N4Py)(CH_3CN)]^{2+}$ gives rise to a very low A/K ratio (for cyclohexane oxidation) of 1.4 along with a KIE of 1.5 (using C_6D_{12}) which are altered when the reaction is carried out under O_2 (air). Similarly, a much lower regioselectivity 3°/2° factor for adamantane of ~3.3 is seen compared with $[Fe(TPA)(CH_3CN)]^{2+}$ (~15-17) and the reaction is not stereospecific for oxidation of *cis* and *trans* 1,2-dimethylcyclohexane. These results indicate for $[Fe(N4Py)(CH_3CN)]^{2+}$ the presence of long lived alkyl radicals generated via reaction of the alkane with hydroxyl radical. In the case of both $[Fe(TPA)(OOH)(S)]^{2+}$ and $[Fe(N4Py)(OOH)]^{2+}$ the low O-O stretching frequency indicates a tendency to cleave at the

O-O bond. In each case low temperature trapping experiments have subsequently led to characterisation of a green species resulting from decay of the hydroperoxoiron(III) complex believed to contain the iron(IV) oxo complexes $[Fe(TPA)(O)(S)]^{2+}$ and $[Fe(N4Py)(O)]^{2+}$.[3, 56] The different catalytic behaviour suggests for TPA as ligand that the high valent species is more reactive and intercept the alkyl radicals as they are formed. For pentadentate (L_4) N4py it appears the high valent iron oxo species generated is a less potent reactant allowing long lived alkyl radicals to be generated via free hydroxyl radical. It is now believed that the difference between TPA and N4py lies in the denticity of the ligand which for TPA allows a labile *cis* site to be present adjacent the OOH^- ligand which appears to be involved in its activation to give a more highly potent oxidising species. In the case of pentadentate N4py the extra labile *cis* site is absent. Nonetheless ready O-O cleavage within $[Fe^{IV}(N4Py)OOH]^{2+}$ is suggested from the low O-O stretching frequency implying ready formation of $[Fe^{IV}(N4Py)(O)]^{2+}$. This then argues for $[Fe^{IV}(N4Py)(O)]^{2+}$ being a much weaker oxidant than $[Fe^{IV}(TPA)(O)(S)]^{2+}$ or

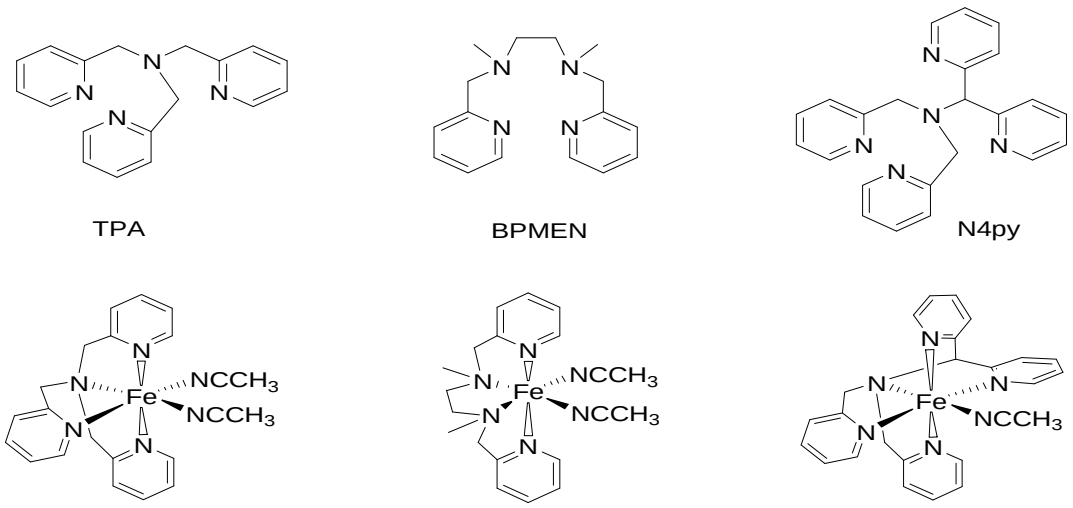

Figure 1.13: Schematic representation of ligands; TPA (L_1), BPMEN (L_3) and N4Py (L_4) and their corresponding iron(II) complexes; $[Fe(TPA)(CH_3CN)_2]^{2+}$ [1], $[Fe(BPMEN)(CH_3CN)_2]^{2+}$ [1] and $[Fe(N4Py)(CH_3CN)_2]^{2+}$.[1]

a species generated there from. Indeed more recent studies by Que et al have shown that $[Fe^{IV}(N4Py)(O)]^{2+}$, generated separately via the reaction of $[Fe(N4Py)(CH_3CN)]^{2+}$ with PhIO, is a relatively sluggish oxidant and as a result one of the longest lived iron(IV) oxo species known with a half life of ~60h at 25°C.[110] The marked selectivity of $[Fe(TPA)(CH_3CN)_2]^{2+}$ and $[Fe(BPMEN)(CH_3CN)_2]^{2+}$ compared with $[Fe(N4Py)(CH_3CN)]^{2+}$ towards hydroxylation of cycloalkanes by H_2O_2 appears for the former to be related to the presence of two *cis* labile sites on the iron. Initially this was believed to relate to the rapid formation of the hydroperoxoiron(III) intermediate and, in turn, the high valent iron(IV) oxo species allowing it to be available for reaction with alkyl radicals. However recent work in regard to alkene epoxidation activity has suggested that it may be due to the accessing for the former of the more potent iron(V) oxidant, figure 1.7 pathway (iii). The behaviour of $[Fe(N4Py)(CH_3CN)]^{2+}$ indicates that the homolytic O-O cleavage pathway (ii), figure 1.7, is involved generating LFe^{IV}=O and OH·. Iron(IV) oxo species have now been characterised for a number of biological non-heme systems such as the 2–oxoglutarate-dependent enzyme TauD.[111, 112] A number of iron(IV) oxo compounds have proved stable enough to crystallise. Reaction of $[Fe(TMC)(O_3SCF_3)_2]$ with PhIO in CH_3CN gives the crystallographically characterised $[Fe^{IV}(O)(TMC)(CH_3CN)]^{2+}$(TMC–1,4,8,11-tetramethyl-1,4,8,11-tetraazacyclotetradecane) (L_5).[113] On the other hand C_2 $[Fe^{IV}(O)(TPA)(S)]^{2+}$ (S = CH_3CN or H_2O) generated via the reaction of $[Fe(TPA)(CH_3CN)_2]^{2+}$ with CH_3CO_3H is only stable below -40°C. Both iron(IV) oxo complexes have been tested towards the stoichiometric oxidation of alkane and alkene substrates. While $[Fe^{IV}(O)(TMC)(CH_3CN)]^{2+}$ can transfer oxygen only to PPh_3 at -40°C,[114] $[Fe^{IV}(O)(TPA)(S)]^{2+}$ is able to epoxidise cyclooctane at this temperature. In the reaction between ^{t}BuOOH and various non-heme iron(II) polypyridine complexes the products are characterised by absorption band between 550 and 650 nm ($\varepsilon_m \sim 2000\ M^{-1}cm^{-1}$).[92] For TPA as ligand the maximum is at 600 nm ($\varepsilon_m \sim 2000\ M^{-1}cm^{-1}$) assigned to the blue low-spin iron(III) complex C_1 $[Fe^{III}(TPA)(OO^tBu)(S)]^{2+}$. In these solutions the formation of small amounts of

pale green $[Fe^{IV}(O)(TPA)(S)]^{2+}$ could have been overlooked in the beginning due to the dominant absorption from low spin $[Fe^{III}(TPA)(OO^tBu)(S)]^{2+}$. However direct evidence for the formation of $[Fe^{IV}(O)(TPA)(S)]^{2+}$ from $[Fe^{III}(TPA)(OO^tBu)(S)]^{2+}$ has now been obtained in the presence of added Lewis bases, figure 1.14.[115] It is believed that the higher detectable yields of $[Fe^{IV}(O)(TPA)(S)]^{2+}$ is due to accelerated formation via a 'push' effect from the Lewis base facilitating rapid homolytic cleavage of the O-O bond.[115] For example when $[Fe^{III}(TPA)(OO^tBu)(S)]^{2+}$ is reacted with 12 equivalents of 4-picolinate it increases its first order decay by 10 fold resulting in a 90% yield of $[Fe^{IV}(O)(TPA)(S)]^{2+}$ (from Mössbauer measurements). With pyridine-N-oxide the yield of the iron(IV) oxo complex is 95%. The need to generate $[Fe^{IV}(O)(TPA)(S)]^{2+}$ rapidly in order to maximise its yield is because of the thermal instability of the iron(IV) oxo complex. Both the Mössbauer and UV-visible spectrum of $[Fe^{IV}(O)(TPA)(S)]^{2+}$ are dependent of the nature of the Lewis base. The peak maximum shifts from 700 nm (no added base) to 718 nm (for 4-picolinate) or to 742 nm (for pyridine-N-oxide). As shown in figure 1.14, these changes in the λmax indicate that the S (CH_3CN) ligand in $[Fe^{IV}(O)(TPA)(S)]^{2+}$ is likely replaced by the Lewis base. It is interesting to note that here pyridine-N-oxide acts does not function itself as an oxygen transfer agent as in other literature examples.[116] If it had functioned in this way

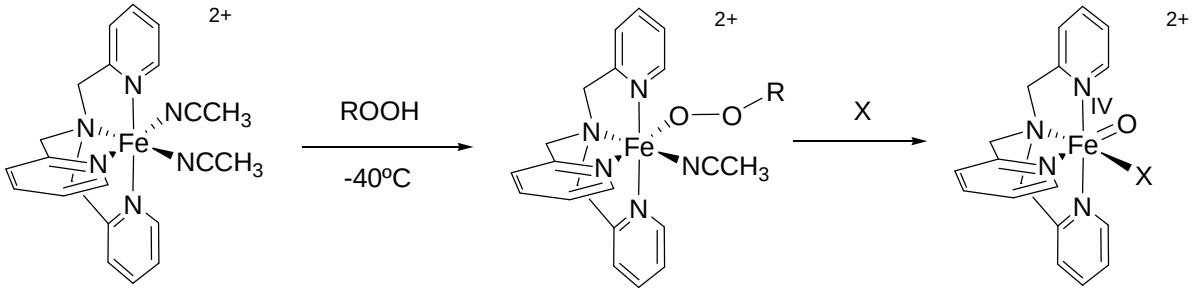

Figure 1.14 Schematic representation of $[Fe^{IV}(O)(TPA)(X)]$ (C_2) formation by reaction of $[Fe^{II}(TPA)(CH_3CN)_2]^{2+}$ with ROOH.[115]

pyridine would have replaced the S in $[Fe^{IV}(O)(TPA)(S)]^{2+}$ resulting in a much lower λ_{max} similar to that for S = CH_3CN (similar donor properties). Recently Que et al reported that the introduction of a carboxylate ligand $CF_3CO_2^-$ trans to the oxo group in the S = 1 complex *trans*-$[Fe^{IV}(O)(TMC)(CH_3CN)]^{2+}$ (C_3) enhance its reactivity.[117] This is believed to occur through a weakening of the Fe=O bond providing greater access to the more reactive S = 2 surface, figure 1.15.

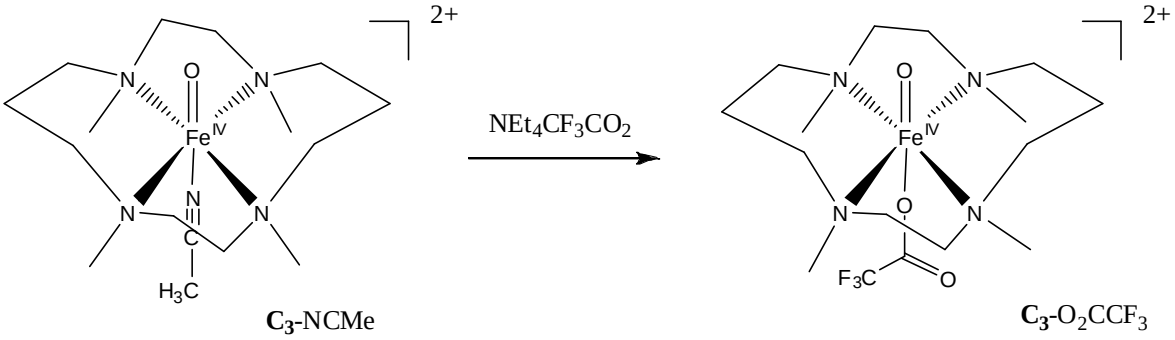

Figure 1.15: Conversion of S = 1 *trans*-$[Fe^{IV}(O)(TMC)(CH_3CN)]^{2+}$ (C_3-NCMe) into S = 2 *trans*-$[Fe^{IV}(O)(TMC)(O_2CCF_3)]^{+}$ (C_3- $CF_3CO_2^-$) via the addition of $CF_3CO_2^-$. [117]

Several non-heme iron metalloenzymes such MMO, TauD and ribonuclotide reductase are believed to form reactive S = 2 iron centres in carrying out their enzymic reactions. All three enzymes have an iron coordination sphere rich in carboxylate ligands. Recently the number of persistent iron(IV) oxo complexes has been expanded. In addition to $[Fe^{IV}(N4Py)(O)]^{2+}$ mentioned earlier a long lived iron(IV) oxo complex of pentadentate Bn–tpen, figure 1.16, has

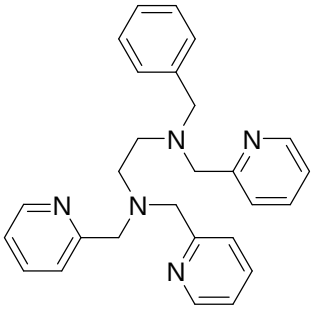

Figure 1.16: Structure of Bn-tpen (L_6).

been characterised. The most striking properties of $[Fe^{IV}(N4Py)(O)]^{2+}$ and $[Fe^{IV}(Bn\text{-}tpen)(O)]^{2+}$ containing (L_6) are the higher temperature stability[110] and their ability to hydroxylate C–H bonds as strong as those in cyclohexane. $[Fe^{IV}(L)(O)(S)]^{2+}$ complexes are usually prepared by treatment of the iron(II) derivative $[Fe^{II}(L)(CH_3CN)_x]^{2+}$ with the oxygen transfer agent PhIO and are noted by their green colour. For L = N4py the green colour is associated with a band at 695 nm (ϵ = 400 M^{-1} cm^{-1}) with a shoulder near 800 nm. Treatment of $[Fe^{II}(Bn\text{-}tpen)(O_3SCF_3)]^{2+}$ with PhIO also yields green $[Fe^{IV}(O)(Bn\text{-}tpen)(O_3SCF_3)]^{2+}$ with λ_{max} at 739 nm (ϵ = 400 M^{-1} cm^{-1}) and a shoulder near 900 nm but this species has a much shorter lifetime ($t_{1/2}$ ~ 6 h).[118] Similar near-IR bands ~ 700nm have been reported for the iron(IV) oxo complexes $[Fe^{IV}(O)(TMC)(CH_3CN)]^{2+}$ and $[Fe^{IV}(O)(TPA)(CH_3CN)]^{2+}$[113, 114]. $[Fe^{IV}(O)(Bn\text{-}tpen)(O_3SCF_3)]^{2+}$ exhibits the highest KIE value (KIE = 50) so far observed at ambient temperature for catalysis of cyclohexane oxygenation by a synthetic non-heme iron complex. Similar KIE value were reported for the reaction of ethylbenzene with $[Fe_2O(TPA)_2]^{4+}$ at -40°C[119]. Such large isotopic effects have been observed in the case of some non-heme iron enzymes such as TauD enzyme which has led to the proposal that the hydrogen atom abstracting agent is a high valent iron(V) oxo species.[111, 112, 120] Similarly large KIE values have also been reported for MMO for which a hydrogen tunnelling mechanism has been proposed.[6, 117, 121]

The high activity towards preferential hydroxylation of cyclohexane shown by iron(II/III)-TPA and related polypyridine ligand complexes was discovered thanks to an important observation which was the use of diluted H_2O_2.[42] Moreover, by adding diluted solutions of H_2O_2 via syringe pump at a steady rate equalling its H_2O_2 consumption was found to have a significant effect on the A/K ratio due to suppression of reactions that stem from the production of highly reactive but non-selective hydroxyl radicals.[122] Thus, under these conditions the observed A/K ratio for catalytic ROOH oxidation of cyclohexane increased and moreover it was not influenced by the presence of O_2. Furthermore when *cis*-

1,2-dimethylcyclohexane is used as substrate, the stereospecific hydroxylation of the *cis*-1,2-dimethyl groups was detected.[123] Such reactivity patterns suggest very short lived alkyl radicals not consistent with reactions involving RO·. A further characteristic of this family of non heme iron complexes is that they will catalyse the epoxidation of alkenes by H_2O_2 as well as stereospecific *cis*-dihydroxylation.[124].

Several non-heme iron-based catalytic oxidation systems with relevant potential applications have been developed. For instance, the iron(II) complexes of N4py and TPA catalyse alcohol oxidation via oxygen transfer from the $[Fe^{IV}(N4Py)(O)]^{2+}$ and $[Fe^{IV}(TPA)(O)]^{2+}$ complexes.[125, 126]Another important observation is that of Jacobsen et al[127] who found that the addition of acetic acid enhanced the catalytic alkene epoxidising activity of several non-heme iron complexes. The acetic acid was found to significantly enhance the yield of epoxide. Using acetic acid as a 30% additive the epoxidation of terminal alkenes by $[Fe(BPMEN)(CH_3CN)_2]^{2+}$ could be carried out in 90% yield, using only 3% of the iron catalyst and H_2O_2 at 4°C in 50% excess. A similar enhancement of alkene epoxidation activity, at the expense of *cis*-dihydroxylation, was observed when acetic acid was added to $[Fe(TPA)(CH_3CN)_2]^{2+}$.[128] Such activity has been attributed to the *in-situ* generation of peracetic acid in these solutions on the basis of largely identical behaviour (enhancement of epoxidation) seen on substituting acetic acid/H_2O_2 by peracetic acid.[129] It has been well documented that cyclohexane oxidations by peracids such as m-chloroperbenzoic acid (mCPBA) when catalysed by the tetradentate $[Fe(BPMEN)(CH_3CN)_2]^{2+}$ and $[Fe(TPA)(CH_3CN)_2]^{2+}$ give significantly higher A/K ratios than when using H_2O_2 or ^tBuOOH. This a feature attributed to heterolytic O-O cleavage of the percarboxylatoiron(III) precursor to generate a formally $LFe^V=O$ species. The formation of this species has been proposed to account for enhanced epoxidation activity, in particular when seen at the expense of *cis*–dihydroxylation. A correlation between high A/K ratios in cyclohexane oxygenation catalysis with high alkene epoxidation activity can be observed and particularly when at the expense of

cis-dihydroxylation offers the best marker yet for the presence of an active formally $LFe^{V}=O$ centre. However it appears that formally $LFe^{V}=O$ may not be formed in all cases of iron catalysis of peracid oxygenations. The percarboxylatoiron(III) adduct formed from reaction of pentadentate $[Fe(N4Py)(CH_3CN)]^{2+}$ with m-CPBA parallels the behaviour of the hydroperoxo adduct in as it appears to only undergo homolytic O-O cleavage to access an $Fe^{IV}=O$ oxidant reflecting the need for a second labile (*cis*) site to be present in order to access the more potent $LFe^{V}=O$ oxidant[128]. The homolytic O-O behaviour is apparent in a significantly lower cyclohexane A/K ratio (1.3) when oxygen is present compared to when the reaction is carried our under inert atmosphere (5.6) implying both a metal based oxidant but also the presence of O_2 trappable long lived alkyl radicals presumably via competing H abstraction by C- or O-centred radicals.[130]

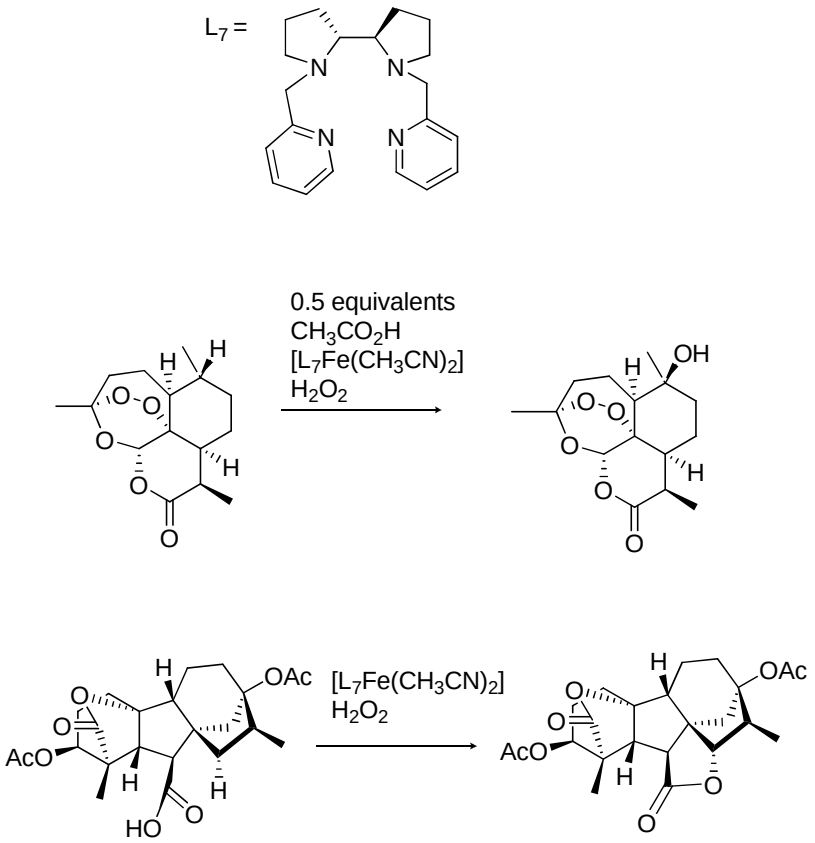

Figure 1.17: Enantioselective catalysis of H_2O_2 hydroxylation at 2^o and 3^o C-H bonds in the antimalarial drug artemisinin, and tetrahydrogibberellic acid, respectively, by the asymmetric complex; $[Fe(L_7)(CH_3CN)_2]^{2+}$ (L_7 = S,S-PDP) in the presence of acetic acid.[131]

One of the most remarkable applications of the Fe(BPMEN)-H_2O_2-acetic acid system was recently reported by White and Chen using an iron complex of an asymmetric BPMEN-type ligand; $[Fe(L_7)(CH_3CN)_2]^{2+}$ (L_7 = S,S-PDP), figure 1.17. It was discovered that tertiary C-H bonds such as C10 in the antimalarial drug artemisinin are catalytically hydroxylated by this metal complex and H_2O_2 in the presence of acetic acid, without altering other functional groups. The enantioselective hydroxylation was carry out using 5 mol% catalyst; the product being obtained in 40-60% yield.[131] In most cases, the tertiary C-H bonds hydroxylated are the most rich electronically as well as the most accessible. It was also found that if the substrate possessed carboxylate functionality, such as in the case of the tetrahydrogibberellic acid analogue, it was able to direct the iron-based oxidant to attack at a particular nearby C-H bond, to give the lactone, figure 1.17. This implies that the promoting effect of the acetic acid might, at least in part, be through coordination of acetate (or indeed any other available carboxylate moiety) to the iron active species. These two examples show how simple biomimetic iron-based catalysts can be active in promoting enantioselective and regioselective hydroxylation of organic molecules with complex structures.

Another family of iron complexes highly active towards promoting peroxide oxygenations in aqueous media are those of the macrocyclic tetraamide ligand TAML (L_8), figure 1.18, developed by Collins et al. Several of these have moreover been investigated for

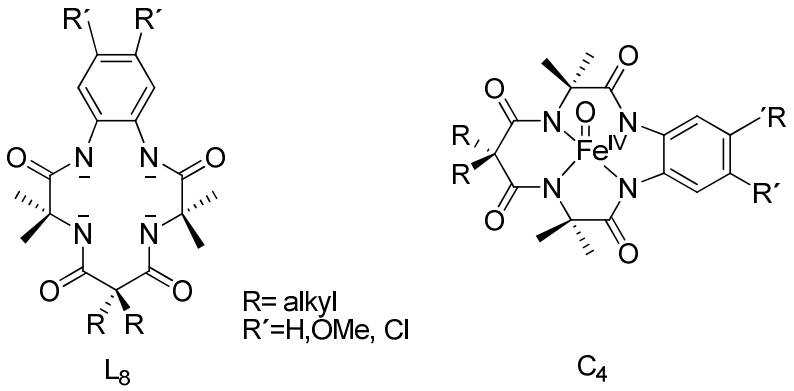

Figure 1.18: Structures of the tetraamide macrocycle ligand TAML (L_8) (left) and its S = 1 d^4 iron(IV) complex $[Fe(O)(TAML)]^{2-}$ complex (C_4).

the removal (complete oxidative degradation) of various toxic environmental POMs such as PCPs. Fe-TAML species show promising activity towards activating H_2O_2 for this purpose and wide scale environmental use is a possibility. Possible uses include the removal of persistent organic molecules (POMs) associated with textile, pulp, paper and pesticide industries, the removal of sulfur from hydrocarbon fuels[132] and the rapid killing of anthrax-like spores. An extremely powerful oxidant appears relevant to this system and very recently chemical and spectroscopic evidence has been found for generation of two high valent iron species consisting of both S = 1 and S = 2 d^4 iron(IV) oxo centres[133, 132] and, most interestingly, an S = ½ d^3 perferryl iron(V) oxo centre. The S = ½ d^3 iron(V) species $[Fe^{V}(O)(TAML)]^-$ was only characterised at low temperature in solution (-70^{o}C) following reaction of the iron(III) complex $[Fe^{III}(OH_2)(TAML)]^-$ with mCPBA.[134] However it proved stable enough at this temperature to allow its full characterisation by MS, Mössbauer, EPR and XAS supported by DFT calculations. This S = ½ species represents the first example of a fully characterized iron(V) oxo complex which is believed to be the active oxidant species in catalysis of the degradation of numerous environmental POMs by H_2O_2 in the presence of Fe-TAML complexes.[42] Evidence for the involvement of discrete iron(V) oxo centres in biological processes is increasing. Following ^{18}O labelling experiments Que and co-workers have concluded that an iron(V) oxo species formulated as HO-Fe^{V}=O is the relevant oxidant in most enzymatic transformations carried out by the Rieske dioxygenase family.[121] Examples of genuine iron(V) complexes are still however rare. Wieghardt et al have spectroscopically characterized an S = ½ iron(V) complex with a terminal nitrido group obtained by a photochemical N-N bond cleavage reaction on an iron(III)-azido complex.[135]

1.3.7 Mimicking the iron oxygenase enzyme macro environment.

Methane monooxygenase and cytochrome P-450 both possess structures wherein the

non-heme diiron and the heme-iron active sites respectively are embedded within a hydrophobic pocket, partly to attract (solubilise) the hydrophobic C-H substrate but also to assist selective uptake and subsequent hydroxylation (oxygenation).[136] Both enzymes work in aqueous media. However the feasibility of creating a local hydrophobic macro environment within an aqueous soluble lab-based hydroxylating catalyst has received little attention. Fish et *al.* have reported studies on alkane functionalization by (^{t}BuOOH)/O_2 in aqueous media using $[Fe_2O(\mu\text{-}OAc)(TPA)_2]^{3+}$ as a pre-catalyst embedded within amorphous silica modified by alternate incorporation of hydrophilic and hydrophobic polyethylene oxide (PEO) and polypropylene oxide (PPO) pendant groups. It was observed that this artificial scaffold mimics the hydrophobic active site of MMO enzyme facilitating the oxidation of alkanes using t-BuOOH/O_2 as oxidant in aqueous medium (pH 4.2). The results of these experiments are shown in table 1.4[137]. The products obtained were cyclohexanol, cyclohexanone and

Table 1.4: Oxidation of Alkanes with 1wt% $[Fe_2O(\mu\text{-}OAc)(TPA)_2]^{3+}$, 10% PPO,10% PeO-$SiO_2$[a]

Substrate	**Total TON**	**Products**	**%**
cyclohexane	238	cyclohexanone	51
		cyclohexanol	16
		cyclohexyl-tert-butyl peroxide	33
cycloheptane	146	cycloheptanone	55
		cycloheptanol	16
		cycloheptyl-tert-butyl peroxide	26
tetrahydronaphthalene	141	α-tetralone	94
		α -tetralol	6
ethylbenzene	157	acetophenone	72
		1-phenylethanol	28
n-nonane	31	2-,3-,4-nonanone	68
		2-,3-,4-nonanol	32

[a] Reactions were carried out by mixing 0.38 mmol alkane, 3.8 mmol TBHP in 5 cm^3 water at pH 4.2, with 0.38 mmol precatalyst (as 1 wt% $[Fe_2O(\mu\text{-}OAc)(TPA)_2]^{3+}$on 10% PPO,10% PEO-$SiO_2$) for 3 h at room temperature.

[b]Product as mol % total products. Yields cased on TBHP were 80-90%.

cyclohexyl-tert-butyl-peroxide with a 1:3:2 ratio when cyclohexane was used as substrate. The catalytic activity was found to be crucially dependent on the balance between PEO and PPO tethered on the silica surface. The silica-based assembly showed reactivity somewhat higher in comparison to an aqueous micelle system utilising cetyltrimethylammonium hydrogen sulphate as a surfactant.

An alternative way of creating a local hydrophobic microenvironment for the iron-TPA system is to attach hydrophobic groups to the TPA ligand itself. Possible synthons for this are tris(6-amino-2-pyridylmethyl)amine (6-$(NH_2)_3$-TPA) (attachment via amide/urea/amine),[138,139] figure 1.19a, and tris(6-hydroxymethyl-2-pyridylmethyl)amine (6

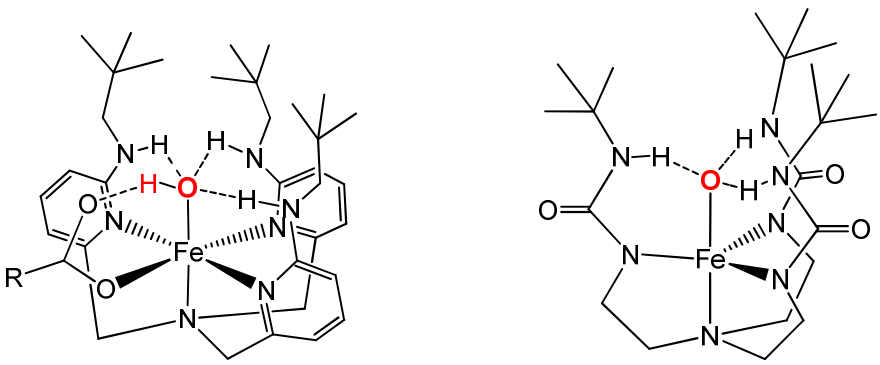

Figure 1.19: (a): Iron(III) complexes of (L_9) tris(6-neopentylamino-2-pyridylmethyl)amine (R = C_6H_5) (a) and (L_{10}) N',N'',N'''-tris(t-butylamidoaminoethyl)amine (b) showing hydrogen bonding from N-H to stabilize terminal hydroxo and oxo ligands respectively.[138, 140]

-$(OH)_3$-TPA) (attachment via ether/ester). Studies have shown that when TPA coordinates to transition metal centres the 6-py positions are orientated along the same direction. Thus attachment of peralkyl substituents at the 6-position should lead to the creation of a hydrophobic pocket which moreover might lead to a substrate orientation/proximity effect to facilitate oxygenation on the usually more inert C-1 position on a linear alkane, figure 1.20. Metal complexes containing such ligands could also be studied for activity towards alkane oxygenation in a micellar aqueous system.

An additional feature of several of the alkane oxygenase enzymes alongside the active site hydrophobicity is the presence of intra molecular hydrogen-bonding networks which may regulate the properties/creation of the oxo-metal centres. The X-ray structure of compound I of cytochrome *c* peroxidase shows the presence of hydrogen-bonding from an active site arginine (Arg 48) to the Fe^{IV}=O centre[141] which may be important in stabilizing (prolonging the lifetime) of this reactive high valent species as well as tuning its reactivity.

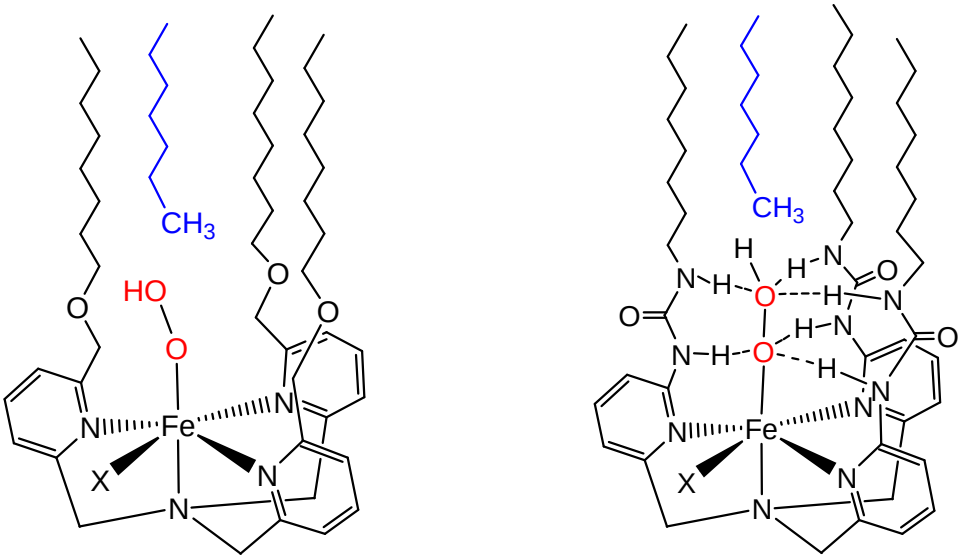

Figure 1.20: Putative hydroperoxo-iron(III) complexes of peralkylated TPA derivatives tris(6-n-octyloxymethyl-2-pyridylmethyl)amine (a) (see chapter 3) and tris(6-n-octylureayl-2-pyridylmethyl)amine (b) (see chapter 4) showing hydrogen bonding from urea N-H groups to stabilize the hydroperoxo group. In both a putative n-heptane molecule is shown orientated in the pocket in such a way as to facilitate possible oxygenation at the less reactive C-1 position.

In this regard Borovik et al have reported rare examples of mononuclear $Mn^{II/III}$ and $Fe^{III/II}$ complexes containing hydroxo and oxo ligands coordinated within a tripodal TPA-like ligand, stabilised through intramolecular hydrogen-bonding. Use of the tripodal ligand; (L_{10}) N',N'',N'''-tris(t-butylamidoaminoethyl)amine , figure 1.19b, creates a protective hydrogen-bonded cavity around the M^{III}-O(H) units (M^{III} = Fe and Mn).[140] Here the t-butyl groups are orientated upwards to encapsulate the hydrogen-bonded Fe(III)-'O' centre. Thus one finds the

intriguing situation of a high valent metal centre located inside a hydrophobic pocket where the oxo ligand is stabilized through N-H hydrogen bonds. The catalytic behaviour of such derivatives has yet to be fully explored.

The only 6-py substituted iron-TPA complexes to have received detailed investigations as to their catalytic alkane hydroxylating ability are those of the 6-Me_n-TPA (n = 1-3) derivatives.[122] $[Fe(6\text{-}Me\text{-}TPA)(CH_3CN)_2]^{2+}$ shows comparable activity in H_2O_2 oxygenation catalysis on cyclohexane (A/K = 7.0) and adamantane ($3^o/2^o$ = 30) to that shown by $[Fe(TPA)(CH_3CN)_2]^{2+}$ and $[Fe(BPMEN)(CH_3CN)_2]^{2+}$ implying a metal–based oxidant. However the presence of 6-Me substituents on two or all three of the pyridines results in high spin peroxoiron(III); $[Fe(L)(OOH)]^{2+}$ intermediates and a product profile more consistent with the involvement of hydroxyl and long lived alkyl radicals (A/K = 1 - 2) despite some evidence of a higher selectivity than OH radicals towards C-H bond cleavage (cyclohexane KIE 3.3 – 4.0, adamantane $3^o/2^o$ = 15 - 33).[122] This shows that some of the selectivity demonstrated by the iron TPA family of complexes is encouragingly retained upon 6-py substitution.

1.3.8 Adaptation of iron-TPA based oxidants to the fluorous biphase.

A number of approaches have been devised in homogeneous catalysis to overcome the problem of catalyst separation from the substrate-product mixture. Use of fluorous biphasic (FBC) solvent system is one of them wherein a catalyst saturated with fluorous groups is retained in a perfluorinated solvent while the products and substrate are retained in a different phase. At low temperature the two phases separate allow easy removal and recovery of the catalyst.[142] It is well known that perfluorohydrocarbons have unusual properties that entail being extremely hydrophobic and lacking hydrogen bonding capability which renders them to be relatively insoluble in their hydrocarbon analogues. They also have the propensity to dissolve various gases very efficiently such as oxygen, hydrogen and carbon dioxide. Fish and

co-workes have shown how the FBC concept is a practical way to separate the catalyst from the substrate or product containing phase in the oxidation of alkanes and alkenes using ^{t}BuOOH and O_2 gas as oxidating agent.[142] The synthesis of R_f-perfluoroalkyl synthons such as 3-perfluorooctyl-1-iodopropane, 3-perfluorooctyl-1-propanol (R_f =-$(CH_2)_3$-$(CF_2)_7$-CF_3) was reported along with a variety of new R_f-perfluoroalkylated ligands with amines such as 1,4,7-triazacyclononane (TACN), bis-picolylamine and bis(1,2-picolylamino)diethylenediamine. It was found that only 1,4,7-tris-*N*-(4,4,5,5,6,6,7,7,8,8,9,9,10,10,11,11,11-heptadecafluoro undecyl)-1,4,7-triazacyclononane (R_f-TACN) is completely soluble. The ligand must contain at least 57% of fluorine in order to be fully soluble. The R_f-TACN ligand was combined with $[Mn(O_2C(CH_2)_2C_8F_{17})_2]$ and $[Co(O_2C(CH_2)_2C_8F_{17})_2]$ metal complexes with R_f-perfluoroalkylcarboxylate coordinated to the metal, to produce the corresponding R_fMn^{2+}-R_fTACN and R_fCo^{2+}-R_fTACN pre-catalyst for the oxidation by these metals. Use of R_f-perfluoroalkyl synthons like 3-perfluoroctyl-1-iodopropane with deprotonated synthons such as 6-$(OH)_3$-TPA (ether link formation) offers a route to generating interesting hydrophobic fluorocarbon-soluble perfluoro iron-TPA systems, e.g., figure 1.21, analogous to those in figure 1.20, for investigating iron-based FBC of peroxide alkane oxygenation.

1.4 Summary and conclusions

The considerable progress in the understanding of the mechanisms underpinning how iron or copper-based oxygenase enzymes catalyse a variety of C-H bond oxygenation processes over the last 30 years has motivated the increase of a range of new synthetic biomimetic systems. A promising number of iron, manganese, nickel and copper complexes armed with non-porphyrin ligands active in the catalytic oxidation of alkanes and alkenes with H_2O_2 or even O_2 have been discovered. A recurring theme especially concerning those reactions utilising H_2O_2 as oxidant has been to determine the optimum reaction conditions

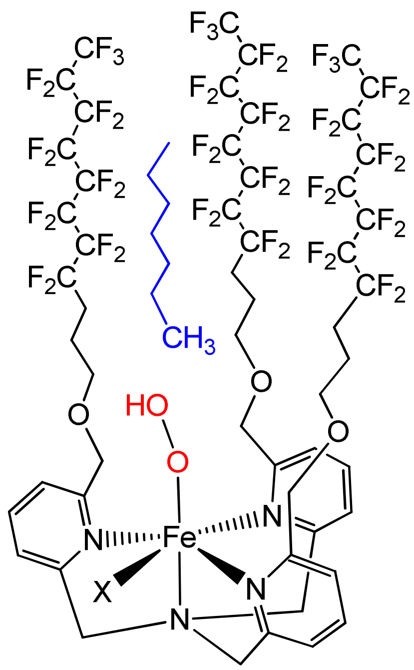

Figure 1.21: A putative fluorous-soluble hydroperoxo-iron(III) complex of a tris(6-perfluoralkyloxymethyl-2-pyridylmethyl)amine ligand.

that prevents generation of OH radicals which are unselective and facilitate the formation of a high valent oxidant via O-O bond heterolysis of its peroxo precursor. The generation of a more selective metal-based oxidant makes possible substrate oxidations with noteworthy chemo-, region- and steroselectivity; and it could be applied in the chemical industry. The catalytic oxidation of n-alkane C-1 bonds to 1-oxygenates constitute still one of the most challenging chemical processes. Ultimately the use of O_2 as oxidant (source of O) is most desired from a cost point of view since aqueous H_2O_2 still remains a relatively expensive commodity oxidant to both use and transport. Important features in ligand design also need to be taken in account. The tunnelling effect could be the key factor towards achieving efficient alkane oxidation and selectivity. It is also important to address what is the best ligand donor set for generating the right kind of reactive oxygenating species. The role of ancillary ligands, such as pyridine or carboxylate requires further investigation. Finding a sophisticated ligand which could facilitate a tunnelling effect and at the same time increase the alkane solubility /

regioselective reaction is still the goal for future research. Finally adapting the metal-based oxidant system to work under fluorous biphasic conditions could allow the easy removal and recycling of catalysts by solubilisation in the fluorous media which could be a key feature for industrial commercialization.

In the subsequent chapters the chemistry of iron complexes of a number of new 6-py peralkylated derivatives of TPA is explored with a view to the design of a hydrophobic catalyst ultimately aimed at enhanced activity for the regioselective H_2O_2 oxygenation of n-alkanes at the C-1 position to give 1-oxygenates. In chapter 2 the chemistry of iron(III) and manganese(II) complexes containing the precursor ligand tris(6-hydroxymethyl-2-pyridylmethyl)amine ((6-OH)$_3$-TPA) is described, while the iron chemistry of several completely new tris(6-alkyloxymethyl)TPA derivatives, synthesized from 6-(OH)$_3$-TPA, is explored in chapter 3. Chapter 4 describes the characterisation and chemistry of iron complexes of a family of new 6-peralkylureido-TPA ligands, while chapter 5 discusses the results of catalytic H_2O_2 oxygenations on cyclohexane carried out by the entire family of new iron-TPA complexes synthesised in the preceding chapters. The studies with 6-(OH)$_3$-TPA in chapter 2 have already been published.[143]

1.5 References

1. M. Costas, K. Chen and L. Que, *Coord. Chem. Rev.*, 2000, **200-202**, 517-544.
2. D. H. R. Marton, A. E. Martell, D. T. Sawyer and Editors, *The Activation of Dioxygen and Homogeneous Catalytic Oxidation. (Proceedings of the Fifth International Symposium on the Activation of Dioxygen and Homogeneous Catalytic Oxidation, held March 14-19, 1993, in College Station, Texas.)*, 1993.
3. R. A. Sheldon and J. K. Kochi, *Metal-Catalyzed Oxidations of Organic Compounds*, 1981. Publisher: (Academic Press, New York, N. Y.)
4. D. Riley, M. Stern and J. Ebner, *Act. Dioxygen Homogeneous Catal. Oxid., [Proc. Int. Symp.], 5th* 1993, 31-44.
5. A. L. Feig and S. J. Lippard, *Chem. Rev.* , 1994, **94**, 759-805.
6. B. J. Wallar and J. D. Lipscomb, *Chem. Rev.* , 1996, **96**, 2625-2657.
7. Z. Wang, L. Martins, W. R. Ellis, Jr. and L. Que, Jr., *JBIC, J. Biol. Inorg. Chem.*, 1997, **2**, 56-64.
8. J. Reedijk, E. Bouwman and Editors, *Bioinorganic Catalysis, Second Edition, Revised and Expanded*, 1999. Publisher: Marcel Dekker, Inc., New York
9. C. R. Randall and L. Que, Jr., *Handbook of Metal-Ligand Interactions in Biological Fluids: Bioinorganic Chemistry*, 1995, **1**, 388-398. Publisher: Dekker, New York, N.Y
10. J. Stubbe and J. W. Kozarich, *Chem. Rev* , 1987, **87**, 1107-1136.
11. S. Atsumi, T. Hanai and C. Liao James, *Nature* 2008, **451**, 86-89.
12. B. Meunier, *Chem. Rev.* , 1992, **92**, 1411-1456.
13. C. S. Raman, H. Li, P. Martasek, V. Kral, B. S. Masters and T. L. Poulos, *Cell* 1998, **95**, 939-950.

14. B. R. Crane, A. S. Arvai, D. K. Ghosh, C. Wu, E. D. Getzoff, D. J. Stuehr and J. A. Tainer, *Science*, 1998, **279**, 2121-2126.

15. H. Li and T. L. Poulos, *Structure*, 1994, **2**, 461-464.

16. M. Sono, M. P. Roach, E. D. Coulter and J. H. Dawson, *Chem. Rev. (Washington, D. C.)* 1996, **96**, 2841-2887.

17. D. Picot, P. J. Loll and R. M. Garavito, *Nature*, 1994, **367**, 243-249.

18. L. J. Marnett, *Adv. Exp. Med. Biol.*, 1991, **283**, 65-70.

19. *Cytochrome P-450: Structure, Mechanism and Biochemistry*, Plenum Press, New York, 1995.

20. R. Davydov, I. D. G. Macdonald, T. M. Makris, S. G. Sligar and B. M. Hoffman, *J. Am. Chem. Soc.*, 1999, **121**, 10654-10655.

21. D. L. Harris and G. H. Loew, *J. Am. Chem. Soc.*, 1998, **120**, 8941-8948.

22. A. C. Rosenzweig, P. Nordlund, P. M. Takahara, C. A. Frederick and S. J. Lippard, *Chem. Biol.*, 1995, **2**, 409-418.

23. A. C. Rosenzweig, C. A. Frederick, S. J. Lippard and P. Nordlund, *Nature* 1993, **366**, 537-543.

24. K. E. Liu, A. M. Valentine, D. Wang, B. H. Huynh, D. E. Edmondson, A. Salifoglou and S. J. Lippard, *J. Am. Chem. Soc.*, 1995, **117**, 10174-10185.

25. A. M. Valentine, S. S. Stahl and S. J. Lippard, *J. Am. Chem. Soc.*, 1999, **121**, 3876-3887.

26. L. Shu, J. C. Nesheim, K. Kauffmann, E. Munck, J. D. Lipscomb and L. Que, Jr., *Science* 1997, **275**, 515-518.

27. S. K. Lee, J. C. Nesheim and J. D. Lipscomb, *J. Biol. Chem.*, 1993, **268**, 21569-21577.

28. P. E. M. Siegbahn and R. H. Crabtree, *J. Am. Chem. Soc.*, 1997, **119**, 3103-3113.

29. P. E. M. Siegbahn, *Inorg. Chem.*, 1999, **38**, 2880-2889.

30. H. Basch, K. Mogi, D. G. Musaev and K. Morokuma, *J. Am. Chem. Soc.*, 1999, **121**, 7249-7256.

31. B. D. Dunietz, M. D. Beachy, Y. Cao, D. A. Whittington, S. J. Lippard and R. A. Friesner, *J. Am. Chem. Soc.*, 2000, **122**, 2828-2839.

32. P. E. M. Siegbahn, R. H. Crabtree and P. Nordlund, *JBIC, J. Biol. Inorg. Chem.*, 1998, **3**, 314-317.

33. K. Yoshizawa, *JBIC, J. Biol. Inorg. Chem.*, 1998, **3**, 318-324.

34. A. A. Shteinman, *JBIC, J. Biol.* , 1998, **3**, 325-330.

35. J. D. Lipscomb and L. Que, Jr., *JBIC, J. Biol. Inorg. Chem.*, 1998, **3**, 331-336.

36. Y. Lindqvist, W. Huang, G. Schneider and J. Shanklin, *EMBO J.*, 1996, **15**, 4081-4092.

37. J. A. Broadwater, C. Achim, E. Munck and B. G. Fox, *Biochemistry*, 1999, **38**, 12197-12204.

38. R. M. Burger, *Chem. Rev.* , 1998, **98**, 1153-1169.

39. R. M. Burger, T. A. Kent, S. B. Horwitz, E. Munck and J. Peisach, *J. Biol. Chem.*, 1983, **258**, 1559-1564.

40. R. M. Burger, J. Peisach and S. B. Horwitz, *J. Biol. Chem.*, 1981, **256**, 11636-11644.

41. J. W. Sam, X.-J. Tang and J. Peisach, *J. Am. Chem. Soc.*, 1994, **116**, 5250-5256.

42. L. Que, Jr. and B. Tolman William, *Nature*, 2008, **455**, 333-340.

43. C. Walling, *Acc. Chem. Res.*, 1975, **8**, 125-131.

44. D. T. Sawyer, A. Sobkowiak and T. Matsushita, *Acc. Chem. Res.*, 1996, **29**, 409-416.

45. P. A. MacFaul, D. D. M. Wayner and K. U. Ingold, *Acc. Chem. Res.*, 1998, **31**, 159-162.

46. S. Goldstein and D. Meyerstein, *Acc. Chem. Res.*, 1999, **32**, 547-550.

47. N. D. Priestley, H. G. Floss, W. A. Froland, J. D. Lipscomb, P. G. Williams and H. Morimoto, *J. Am. Chem. Soc.*, 1992, **114**, 7561-7562.

48. A. M. Valentine, B. Wilkinson, K. E. Liu, S. Komar-Panicucci, N. D. Priestley, P. G. Williams, H. Morimoto, H. G. Floss and S. J. Lippard, *J. Am. Chem. Soc.*, 1997, **119**, 1818-1827.

49. G. H. McGall, L. E. Rabow, J. Stubbe and J. W. Kozarich, *J. Am. Chem. Soc.*, 1987, **109**, 2836-2837.

50. L. E. Rabow, J. Stubbe, J. W. Kozarich and G. H. McGall, *J. Am. Chem. Soc.*, 1990, **112**, 3203-3208.

51. R. J. Guajardo, S. E. Hudson, S. J. Brown and P. K. Mascharak, *J. Am. Chem. Soc.*, 1993, **115**, 7971-7977.

52. M. E. J. Coronel and A. J. Colussi, *Int. J. Chem. Kinet.*, 1988, **20**, 749-752.

53. G. V. Buxton, C. L. Greenstock, W. P. Helman and A. B. Ross, *J. Phys. Chem. Ref.* , 1988, **17**, 513-886.

54. P. A. MacFaul, K. U. Ingold, D. D. M. Wayner and L. Que, Jr., *J. Am. Chem. Soc.*, 1997, **119**, 10594-10598.

55. R.Y.N. Ho, G. Roelfes, B.L. Feringa and L. Que, Jr., *J. Am. Chem. Soc.*,1999,**121**, 264-265.

56. D. H. Barton, A. H. Beck and D. K. Taylor, *Tetrahedron*, 1995, **51**, 5245-5254.

57. J. T. Groves and T. E. Nemo, *J. Am. Chem. Soc.*, 1983, **105**, 6243-6248.

58. K. U. Ingold and P. A. MacFaul, *Biomimetic Oxid. Catal. Transition Met. Complexes* B.Meunier. Ed.ICP, London ,2000, 45-89.

59. G. A. Russell, *J. Am. Chem. Soc.*, 1957, **8**, 3871.

60. H. C. Tung, C. Kang and D. T. Sawyer, *J. Am. Chem. Soc.*, 1992, **114**, 3445-3455.

61. J.-M. Vincent, S. Bearnais-Barbry, C. Pierre and J.-B. Verlhac, *J. Chem. Soc., Dalton Trans.*, 1999, 1913-1914.

62. C. Nguyen, R. J. Guajardo and P. K. Mascharak, *Inorg. Chem.*, 1996, **35**, 6273-6281.

63. T. Kojima, R. A. Leising, S. Yan and L. Que, Jr., *J. Am. Chem. Soc.*, 1993, **115**, 11328-11335.

64. R. A. Leising, R. E. Norman and L. Que, Jr., *Inorg. Chem.*, 1990, **29**, 2553-2555.

65. P. A. MacFaul, I. W. C. E. Arends, K. U. Ingold and D. D. M. Wayner, *J. Chem. Soc., Perkin Trans. 2*, 1997, 135-145.

66. S. Menage, J. M. Vincent, C. Lambeaux, G. Chottard, A. Grand and M. Fontecave, *Inorg. Chem.*, 1993, **32**, 4766-4773.

67. S. Menage, J.-M. Vincent, C. Lambeaux and M. Fontecave, *J. Mol. Catal. A: Chem.*, 1996, **113**, 61-75.

68. R. M. Buchanan, S. Chen, J. F. Richardson, M. Bressan, L. Forti, A. Morvillo and R. H. Fish, *Inorg. Chem.*, 1994, **33**, 3208-3209.

69. R. H. Fish, K. J. Oberhausen, S. Chen, J. F. Richardson, W. Pierce and R. M. Buchanan, *Catal. Lett.*, 1993, **18**, 357-365.

70. D. Tetard and J.-B. Verlhac, *J. Mol. Catal. A: Chem.*, 1996, **113**, 223-230.

71. A. Rabion, R. M. Buchanan, J.-L. Seris and R. H. Fish, *J. Mol. Catal. A: Chem.*, 1997, **116**, 43-47.

72. R. A. Leising, J. Kim, M. A. Perez and L. Que, Jr., *J. Am. Chem. Soc.* 1993, **115**, 9524-9530.

73. J. Kim, R. G. Harrison, C. Kim and L. Que, Jr., *J. Am. Chem. Soc.*, 1996, **118**, 4373-4379.

74. S. Miyajima and O. Simamura, *Bull. Chem. Soc. Jpn.* 1975, **48**, 533-535.

75. A. F. Trotman-Dickenson, *Adv. Free-Radical Chem.*, 1965, **1**, 1-38.

76. A. M. Khenkin and A. E. Shilov, *New J. Chem.*, 1989, **13**, 659-667.

77. M. das Dores Assis and J. R. L. Lindsay Smith, *J. Chem. Soc., Perkin Trans. 2*, 1998, 2221-2226.

78. A. B. Sorokin and A. M. Khenkin, *New J. Chem.*, 1990, **14**, 63-67.

79. R. H. Fish, M. S. Konings, K. J. Oberhausen, R. H. Fong, W. M. Yu, G. Christou, J. B. Vincent, D. K. Coggin and R. M. Buchanan, *Inorg. Chem.*, 1991, **30**, 3002-3006.

80. S. Ito, M. Suzuki, T. Kobayashi, H. Itoh, A. Harada, S. Ohba and Y. Nishida, *J. Chem. Soc., Dalton Trans.*, 1996, 2579-2580.

81. Y. Nishida, T. Okuno, S. Ito, A. Harada, S. Ohba, H. Matsushima and T. Tokii, *Chem. Lett.*, 1995, 885-886.

82. T. Okuno, S. Ito, S. Ohba and Y. Nishida, *J. Chem. Soc., Dalton Trans.*, 1997, 3547-3551.

83. C. Sheu and D. T. Sawyer, *J. Am. Chem. Soc.*, 1990, **112**, 8212-8214.

84. V. S. Kulikova, O. N. Gritsenko and A. A. Shteinman, *Mendeleev Commun.*, 1996, 119-120.

85. S. Menage, J. M. Vincent, C. Lambeaux and M. Fontecave, *J. Chem. Soc., Dalton Trans.*, 1994, 2081-2084.

86. C. Duboc-Toia, S. Menage, C. Lambeaux and M. Fontecave, *Tetrahedron Lett.*, 1997, **38**, 3727-3730.

87. G. Roelfes, M. Lubben, R. Hage, L. Que, Jr. and B. L. Feringa, *Chem.--Eur. J.*, 2000, **6**, 2152-2159.

88. K. Chen, M. Costas, J. Kim, K. Tipton Adrianne and L. Que, Jr., *J Am Chem Soc*, 2002, **124**, 3026-3035.

89. J. T. Groves, *J. Chem. Educ.*, 1985, **62**, 928-931.

90. V. W. Bowry and K. U. Ingold, *J. Am. Chem. Soc.*, 1991, **113**, 5699-5707.

91. M. Newcomb, M.-H. Le Tadic-Biadatti, D. L. Chestney, E. S. Roberts and P. F. Hollenberg, *J. Am. Chem. Soc.*, 1995, **117**, 12085-12091.

92. J. C. Nesheim and J. D. Lipscomb, *Biochemistry*, 1996, **35**, 10240-10247.

93. P. J. Krusic and J. K. Kochi, *J. Amer. Chem. Soc.*, 1971, **93**, 846-860.

94. M. P. Mehn, S. D. Brown, D. M. Jenkins, J. C. Peters and L. Que, Jr., *Inorg. Chem.*, 2006, **45**, 7417-7427.

95. R. A. Leising, J. Kim, M. A. Perez and L. Que, Jr., *J. Am. Chem. Soc.*, 1993, **115**, 9524-9530.

96. I. Tabushi, T. Nakajima and K. Seto, *Tetrahedron Lett.*, 1980, **21**, 2565-2568.

97. D. H. R. Barton, M. J. Gastiger and W. B. Motherwell, *J. Chem. Soc., Chem. Commun.*, 1983, 731-733.

98. D. H. R. Barton, S. D. Beviere, W. Chavasiri, E. Csuhai, D. Doller and W. G. Liu, *J. Am. Chem. Soc.*, 1992, **114**, 2147-2156.

99. E. About-Jaudet, D. H. R. Barton, E. Csuhai and N. Ozbalik, *Tetrahedron Lett.*, 1990, **31**, 1657-1660.

100. D. H. R. Barton, B. Hu, D. K. Taylor and R. U. R. Wahl, *J. Chem. Soc., Perkin Trans. 2*, 1996, 1031-1041.

101. D. T. Richens, S. L. Jain and A. C. Gale, *Inorg. React. Mech. (Philadelphia, PA, U. S.)* 2007, **6**, 169-183.

102. U. Schuchardt, W. A. Carvalho and E. V. Spinace, *Synlett*, 1993, 713-718.

103. D. H. R. Barton, S. D. Beviere and D. R. Hill, *Tetrahedron*, 1994, **50**, 2665-2670.

104. P. Jensen Michael, J. Lange Steven, P. Mehn Mark, L. Que Emily and L. Que, Jr., *J. Am. Chem. Soc.*, 2003, **125**, 2113-2128.

105. I. W. C. E. Arends, K. U. Ingold and D. D. M. Wayner, *J. Am. Chem. Soc.*, 1995, **117**, 4710-4711.

106. J. Kim, Y. Dong, E. Larka and L. Que, Jr., *Inorg. Chem.*, 1996, **35**, 2369-2372.

107. R. D. Oldroyd, J. M. Thomas, T. Maschmeyer, P. A. MacFaul, D. W. Snelgrove, K. U. Ingold and D. D. M. Wayner, *Angew. Chem., Int. Ed. Engl.*, 1997, **35**, 2787-2790.

108. S. J. Lange, H. Miyake and L. Que, Jr., *J. Am. Chem. Soc.*, 1999, **121**, 6330-6331.

109. J. Bernadou and B. Meunier, *Chem. Commun.*, 1998, 2167-2173.

110. M. Lubben, A. Meetsma, E. C. Wilkinson, B. Feringa and L. Que, Jr., *Angew. Chem., Int. Ed. Engl.*, 1995, **34**, 1512-1514.

111. J. C. Price, E. W. Barr, T. E. Glass, C. Krebs and J. M. Bollinger, Jr., *J. Am. Chem. Soc.*, 2003, **125**, 13008-13009.

112. J. C. Price, E. W. Barr, B. Tirupati, J. M. Bollinger, Jr. and C. Krebs, *Biochemistry*, 2003, **42**, 7497-7508.

113. J.-U. Rohde, J.-H. In, M. H. Lim, W. W. Brennessel, M. R. Bukowski, A. Stubna, E. Muenck, W. Nam and L. Que, Jr., *Science (Washington, DC, U. S.)*, 2003, **299**, 1037-1039.

114. H. Lim Mi, J.-U. Rohde, A. Stubna, R. Bukowski Michael, M. Costas, Y. N. Ho Raymond, E. Munck, W. Nam and L. Que, Jr., *Proc. Natl. Acad. Sci. U. S. A.*, 2003, **100**, 3665-3670.

115. J. Kaizer, M. Costas and L. Que, Jr., *Angew. Chem., Int. Ed.*, 2003, **42**, 3671-3673.

116. Y. Wang and J. H. Espenson, *Inorg. Chem.*, 2002, **41**, 2266-2274.

117. J.-U. Rohde and L. Que, Jr., *Angew. Chem., Int. Ed.*, 2005, **44**, 2255-2258.

118. J. Kaizer, J. Klinker Eric, Y. Oh Na, J.-U. Rohde, J. Song Woon, A. Stubna, J. Kim, E. Munck, W. Nam and L. Que, Jr., *J Am Chem Soc*, 2004, **126**, 472-473.

119. C. Kim, Y. Dong and L. Que, Jr., *J. Am. Chem. Soc.*, 1997, **119**, 3635-3636.

120. L. Que, Jr. and R. Y. N. Ho, *Chemical Reviews* 1996, **96**, 2607-2624.

121. M. Costas, M. P. Mehn, M. P. Jensen and L. Que, Jr., *Chem. Rev. (Washington, DC, U. S.)*, 2004, **104**, 939-986.

122. K. Chen, M. Costas and L. Que, Jr., *Journal of the Chemical Society, Dalton Transactions*, 2002, 672-679.

123. K. Chen and L. Que, Jr., *J. Am. Chem. Soc.*, 2001, **123**, 6327-6337.

124. K. Chen, M. Costas, J. Kim, A. K. Tipton and L. Que, Jr., *J. Am. Chem. Soc.*, 2002, **124**, 3026-3035.

125. N. Y. Oh, Y. Suh, M. J. Park, M. S. Seo, J. Kim and W. Nam, *Angew. Chem., Int. Ed.*, 2005, **44**, 4235-4239.

126. C. V. Sastri, K. Oh, Y. J. Lee, M. S. Seo, W. Shin and W. Nam, *Angew. Chem., Int. Ed.*, 2006, **45**, 3992-3995.

127. M. C. White, A. G. Doyle and E. N. Jacobsen, *J. Am. Chem. Soc.*, 2001, **123**, 7194-7195.

128. R. Mas-Balleste and L. Que, Jr., *J. Am. Chem. Soc.*, 2007, **129**, 15964-15972.

129. M. Fujita and L. Que, Jr., *Adv. Synth. Catal.*, 2004, **346**, 190-194.

130. K. Ray, S. M. Lee and L. Que, Jr., *Inorg. Chim. Acta*, 2008, **361**, 1066-1069.

131. M. S. Chen and M. C. White, *Science (Washington, DC, U. S.)* 2007, **318**, 783-787.

132. A. Chanda, X. Shan, M. Chakrabarti, W. C. Ellis, D. L. Popescu, F. Tiago de Oliveira, D. Wang, L. Que, T. J. Collins, E. Muenck and E. L. Bominaar, *Inorg. Chem.* 2008, **47**, 3669-3678.

133. A. Chanda, D.-L. Popescu, F. Tiago de Oliveira, E. L. Bominaar, A. D. Ryabov, E. Muenck and T. J. Collins, *J. Inorg. Biochem.*, 2006, **100**, 606-619.

134. F. Tiago de Oliveira, A. Chanda, D. Banerjee, X. Shan, S. Mondal, L. Que, Jr., L. Bominaar Emile, E. Munck and J. Collins Terrence, *Science* 2007, **315**, 835-838.

135. N. Aliaga-Alcalde, S. D. George, B. Mienert, E. Bill, K. Wieghardt and F. Neese, *Angew. Chem., Int. Ed.*, 2005, **44**, 2908-2912.

136. K. Neimann, R. Neumann, A. Rabion, R. M. Buchanan and R. H. Fish, *Inorg. Chem.*, 1999, **38**, 3575-3580.

137. R. H. Fish, A. Rabion, K. Neimann, R. Neumann, J.-M. Vincent, M. Contel, C. Izuel, P. R. Villuendas and P. J. Alonso, *Top. Catal.*, 2005, **32**, 185-196.

138. S. Ogo, S. Wada, Y. Watanabe, M. Iwase, A. Wada, M. Harata, K. Jitsukawa, H. Masuda and H. Einaga, *Angew. Chem., Int. Ed.*, 1998, **37**, 2102-2104.

139. J. C. Mareque Rivas, E. Salvagni, R. T. Martin de Rosales and S. Parsons, *Dalton Trans.*, 2003, 3339-3349.

140. C. E. MacBeth, R. Gupta, K. R. Mitchell-Koch, V. G. Young, Jr., G. H. Lushington, W. H. Thompson, M. P. Hendrich and A. S. Borovik, *J. Am. Chem. Soc.*, 2004, **126**, 2556-2567.

141. V. Fueloep, R. P. Phizackerley, S. M. Soltis, I. J. Clifton, S. Wakatsuki, J. Erman, J. Hajdu and S. L. Edwards, *Structure (London)*, 1994, **2**, 201-208.

142. J.-M. Vincent, A. Rabion, V. K. Yachandra and R. H. Fish, *Can. J. Chem.*, 2001, **79**, 888-895.

143. G. Guisado-Barrios, Y. Li, A. M. Z. Slawin, D. T. Richens, I. A. Gass, P. R. Murray, L. J. Yellowlees and E. K. Brechin, *Dalton Trans.*, 2008, 551-558.

Chapter 2

Synthesis of Tris(6-hydroxymethyl-2-pyridylmethyl)amine (H_3L_{11}) and a study of its coordination chemistry with Cu^{II}, Mn^{II} and Fe^{III}.

2.1 Introduction

Transition metal complexes of tris(2-pyridylmethyl)amine (TPA) and its substituted derivatives have been studied extensively in recent years as providing models for the active sites of various metalloproteins.[1-5] Considerable interest has particularly surrounded models for a range of non-heme iron[1,2] and copper[3–5] oxygenases as well as to provide bio-inspired C-H oxidation catalysts.[1-3] Several TPA complexes have moreover been patented as catalysts for alkaline bleaching.[6] Further interest stems from the effects of introducing substituents α to the pyridyl nitrogen which can be used to provide further functionality and/or to generate steric interactions that modify the properties such as spin state and redox potentials.[7-11] The metal complex $[Fe^{II}(TPA)(CH_3CN)_2]^{2+}$ and its corresponding t-butylperoroxoiron(III) derivative are both low spin, the introduction of only one CH_3 at the 6-position of the py ring originates a significant change, while the t-butylperoxoiron(III) derivative remains low spin the iron(II) complex $[Fe^{II}(6\text{-MeTPA})(CH_3CN)_2]^{2+}$ is high spin. The introduction of two or three 6-Me substituens results exclusively in high spin iron(II) and iron (III) complexes.[7] This has important consequences for subsequent reactions of these species in the context of H_2O_2 or ^{t}BuOOH-dependent oxidation catalysis. The introduction of co-ordinating substituents also serves to access multinuclear metal derivatives.[12-15] Colbran et al have described the synthesis of three TPA derivatives bearing one, two or three hydroxymethyl group(s), respectively, at the 6-position on the pyridine rings and have described the chemistry of both mono and polynuclear copper(II) derivatives.[16,17] Tris(6-hydroxymethyl-2-pyridylmethyl)amine (H_3L_{11}) is

particularly attractive since unlike TPA itself it is water soluble and stable to alkaline pH offering potential as a ligand for developing aqueous-based oxygenation (bleaching) catalysts.[6] On the other hand peralkylation of the OH groups (ether formation) quickly introduces hydrophobicity for the synthesis of hydrocarbon-soluble/micellar transition metal oxidation catalysts.[18] Studies on several alkylated derivatives of H_3L_{11} are reported in chapter 3. Finally, oxidation of the hydroxymethyl substituent offers a ready route to the synthesis of further 6-substituted derivatives having carboxylato[17] and carboxamido groups. Previously reported samples of H_3L_1 were contaminated by the presence of co-crystallised NaBr which led to disordered Cl^- and Br^- ion occupancy in the crystal structure of the copper(II) chloride complex C_5 $[Cu(H_3L_{11})Cl]Cl$.[16] In this work a bromide-free pure sample of H_3L_{11} has been prepared which has allowed isolation of a pure sample of the chloride salt; $[Cu(H_3L_{11})Cl]Cl$ as well as a new structural isomer of the bromide salt; C_6 $[Cu(H_3L_{11})Br]Br$. The coordination chemistry has also been expanded here to include hepta-co-ordinated manganese(II) and iron(III) derivatives. The iron(III) complex is linear trinuclear possessing a novel alkoxide-bridged cationic unit with the tightest Fe-O-Fe angle (87.6^o) and shortest Fe…Fe distance (2.834 Å) yet found for a pair of weakly antiferromagnetically-coupled alkoxide-bridged Fe(III) centres. These findings have challenged current theories involved in correlating the extent/nature of magnetic interactions in such species based on Fe-O(bridge) distances and Fe-O-Fe angles. The Cu(II), Mn(II) and trinuclear Fe(III) complexes of H_3L_{11} have been tested as low temperature bleaching catalysts in comparison with the patented complexes of TPA.

2.2 Results and Discussion

2.2.1. Synthesis of Tris(6-hydroxymethyl-2-pyridylmethyl)amine (H_3L_{11}). In this work H_3L_{11} was prepared by a slight modification of the literature method[16] following treatment of 6-(bromomethyl)-2-(hydroxymethyl)pyridine[19] in acetonitrile with ammonium acetate and sodium carbonate. Flash chromatography (35-70μ 60Å silica gel column) of the filtered and combined acetonitrile fractions ensured no residual bromide was present which had contaminated previously reported samples.[16] The improvement in purity was illustrated by successful isolation of an analytically pure sample of the Cu(II) complex $[Cu(H_3L_{11})Cl]Cl$.

2.2.2. Synthesis and characterisation of monochloro(tris(6-hydroxymethyl-2-pyridylmethyl)amine)copper(II) chloride, $[Cu(H_3L_{11})Cl]Cl$. (C_5)

Blue-green blocks of $[Cu(H_3L_{11})Cl]Cl$ were obtained after 3 days by diethyl ether vapour diffusion into a methanol solution of anhydrous copper(II) chloride and H_3L_{11}. Using anhydrous copper(II) chloride we did not encounter the blue oils that had impaired crystallisation of copper(II) complexes in previous work.[16] Figure 2.1 illustrates the molecular structure with relevant bond lengths and angles shown in table 2.1. The molecular structure of $[Cu(H_3L_{11})Cl]Cl$ is very similar to that for the disordered Br^-/Cl^- derivative obtained previously[16] with a single hydroxymethyl arm attached to the copper *trans* to the amine nitrogen along with the other 3 nitrogens and single chloride. The hydrogen atoms are included in idealised positions apart from on the co-ordinated hydroxymethyl arm. The co-ordination geometry at copper can be viewed as 4+2 with a significant tetragonal distortion along two Cu-N bonds to the two pyridyls that are approximately *trans*, Cu-N(24) (2.47 Å) and Cu-N(14) (2.57 Å). The remaining bond lengths from copper(II) to the other two nitrogens,

hydroxymethyl oxygen and chloride are normal for equatorial plain positioning within such a tetragonally-distorted structure. As observed previously with co-ordination of H_3L_{11} versus its mono- and bis-(6-hydroxymethyl) counterparts coordination of the single hydroxymethyl arm necessitates it to be *trans* to the amine nitrogen. The single chloride counter anion is hydrogen-bonded to the acidic hydrogen of the bound hydroxymethyl group. As a result there is no hydrogen-bonding observed here between OH groups on adjacent hydroxymethyl arms of the cation as was observed previously[16] showing this to be not a hugely important templating interaction.

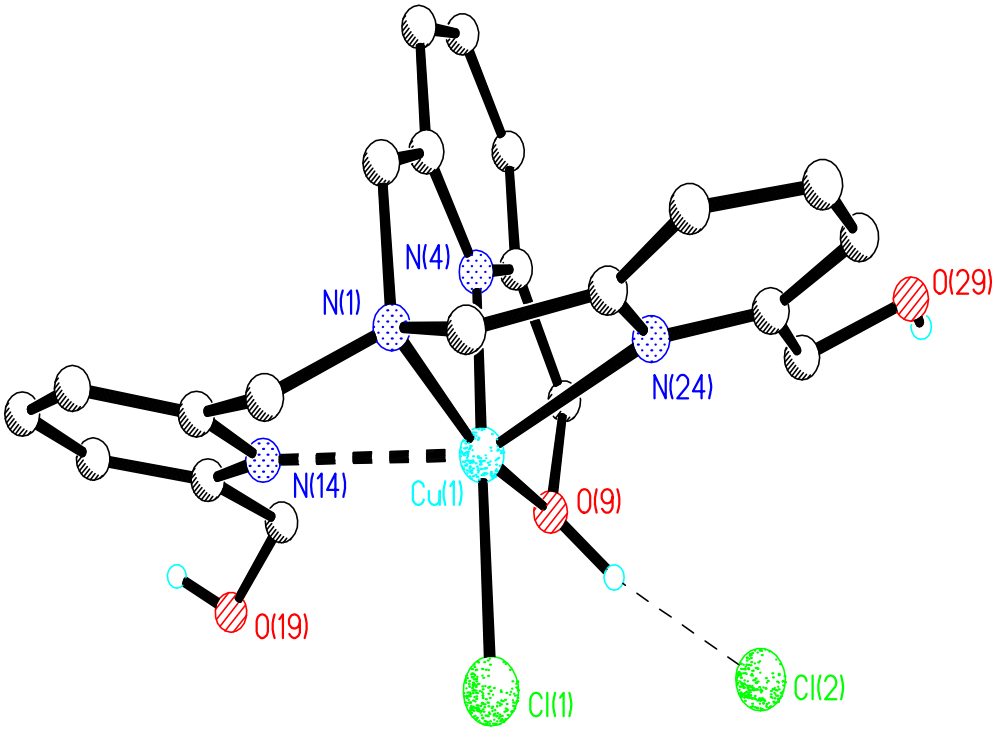

Figure 2.1: View of the coordination geometry around Cu(II) in $[Cu(H_3L_{11})Cl]Cl$

Table 2.1: Selected bond lengths (Å) and angles (°) for $[Cu(H_3L_{11})Cl]Cl$ (esd's in parentheses).

Cu(1)-N(4)	1.939(17)	Cu(1)-O(9)	2.065(15)
Cu(1)-N(1)	2.096(17)	Cu(1)-N(14)	2.567(17)

Cu(1)-N(24)	2.466(17)	Cu(1)-Cl(1)	2.222(5)
N(4)-Cu(1)-O(9)	78.7(6)	O(9)-Cu(1)-N(24)	106.9(6)
N(4)-Cu(1)-N(1)	84.2(7)	N(1)-Cu(1)-N(24)	74.8(6)
O(9)-Cu(1)-N(1)	162.7(6)	Cl(1)-Cu(1)-N(24)	96.5(4)
N(4)-Cu(1)-Cl(1)	173.9(5)	O(9)-Cu(1)-Cl(1)	95.5(4)
N(1)-Cu(1)-Cl(1)	101.5(5)	N(4)-Cu(1)-N(24)	87.1(6)

2.2.3. Synthesis and characterisation of monobromo(tris(6-hydroxymethyl-2-pyridylmethyl)amine)copper(II) bromide, [Cu(H_3L_{11})Br]Br. C_6

Orange crystals of (C_6) [Cu(H_3L_{11})Br]Br were obtained following diethyl ether vapour diffusion into a solution of anhydrous copper(II) bromide and H_3L_{11} in methanol. The X-ray structure is shown figure 2.2 with selected bond lengths and angles shown in table 2.2. In contrast to [Cu(H_3L_{11})Cl]Cl the copper(II) in [Cu(H_3L_{11})Br]Br is in a distorted square-pyramidal geometry with only two of the three pyridyl groups coordinated and the copper slightly above the distorted basal plane. The basal positions are occupied by two pyridines, the tertiary amine and one of the hydroxymethyl arms. The single coordinated bromide ion is apical. The Cu-N distance to the third pyridine is 3.130 (4) Å.

The two non-coordinated hydroxymethyl groups are in a hydrogen-bonded network with the free bromide counter anion located close by (av O---Br 3.26 Å). The co-ordinated hydroxymethyl arm is further hydrogen-bonded to the hydroxo group of one of the non co-ordinated arms (O(9)---O(29) 2.62 Å). The important hydrogen-bonding parameters are shown in table 2.3.

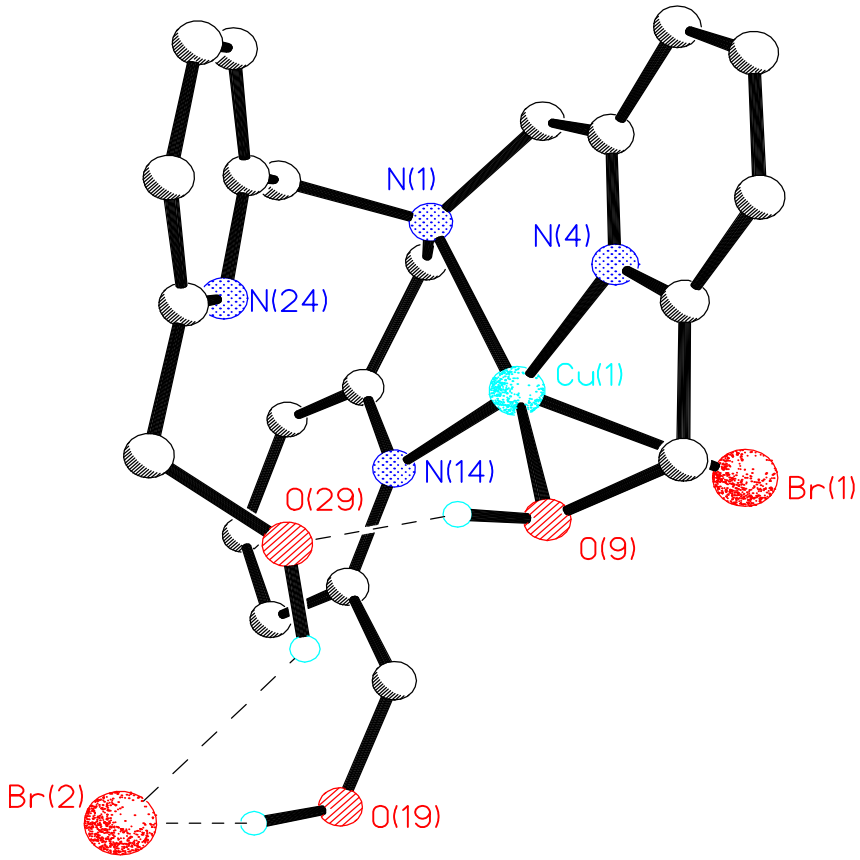

Figure 2.2: View of the coordination geometry around Cu(II) in $[Cu(H_3L_{11})Br]Br$

Table 2.2: Selected bond lengths (Å) and angles (°) for $[Cu(H_3L_{11})Br]Br$ (esd's in parentheses).

Cu(1)-N(1)	2.089(4)	Cu(1)-O(9)	2.068(4)
Cu(1)-N(4)	1.938(4)	Cu(1)-Br(1)	2.4841(7)
Cu(1)-N(14)	1.968(4)	Cu(1)-N(24)	3.000(4)
N(4)-Cu(1)-N(14)	164.53(15)	N(1)-Cu(1)-O(9)	144.63(13)
N(4)-Cu(1)-N(1)	82.13(15)	N(4)-Cu(1)-Br(1)	96.58(11)
N(14)-Cu(1)-N(1)	82.88(14)	N(14)-Cu(1)-Br(1)	94.03(10)
N(4)-Cu(1)-O(9)	76.69(14)	N(1)-Cu(1)-Br(1)	119.15(10)

N(14)-Cu(1)-O(9)	114.34(13)	O(9)-Cu(1)-Br(1)	91.42(9)

Table 2.3: Hydrogen-bonding parameters for [Cu(H_3L_{11})Br]Br (esd's in parentheses).

D-H--A	d(D-H)/ Å	d(H--A)/ Å	d(D--A)/ Å	>(DHA)/^{o}
O(9)-H(9O)--O(29)	0.9800(11)	1.65(2)	2.616(2)	166(8)
O(19)-H(19O)--Br(2)	0.9800(11)	2.35(3)	3.247(4)	152(6)
O(29)-H(29O)--Br(2)	0.9800(11)	2.56(10)	3.282(7)	130(10)

This structure is markedly different to that reported previously[16] for the same compound [Cu(H_3L_{11})Br]Br and illustrates the flexible co-ordination chemistry apparent for H_3L. In Colbran's structure the copper(II) centre is in a tetragonally-distorted octahedral geometry, similar to the copper(II) chloride complex here, but with highly differing Cu-N bonds to the two *trans* pyridyls (2.32 A and 2.78 A). However the donor atom positions are completely different to the structure obtained here with the co-ordinated bromide in an equatorial position *cis* to long a Cu-N(py) bond. In the structure here the bromide is *cis* to both co-ordinated pyridyl groups and the tetragonal distortion is more extreme leading to a five co-ordinated square-pyramidal geometry with only two pyridyl groups coordinated and the bromide apical. It is concluded that these two structural forms for this complex must be very close in energy given the similar methods of preparation and isolation. The greater degree of tetragonal distortion towards five co-ordination with bromide as coordinated halogen compared with chloride could be due to increased steric repulsion from the larger ion.

2.2.4. Synthesis and characterization of (tris(6-hydroxymethyl-2-pyridylmethyl) amine)manganese(II) chloride trihydrate, $[Mn(H_3L_1)]Cl_2.3H_2O$. (C_7)

Colourless crystals of (C_7) $[Mn(H_3L_{11})]Cl_2.3H_2O$ suitable for X-ray investigation were obtained following diethyl ether vapour diffusion into a solution of $MnCl_2.4H_2O$ and H_3L_{11} in methanol. Here the structure revealed co-ordination of all seven donors from H_3L_{11} to the Mn(II) centre, figure 2.3, in a distorted capped trigonal prismatic arrangement. Selected bond lengths and angles are shown in table 2.4. Three hydroxymethyl arms occupy the basal positions of the distorted trigonal prism with the longer bond to the tertiary amine nitrogen (2.44Å) capping the expanded triangular face formed by Mn-N bonds to the three pyridyl nitrogens at the apex of the distorted prism. Co-ordination of all three hydroxymethyl arms to the metal here is not unexpected given the higher affinity for oxygen as donor by the hard Mn(II) centre. The common co-ordination number for Mn(II) is six but the appearance here of a hepta-co-ordinated complex is not unexpected[20] given the high spin d^5 configuration, relatively large radius and zero associated crystal field stabilisation energy.

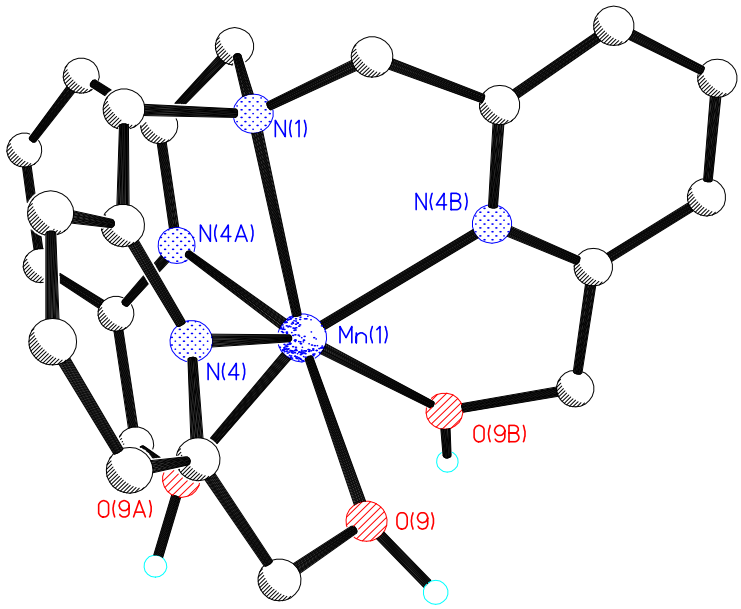

Figure 2.3: View of the coordination geometry around Mn(II) in $[Mn(H_3L_{11})]Cl_2.3H_2O$

Table 2.4: Selected bond lengths (Å) and angles (°) for $[Mn(H_3L_{11})]Cl_2.3H_2O$ (esds in parentheses).

Mn(1)-O(9)	2.253(3)	Mn(1)-N(1)	2.440(7)
Mn(1)-N(4)	2.268(4)		
N(4a)-Mn(1)-N(4)	108.93(9)	O(9a)-Mn(1)-O(9)	81.12(15)
N(4)-Mn(1)-N(1)	69.99(9)	O(9)-Mn(1)-N(1)	131.34(10)
O(9)-Mn(1)-N(4a)	98.38(13)	O(9a)-Mn(1)-N(4)	150.83(13)
O(9)-Mn(1)-N(4)	70.07(13)		

2.2.4. Synthesis and characterization of bis(tris(6-oxymethyl-2-pyridylmethyl)amine)triiron(III) perchlorate acetonitrile solvate, $[Fe_3(L_{11})_2](ClO_4)_3.nCH_3CN$ (n = 1 or 2). (C_8)

The synthesis of $[Fe_3(L_{11})_2](ClO_4)_3.nCH_3CN$ followed the procedure of Masuda et al[21] for the preparation of the Fe(III) complex of tris(6-pivalamido-2-pyridylmethyl)amine. Masuda used sodium benzoate to introduce a carboxylate ligand for the purpose of successfully modelling the active ferric site of soybean lipoxygenase-1.[22] We therefore adopted the same approach in the expectation of making an analogous mononuclear Fe(III) complex. As in the reported synthesis oxidation of Fe(II) to Fe(III) occurs spontaneously in the air. However in the case of H_3L_{11} the greater affinity for oxygen donors by the hard Fe(III) centre leads to coordination of all three hydroxymethyl arms as in the case of the Mn(II) complex above. Furthermore the increased acidity of the hydroxyl protons as a result of coordination to Fe(III) leads to deprotonation in the presence of benzoate (acting here as base) and formation of an alkoxide-bridged linear trinuclear complex via incorporation of an additional Fe(III) centre. This was further confirmed by the analytical presence of co-crystallised benzoic acid along with sodium

perchlorate in the initially analysed yellow-brown solid residue although vapour diffusion of diethyl ether into an acetonitrile solution of a recrystallised sample gave X-ray quality crystals solvated by two acetonitriles. The structure of $[Fe_3(L_{11})_2](ClO_4)_3.2CH_3CN$, figure 2.4, consists of a six-coordinated Fe(III) bound only to the bridging alkoxide groups flanked by two hepta-coordinated Fe(III) centres coordinated to the three bridging alkoxides and the four nitrogen donors of L_{11}. Selected bond lengths and angles are listed in table 2.5. The central hexa-coordinated iron(III) is distorted from octahedral towards trigonal antiprismatic geometry (range Fe-O = 1.99-2.10 Å; tight O-Fe-O = ~80°, open O-Fe-O ~100°). The two hepta-coordinated iron(III)'s are in a distorted capped trigonal prismatic geometry similar to that found in $[Mn(H_3L_{11})]Cl_2$ with the bond to the tertiary amine distinctly longer (Fe-N = 2.366 Å) than those to the pyridine nitrogens (av Fe-N = 2.13 Å) and capping the expanded triangular face of the trigonal prism formed by the latter. Crystal data for all four complexes reported in this chapter are shown in table 2.6.

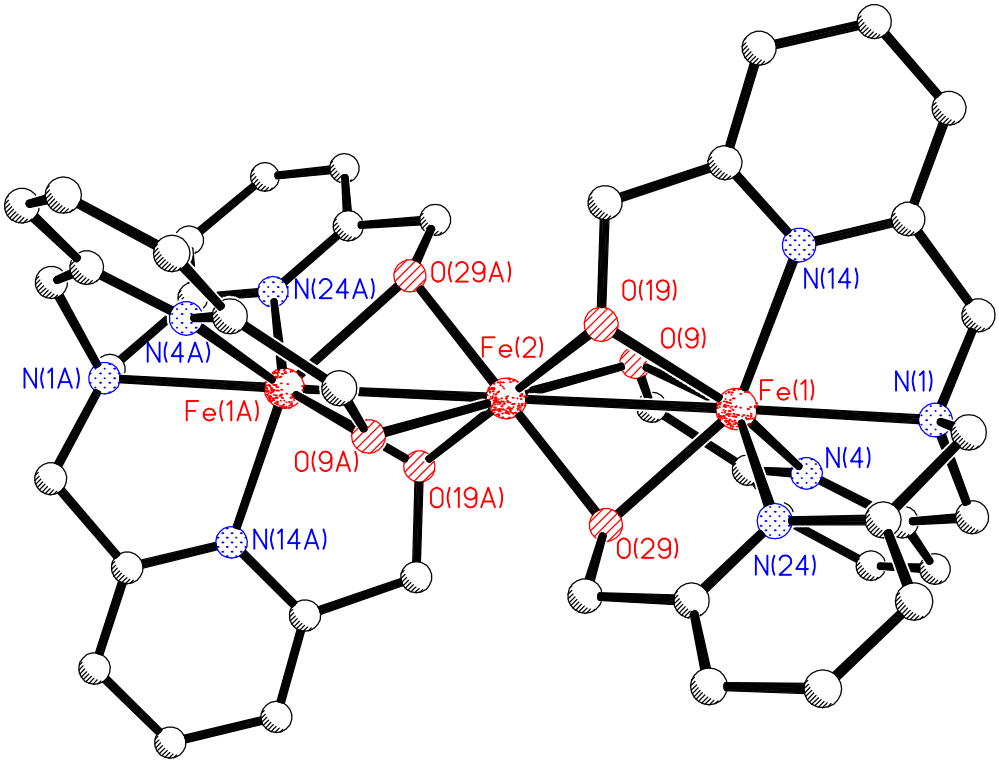

Figure 2.4: View of the trinuclear Fe(III) cationic unit of $[Fe_3(L_{11})_2](ClO_4)_3.2CH_3CN$

Table 2.5: Selected bond lengths (Å) and angles (°) for $[Fe_3(L_{11})_2](ClO_4)_3.2CH_3CN$ (esds in parentheses).

Fe(1)-O(29)	2.102(2)	Fe(1)-O(9)	2.082(2)
Fe(2)-O(9)	1.989(2)	Fe(1)-O(19)	2.097(2)
Fe(2)-O(19)	2.003(2)	Fe(1)-N(4)	2.133(3)
Fe(2)-O(29)	2.010(2)	Fe(1)-N(24)	2.143(3)
Fe(2)-Fe(1)	2.8343(5)	Fe(1)-N(14)	2.115(2)
		Fe(1)-N(1)	2.366(3)
O(29)-Fe(2)-O(29a)	180.000	O(19)-Fe(1)-N(4)	150.30(10)
O(29)-Fe(2)-O(9)	79.62(9)	O(9)-Fe(1)-N(4)	75.16(10)
O(29a)-Fe(2)-O(9)	100.38(9)	O(29)-Fe(1)-N(24)	74.69(9)
O(9)-Fe(2)-O(9a)	180.000	O(19)-Fe(1)-N(24)	94.59(9)
O(29)-Fe(2)-O(19a)	100.79(9)	O(9)-Fe(1)-N(24)	150.05(9)
O(19)-Fe(2)-O(29)	79.21(9)	N(4)-Fe(1)-N(24)	109.33(10)
O(9)-Fe(2)-O(19)	79.56(8)	O(29)-Fe(1)-N(14)	150.20(9)
O(9a)-Fe(2)-O(19)	100.44(8)	O(19)-Fe(1)-N(14)	75.20(9)
O(19a)-Fe(2)-O(19)	180.000	O(9)-Fe(1)-N(14)	95.37(9)
O(29)-Fe(1)-O(9)	75.45(8)	N(4)-Fe(1)-N(14)	111.16(10)
O(29)-Fe(1)-O(19)	75.05(8)	O(29)-Fe(1)-N(4)	94.09(9)

Table 2.6: Numerical crystal and refinement data for complexes of H_3L_{11} determined by X-ray crystallography at 93(2)K

	$[Cu(H_3L_{11})Cl]Cl$	$[Cu(H_3L_{11})Br]Br$	$[Mn(H_3L_{11})]Cl_2.3H_2O$	$[Fe_3(L_{11})_2](ClO_4)_3.2CH_3CN$
Formula	$C_{21}H_{24}Cl_2CuN_4O_3$	$C_{21}H_{24}Br_2CuN_4O_3$	$C_{21}H_{30}Cl_2MnN_4O_6$	$C_{46}H_{42}Cl_3Fe_3N_{10}O_{18}$
M	514.88	603.80	560.33	1296.80
Crystal system	Monoclinic	Monoclinic	Trigonal	Monoclinic
Space Group	$P2_1/c$	$P2_1/n$	$R\text{-}3c$	$P2_1/c$
a/Å	9.2202(14)	8.6000(13)	13.0839(4)	11.4502(11)
b/Å	25.647(4)	8.2400(13)	13.0839(4)	20.814(2)
c/Å	10.0745(16)	33.120(5)	54.374(2)	11.5548(11)
$\alpha/^o$	90	90	90	90
$\beta/^o$	113.014(4)	96.5	90	108.197(2)
$\gamma/^o$	90	90	120	90
$V/Å^3$	2192.7(6)	2331.9(6)	8061.1(5)	2616.1(4)
Z	4	4	12	2
μ/cm^{-1}				
Reflections collected	11331	14320	13811	14484
R_{int} (no. of equivalent reflections)	0.0549	0.0309	0.0406	0.0379
Observed reflections [$I/\sigma(I) > 2$]	3645	3942	1753	4894
Final R, R_w [$I/\sigma(I) > 2$]	0.0629, 0.1395	0.0421, 0.1079	0.0850, 0.2262	0.0551, 0.1115

2.2.6. DC Magnetic Susceptibility Studies on $[Fe_3(L_{11})_2](ClO_4)_3.2CH_3CN$.

Direct current magnetic susceptibility studies were performed on a powdered polycrystalline sample of $[Fe_3(L_{11})_2](ClO_4)_3.2CH_3CN$ in the 5 – 300 K range in an applied field of 0.1 T. The results are plotted as the $\chi_M T$ product versus T in figure 2.5. The room temperature $\chi_M T$ value of approximately 11.4 cm^3 K mol^{-1} is slightly lower than that expected for three non-interacting Fe(III) ions (13.125 cm^3 K mol^{-1}). Upon cooling, the value of $\chi_M T$ decreases gradually to approximately 4 cm^3 K mol^{-1} at 5 K. This behaviour is indicative of weak antiferromagnetic exchange between the metal centres with the low temperature maximum suggesting an $S = 5/2$ ground state.

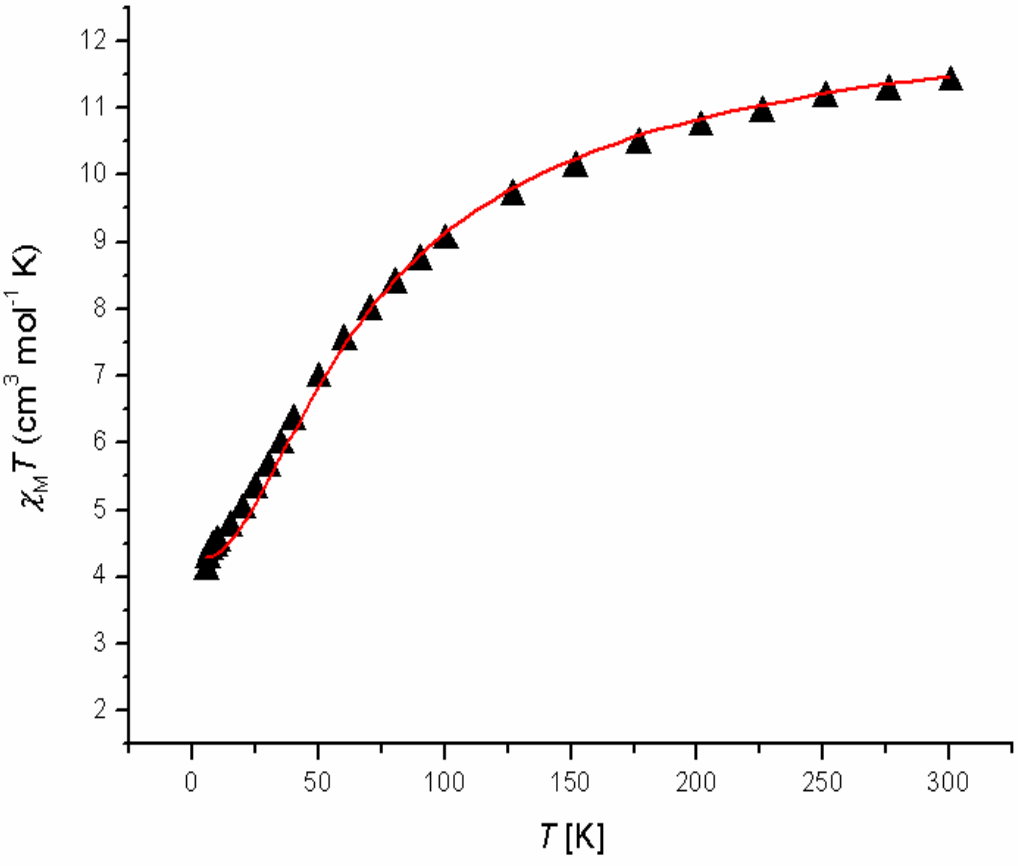

Figure 2.5: Plot of $\chi_M T$ versus T for $[Fe_3(L_{11})_2](ClO_4)_3.2CH_3CN$ in the temperature range 5 - 300 K. The solid line is a simulation of the experimental data.

Inspection of the molecular structure suggests the presence of only one exchange interaction (J_1) between the central metal ion Fe(2) and the peripheral Fe ions (Fe(1) and symmetry equivalent) mediated by the μ-bridging alkoxide ligands. However, attempts to simulate the experimental data with this simple model failed, and so the 2*J*-model, depicted in figure 2.6, including the Fe(1)…Fe(1') interaction (J_2) was employed. Using the program MAGPACK[23] and employing the Hamiltonian

$$\hat{H} = -2J_1(\hat{S}_1 \cdot \hat{S}_2 + \hat{S}_2 \cdot \hat{S}_{1'}) - 2J_2(\hat{S}_1 \cdot \hat{S}_{1'})$$

allowed us to satisfactorily simulate the data with the parameters J_1 = - 3.1 cm^{-1}, J_2 = + 0.2 cm^{-1} and g = 2.00(2). This results in a spin ground state of S = 5/2 with the first S = 3/2 excited state 17.5 cm^{-1} higher in energy, and the second excited state, S = 7/2, 22.5 cm^{-1} higher in energy.

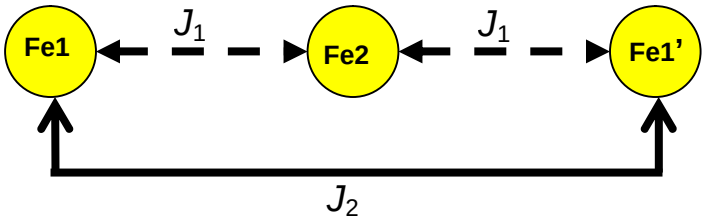

Figure 2.6: The exchange interaction model employed for the $[Fe_3(L_{11})_2]^{3+}$ core.

The magnetic properties of exchanged coupled *dinuclear* complexes have, for some time, been known to depend on the identity of the metal ions, the nature of the bridging ligands providing the super-exchange pathway, and the bridging geometry, *i.e.* the angles and distances. There have been a number of magneto-structural correlations published for the Fe-O-Fe moiety, which have attempted to describe the relationship between the strength of interaction (*J*) and the Fe…Fe distance, the Fe…O distance and the Fe-O-Fe bridging angle, with, in almost all cases, the central bridging ion being an oxide rather than a hydroxide or alkoxide. As yet, none have appeared universally correct. For example, Gerloch suggested a

rapid decrease in *J* with decreasing Fe-O-Fe angle, with the maximum value expected for a bridging angle of 180°.[24] Gorun and Lippard suggested the main contribution to the exchange was the average Fe-O distance[25] whilst Güdel and Weihe concluded that both the Fe-(μ-O) distance and the Fe-(μ-O)-Fe angle were important.[26] To our knowledge, the only attempted magneto-structural correlation for alkoxide-bridged diiron(III) species was published by Caneschi and co-workers in 1997 who investigated molecules of the type $[Fe_2(OR)_2L_{12}]$, Table 2.7, where L_{12} is a β-diketonate ligand.[27] Based on their experimental evidence they suggested a linear dependence of *J* with the Fe-O-Fe bridging angle (α), expressed as $J = 1.48\alpha - 135$, with the switch from antiferromagnetic to ferromagnetic occurring at $\alpha = 91°$. DFT calculations later refined the expression to $J = 5.0(1)\alpha - 450(10)$.[28] $[Fe_3(L_{11})_2]^{3+}$ with Fe-O-Fe bridging angles of 87.12, 87.42 and 88.21° ($\alpha_{av} = 87.58°$), appears not follow these experimentally or theoretically derived trends. All three bridging angles in $[Fe_3(L1_1)_2]^{3+}$ are below that expected for a ferromagnetic interaction, and the predicted exchange of +5.4 cm^{-1} (+12 cm^{-1} via DFT) is some way off the observed value of -3.1 cm^{-1}. Given that there are only a few structurally related trinuclear iron complexes reported (see below), and almost none with reliable magnetic data, it is not possible at this stage to provide a deep understanding of the origins of these differences, but clearly $[Fe_3(L_{11})_2]^{3+}$ "bucks the trend". Thus it appears that, as with the oxo-bridged species before them, there may not be a simple correlation for alkoxo-bridged Fe clusters between *J* and any single structural parameter, and that any universal correlation must invoke other relationships.

2.2.7. Thin-layer Spectroelectrochemistry on $[Fe_3(L_{11})_2](ClO_4)_3.2CH_3CN$.

Cyclic voltammograms of 3.15 $x10^{-4}$ M solutions of $[Fe_3(L_{11})_2](ClO_4)_3.2CH_3CN$ at a Pt electrode in CH_3CN solvent containing 0.1M $[^nBu_4N][BF_4]$ show two clean reversible one-electron reduction processes to formally $[Fe_3(L_1)_2]^{2+}$ and $[Fe_3(L_{11})_2]^{+}$ species at +0.36 V and 0.0 V vs Ag/AgCl, figure 2.7. The potentials are invariant with temperature down to 233 K.

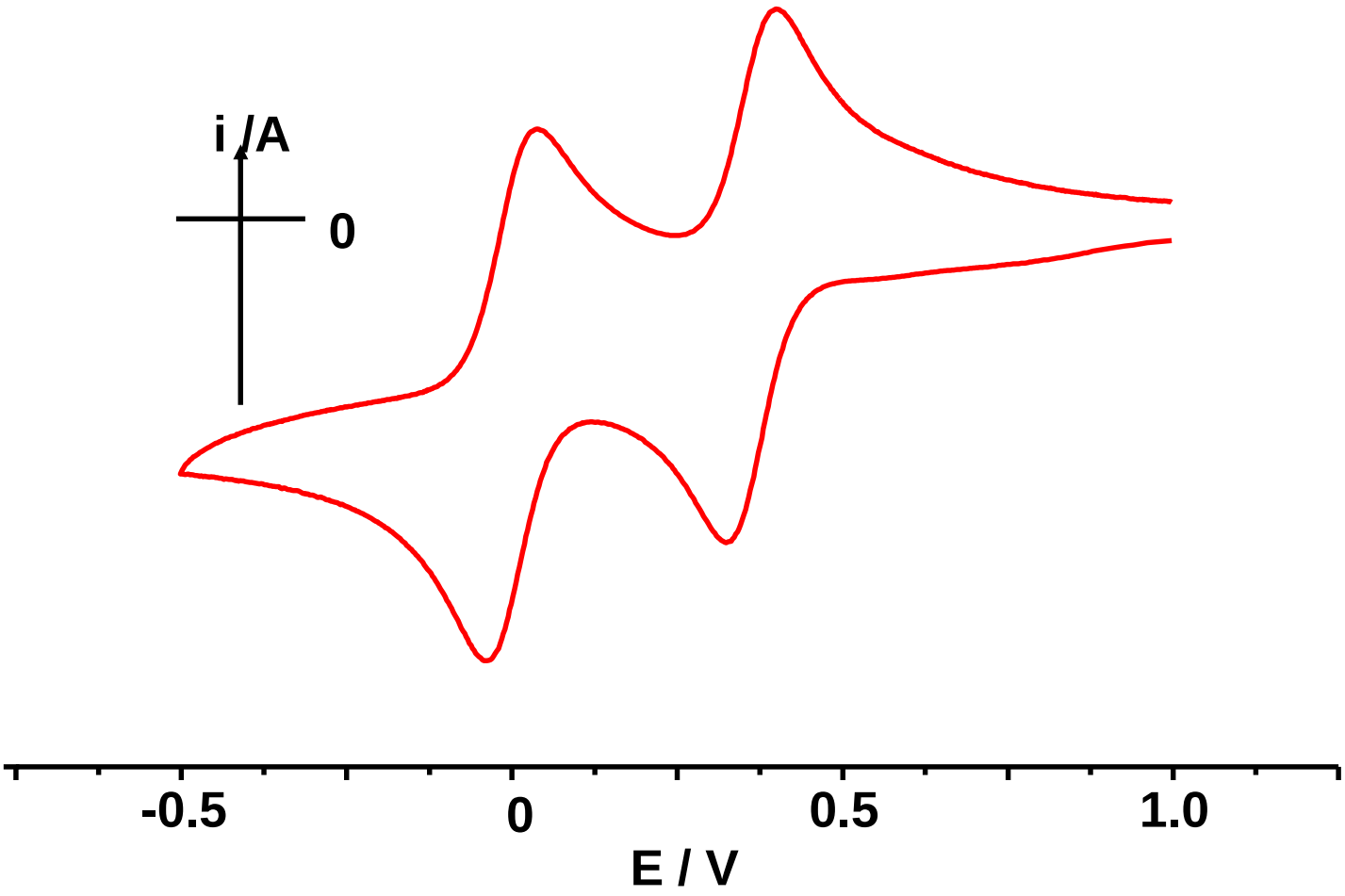

Figure 2.7: Cyclic voltammogram of $[Fe_3(L_{11})_2](ClO_4)_3$ (3.15 x 10^{-4} M) in CH_3CN at a Pt electrode containing 0.1M $[^nBu_4N][BF_4]$ (E/V vs AgCl).

The presence of only two relatively close $1e^-$ redox processes[29] tentatively suggests that they are due to successive reduction of the two peripheral hepta-coordinated Fe(III)s to Fe(II) with the central hexa-coordinated iron(III) stabilised towards reduction as a result of the strong field of six alkoxide donors, figure 2.8. Subsequent controlled potential spectro-electrochemistry using an optically transparent thin layer Pt electrode (OTTLE) at +0.3 V and -0.5 V vs Ag/AgCl reveals distinct UV-vis-NIR spectra for the $1e^-$ reduced $[Fe_3(L_{11})_2]^{2+}$ and

$2e^-$ reduced $[Fe_3(L_{11})_2]^+$ species for comparison with the spectrum of $[Fe_3(L_{11})_2]^{3+}$, figures. 2.8 and 2.9.

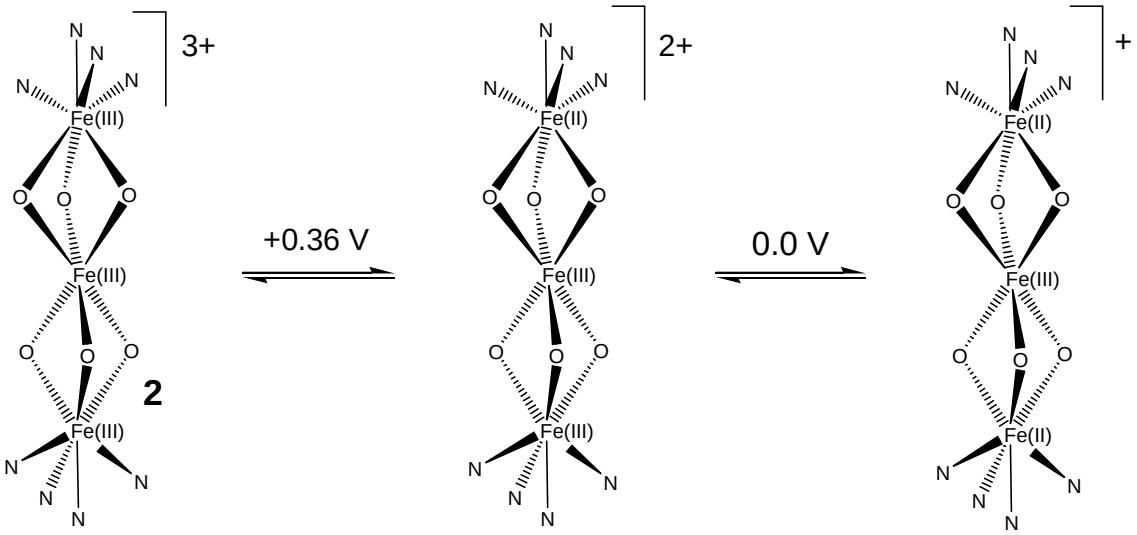

Figure 2.8: Redox processes involving $[Fe_3(L_{11})_2]^{3+}$ in CH_3CN solution.

The reversibility of the two successive $1e^-$ reduction processes was confirmed in each case by the presence of a well defined isosbestic point. The intensity of the absorption peaks for all three forms suggests an assignment to charge-transfer transitions. The broad absorption peak for $[Fe_3(L_{11})_2]^+$ at 470nm (ε = 3,200 $M^{-1}cm^{-1}$) **,** figure 2.9, is tentatively assigned to an $Fe(III)_{mid}$-$Fe(II)_{end}$ inter-valence charge transfer transition on the basis of its absence from the spectrum of $[Fe_3(L_{11})_2]^{3+}$ although further studies would be needed to confirm this especially in the absence of a similar well defined absorption peak for the $1e^-$ reduced $[Fe_3(L_{11})_2]^{2+}$ complex.

$[Fe_3(L_{11})_2]^{3+}$ is the first example of a six-coordinated Fe(III) centre flanked by two hepta-coordinated Fe(III) centres and has the tightest Fe-O(bridge)-Fe angle and as a result shortest Fe….Fe distance (2.8343(5) Å) of all the linear trinuclear Fe(III) complexes so far characterized (table 2.7, figure 2.11). The only other close structural match is the linear methoxide-bridged trinuclear Fe(III) complex **C_{11}** (figure 2.11) reported in 2005 by Mak et al via methanolysis of the tripyridine ligand L_{13} = 2,6-pyridyldiylbis(2-pyridyl)methanone.[30]

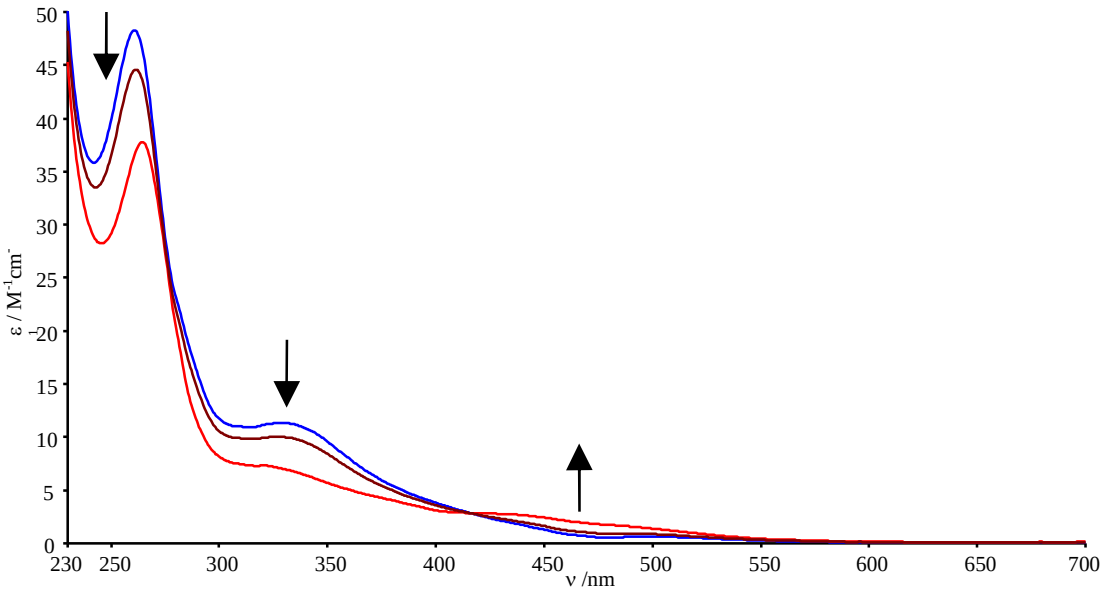

Figure 2.9: UV/Vis/NIR spectra of $[Fe_3(L_{11})_2]^{3+}$ (blue) and its $1e^-$ reduction product $[Fe_3(L_{11})_2]^{2+}$ (red) in 0.1 M $[^nBu_4N][BF_4]$ / CH_3CN at 233 K showing partially reduced curves. The potential was held at +0.3 V vs. Ag/AgCl.

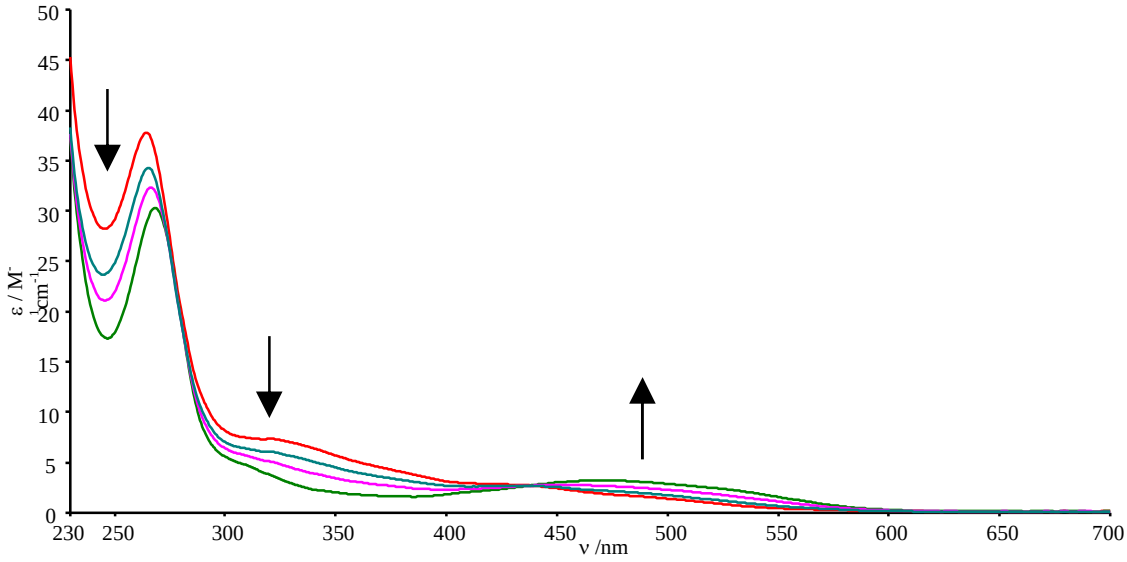

Figure 2.10: UV/Vis/NIR spectra for the $1e^-$ reduced species $[Fe_3(L_{11})_2]^{2+}$ (red) and $2e^-$ reduced species $[Fe_3(L_{11})_2]^{+}$ (green) in 0.1 M $[^nBu_4N][BF_4]$ / CH_3CN at 233 K showing partially reduced curves. The potential was held at -0.5 V vs. Ag/AgCl.

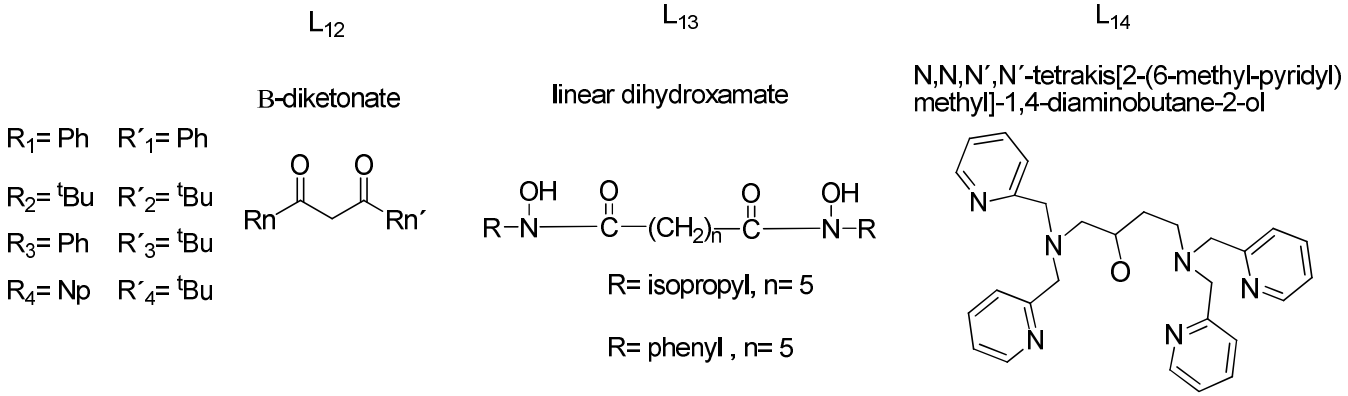

Figure 2.11: Schematic representation of L_{12}-L_{14}

Complex	Single O-bridge	CN	Fe^{III}-O(bridge) / Å	Fe-O-Fe / $^{o\ a}$	Fe….Fe / Å	Ref
linear Fe^{III}_3 species						
C_8	tri-alkoxide	7,6,7	2.047 [a]	87.6	2.834 [a]	This work
C_9	tri-alkoxide	6,8,6	2.090 [a]	88.5	2.907 [a]	30
C_{10}	oxide/hydroxide	6,6,6	1.910 [a]	125.3	3.392(1)	31
C_{11}	hydroxide	6,6,6	1.949 [a]	123.9	3.440 [a]	33
$Fe^{III}_2(OR)_2L_{12}$						
C_{12}	OMe	6,6	1.987 [a]	102.0	3.087(1)	27
C_{13}	OMe	6,6	1.974 [a]	103.7	3.105 [a]	“
C_{14}	OEt	6,6	1.965 [a]	101.8	3.049(3)	“
C_{15}	OPr^n	6,6	1.974 [a]	103.1	3.093(3)	“
$Fe^{III}_2(OR)_2L_{13}$	OMe	6,6	2.002 [a]	104.6	3.168(1)	39
$[Fe^{II,III}_2L_{14}(O_2CPh)_2]^{2+}$	alkoxide	6,6	1.909(7)	111.2	3.300(2)	40

Table 2.7: Structural data for oxygen-bridged linear triiron(III) and alkoxide-bridged diiron(III) complexes
a-average value

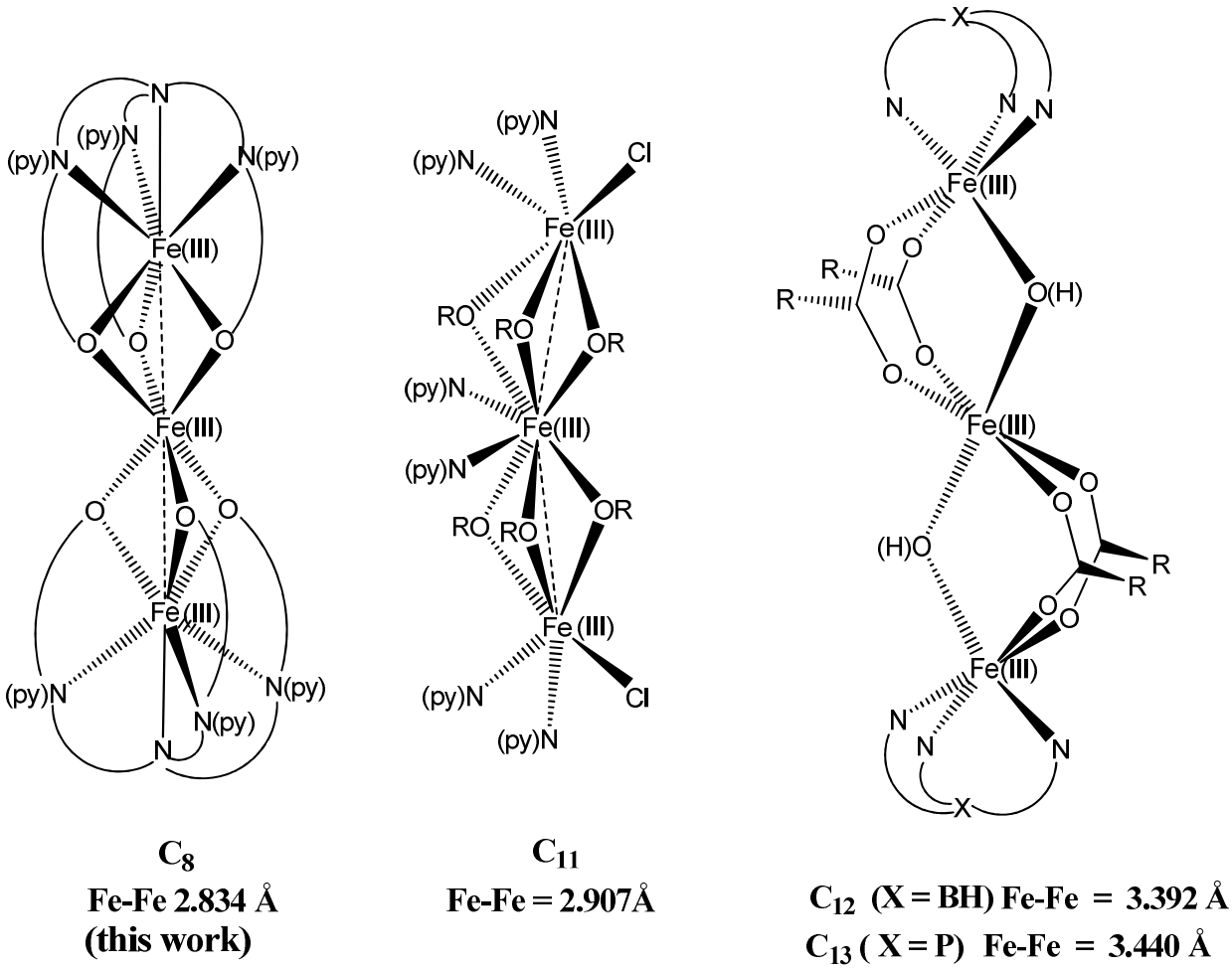

Figure 2.12: Core Structures of Various Linear Oxygen-bridged Triferric complexes

Here an unusual octa-coordinated central Fe(III) is co-ordinated to six alkoxide/methoxide oxygen donors and two nitrogen donors from the middle pyridine of both coordinated ligands, each flanked by two six-coordinated Fe(III)s. The three Fe(III) centres are in a bent configuration (Fe-Fe-Fe = 152.63(3)^{o}) with the slightly more open angle at the bridging alkoxide oxygens (av 88.5^{o}) leading to a slightly longer Fe…Fe separation (av 2.907 Å) than for $[Fe_3(L_{11})_2]^{3+}$.

The only other reported linear triferric complexes have the Fe(III) centres bridged by two μ-carboxylates and a single μ-oxo or hydroxo ligand. Reed and Kitajima et al isolated the oxo-bridged complex **C_{12}**, figure 2.12, using the ligand tris(3,5-diisopropylpyrazolyl)borate.[31] Here all three Fe(III) centres are hexa-coordinated with the central Fe(III), like in $[Fe_3(L_{11})_2]^{3+}$,

co-ordinated to only oxygen donors (six); four from μ-carboxylates and two from disorded μ-oxo/μ-hydroxo ligands. The Fe-O-Fe angle at the bridging oxygen in **C_{12}** is much larger (av 125.3^o) leading to a larger Fe….Fe separation (3.392(1) Å). A similar linear μ-oxo, bis-μ-carboxylato-triiron(III) complex has been characterised using tris(3,5-dimethylpyrazolyl)borate.[32] The μ-hydroxo,bis-μ-benzoato-triiron(III) complex **C_{13}**, figure 2.11 has been reported by Kurtz et al using the ligand tris(1,4-dimethylimidazol-2-yl)phosphine.[33] **C_{13}** appears to be a rare example of an exclusively hydroxo-bridged linear triferric complex. The Fe-O-Fe angle (av 125.9^o) is similar to that in **C_{12}**.

$[Fe_3(L_{11})_2]^{3+}$ provides a further relatively rare example of hepta-co-ordinated Fe(III). Other examples include $Fe(dapsox)(H_2O)_2]^+$ (H_2dapsox = 2,6-diacetylpyridine-bis(semioxamazide)[34] and salts of polyaminocarboxylatoiron(III) complexes obtained with large radius cations such as $Ca[Fe(CDTA)(H_2O)]_2$ (H_4CDTA = trans-1,2-cyclohexanediamminetetraacetic acid)[35] and $Rb[Fe(EDTA)(H_2O)]$.[36] In the latter two complexes the Fe(III) centre is in a triangular-capped distorted trigonal prismatic geometry similar to that found in $[Fe_3(L_1)_2]^{3+}$. Figure 2.13 illustrates the range of coordination geometries found for H_3L_{11} as ligand.

Finally complexes $[Fe_3(L_{11})_2]^{3+}$ and **C_{11} – C_{13}** can be considered to be putative models for the triferric site 3 of ferreascidin, a glycoprotein isolated from the blood cells of the stolidobranch ascidian Pyura stolonifera.[37, 38] The site 3 cluster consists of a rare linear unit containing three antiferromagnetically coupled high-spin Fe(III) centres resulting in a RT paramagnetic S = 5/2 ground state.[37] The absence of sulfur and sulfide in ferreascidin indicates that the bridging atoms must be oxygen and/or nitrogen atoms.

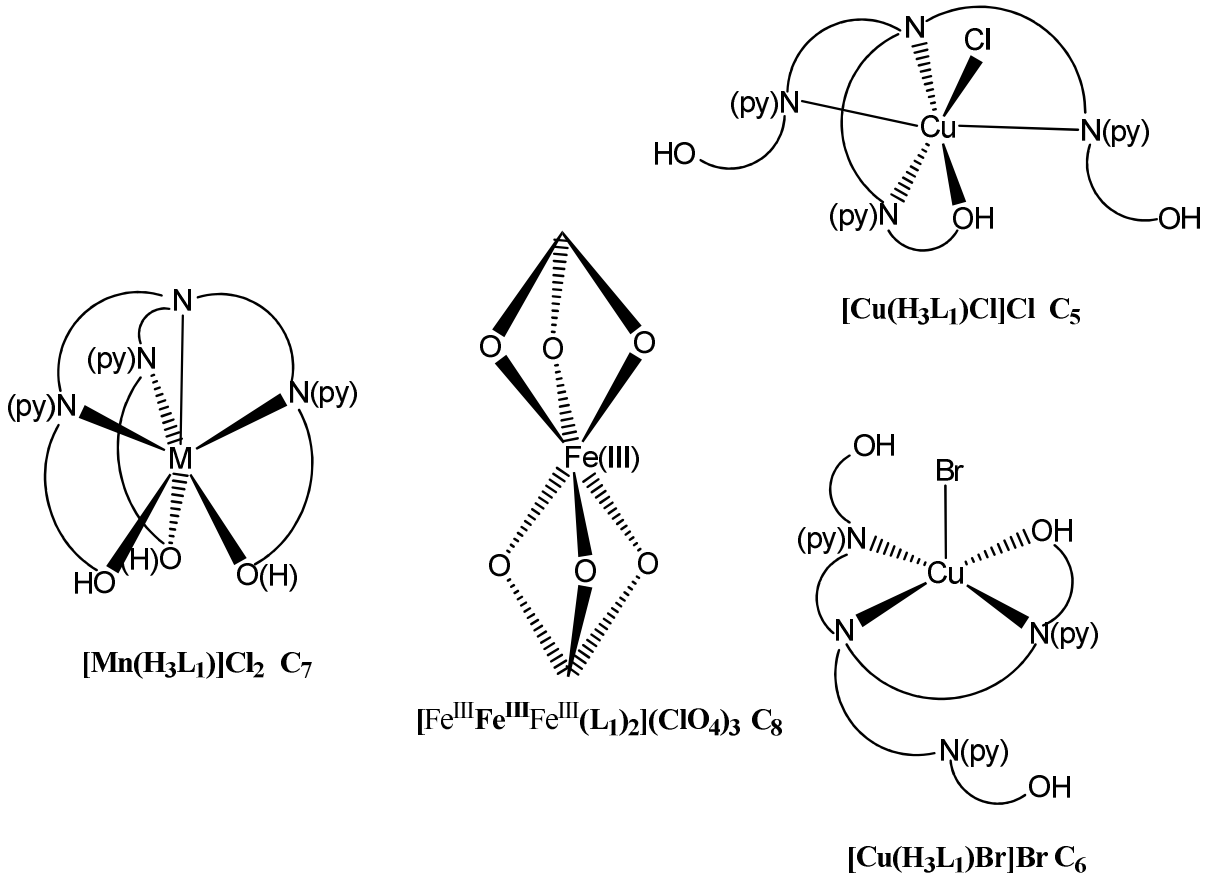

Figure 2.13: Ligand co-ordination modes found in metal complexes of H_3L_{11}

2.3. Experimental

2.3.1. Physical Measurements

X-ray crystallography was carried out at 93(2)K using Mo Kα radiation from a Rigaku MM007 rotating anode diffractometer operating with a low temperature attachment, see Table 2.6 for further relevant details. ^{1}H and ^{13}C NMR spectra were recorded on a Bruker Advance 300 Spectrometer (300MHz for ^{1}H, 75.4 MHz for ^{13}C).

Mass spectra were acquired on a Water's 2795 HPLC with Micromass LCT equipped with a "lock spray" for accurate mass measurements.

Elemental analysis for C, H and N were determined on dried samples using a Carlo Erba CHNS analyser.

Variable-temperature, solid-state direct current (dc) magnetic susceptibility data down to 5 K were collected on a powdered microcrystalline sample using a Quantum Design MPMS-XL SQUID magnetometer in an applied field of 0.1 T. Diamagnetic corrections were applied to the observed paramagnetic susceptibilities using Pascal's constants.

Electrochemical measurements were carried out on a 3.15 x 10^{-4} M solution of **2** in CH_3CN containing 0.1M $[^{n}Bu_4N][BF_4]$. A standard three electrode system was used comprising a Metrohm 6.1241.060 Pt working electrode, Metrohm 6.0726.100 Ag/AgCl reference electrode and a Pt wire reference electrode. Data were captured on a DELL Pentium III desktop PC with General Purpose Electrochemistry system (GPES) version 4.8 connected to an Autolab PGSTAT30 potentiostat. Quoted data were recorded using a scan rate ν = 0.1 Vs^{-1} and are displayed in the form $(E_{pa} + E_{pc})$ /2 V $(E_{pa} - E_{pc})$. Potentals are vs Ag/AgCl referenced to the ferrocinium/ferrocene couple taken as +0.55 V.

In situ UV/Vis/NIR spectroelectrochemistry was performed on the same solutions of **2** above using an optically transparent thin layer electrode (OTTLE) cell using a Perkin-Elmer Lambda 9 spectrophotometer. The spectra were captured on a Datalink Pentium desktop PC running UV Winlab software, version 2.70.01. A platinum gauze working electrode

(transparency = 40 %) was used in the quartz cell (path length = 0.5 mm). The platinum wire counter and Ag/AgCl reference electrodes were separated from the test solution by sintered frits in a quartz reservoir above the flat cell. A tight fitting PTFE lid prevented the oxygen-purged solutions being exposed to the atmosphere. The assembly was then placed in a PTFE block fitted with two pairs of quartz windows, inside the spectrometer. Dry, pre-cooled N_2 was passed between the cell and the inner pair of quartz windows to cool the solution. Dry, room temperature N_2 was passed between the outer and inner quartz windows of the PTFE block to prevent frosting of the cell and windows. The spectrometer cavity was kept under N_2. The temperature was monitored using a thermocouple connected to a digital thermometer and could be controlled by careful adjustment of the N_2 flow rate. Potential was applied and bulk electrolysis performed with UV/Vis/NIR spectra measured every ten minutes. Conversion of the electroactive species was deemed complete when the spectrum became constant and current flow ceased. The potential was then set back to re-generate the original species to ensure reversibility of the redox process.

2.3.2. Materials and Reagents

All metal salts and reagents were used as supplied from Sigma-Aldrich without further purification. Solvents; acetonitrile, methanol, diethyl ether and dichloromethane were all used as supplied without further purification. Flash chromatography was carried out using a 30cm x 1cm column of Fluorochem silica gel 35-70μ 60Å.

2.3.3. Tris(6-hydroxymethyl-2-pyridylmethyl)amine (H_3L_{11})

The title compound was prepared by a slight modification of the literature method[16] following treatment of 6-(bromomethyl)-2-(hydroxymethyl)pyridine[19] in acetonitrile with ammonium acetate and sodium carbonate. When no more starting material was evident by ^{1}H NMR and tlc the solution was filtered, washed with acetonitrile, and the combined acetonitrile fractions

evaporated to give a white solid which was flash chromatographed on silica gel (eluent dichloromethane-methanol gradient, 1-10% vv dichloromethane) until pure by ^{1}H NMR. Yield 3.5 g (57%), mp 159-161^{o}C. δ_H (DMSO) 3.37 (6H, s, 3CH_2), 4.50 (6H, d 3CH_2), 5.42 (3H, br, 3OH), 7.25 (3H, d, 3CH arom), 7.42 (3H, d, 3CHarom), 7.75 (3H, t, 3CH arom)**.** MS: ES+: m/z: 403 [$(M+Na)^+$ 100%]**.**

2.3.4. [Cu(H_3L_{11})Cl]Cl. (C_5)

A green solution of anhydrous copper(II) chloride (35,38 mg, 0.236 mmol) in methanol (3 cm^3) was added to a solution of H_3L_1 (0.1g, 0.236 mmol) in methanol (12 cm^3). The resulting deep bluish-green solution was placed in an open vial and diethyl ether was allowed to mix in slowly using vapour diffusion. After 3 days blue-green crystals were obtained which were found to be suitable for X-ray diffraction. Yield 29 mg, 21.4 %. Found: C, 47,21; H, 4.38; N, 10.51. $C_{21}H_{24}Cl_2CuN_4O_3$, requires C, 48.98 ; H, 4.69 ; N, 10.88.

2.3.5. [Cu(H_3L_{11})Br]Br. (C_6)

A yellow solution of anhydrous copper(II) bromide (58.77 mg, 0.236 mmol) in methanol (3 cm^3) was added to a solution of H_3L_1 (0.1 g, 0.236 mmol) in methanol (12 cm^3). The resulting dark green-brown solution was placed in an open vial and diethyl ether was allowed to mix in slowly using vapour diffusion. After 3 days a few small orange crystals were obtained which were found to be suitable for X-ray analysis.

2.3.6. [Mn(H_3L_{11})]Cl_2.3H_2O. (C_7)

A colourless solution of $MnCl_2.4H_2O$ (0.034 g, 0.236mmol) in methanol (3 cm^3) was added to a solution of H_3L_1 (0.1g, 0.236mmol) in methanol (12 cm^3). The clear colourless solution was placed in an open vial and diethyl ether was allowed to mix in slowly using vapour diffusion. After 2 days colourless crystals were obtained. Yield 0.035g (26.3%). Found (%): C, 35.74; H,

4.26; N, 7.69. $C_{22}H_{34}Cl_{4.4}Mn_{2.2}N_4O_7$ ($[Mn(H_3L_1)]Cl_2.(MnCl_2)_{1.2}.CH_3OH.3H_2O$) requires (%): C, 35.52; H, 4.61; N, 7.53. Redissolution in methanol and allowing diethyl ether to mix in by vapour diffusion eventually produced colourless crystals of the pure chloride trihydrate salt suitable for X-ray analysis.

2.3.7. $[Fe_3(L_{11})_2](ClO_4)_3.nCH_3CN$ (n = 1 or 2) (C_8)

The synthesis was based upon that described by Masuda et al for the mononuclear Fe(III) complex of tris-(6-pivalamido-2-pyridylmethyl)amine.[21] A solution of $C_6H_5CO_2Na$ (0.032g, 0.236 mmol) in H_2O (2 cm^3) was added to a red solution of $Fe(ClO_4)_2.6H_2O$ (0.093 g, 0.236 mmol) and H_3L_{11} (0.1 g, 0.236 mmol) in acetonitrile (20 cm^3) giving a yellow solution. The reaction mixture was stirred for 5 hours after which the solvent was evaporated to leave a yellow-brown solid which was washed with a small amount of diethyl ether. Dissolution of the solid in acetonitrile followed by slow precipitation by the addition of diethyl ether gave rise to a golden brown crystalline solid of the mono acetonitrile solvate, yield 0.088g, (52%). Found (%): C, 41.36; H, 3.56; N 9.96. $C_{44}H_{45}Cl_3Fe_3N_9O_{18}$ ($[Fe_3(L_1)_2](ClO_4)_3.CH_3CN$; M_r 1261.78) requires (%): C, 41.88; H 3.59; N 9.99. Golden-brown single crystals of the bis acetonitrile solvate ($[Fe_3(L_{11})_2](ClO_4)_3.2CH_3CN$; M_r = 1302.84) were subsequently obtained by vapour diffusion of diethyl ether into a dry acetonitrile solution of the above solid and were found suitable for X-ray structural analysis.

2.4. References

1. A. Bassan, M. R. A. Blomberg, P. E. M. Siegbahn and L. Que, Jr. *Angew. Chem. Int. Ed.*, 2005, **44**, 2939; M. Costas, M. P. Mehn, M. P. Jensen and L. Que, Jr., *Chem. Revs.*, 2004, **104**, 939; M. Costas, K. Chen and L. Que, Jr., *Coord. Chem. Revs*., 2000, **200-202**, 517; L. Que, Jr. and R. Y. N. Ho., *Chem. Revs.*, 1996, **96**, 2607; L. Que, Jr. and Y. Dong, *Acc. Chem. Res*., 1996, **29**, 190.
2. H. -F. Hsu, Y. Dong, L. Shu, V. G. Young, Jr. and L. Que, Jr., *J. Am. Chem. Soc.*, 1999, **121**, 5230; J. Kim, R. G. Harrison, C. Kim and L. Que, Jr., *J. Am. Chem. Soc*., 1996, **118**, 4373; R. A. Leising, R. E. Norman and L. Que, Jr., *Inorg. Chem*., 1990, **29**, 2553.
3. H. C. Liang, M. Dahan and K. D. Karlin, *Curr. Opin. Chem. Biol*., 1999, **3**, 168.
4. K. D. Karlin, S. Kaderli and A. D. Zuberbuhler, *Acc. Chem. Res*., 1997, **30**, 139; K.D. Karlin, D. H. Lee, H. V. Obias and K. J. Humphries, *Pure Appl. Chem.,* 1998, **70,** 855.
5. P. A. Goodson, A. R. Oki, J. Glerup and D. J. Hodgson, *J. Am. Chem. Soc*., 1990, **112**, 6254; J. E. McGrady and R. Stranger, *J. Am. Chem. Soc.*, 1997, **119**, 8512; A. Diebold and K. S. Hagen, *Inorg. Chem*., 1998, **37**, 215.
6. R. Hage and A. Lienke, *Angew. Chem. Int. Ed.,* 2006, **45**, 1206; L. Que, Jr., C. Kim, J. Kim and Y. Zang, *US Patent WO-A-9748710* [Chem. Abs., 1997, **128**, 90357].
7. K. Chen and L. Que, Jr., *J. Am. Chem. Soc.*, 2001, **123**, 6327.
8. R. Y. N. Ho, G. Roelfes, B. L. Feringa and L. Que Jr., *J. Am. Chem. Soc.*, 1999, **121**, 264.
9. N. Lehnert, R. Y. N. Ho, L. Que Jr. and E. I. Solomon, *J. Am. Chem. Soc*., 2001, **123**, 8271 and 12802.
10. Y. Zang, J. Kim, Y. Dong, E. C. Wilkinson, E. H. Appleman and L. Que, Jr., *J. Am. Chem. Soc.*, 1997, **119**, 4197; J. –J. Girerd, F. Banse and A. Samaan, *J. Struct. Bonding*, 2000, **97**, 143.

11. M. Harata, K. Jitsukawa, H. Masuda and H. Einaga, *Chem. Lett.*, 1995, 61; A. Wada, M. Harata, K. Hasegawa, K. Jitsukawa, H. Masuda,. M. Mukai, T. Kitagawa and H. Einaga, *Angew. Chem. Int. Ed.*, 1998, **37**, 798.
12. D. H. Lee, N. Wei, N. N. Murthy, Z. Tyelkar, K. D. Karlin, S. Kalderli, B. Jung and A. Zuberbuhler, *J. Am. Chem. Soc.*, 1995, **117**, 12498.
13. D. H. Lee, N. N. Murthy and K. D. Karlin, *Inorg. Chem.*, 1997, **36**, 5785; J. E. Bol, W. L. Driessen, R. Y. N. Ho, B. Maase, L. Que, Jr. and J. Reedijk, *Angew. Chem., Int. Ed. Engl.*, 1997, **36**, 998; P. Comba, P. Hilfenhaus and K. D. Karlin, *Inorg. Chem.*, 1997, **36**, 2309.
14. H. V. Obias, G. P. Van Strijdonck, D. H. Lee, M. Ralle, N. J. Blackburn and K. D. Karlin, *J. Am. Chem. Soc.*, 1998, **120**, 9696; T. D. Ju, R. A. Ghiladi, D. H. Lee, G. P. Van Strijdonck, A. S. Woods, R. J. Cotter, V. G. Young and K. D. Karlin, *Inorg. Chem.*, 1999, **38**, 2244.
15. C.-L. Chuang, K. Lim, O. dos Santos, X. Xu and J. W. Canary, *Inorg. Chem.*, 1997, **36**, 1967.
16. Z. He, P. J. Chaimungkalanont, D. C. Craig and S. B. Colbran, *Dalton Trans.*, 2000, 1419; D. G. Lonnon, D. C. Craig and S. B. Colbran, *Dalton Trans*., 2006, 3785.
17. D. G. Lonnon, D. C. Craig and S. B. Colbran, Inorg. Chem. Commun., 2003, 1351.
18. G. Guisado-Barrios and D. T. Richens, 2007, to be submitted.
19. B. Kaptein, G. Barf, R. M. Kellog and F. V. Bolhuis, *J. Org. Chem.*, 1990, **55**, 1890; M. Newcombe, G. W. Gokel and D.J. Cram, *J. Am. Chem. Soc.*, 1974, **96**, 6810.
20. See the following for other examples of hepta-co-ordinated Mn(II) complexes: S. El Ghachtouli, A. Mohamadou and J .-P. Barbier, *Inorg. Chim. Acta.*, 2005, **358**, 3873; C. Baffert, I. Romero, J. Pécaut, A. Llobert, A. Deronzier and M. N. Collomb, *Inorg. Chim. Acta.*, 2004, **357**, 3430; C. Ma, C. Chen, Q liu, D. Liao and L. Li, *Eur. J. Inorg. Chem.*, 2003, 1227; O. Horner, J. -J. Girerd, C. Philouze, L. Tchertanov, *Inorg. Chim. Acta*., 1999, **290**, 139.

21. S. Ogo, R. Yamahara, M. Roach, T. Suenobu, M. Aki, T. Ogura, T. Kitagawa, H. Masuda, S. Fukuzumi and Y. Watanabe, *Inorg. Chem*., 2002, **41**, 5513; S. Ogo, S. Wada, Y. Watanabe, M. Iwase, A. Wada, M. Harata, K. Jitsukawa, H. Masuda and H. Einaga, *Angew. Chem. Int. Ed.* 1998, **37**, 2102.
22. M. J. Nelson and S. P. Seitz in *Active Oxygen in Biochemistry*, eds. J.S. Valentine, C. S. Foote, A. Greenberg and J. F. Liebman, Chapman and Hall, London, 1995; T. Funabiki, (ed.) *Oxygenases and Model Systems*, Kluwer Academic, Dordrecht, 1997, **69**, 140.
23. J. J. Borrás-Almenar, J. M. Clemente-Juan, E. Coronado, and B. S. Tsukerblat, *Inorg. Chem*., 1999, **38,** 6081 and *Comput. Chem*., 2001, **22,** 985.
24. M. Gerloch and A. D. C. Towl, *J. Chem. Soc. A*, 1969, 2850.
25. S. M. Gorun and S. J. Lippard, *Inorg. Chem.*, 1991, **30,** 1625.
26. H. Weihe and H. U. Güdel, *J. Am. Chem. Soc.*, 1997, **119,** 6539.
27. F. Le. Galli, F. Fabrizi de Biani, A. Caneschi, P. Cinelli, A. Cornia, A. C. Fabretti and D. Gatteschi, *Inorg. Chim. Acta.*, 1997, **262**, 123.
28. A. Caneschi, F. Fabrizi de Biani, L. Kloo and P. Zanello, *Int. J. Quant. Chem.,* 1999, **72**, 61.
29. No further waves were apparent in the cyclic voltammograms of **2** out to the CH_3CN solvent window cut off, +2 V to -2 V vs Ag/AgCl.
30. X. D. Chen, M. Du, X. M. Chen and T. C. W. Mak, *Polyhedron*, 2005, **24**, 1047.
31. N. Kitajima, H. Amagai, N. Tamura, M. Ito, Y. Moro-oka, K. Heerwegh, A. Penicaud, R. Mathur, C. A. Reed and P. D. W. Boyd, *Inorg. Chem*., 1993, **32**, 3583.
32. M. J. Long, D. T. Richens and A. K. Powell, 1989, unpublished results
33. V. A.Vankai, M. G. Newton and D. M. Kurtz, *Inorg. Chem.*, 1992, **31**, 341.
34. K. Andjelkovic, A. Bacchi, D. Jeremic, I. Ivanovic-Burmazovic, *J. Coord. Chem.* 2002, **55**, 1385.
35. A. H. Cohen and J. L. Hoard, *J. Am. Chem. Soc.*, 1966, **88**, 3228.

36. M. D. Lind, M . J. Hamor, T. A. Hamor and J. L. Hoard, *Inorg. Chem.*, 1964, **3**, 34.

37. S. W. Taylor, J. D. Cashion, L. J. Brown, C. J. Hawkins and G. R. Hanson, *Inorg. Chem.*,1995, **34**, 1487.

38. S. W. Taylor, C. J. Hawkins and D. J. Winter, *Inorg. Chem.*, 1993, **32**, 422.

39. S. J. Barclay, P. E. Riley and K. N. Raymond, *Inorg. Chem.*, 1984, **23**, 2005.

40. M. Suzuki, S. Fujinami, T. Hibino, H. Hori, Y. Maeda, A. Uehara and M. Suzuki, Masatatsu, *Inorg. Chim. Acta*, 1998, **283**,124

Chapter 3

Synthesis and Characterisation of a Hydrophobic TPA ligand via O-alkylation (R = n-octyl or methyl) of tris(6-hydroxymethyl-2-pyridylmethyl) amine. Characterisation of iron(II) complexes by paramagnetic ^{1}H NMR.

3.1 Introduction

In chapter 2, the synthesis of the TPA derivative, tris(6-hydroxymethyl-2-pyridylmethyl)amine (H_3L_{11}) was described along with the characterisation of a number of metal complexes with copper(II), manganese(II) and iron(III). It was found that H_3L_{11} possesses a wide and versatile coordination chemistry. H_3L_{11} moreover is water soluble and stable to alkaline pH and as such may have potential as a bleaching catalyst precursor, perhaps superior to TPA itself, within a new generation of low temperature detergents working in alkaline media around pH 10. Several TPA complexes have been patented as catalysts for alkaline bleaching.[1-3] as well as providing models for a range of non-heme iron,[4-9]copper oxygenases.[10–15] and bio-inspired C-H oxidation catalysts.[4-9, 16, 17] It has been already established that the introduction of substituents α to the pyridyl nitrogen leads not only to further functionality but to additional steric and electronic properties that can modify properties such as spin state and redox potentials.[18-20] For example whereas $[Fe^{II}(TPA)(CH_3CN)_2]^{2+}$ and its corresponding t-butylperoxoiron(III) derivative are both low spin, significant changes occur on introducing a CH_3 group at the 6-position on just one of the pyridine rings. Here while the t-butylperoxoiron(III) complex remains low spin, the corresponding iron(II) complex is high spin. Finally the introduction of 6-Me substituents on two or all of the pyridine rings results exclusively in high spin iron(II) and iron(III) complexes. This has important consequences in the subsequent reactions of these iron TPA-derived complexes as catalysts of H_2O_2 or ^{t}BuOOH-dependent oxidations.[18] Tris(6-hydroxymethyl-2-pyridylmethyl)amine (H_3L_{11}) on the other hand, however, offers the

opportunity to build hydrophobicity into the ligand backbone via simple alkylation of the hydroxymethyl groups. Building in hydrophobicity is an aspect that has been little explored to date in model complexes especially given the evidence now from structural data that monooxygenase enzymes like cytochrome P-450 and bacterial methane monooxygenase contain their active iron sites embedded within a deeply hydrophobic region of the protein enabling the ready uptake, correct orientation and subsequent functionalization (hydroxylation) of the C-H compound.[21] There is evidence from the literature that embedding biomimetic models within a hydrophobic environment can lead to enhanced activity. By using the dinuclear iron(III) TPA complex $[Fe_2O(\eta^1\text{-}OAc)(TPA)_2]^{3+}$ as a close structural model for MMO Fish et al have described formation of $[Fe_2O(\eta^1\text{-}H_2O)(\eta^1\text{-}OAc)(TPA)_2]^{3+}$ *in-situ* at pH 4.2 from $[Fe_2O(\eta^1\text{-}OAc)(TPA)_2]^{3+}$ which previously had been determined by UV/VIS and ^1H NMR analysis that $[Fe_2O(\mu\text{-}OAc)\ (TPA)_2]^{3+}$ was converted to the $[Fe_2O(\eta^1\text{-}H_2O)(\eta^1\text{-}OAc)(TPA)_2]^{3+}$ complex, at pH 4.2 and that, this $\eta^1\text{-}H_2O$ was thought to be responsible for the dramatic increase in the oxidation of water soluble alcohols to the corresponding aldehydes and ketones in the presence of TBHP/ O_2.[22]

The $[Fe_2O(\eta^1\text{-}H_2O)(\eta^1\text{-}OAc)(TPA)_2]^{3+}$ complex was embedded in an amorphous silicate surface modified by a combination of hydrophilic poly(ethylene oxide) and hydrophobic poly(propylene oxide), figure 3.1.

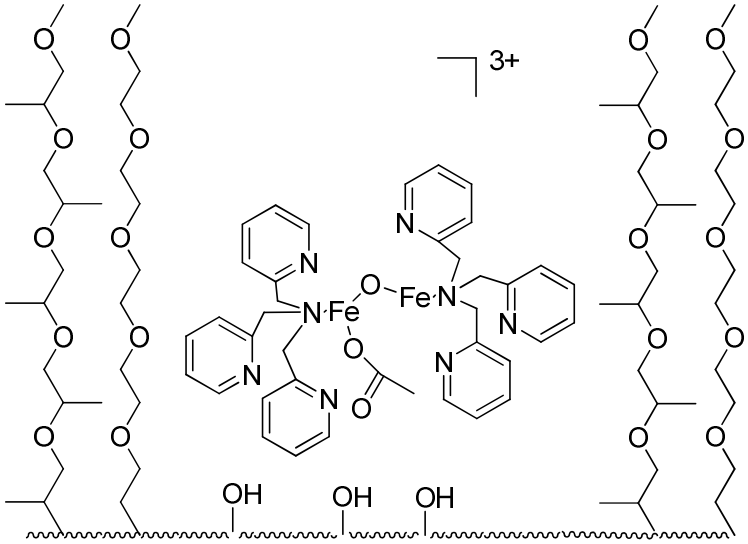

Figure 3.1: A schematic representation of in-situ formed $[Fe_2O(\eta^1\text{-}H_2O)(\eta^1\text{-}OAc)(TPA)_2]^{3+}$, embedded in te PEO, PPO derivatized silica, for alkane functionalization in water at pH 4.2

The idea was to simulate the hydrophobic MMO macroenviroment. The resulting assembly was found to be active towards the catalysis of the oxygenation of cycloalkanes with tert-butyl hydroperoxide (TBHP)/O_2 in an aqueous medium at pH 4.2.[23]

Even more intriguing was that the silica-based assembly showed higher reactivity when the $[Fe_2O(\eta^1\text{-}H_2O)(\eta^1\text{-}OAc)(TPA)_2]^{3+}$ complex was similarly studied at pH 4.2 within an aqueous micellar system utilizing the surfactant, cetyltrimethylammonium hydrogen sulfate at its critical micelle concentration, figure 3.2.[23]

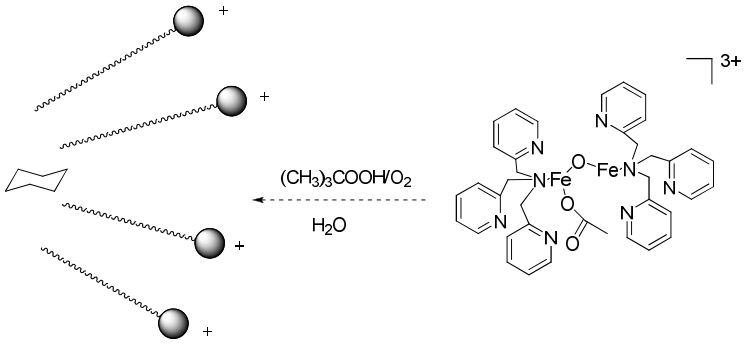

Figure 3.2: A schematic representation of *in-situ* formed $[Fe_2O(\eta^1\text{-}H_2O)(\eta^1\text{-}OAc)(TPA)_2]^{3+}$ difussing, along with oxidants, TBHP/ O_2, into aqueous micelles formed with the surfactant, cetyltrimethylaamonium hydrogensulfate, for alkane functionalization in water at pH 4.2

Thus there is much interest and scope in ligands allowing the introduction of a degree of hydrophobicity into the structure in the expectation of enhancing C-H oxygenating activity. Such hydrophobicity could be easily introduced into H_3L_{11} via peralkylation (ether formation) of the hydroxymethyl groups in order to synthesize a new family of possibly hydrocarbon-soluble/micellar transition metal oxidation catalysts. Similarly functionalisation of the hydroxymethyl groups with peralkylated substituents containing fluorine could lead to catalysts soluble in fluorous solvents for oxygenations on hydrocarbons, alkenes and alcohols under fluorous biphasic conditions (FBC).[24] Figure 3.3 below shows a catalytic system based upon a N-perfluoroalkylated triazacyclononane macrocycle developed by Fish *et al* for FBC oxidations of hydrocarbons and olefins with TBHP/O_2. Good activity was found and moreover the presence of the fluorous tails allowed the copper complex to be totally separated from the organic phase by a simple decantation process and thus recycled three times.[24]

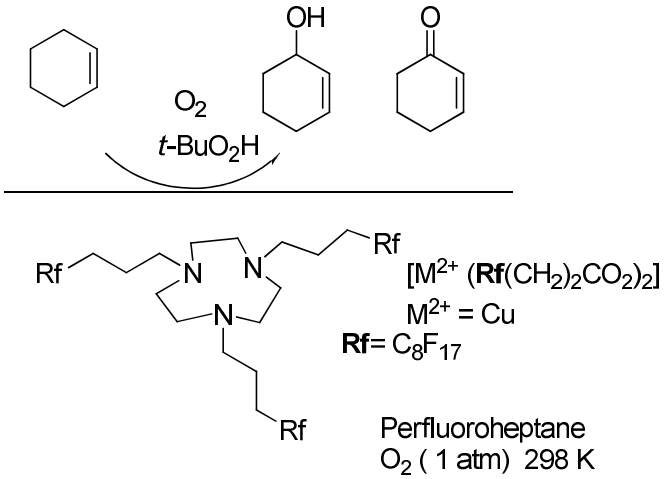

Figure 3.3: FBC system for oxidations of hydrocarbons and olefins with TBHP/O_2 based on a Cu^{II} complex of a tris(N-perfluoroalkyl)triazacyclononane.

Chapter 3

This chapter reports studies on the peralkylation of the hydroxymethyl groups of H_3L_{11} in order to synthesize and characterise a new family of hydrophobic lipophilic TPA-derived iron catalysts for C-H oxygenations with H_2O_2 and t-BuOOH, figure 3.4. Of particular interest was to create a hydrophobic channel above the active hydroperoxo or oxo iron centre that might orientate an n-alkane substrate towards C-H oxygenation preferentially at the C-1 position. A ready cheap supply of medium length (C_7-C_9) 1-oxygenates (alcohols and aldehydes) is sought after as plasticizer and detergent additives.[25] These are currently made via expensive catalytic hydroformylation of the corresponding long chain C_7-C_9 alkenes.[26]

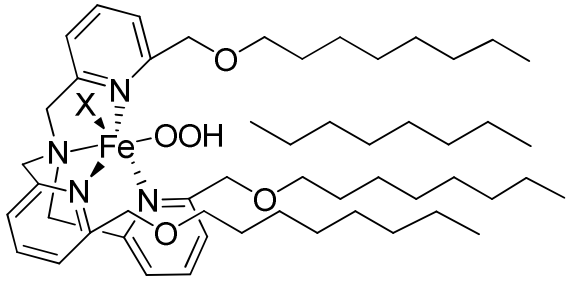

Figure 3.4: Schematic representation of the hydrophobic pocket generated next to a putative hydroperoxo-iron(III) centre trapping an alkane and orientating it for C-1 functionalisation.

The use of C_7-C_9 n-alkanes for this conversion (cheaper - mostly used as additives to petrol) would be a huge advance. However use of n-alkanes poses huge challenges since there are no functional groups serving to direct regio reactivity and moreover the internal CH_2 bonds are many times more reactive than those at terminal CH_3. The design and use of a catalyst allowing only the approach of and thus reaction with the terminal CH_3 group at the active site would seem the only way of achieving such regioselective partial 1-oxygenation of n-alkanes to 1-alcohol/aldehydes in reasonable yield. This might be achievable with restricted substrate orienation such as within a catalyst containing a hydrophobic channel such as in figure 3.4. In the sections below the synthesis of two alkylated derivatives of H_3L_{11}; tris-(6-methoxymethyl-2-pyridylmethyl) amine, L_{15} and tris-(6-n-octyloxymethyl-2-pyridylmethyl)amine, L_{16} are

reported along with characterisation of their paramagnetic iron(II) complexes in solution using NMR. The activity of the iron(II) complexes towards the catalysis of alkane oxygenation with H_2O_2 is reported later in chapter 5.

3.2. Results and Discussion.

3.2.1. Synthesis of tris(6-methoxymethyl-2-pyridylmethyl)amine, L_2 and of tris-(6-n-octyloxymethyl-2-pyridylmethyl)amine, L_{15}.

The synthesis of the simpler tris(6-methoxymethyl)TPA derivative, L_{15} was important for the purpose of identifying any regioselectivity effect stemming from the introduction of the C_8 peralkyl chain in L_{16} as well as assisting in the assignment of ^{1}H NMR resonances of L_{16} and its iron complexes later. The synthesis of L_{15} and L_{16} initially followed procedures reported for the alkylation of 6-hydroxymethylpyridine derivatives[27, 28] involving generation of the tris-alkoxide from H_3L_{11} using sodium hydride (NaH) in the ethereal solvents; tetrahydrofuran (THF) or dioxane followed by alkylation with the corresponding haloalkane. Use of this method was not however successful for synthesizing L_{15} or L_{16}. This was a surprise but success was eventually achieved on switching to dimethylformamide (DMF) as the solvent as had been reported in one isolated case.[29] The successful synthesis of L_{15} was achieved by the addition of a solution of NaH in DMF at 0ºC to a DMF solution of H_3L_{11} followed by addition of iodomethane after 1 hour stirring, stirring for further 36 h, work up and chromatographic purification to a yellow oil in 68% yield. A similar procedure but using 1-bromooctane was used successfully to synthesize L_3 in 72% yield after chromatography. Both L_{15} and L_{16} have been fully characterised by ^{1}H NMR and ^{13}C NMR and MS.

3.2.2. ^{1}H NMR characterisation of tris-(6-methoxymethyl-2-pyridylmethyl)amine, L_{15} and of tris-(6-n-octyloxymethyl-2-pyridylmethyl)amine, L_{16}.

All ^{1}H NMR spectra were recorded on samples in standard 5mm tubes. The ^{1}H NMR of L_{15} in CD_3CN, figure 3.5 and 3.6, shows the expected resonances; a singlet at 3.4 ppm for the methoxy methyl, along with two further singlets at 3.8 ppm and 4.5 ppm for 6-CH_2 and 2-CH_2 groups respectively on the py ring. The β, β' and γ protons of the pyridine ring are seen as the expected triplet and two doublets at 7.29 ppm, 7.55 ppm and 7.69 ppm respectively, figure 3.6.

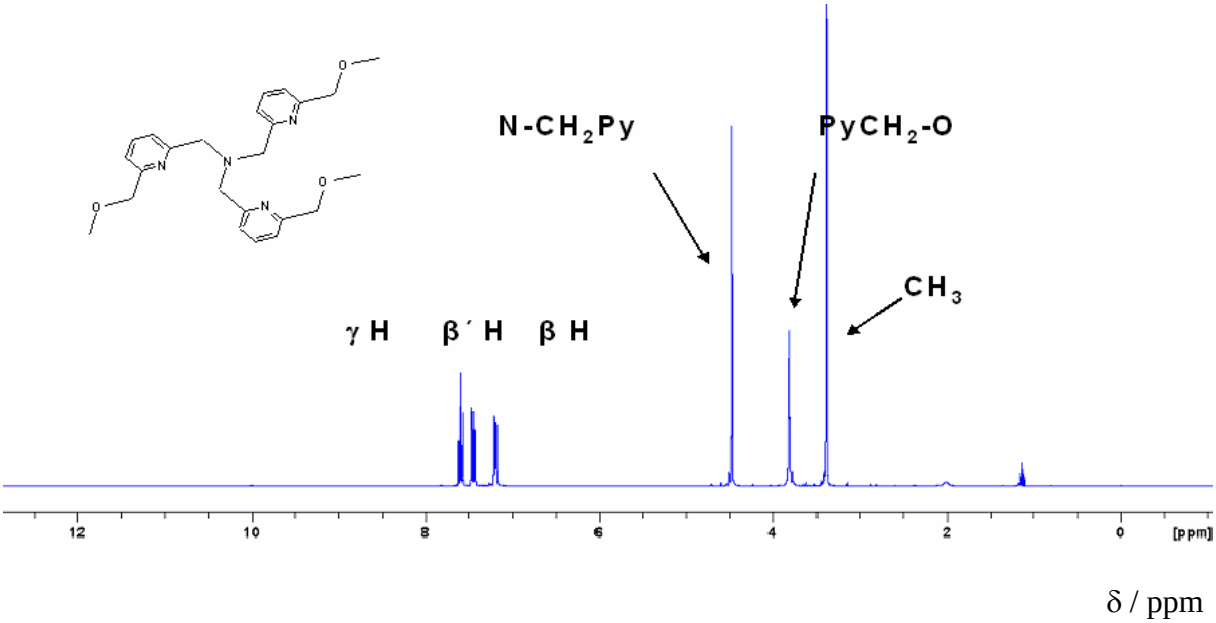

Figure 3.5: ^{1}H NMR spectrum of **L_{15}** in CD_3CN

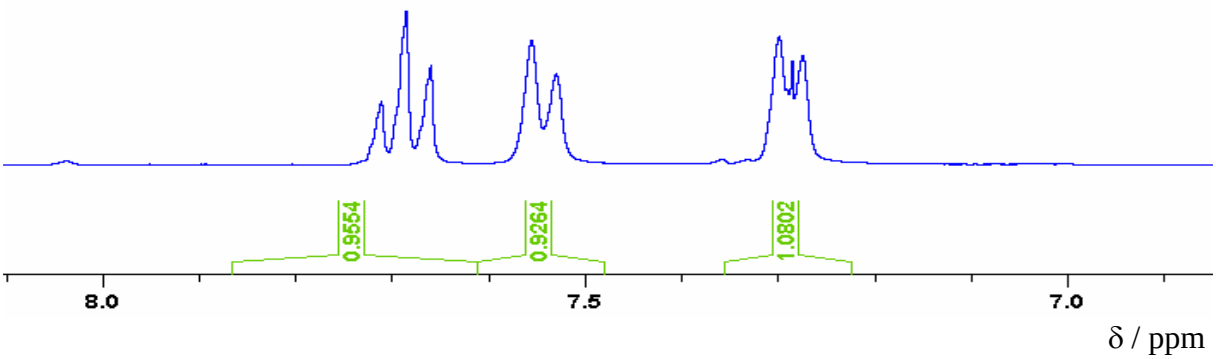

Figure 3.6: ^{1}H NMR spectrum of **L_{15}** in CD_3CN, expanded region between 7 - 8 ppm.

The ^{1}H NMR spectrum of L_{16} in CD_3CN, figure 3.7 and 3.8, shows the β and β' protons of the pyridine groups as doublets at 7.22 ppm and 7.42 ppm respectively with the γ proton (triplet) more downfield at 7.59 ppm. The protons of the methylene group adjacent to the tertiary

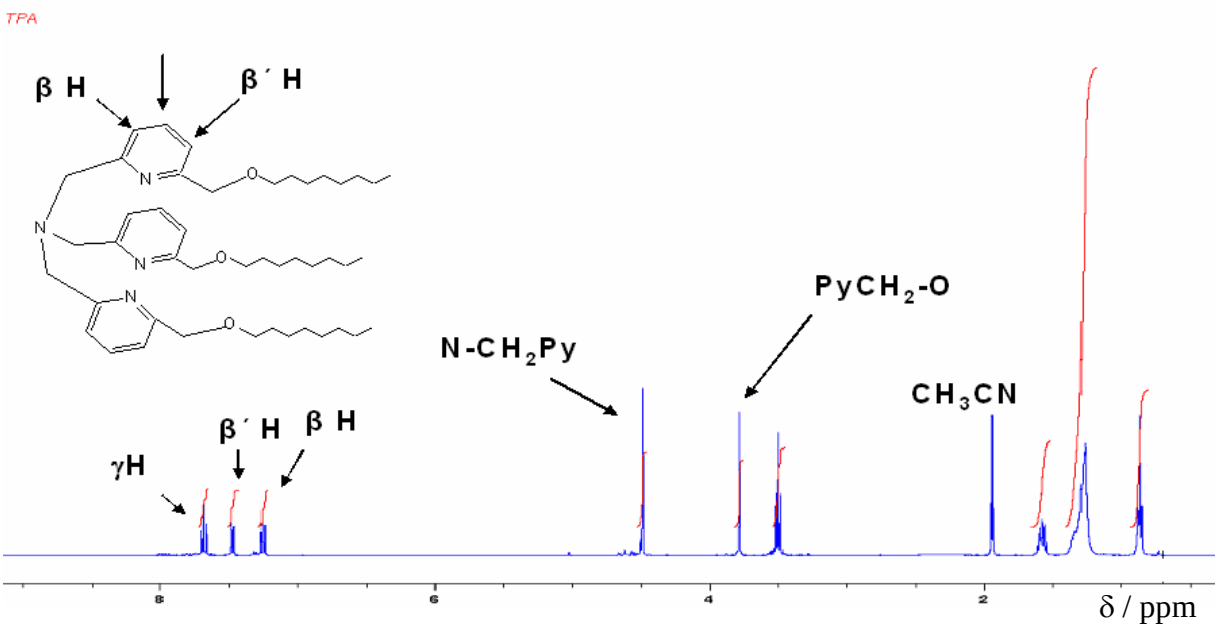

Figure 3.7: ^{1}H NMR spectrum for **L_{16}** in CD_3CN

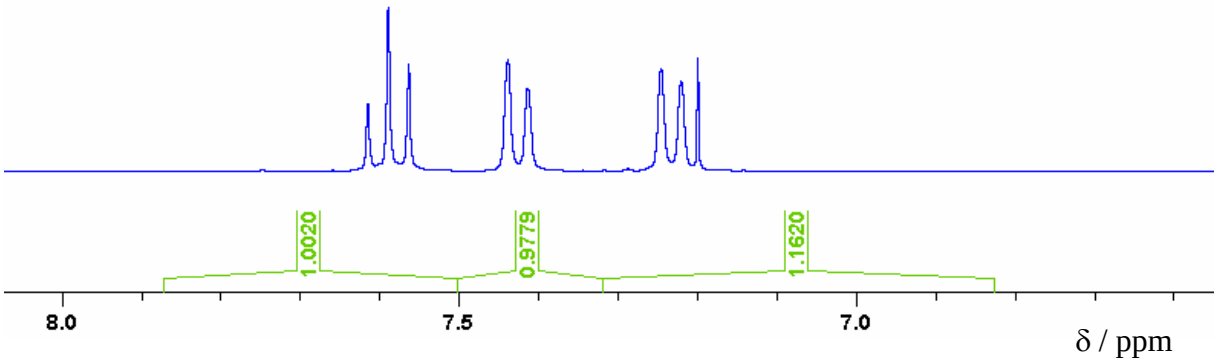

Figure 3.8: ^{1}H NMR spectrum of **L_{16}** in CD_3CN, expanded region between 7 - 8 ppm.

amine is present as in L_{15} as a singlet at 4.5 ppm with the α-CH_2 methylene between the pyridine and the oxygen assigned to the singlet at 3.7 ppm. The first methylene of the C_8 chain (showing the expected triplet coupling to its neighbour) is apparent at 3.5 ppm well separated

from the rest of the C_8 chain. Finally the terminal CH_3 group of the C_8 chain is seen most upfield as expected as a triplet at 0.8 ppm.

3.2.3. Synthesis and characterisation of iron(II) complexes.

Iron(II) complexes of L_{15} and L_{16} were prepared by mixing equimolar amounts of the ligand and either $[Fe(H_2O)_6](ClO_4)_2$ (commercially available) or $[Fe(CH_3CN)_2(O_3SCF_3)_2]$ (synthesized in house)[30] in either CH_3CN or CH_2Cl_2 solvent. The triflate complex was most widely employed owing to the small, but real, risk of explosion from handling perchlorate salts. Vapour diffusion techniques (diffusion of diethyl ether into CH_3CN or CH_2Cl_2 solutions) were used in attempts to grow crystals of the iron(II) complexes as reported for the complexes with H_3L_{11} in chapter 2. However, in all cases, the iron(II) complexes of L_{15} and L_{16} were obtained as oils and all attempts to grown crystals suitable for X-ray analysis were unsuccessful.

3.2.4. Bis(acetonitrile)(tris-(6-methoxymethyl-2-pyridylmethyl)amine)iron(II) perchlorate; (C_{16}) $[Fe(L_{15})(CH_3CN)_2](ClO_4)_2$ and bis(acetonitrile) (tris- (6-n-octyloxy methyl- 2-pyridylmethyl)amine)iron(II) perchlorate,(C_{17}) $[Fe(L_{16})(CH_3CN)_2](ClO_4)_2$.

A solution of L_{15} was added under nitrogen to a pale yellow solution of $[Fe(H_2O)_6](ClO_4)_2$ in CH_3CN yielding a reddish-orange solution. The reaction mixture was stirred for 3 h. The solvent was evaporated yielding $[Fe(L_{15})(CH_3CN)_2](ClO_4)_2$ as a reddish-orange oil. A similar procedure was used to prepare $[Fe(L_{16})(CH_3CN)_2](ClO_4)_2$ again as a reddish-orange oil.

3.2.5. Bis(acetonitrile)(tris(6-methoxymethyl-2-pyridylmethyl)amine)iron(II) trifluoro methanesulfonate, (C_{18}) [Fe(L_{15})(CH_3CN)$_2$](CF_3SO_3)$_2$ and bis(acetonitrile)(tris-(6-octyloxy methyl-2-pyridylmethyl)amine)iron(II) trifluoromethanesulfonate, (C_{19}) [Fe(L_{16})(CH_3CN)$_2$](CF_3SO_3)$_2$.

A solution of L_{15} was added under nitrogen to a pale yellow solution of [Fe(CH_3CN)$_2$(O_3SCF_3)$_2$] in THF yielding a reddish-orange solution. The reaction mixture was stirred for 12 h. The solvent was evaporated to yield [Fe(L_{15})(CH_3CN)$_2$](CF_3SO_3)$_2$ as a reddish-orange oil. A similar procedure was used to prepare [Fe(L_{16})(CH_3CN)$_2$](CF_3SO_3)$_2$ again as a reddish-orange oil.

3.2.6. Characterisation of [Fe(L)(CH_3CN)$_2$](CF_3SO_3)$_2$ (L = L_{15} or L_{16}) in solution by ^{1}H NMR.

Each iron(II) complex was prepared *in-situ* by mixing equimolar quantities of [Fe(CH_3CN)$_2$(O_3SCF_3)$_2$] and the appropriate ligand in either CD_3CN and CD_2Cl_2. In each case the solvents were first degassed by 3 freeze-thaw cycles and left under argon.

3.2.6.1. ^{1}H NMR study of [Fe(L_{15})(CH_3CN)$_2$](O_3SCF_3)$_2$ in CD_3CN.

An equimolar amount of **L_{15}** in CD_3CN or CD_2Cl_2 under nitrogen atmosphere was added to a pale yellow deoxygenated solution of [Fe(CH_3CN)$_2$(O_3SCF_3)$_2$] in CD_3CN or CD_2Cl_2 to yield a reddish-orange solution which was rapidly transferred under nitrogen to a 5mm NMR tube. ^{1}H NMR resonances appear over a range from 0 to +100 ppm, figure 3.9 and 3.10**,** consistent with the presence of a high spin iron(II) complex.

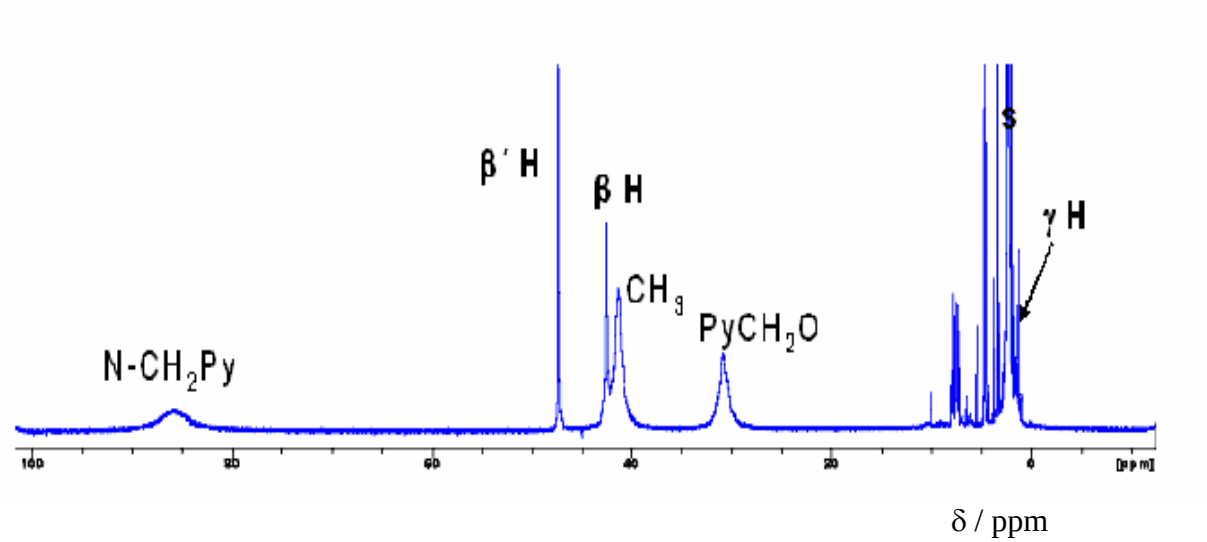

Figure 3.9: ^{1}H NMR spectrum of $[Fe(L_{15})(CH_3CN)_2](O_3SCF_3)_2$ in CD_3CN region (0-100 ppm)

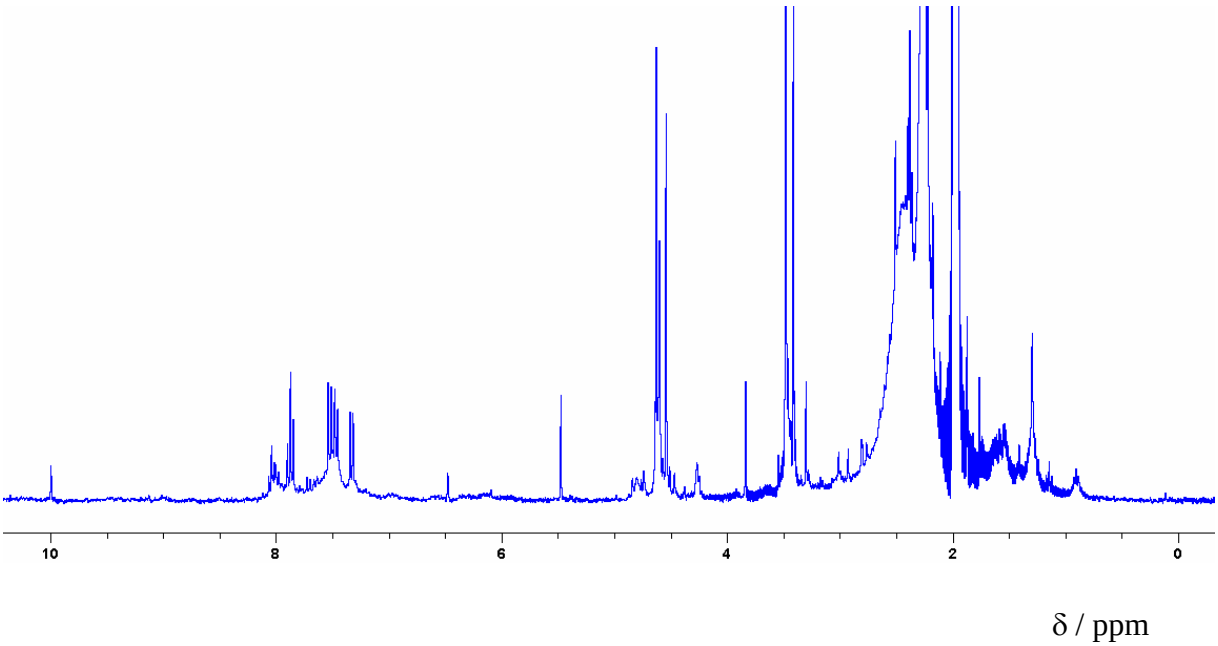

Figure 3.10: ^{1}H NMR spectrum of $[Fe(L_{15})(CH_3CN)_2](O_3SCF_3)_2$ in CD_3CN region (0-10 ppm)

The protons from the methylene group between the tertiary amine and the pyridine rings are observed very downfield at ~86 ppm, with the two β and β' protons of the pyridine ring at 43 and 47 ppm respectively. Two well separated peaks are seen at 31 and 41 ppm corresponding to the methoxy methyl and the methylene between the ether oxygen and pyridine respectively. This in turn confirms the assignment of the two overlapping methylene peaks at ~35 ppm in $[Fe(L_{15})(CH_3CN)_2](O_3SCF_3)_2$. In order to confirm the assignment a paramagnetic ^1H COSY NMR spectrum was recorded. This is shown in figure 3.11. Cross peaks are clearly seen in the spectrum arising from correlation of the broad upfield peak at ~ 5 ppm and the two β and β' protons of the pyridine ring in the 40-50 ppm region. This assigned the broad upfield resonance at ~ 5 ppm to the γ proton of the pyridine ring.[31] What is also apparent in figure 3.9, are sharp ligand-derived resonances in the normal region 0-10 ppm for a diamagnetic species. This region is shown clearly in figure 3.10. Three situations could be responsible.

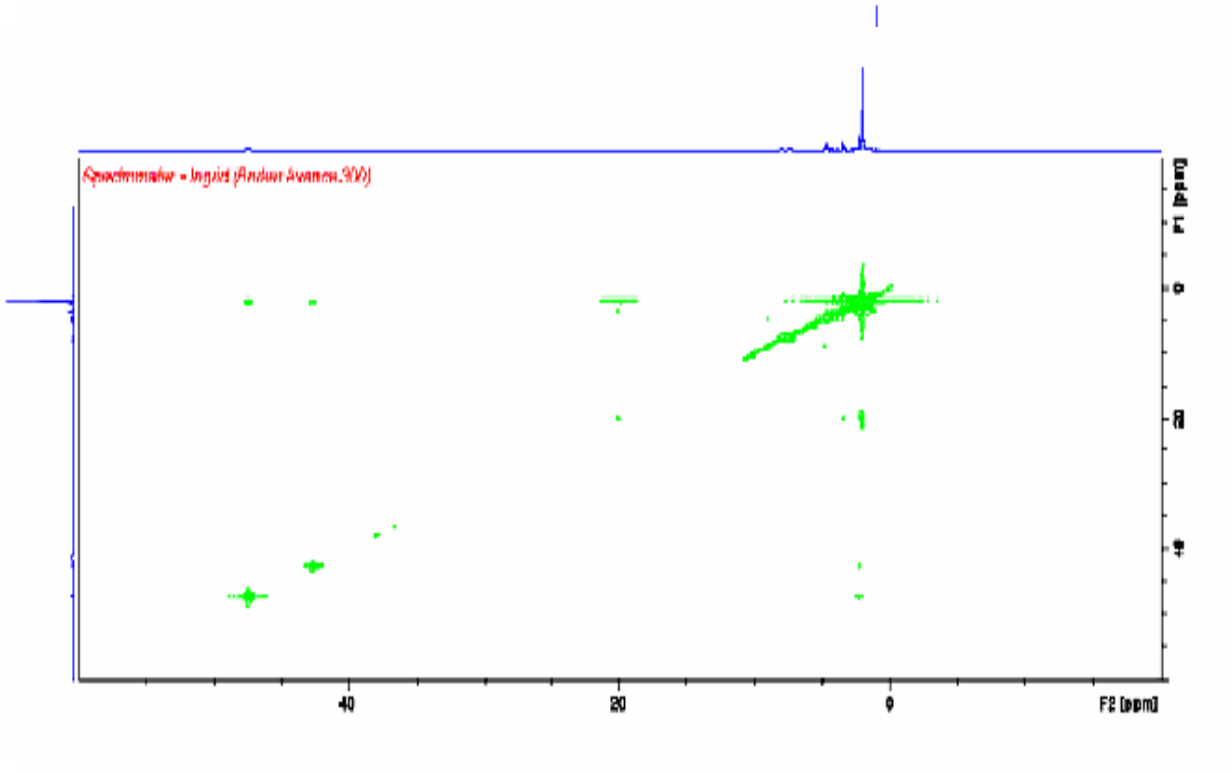

Figure 3.11: ^1H COSY NMR spectrum of $[Fe(L_{15})(CH_3CN)_2](O_3SCF_3)_2$ in CD_3CN

(i) the presence of amounts of free uncomplexed ligand L_{15} as a result of the equimolar Fe:L_{15} addition not being absolutely exact; (ii) amounts of free or decomposed ligand as a result of complex degradation or (iii) a small amount of a diamagnetic low spin iron(II) complex in equilibrium with the high spin form (SC equilibrium). (iii) was ruled out by a temperature dependent ^{1}H NMR investigation[32] which showed no change in relative intensity of the diamagnetic and paramagnetic features over the range +60^{o}C to -30^{o}C, figure 3.12 (a) and (b). The resonances assigned to paramagnetic high spin $[Fe(L_2)(CH_3CN)_2]^{2+}$ gradually became sharper and shifted upfield while no change was observed to the diamagnetic features. A further clue as to the origin of the diamagnetic features, figure 3.10, came from re-running the ^{1}H NMR spectrum after standing for a period of 1 month. The ^{1}H NMR spectrum obtained,

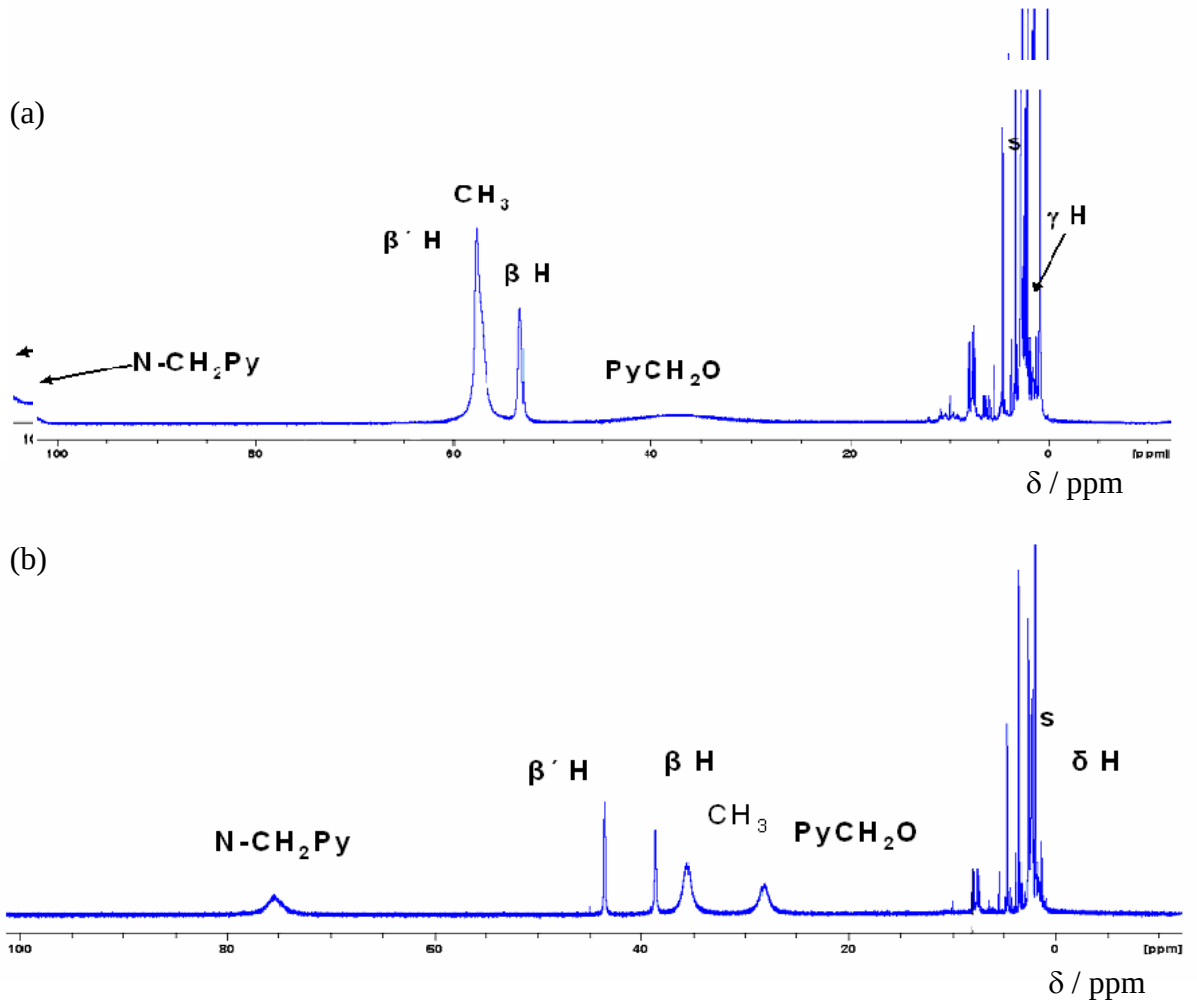

Figure 3.12: ^{1}H NMR spectrum of $[Fe(L_{15})(CH_3CN)_2](O_3SCF_3)_2$ in CD_3CN at (a) -30^{o}C and (b) + 60^{o}C.

figure 3.13, shows a clear increase in intensity of the sharp features in the diamagnetic region in comparison to the paramagnetic features for high spin $[Fe(L_{15})(CH_3CN)_2]^{2+}$. In also ruling out possibility (i) above it was thus concluded that the diamagnetic features are due to complex decomposition. Que et al have observed that introducing 6-substituents on the pyridine rings

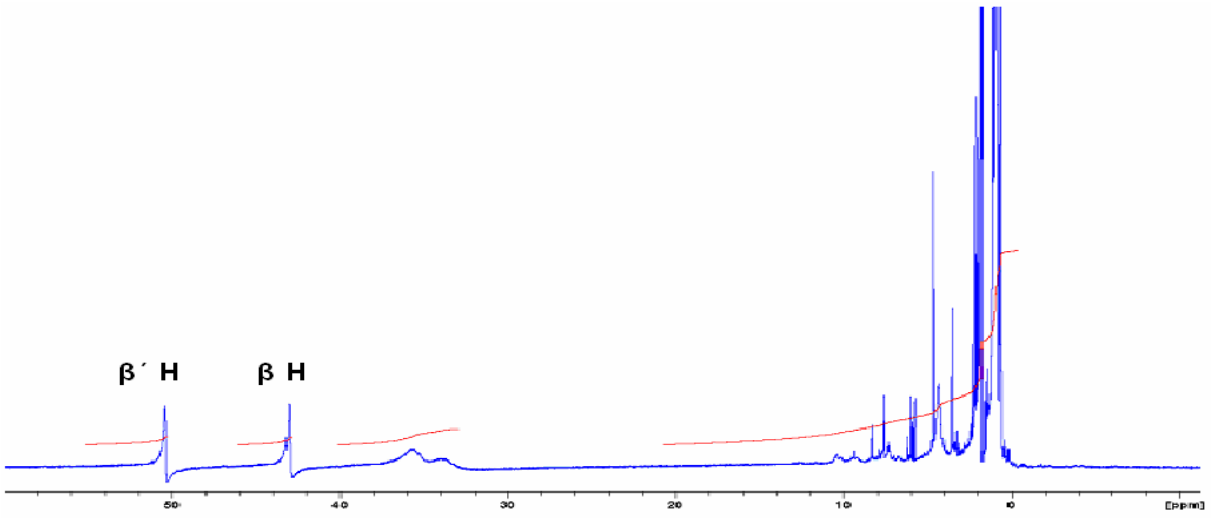

δ / ppm

Figure 3.13: ^{1}H NMR spectrum of $[Fe(L_{15})(CH_3CN)_2](O_3SCF_3)_2$ in CD_3CN re-recorded after standing at RT for 1 month at 25^{o}C.

of TPA quickly reduces the stability of the corresponding iron(III) complexes.[33] Unlike the high stability of iron(II) and iron(III) complexes of TPA they observed that introducing even just one 6-Me substituent as in 6-MeTPA reduces the stability such that decomposition is quickly observed over a period of one month. This indicates that the diamagnetic features, figures 3.10 and 3.13, are due to free or partly decomposed L_2 as a result of complex degradation involving air oxidation of the iron(II) complexes to iron(III) followed by ligand dissociation/decomposition.

3.2.6.2. ^{1}H NMR study of $[Fe(L_{16})(CH_3CN)_2](O_3SCF_3)_2$ in CD_3CN.

An equimolar amount of **L_{16}** in CD_3CN under nitrogen atmosphere was added to a pale yellow deoxygenated solution of $[Fe(CH_3CN)_2(O_3SCF_3)_2]$ in CD_3CN to yield a reddish-orange solution which was rapidly transferred under nitrogen to a 5mm NMR tube. The ^{1}H NMR spectrum, (figure 3.14 and 3.15), is typical of a high-spin iron(II) complex with broad ^{1}H peaks appearing over the range from -5 to +90 ppm. Peaks have been assigned from comparisons with the spectrum of free **L_{16}**, (figure 3.7), and other related high spin iron(II) complexes such as those of 6-Me$_3$TPA (see table 3.2).[31] The protons from the methylene group linking the tertiary amine and pyridine rings are shifted strongly downfield, at ~84 ppm with the two β and β' protons of the pyridine appearing at 50 and 43 ppm respectively. The two broad overlapping resonances seen at 34 and 36 ppm are assigned to the two other methylenes either side of the ether oxygen with the one at slightly higher chemical shift (36 ppm) assigned to the methylene attached to the pyridyl ring. The protons of the next methylene group of the n-octyl chain are assigned to the broad resonance at 5 ppm.

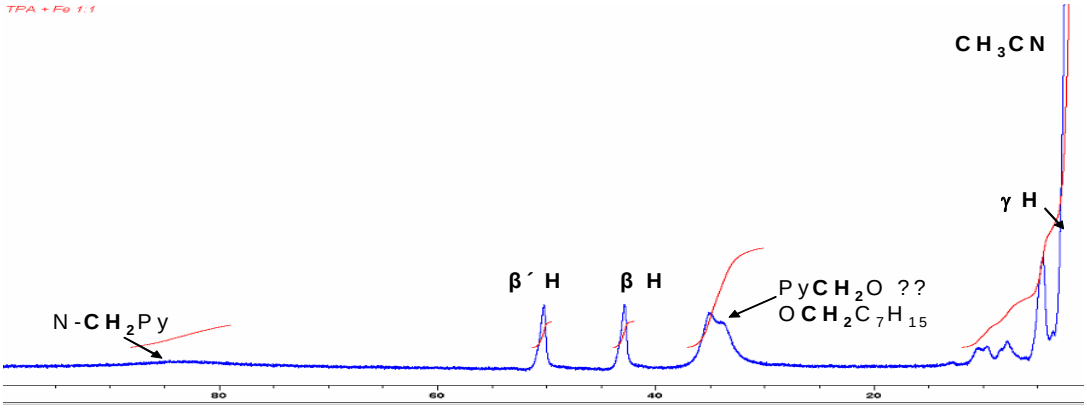

Figure 3.14: ^{1}H NMR spectrum of $[Fe(L_{16})(CH_3CN)_2](O_3SCF_3)_2$ in CD_3CN region (0-100 ppm)

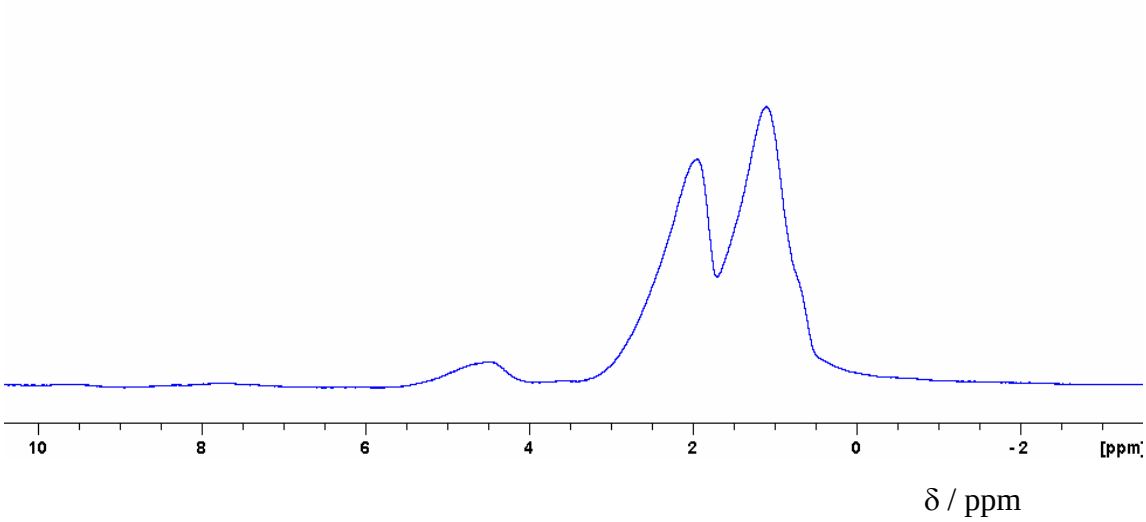

Figure 3.15: ^{1}H NMR spectrum of $[Fe(L_{16})(CH_3CN)_2](O_3SCF_3)_2$ in CD_3CN region (0-10 ppm)

The γ proton of the pyridine rings of $[Fe(L_{15})(CH_3CN)_2]^{2+}$ were assigned to a broad resonance at 5ppm. In the case of $[Fe(L_{16})(CH_3CN)_2]^{2+}$ assignment is more difficult within the broad envelope from -5 to +5 ppm which correspond to protons from CH_3CN and the rest of the n-octyl chain. The entire region between 0-10 ppm was broad with no evidence of the sharp features that had characterised the spectrum of $[Fe(L_{15})(CH_3CN)_2]^{2+}$.

The paramagnetic nature of the iron(II) complexes of L_2 and L_3 is apparent from comparisons with those of the corresponding complexes of TPA and 6-Me substituted derivatives, (Table 3.1). Whereas $[Fe(TPA)(CH_3CN)_2]^{2+}$ is low spin the introduction of only one 6-Me pyridyl substituent as in $[Fe(6\text{-}MeTPA)(CH_3CN)_2]^{2+}$ is enough to switch the complex to the high spin form.

Table 3.1: ^{1}H NMR spectral parameters for the low and high spin iron(II) complexes of TPA and 6-substituted TPA derivatives (determined in CD_3CN).[19]

Complex	CH_2-N-	α-H	β,β'-H	γ-H	α-X
$[Fe(L_{15})(CH_3CN)_2]^{2+}$	86	-	47, 43	5	41 (-CH_2O-) 31 (-OCH_3)
$[Fe(L_{16})(CH_3CN)_2]^{2+}$	84	-	50, 43	~3	36 (-CH_2O-) 34 (-O**H_2**C_7H_{15}-n)
$[Fe(6\text{-}Me_3TPA)(CH_3CN)_2]^{2+}$ *	83	-	49, 54	-5	-28 (CH_3)
$[Fe(6\text{-}Me_2TPA)(CH_3CN)_2]^{2+}$ *	92 86, 75	106 -	56, 59 52, 57	-11 -6	 -25 (CH_3)
$[Fe(6\text{-}MeTPA)(CH_3CN)_2]^{2+}$ *	88 82, 37	95 -	48, 52 50, 51	-7 -6	 -24 (CH_3)
$[Fe(TPA)(CH_3CN)_2]^{2+}$ * (low spin)	6.3	10.9	8.5, 8.4	7.3	-

3.2.6.3. ^{19}F NMR study of $[Fe(L_{15})(CH_3CN)_2](O_3SCF_3)_2$ in CD_3CN.

In the above formulae it is assumed that the trifluoromethane counter anions are uncoordinated with the octahedral iron(II) coordination sphere completed by two molecules of CH_3CN. Britovsek et al[34] have shown that ^{19}F NMR provides a convenient method of ascertaining the presence of coordinated $CF_3SO_3^-$ groups. Using BPMEN complexes of iron(II) Britovsek et al showed that in non-coordinating solvents such as CD_2Cl_2 the ^{19}F NMR chemical shift of $CF_3SO_3^-$ occurs around +20 ppm, indicative of coordination to the iron(II) centre. However in coordinating solvent such as CD_3CN the chemical shift now appears around -80 ppm indicating free (uncoordinated) $CF_3SO_3^-$. The ^{19}F NMR spectra of a solution of $[Fe(L_{15})(CH_3CN)_2](O_3SCF_3)_2$ in CD_3CN, shown in figure 3.16, has a broad feature at ~ -70 ppm. The same resonance was observed from corresponding solutions in CD_2Cl_2. Figure 3.17 It is concluded that in both solvents the two trifluoromethane sulfonate $CF_3SO_3^-$ ions have been replaced in the iron(II) coordination sphere by CH_3CN (either from solvent or

the starting salt) and so the formula $[Fe(L_{15})(CH_3CN)_2]^{2+}$ for the solution species is assumed correct. Althought, since the ^{19}F NMR spectrum in CD_2Cl_2 reveleals uncoordination of the $CF_3SO_3^-$ ions, it could be also possible that the octanoxy oxygen atom is coordinated to the iron centre.

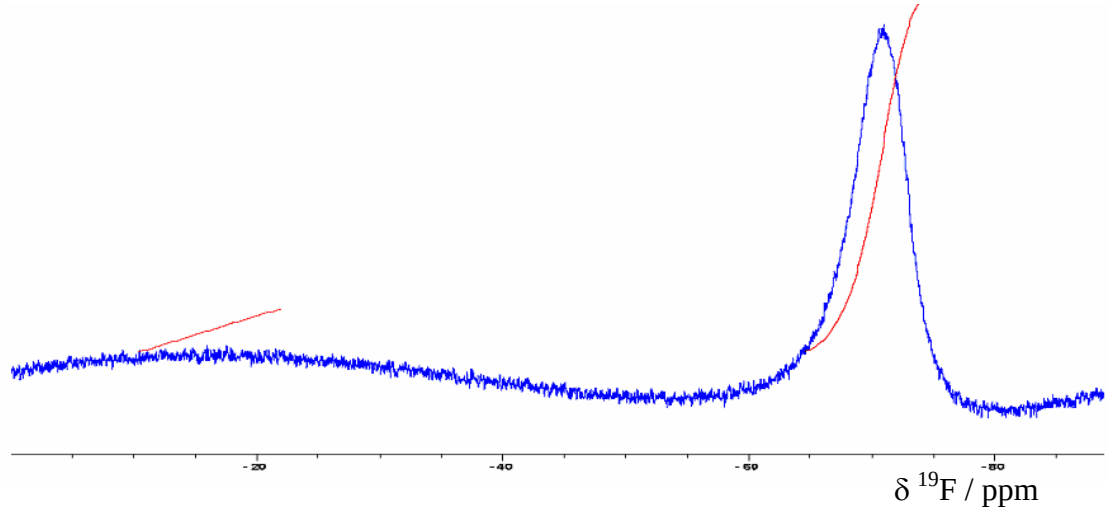

Figure 3.16: ^{19}F NMR spectrum of $[Fe(L_{15})(CH_3CN)_2](O_3SCF_3)_2$ in CD_3CN

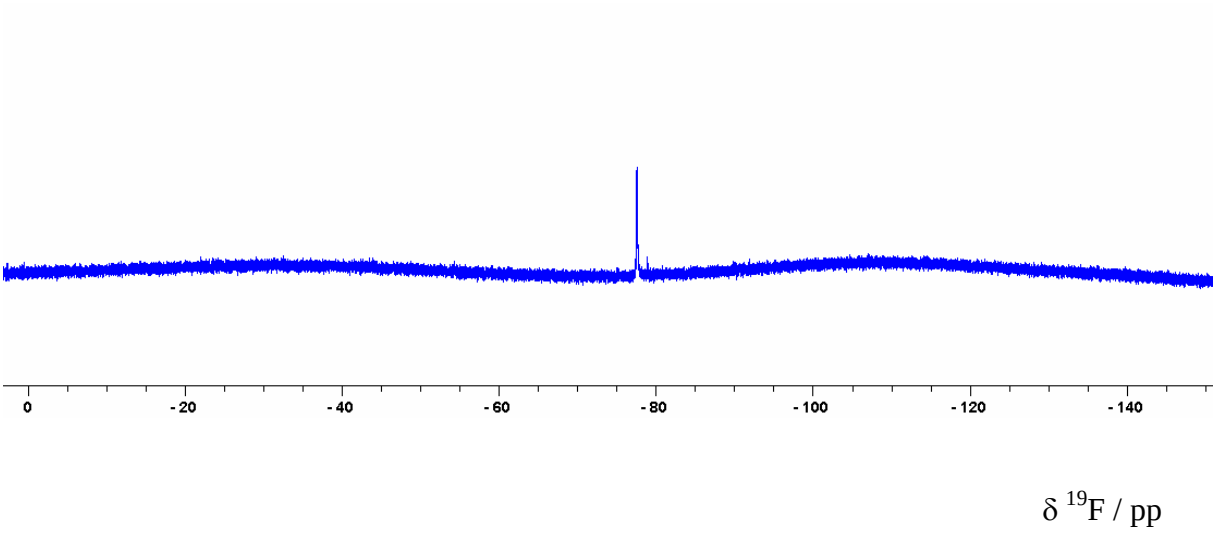

Figure 3.17: ^{19}F NMR spectrum of $[Fe(L_{15})(CH_3CN)_2](O_3SCF_3)_2$ in CD_2C1_2

3.3. Experimental

3.3.1 Instrumental and General Techniques:

NMR spectra were recorded on a Bruker Advance 300 spectrometer (^{1}H 300 MHz, ^{13}C 75.4 MHz. Mass spectra were acquired on a Water's 2795 HPLC with Micromass LCT equipped with a "lock spray" for accurate mass measurements.

3.3.2. Materials and Chemicals:

All chemicals were purchased and used as received from Sigma-Aldrich. DMF and CH_3CN were both dried over CaH_2 overnight followed by distillation. $[Fe(SO_3CF_3)_2(CH_3CN)_2]$ was prepared by reacting Fe metal and anhydrous CF_3SO_3H in acetonitrile followed, attempt to recrystalize in diethyl ether failed. The title compound was obtained as a yellow pale solid in the ethereal solution. The parent TPA ligand, tris(2-pyridylmethyl)amine was synthesized according to a literature procedure[34]. $[Fe(TPA)(SO_3CF_3)_2]$ was synthesized as described by Diebold and Hagen.[15] ^{1}H NMR (CD_3CN), 300 MHz): 11.59 (br s, 3H, $H_{\alpha(pyr)}$), 8.80 (s, 3H, $H_{\beta/\beta'(pyr)}$), 8.70 (s, 3H, $H_{\beta/\beta'(pyr)}$), 7.34 (t, J = 7.5 Hz, 3H, $H_{\gamma(pyr)}$), 6.75 (s, 6 H, CH_2). ^{19}F NMR (CD_3CN), 282 MHz): -79.50 (s,6 F)

3.3.3. Synthesis of Tris-(6-methoxymethyl-2-pyridylmethyl)amine, L_{15}

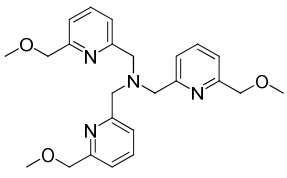

To a solution of NaH (0.339 g, 14.13 mmol) in DMF (15 cm^3) was added a solution of H_3L_{11} (1.3775 g, 3.625 mmol) at 0ºC. The mixture was stirred at 0ºC for 1 h. 1-iodomethane (0.877 cm^3, 14.3 mmol) was then added and the reaction mixture allowed to warm up to room temperature and stirred for 36h. The reaction was quenched by adding 20 cm^3 of water. The

organic phase was extracted with diethyl ether (3x 20 cm^3). The combined extracts were evaporated to give a brown yellow oil which was purified by chromatography (eluent CH_2Cl_2/ MeOH, 95:5) to yield a yellow oil (yield 1.0378 g, 67.84%).

^1H NMR (400.13 MHz, $CDCl_3$, 298 K) δ_H (ppm) = 3.39 (9H, s, $3CH_3$), 3.81 (6H, s, $3CH_2$), 4.78 (6H, s, $3CH_2$), 7.20 (3H, d, $^3J_{HH}$ = 7.7 Hz, 3 H of C_5H_3N), 7.45 (3H, d, $^3J_{HH}$ = 7.8 Hz, 3 H of C_5H_3N), 7.59 (3H, t, $^3J_{HH}$ = 7.7 Hz, 3 H of C_5H_3N)**.** ^{13}C-{^1H} NMR (75.45 MHz, $CDCl_3$, 298 K) δ_C (ppm) = 59.19, 60.57, 119.87, 121.63, 137.44, 158.11, 159.47 MS: ES+: m/z: 423.24 [(M $Cl^+)^+$ 100%]**.**

3.3.4. Synthesis of Tris-(6-n-octyloxymethyl-2-pyridylmethyl)amine, L_{16}

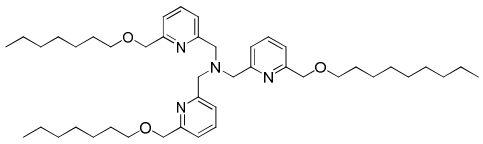

To a solution of NaH (0.2848g, 11.8 mmol) in DMF (15 cm^3) was added a solution of H_3L_{11} (chapter 2) (1g, 2.62 mmol) at 0ºC. The mixture was stirred at 0ºC for 1 h. 1-bromooctane (2.045 cm^3, 11.8 mmol) was then added and the reaction mixture allowed to warm up to room temperature and stirred for 36h. The reaction was quenched by adding 20 cm^3 of water. The organic phase was extracted with diethyl ether (3 x 20 cm^3). The combined extracts were evaporated to give brown-yellow oil which was purified by chromatography (eluent CH_2Cl_2/ MeOH, 95:5) to give a yellow oil, (yield 1.876 g, 72.23%).

^1H NMR (300.06 MHz, $CDCl_3$, 298 K), δ_H = 0.80 (9H, t, $3CH_3$), 1.19 (10H, m, $5CH_2$), 1.56 (6H, quin, $3CH_2$), 3.46 (6H, t, $3CH_2O$), 3.79 (6H, s, $3CH_2$), 4.52 (6H, s, $3CH_2$), 7.22 (3H, d, $^3J_{HH}$ = 7.5 Hz, 3 H of C_5H_3N), 7.43 (3H, d, $^3J_{HH}$ = 7.7 Hz, 3 H of C_5H_3N), 7.59 (3H, t, $^3J_{HH}$ = 7.7 Hz, 3 H of C_5H_3N)**.** ^{13}C-{^1H} NMR (75.45 MHz, $CDCl_3$, 298 K) δ_C**=** 14.50, 23.05, 26.57, 29.65, 29.85, 30.15, 32.22, 60.53, 71.63, 74.14, 119.74, 121.51, 137.39, 158.75, 159.24, CHN

microanalysis: theoretical C 75.37 %, H 10.12 %, N 7.813 %, obtained C 74.24 %, H 10.70 %, N 8.03 %, MS: ES+: m/z: 739 [$(M+Na)^+$ 100%]**.**

3.3.5. Synthesis of $[Fe(L_{15})(CH_3CN)_2](ClO_4)_2$. ($C_{16}$)

CAUTION: Perchlorate salts of metal complexes with organic ligands are potentially explosive and should be handling with care.

A 2 cm^3 solution of L_{15} (0.1g, 1.39 mmol) in CH_3CN was added under nitrogen gas to a pale-yellow solution of $[Fe(H_2O)_6](ClO_4)_2$ (0.035 g, 1.39 mmol) in CH_3CN (2 cm^3) yielding a reddish-orange solution. The reaction mixture was stirred for 3 h. The solvent was evaporated to yield reddish-orange oil. Attempts to obtain crystals suitable for X-ray analysis were unsuccessful. A similar method was used to prepare (C_{17}) the iron(II) perchlorate complex of L_{16} when again a reddish-orange oil was obtained.

3.3.5. Synthesis of $[Fe(CH_3CN)_2(O_3SCF_3)_2]$.

The $[Fe(CH_3CN)_2(O_3SCF_3)_2]$ iron salts was prepared following the reported method.[30]

To a mixture of (5.58 g, 100 mmol) of finely divided powder in dry CH_3CN was added carefully (32 g, 210 mmol) of triflic acid. The reaction is very exothermic. The flask was fitted with a cold finger, and after the initial effervescence subsided (about 1 hour), warmed to 60 ºC. When the effervescence has stopped, the unreacted iron was removed by filtration through a celite pad. The volume of the solution was condensed to approximately 80 ml under vacuum. Although cooling the pale green solution to -25 ºC overnight we were not successful at growing crystals. As reported in the literature, after evaporation of the solvent under vacuum. A pale yellowish solid was obtained. (10.6g, 24.3%).

3.3.6 Synthesis of $[Fe(L_{15})(CH_3CN)_2](CF_3SO_3)_2$. ($C_{18}$)

A 2 cm^3 solution of L_{15} (0.250, 0.349 mmol) in THF was added under nitrogen gas to a pale yellow solution of $[Fe(CH_3CN)_2(O_3SCF_3)_2]$ (0.1522 g, 0.349 mmol) in THF (2 cm^3) yielding a reddish-orange solution. The reaction mixture was stirred for 12 h. The solvent was evaporated to yield reddish-orange oil. Attempts to obtain crystals suitable for X-ray analysis were unsuccessful. A similar method was used to prepare an iron(II) triflate complex of L_{16} when again a reddish-orange oil was obtained.

3.3.7. Synthesis of iron(II) complexes of L_{15} and L_{16} for ^{1}H NMR studies.

Here the iron triflate complexes of L_{15} and L_{16} were prepared *in-situ* in both CD_3CN and CD_2C1_2.

3.3.8. $[Fe(L_{15})(CH_3CN)_2](CF_3SO_3)_2$ in CD_3CN.

A 3 cm^3 solution of L_{15} (0.025 g, 0.0349 mmol) in CD_3CN was added under a nitrogen atmosphere to a pale yellow solution of $[Fe(CH_3CN)_2(O_3SCF_3)_2]$ (0.01522 g, 0.0349 mmol) in CD_3CN (3 cm^3) to yield a reddish-orange solution. 1 cm^3 of this mixture was then transfer under nitrogen into a 5 mm o.d. NMR tube.

3.3.9. $[Fe(L_{15})(CH_3CN)_2](CF_3SO_3)_2$ in CD_2C1_2.

A 3 cm^3 solution of L_{15} (0.025 g, 0.0349 mmol) in CD_2Cl_2 was added under a nitrogen atmosphere to a pale yellow solution of $[Fe(CH_3CN)_2 (O_3SCF_3)_2]$ (0.01522 g, 0.0349 mmol) in CD_2Cl_2 (3 cm^3.) yielding a reddish-orange solution. 1 cm^3 of this mixture was then transfer under nitrogen into a 5 mm o.d. NMR tube.

3.3.10. $[Fe(L_{16})(CH_3CN)_2](CF_3SO_3)_2$ in CD_3CN.

A 3 cm^3 solution of L_{16} (0.0147 g, 0.0349 mmol) in CD_3CN was added under a nitrogen atmosphere to a pale yellow solution of $[Fe(CH_3CN)_2(O_3SCF_3)_2]$ (0.01522 g, 0.0349 mmol) in CD_3CN (3 cm^3) to yield a reddish-orange solution. 1 cm^3 of this mixture was then transfer under nitrogen into a 5 mm o.d. NMR tube.

3.3.11. $[Fe(L_{16})(CH_3CN)_2](CF_3SO_3)_2$ in CD_2C1_2.

A 3 cm^3 solution of L_{16} (0.0147 g, 0.0349 mmol) in CD_2Cl_2 was added under a nitrogen atmosphere to a pale yellow solution of $[Fe(CH_3CN)_2(O_3SCF_3)_2]$ (0.0152 g, 0.0349 mmol) in CD_2Cl_2 (3 cm^3.) yielding a reddish-orange solution. 1 cm^3 of this mixture was then transfer under nitrogen into a 5 mm o.d. NMR tube.

3.4. Summary and Conclusions.

Two new derivatives of TPA have been synthesized and characterised and their corresponding iron(II) complexes characterised by paramagnetic ^{1}H and ^{19}F NMR spectroscopy in CD_3CN and CD_2C1_2 solution. Attempts to obtain crystals suitable for X-ray analysis were unsuccessful and only reddish-orange oils were obtained. ^{19}F NMR spectroscopy confirmed that the $CF_3SO_3^-$ ions in the triflate complexes are not coordinated to iron(II) with the remaining two coordination sites occupied by acetonitrile molecules as observed previously in the cases of iron(II) complexes of TPA, 6-MeTPA, 6-Me_2TPA, 6-Me_3TPA and BPMEN. The synthesis and characterisation of $[Fe(L_{15})(CH_3CN)_2]^{2+}$ with a simpler 6-methoxymethyl-pyridine substituent helped in the assignment of the paramagnetic resonances for the 6-n-octyloxymethyl-pyridine complex $[Fe(L_{16})(CH_3CN)_2]^{2+}$, confirmed by a 2D COSY experiment which in turn identified the upfield shifted γ proton of the pyridine. The iron(II) complexes were exclusively high spin with no evidence from variable temperature NMR studies of a Spin-Crossover equilibrium. A degree of spontaneous decomposition is apparent in the paramagnetic NMR spectra of the two iron(II) complexes in CD_3CN at RT with the presence of diamagnetic resonances for free or decomposed (modified) ligand.

The catalytic activity of both $[Fe(L_{15})(CH_3CN)_2]^{2+}$ and $[Fe(L_{16})(CH_3CN)_2]^{2+}$ towards H_2O_2 oxygenation on alkane substrates is explored in chapter 5 along with a detailed X-band EPR spectroscopy investigation at low temperature (100K) of the reaction products obtained from treatment of both $[Fe(L_{15})(CH_3CN)_2]^{2+}$ and $[Fe(L_{16})(CH_3CN)_2]^{2+}$ separately with H_2O_2 and t-BuOOH in CH_3CN solvent.

.

A different method for attaching 6-peralkyl and ultimately 6- perfluoroalkyl substituents to TPA, which it is hoped could lead to potentially more oxidatively-robust iron complexes, is now explored in chapter 4.

3.5. References

1. H. Masuda, K. Jitsukawa, *JP Pat.*, 2000319291, 2000.
2. Y. Zang, J. Kim, C. Kim, L. Que, Jr. *US Pat.*,9748710, 1997.
3. L. Que, Jr., R. S. Twisker, R. M. Hermant, M. Lubben, B. L. Feringa. EP *Pat.*,9534628, 1995.
4. R. A. Leising, R. E. Norman and L. Que, Jr., *Inorg. Chem.*, 1990, **29**, 2553-2555.
5. A. Bassan, M. R. A. Blomberg, P. E. M. Siegbahn and L. Que, Jr., *Angew. Chem., Int. Ed.*, 2005, **44**, 2939-2941.
6. M. Costas, M. P. Mehn, M. P. Jensen and L. Que, Jr., *Chem. Rev. (Washington, DC, U. S.)*, 2004, **104**, 939-986.
7. M. Costas, M. Ray and L. Que, Jr., *Book of Abstracts, 219th ACS National Meeting, San Francisco, CA, March 26-30, 2000*, 2000, INOR-553.
8. H.-F. Hsu, Y. Dong, L. Shu, V. G. Young, Jr. and L. Que, Jr., *J. Am. Chem. Soc.*, 1999, **121**, 5230-5237.
9. J. Kim, R. G. Harrison, C. Kim and L. Que, Jr., *J. Am. Chem. Soc.*, 1996, **118**, 4373-4379.
10. H.-C. Liang, M. Dahan and K. D. Karlin, *Curr. Opin. Chem. Biol.* 1999, **3**, 168-175.
11. K. D. Karlin, S. Kaderli and A. D. Zueberbuehler, *Acc. Chem. Res.* 1997, **30**, 139-147.
12. K. D. Karlin, D.-H. Lee, H. V. Obias and K. J. Humphreys, *Pure Appl. Chem.* 1998, **70**, 855-862.
13. P. A. Goodson, A. R. Oki, J. Glerup and D. J. Hodgson, *J. Am. Chem. Soc.*, 1990, **112**, 6248-6254.
14. J. E. McGrady and R. Stranger, *J. Am. Chem. Soc.*, 1997, **119**, 8512-8522.
15. A. Diebold and K. S. Hagen, *Inorg. Chem.* 1998, **37**, 215-223.

16. L. Que, Jr. and R. Y. N. Ho, *Chemical Reviews (Washington, D. C.)*, 1996, **96**, 2607-2624.

17. L. Que, Jr. and Y. Dong, *Acc. Chem. Res.*, 1996, **29**, 190-196.

18. K. Chen and L. Que, Jr., *J. Am. Chem. Soc.*, 2001, **123**, 6327-6337.

19. Y. Zang, J. Kim, Y. Dong, E. C. Wilkinson, E. H. Appelman and L. Que, Jr., *J. Am. Chem. Soc.*, 1997, **119**, 4197-4205.

20. S. Ogo, S. Wada, Y. Watanabe, M. Iwase, A. Wada, M. Harata, K. Jitsukawa, H. Masuda and H. Einaga, *Angew. Chem., Int. Ed.*, 1998, **37**, 2102-2104.

21. *Cytochrome P-450: Structure, Mechanism and Biochemistry*, Plenum Press, New York, 1995.

22. R. Neumann and M. Cohen, *Angew. Chem., Int. Ed. Engl.*, 1997, **36**, 1738-1740.

23. K. Neimann, R. Neumann, A. Rabion, R. M. Buchanan and R. H. Fish, *Inorg. Chem.*, 1999, **38**, 3575-3580.

24. M. Contel, C. Izuel, M. Laguna, P. R. Villuendas, P. J. Alonso and R. H. Fish, *Chem.--Eur. J.* 2003, **9**, 4168-4178.

25. P. W. N. M. van Leeuwen, *Homogeneous Catalysis: Understanding the Art*, 2004.

26. P. W. N. M. Van Leeuwen, C. Claver and Editors, *Rhodium Catalyzed Hydroformylation. [In: Catal. Met. Complexes, 2000; 22]*, 2000.

27. J. Gerencser, N. Bathori, M. Czugler, P. Huszthy and M. Nogradi, *Tetrahedron: Asymmetry*, 2003, **14**, 2803-2811.

28. M. Ying, F. Jiang, H. Wei, X. Meng, X. Yu and X. Zeng, *J. Dispersion Sci. Technol.* 2006, **27**, 15-21.

29. D. Banti, E. Groaz and M. North, *Tetrahedron*,2004, **60**, 8043-8052.

30. K. S. Hagen, *Inorg. Chem.* 2000, **39**, 5867-5869.

31. Y.-M. Chiou and L. Que, Jr., *J. Am. Chem. Soc.*, 1995, **117**, 3999-4013.

32. J. England, G. J. P. Britovsek, N. Rabadia and A. J. P. White, *Inorg. Chem. (Washington, DC, U. S.)*, 2007, **46**, 3752-3767.

33. K. Chen, M. Costas and L. Que, Jr., *Journal of the Chemical Society, Dalton Transactions*, 2002, 672-679.

34. G. J. P. Britovsek, J. England and A. J. P. White, *Inorg. Chem.* 2005, **44**, 8125-8134.

Chapter 4

Synthesis and Characterisation of Mono and Bis(6-(n-hexylureyl)pyridine) Derivatives of TPA: Building Blocks to Superior Hydrophobic Iron-Based Catalysts for the 1-Oxygenation of n-Alkanes.

4.1. Introduction

In chapter 3 the synthesis and characterisation of high spin iron(II) complexes of two O-alkylated derivatives of tris(6-hydroxymethyl-2-pyridylmethyl)amine (H_3L_{11}) was described. The n-octyloxymethylpyridine derivative (L_{16}) was synthesized to examine the effect of creating a putative 8 carbon hydrophobic channel above the active iron-hydroperoxo centre towards the catalysis of regioselective 1-oxygenation of n-alkane substrates using H_2O_2 and it will be examined in chapter 5. While synthetically L_{16} and its simpler methoxymethyl counterpart L_{15} were readily synthesized via alkylation of the alkoxide of H_3L_{11} the presence of a reactive benzylic methylene group adjacent to the active iron site makes these TPA derivatives potentially prone to oxidative degradation. This became apparent upon monitoring the ^{1}H NMR spectra of the high spin iron(II) species over time. Masuda at al have reported the synthesis of another family of iron-TPA derivatives which contain alkylated amide/amine groups attached at the 6-position. The initial driving force for synthesizing these was to model the active site of iron dependent non-heme monooxygenase enzymes such as soybean lipoxygenase-1 (SLO-1). Lipoxygenases (LOs) are found in animals and plants and catalyze the regiospecific and stereospecific hydroperoxidation of 1,4-*Z*,*Z*-pentadiene-containing polyunsaturated carboxylic acids such as linoleic and linolenic acids, important species on the biosynthetic path to plant growth hormones and other products aiding response to infection.[1-4] The X-ray crystal structures of several soybean lipoxygenases have been determined. Each one sharing a common high spin iron(II) centre, in a distorted octahedral geometry.[5-9] The iron(II) centre is coordinated by three imidazoles from histidine, a carboxylate from the C-

terminal isoleucine, a carboxamidato carbonyl oxygen from asparagine and a single water molecule.[5-9] In the catalytic cycle of SLO-1, the proposed active species consists of an iron(III) centre coordinated to a hydrogen-bonded hydroxide ligand, figure 4.1, termed ferric-SLO.[5]

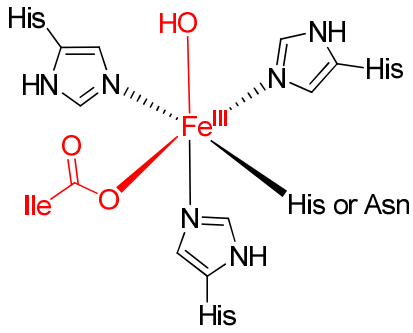

Figure 4.1: Schematic representation of the active ferric form of SLO-1

A number of mononuclear six-coordinate iron(III) complexes with oxygen donor ligands such as methoxo, ethoxo, carboxylato or carboxamidato, and several dinuclear iron(III) complexes with terminal or bridging hydroxo ligands have been characterized as possible models for ferric SLO.[6-11] Of these only one structural model containing a mononuclear iron(III) centre coordinated to a hydrogen-bonded terminal hydroxo ligand has been structurally characterized, $[Fe(TNPA)(PhCO_2)(OH)]ClO_4$**,** figure 4.2a.[5] The similarities to the active site of ferric-SLO are clear. The iron complex $[Fe(TNPA)(PhCO_2)(OH)]ClO_4$ has also been characterized by UV/VIS and EPR spectroscopy and by electrospray ionization mass spectrometry (ESI-MS). In related work Masuda et al also reported a thermodynamically stable iron(III) complex with an alkylperoxide ligand attached in an end-on fashion, whose spectral behaviour was moreover comparable to that of the 'purple' form of SLO-1.[12-15,16]

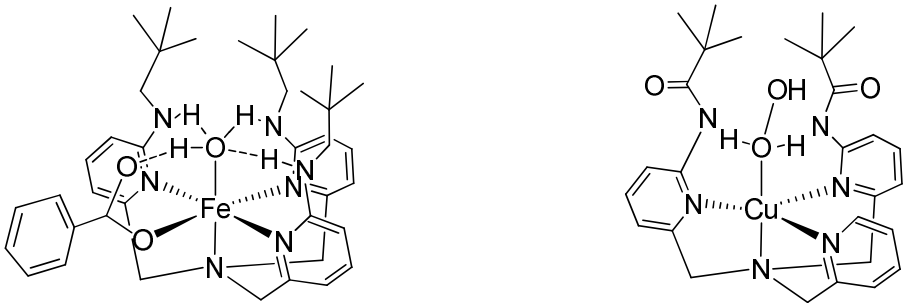

Figure 4.2: Schematic representation of (**a**) [Fe(TNPA)($PhCO_2$)(OH)](ClO_4) (model for SLO-1) and (**b**) [Cu(BPPA)(OOH)](ClO_4). TNPA = tris(6-neopentylamino-2-pyridylmethyl)amine, (L_{17}); BPPA = bis(6-pivaloylamido-2-pyridylmethyl)-2'-pyridylmethylamine, (L_{18}).

The LCu(II)-OH and LCu(II)-OOH(R) complexes (L_{18} = bis(6-pivaloylamido-2-pyridylmethyl)-2'-pyridylmethylamine (BPPA)) have also been synthesized, figure 4.2b.[17, 18] An interesting feature of both complexes is the hydrogen-bonding from the amine/amido N-H groups to the hydroxo/hydroperoxo ligand which results in the t-butyl substituents all pointing upwards above the metal coordination centre.[12-15, 19] Thus one could envisage replacing the neopentyl groups in figure 4.2a with long peralkyl chain substituents in order to create a hydrophobic channel which would moreover self-assemble around the iron(III) centre via hydrogen-bonding to a bound H_2O_2 ligand. Finally, 6-amine/amido substituents attached to pyridine should be more oxidatively robust compared to the benzylic methylenes present in ligands L_{15} and L_{16} (chapter 3). This is an important consideration in the ligand design for a powerful oxidation catalyst.

Finally, in considering the optimum spacer group for attaching the peralkyl substituents at the three 6-py positions of TPA the use of a *urea* group has particular attractions. Borovik and co-workers have reported the reaction of t-butyl isocyanate with tren (tris(aminoethyl)amine) to give tris(t-butylureylethyl)amine (TBUA) (L_{10}), which in the

presence of a strong base (NaH) combines with iron(II) under oxidative conditions to give the first structurally characterised mononuclear iron(III) complex attached to a single terminal oxo ligand, figure 4.3.[20] Strong hydrogen-bonding from the urea N-H groups to the oxo ligand is an important feature in stabilising this moiety. It is believed that initial formation of a high valent iron(IV) or iron(V) species is followed by reduction back to iron(III). Although one could envisage the iron(III) centre in [(H_{-3}TBUA)Fe^{III}=O] as Fe(III)-O^{2-} or Fe(III)-OH_2 hydrogen-bonded to two doubly-deprotonated urea groups the unusually short Fe(III)-O distance suggests an assignment to the former Fe(III)=O^{2-} representation.[20]

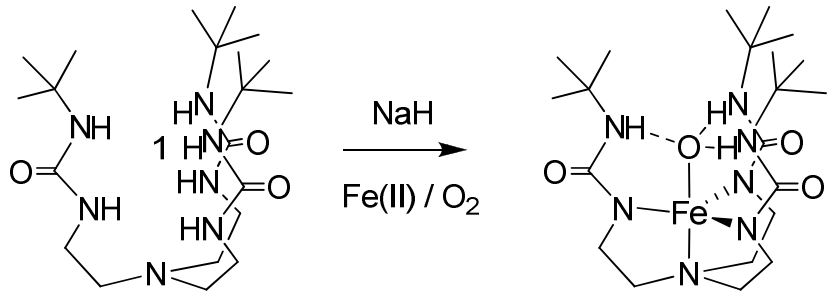

Figure 4.3: Schematic representation of the formation of [(H_{-3}TBUA)Fe^{III}=O] in the presence of a strong base (NaH) and O_2.

Our approach here has been to combine the features of the iron complexes of Masuda and Borovik above by synthesizing a new family of iron-TPA complexes with peralkylurea groups attached at the 6-position on each of the three pyridines. These putative ligands possess many of the important features needed for the design of the optimal iron-based n-alkane oxidation catalyst.

(i) Iron-TPA complexes have already demonstrated activity in the catalysis of H_2O_2 oxygenation on various C-H substrates (see chapter 1)

(ii) The binding of OH_2, OH^- or OOH^- to the iron centre will induce strong and effective hydrogen-bonding from the urea groups at the 6-py position

leading to orientation of the peralkyl substituents upwards above the iron centre (self-assembly) thus creating a hydrophobic channel for both solublisation and orientation of the n-alkane substrate to induce C-1 oxygenation.

(iii) Strong hydrogen-bonding from the remote N-H group of the urea will promote heterolytic O-OH cleavage, figure 4.4, of the Fe(III)-OOH precursor facilitating access to formally iron(V) (perferryl) as representing the optimal and most potent catalytic centre for oxidative reaction at the most inert of C-H substrates like n-alkanes.

(iv) Introducing electron-withdrawing hexylurea groups on the pyridine rings should lower the basicity of the pyridine nitrogens contributing to the thermodynamic stabilization of any mononuclear alkylperoxo iron (III) complex.[19]

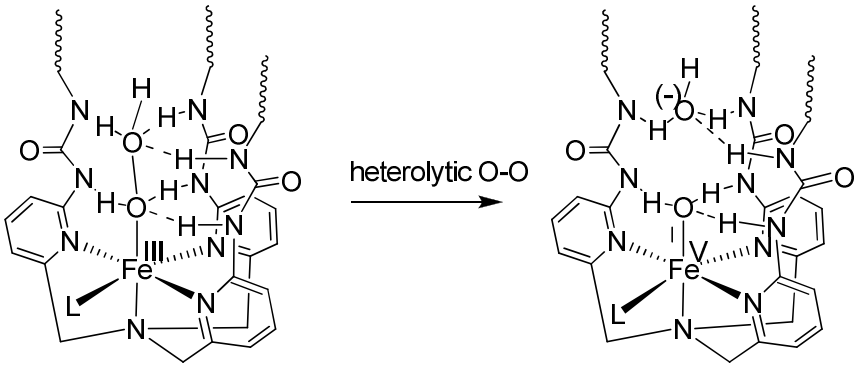

Figure 4.4: Schematic representation of how hydrogen-bonding within a hydroperoxo iron(III) complex of putative tris(6-n-hexylureyl-2-pyridylmethyl)amine could facilitate heterolytic O-O cleavage (abstraction of OH^-) to generate a high valent 'perferryl' iron(V) intermediate.

The use of urea groups might circumvent the behaviour of $[Fe(BPPA)(O_2CBu^t)]^{2+}$ which possesses an interesting seven-coordinated iron centre bound to the four nitrogens of TPA, a

pivalate carboxylate and two amide carbonyls, figure 4.5a. Treatment of $[Fe(BPPA)(O_2CBu^t)]^{2+}$ with ^tBuOOH is believed to give rise to seven-coordinated $[Fe(BPPA)(OOBu^t)]^{2+}$, figure 4.5b, on the basis of retention of the same low field EPR signal, figure 4.5c. $[Fe(BPPA)(OOR)]^{2+}$ is remarkably long lived for a alkylperoxo-iron(III) complex and is reported to persist for 5 h at 25^oC.[21]

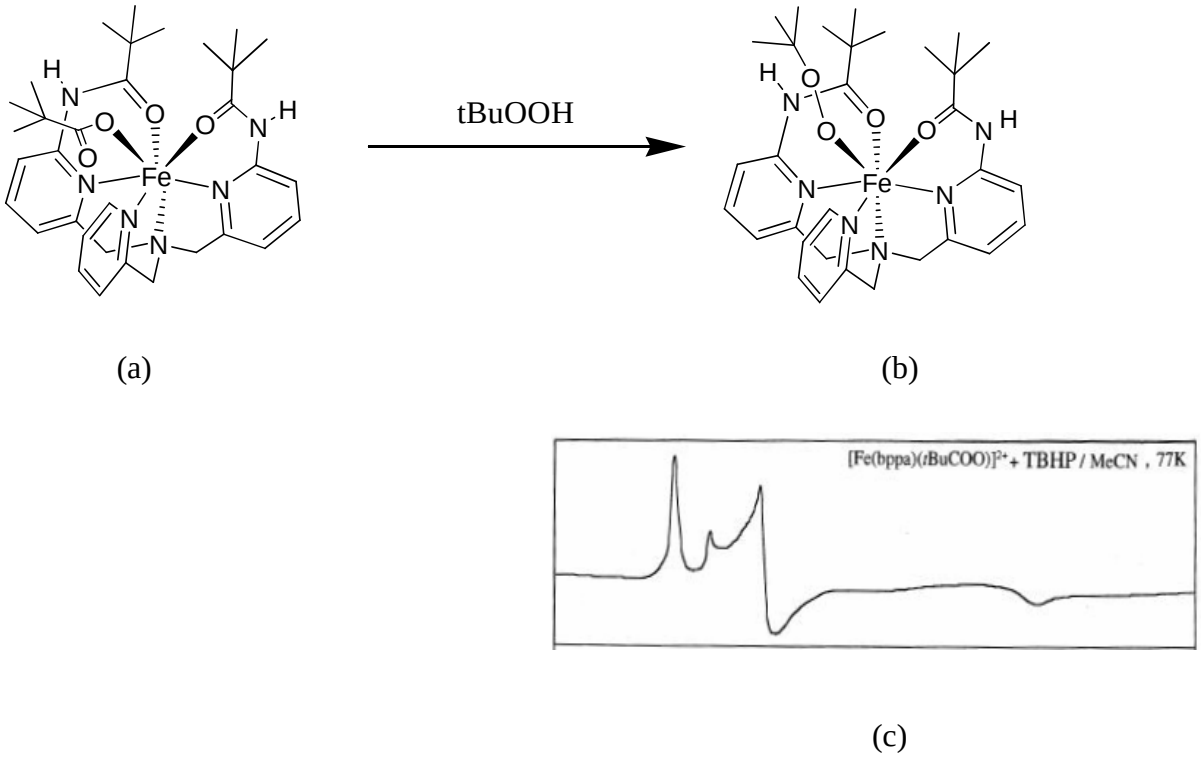

Figure 4.5: (a) Schematic representation of the structure of $[Fe(BPPA)(O_2CBu^t)]^{2+}$; (b) putative $[Fe(BPPA)(OOBu^t)]^{2+}$ and (c) EPR signal from $[Fe(BPPA)(OOBu^t)]^{2+}$ at 77K.

This is believed to be attributable to a degree of electronic and/or steric control by the BPPA ligand.[18] A low field EPR signal, similar to that in figure 4.5(c), is obtained on treating the iron(III) formate complex; $[Fe(BPPA)(O_2CH)]^{2+}$ with H_2O_2.[27] This has been assigned to the seven-coordinated hydroperoxo complex; $[Fe(BPPA)(OOH)]^{2+}$. It was hoped that the use of urea spacer groups could discourage carbonyl binding to iron in favour of hydrogen bonding from both the proximal and remote N-H hydrogens of the urea to bound hydroxo/oxo or hydroperoxo species, see figure 4.4.

There are only brief reports as to the behaviour of iron-BPPA complexes, such as those in figure 4.5, towards oxidation catalysis on C-H substrates. The reactivity towards cyclohexene and cyclohexane in single turnover reactions (high selectivity for hydroxylation over ketonization) is similar to that found in heme iron-based oxidations[22-25] and is not consist with Haber-Weiss[26] or Russell[27] termination radical processes. The reactive species was proposed to be a nucleophilic iron(IV)-oxo based reactant, formulated as (H_2BPPA)Fe(IV)O, deriving from O-O homolysis of a (H_2BPPA)Fe(III)-OOH precursor.[21]

A desirable precursor for the synthesis of a whole range of 6-N-substituted TPA ligands is L_{20} = tris(6-amino-2-pyridylmethyl)amine, figure 4.6, reported by Masuda via hydrolysis of tris(6-pivalamido-2-pyridylmethyl)amine.[28, 29] In the sections below possible new routes to tris(6-amino-2-pyridylmethyl)amine using tris(6-bromo-2-pyridylmethyl)amine

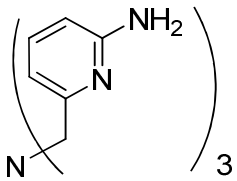

Figure 4.6: Structure of tris(6-amino-2-pyridylmethyl)amine, L_{20}

are described along with the successful synthesis and characterisation of two 6-n-hexylureyl substituted TPA derivatives; L_{21} and L_{22}, figure 4.7. Complexes of L_{21} and L_{22} with iron(II) have been characterised in acetonitrile solution by paramagnetic ^{1}H NMR. The structure of the iron(II) complex of L_{22} has also been characterised by X-ray crystallography. Attempts at making L_{23}, figure 4.7, (unsuccessful to date) are also described.

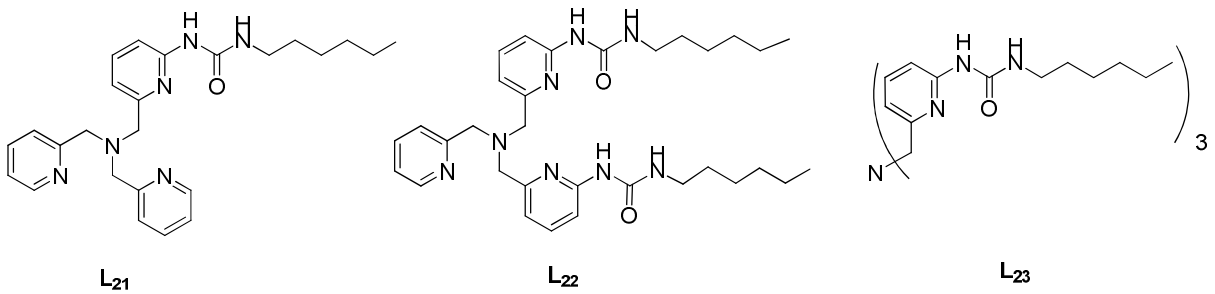

Figure 4.7: Structures of the 6-(n-hexylureyl)-substituted TPA ligands **L_{21} – L_{23}**.

4.2. Results and discussion:

4.2.1. Attempted Synthesis of tris-(6-amino-2-pyridylmethyl)amine L_{20} from tris-(6-bromo-2-pyridylmethyl)amine, L_{24}.

The published route involves acid hydrolysis of tris-(6-pivaloylamino-2-pyridylmethyl)amine.[28,29] However synthesis of this precursor required an NBS radical bromination on 6-pivaloylamino-2-picoline to activate the methyl group followed by a two step amination.[29] However such NBS activated radical brominations on picolines are well documented as favouring preferential reaction on the aromatic ring with monobromination at methyl proceeding only in 10% yield. Although the final amination step involving various 6-N-protected-2-bromomethylpyridines has been recently improved by Berreau et al,[30] using ammonium acetate as ammonium source, potassium carbonate and tetrabutylammonium bromide as phase transfer agent, the problem of obtaining good yields of the 2-bromomethylpyridine precursors remains. Subsequently it was reported that a detectable (usable) yield of radical side chain (methyl) mono-bromination products only results in the case of the 6-N-acetyl or 6-N-pivaloyl-2-picolines.[31] Initial attempts to radical monobromination of the methyl groups of a range of other 6-N-protected amino-2-picolines such as with boc or more desirably n-alkylureyl groups resulted only in ring bromination products.[29] We therefore decided to use a different strategy involving direct amination of the 6-bromoTPA precursor; tris(6-bromo-2-pyridylmethyl)amine. This seemed potentially attractive since the reaction works well for simpler 6-bromopyridine analogues and tris-(6-bromo-2-pyridylmethyl amine is obtainable in very good yield. Moreover it is known that the 6-position can be easily modified for example via Suzuki coupling as reported by Canary et al.[32] Tris(6-bromo-2-pyridylmethyl)amine (L_{24}) is prepared from 2,6-dibromopyridine via monolithiation and reaction with DMF followed by $NaBH_4$ reduction to 6-bromo-2-hydroxymethylpyridine which is then brominated with HBr and finally reacted with ammonium acetate/sodium carbonate to give the TPA. Four methods were then employed for

the direct amination of tris-(6-bromo-2-pyridylmethyl)amine involving (i) potassium in liquid ammonia (KNH_2),[33] (ii) copper-catalyzed reaction with liquid ammonia,[34] and finally (iii) palladium-catalysed reaction with benzophenone imine[35] or (iv) with lithium bis(trimethylsilyl)amide[36] as ammonia equivalents. However, despite repeated attempts, none of these direct amination methods proved successful for the synthesis of tris-(6-amino-2-pyridylmethyl)amine. Therefore, an alternative method to the use of radical bromination for activating the methyl group of a range of 6-N-protected amino-2-picolines was investigated. The method of choice proved to be that reported in 2007 by Berlin et al involving treatment with BuLi to deprotonate the 2-methyl group followed by reaction with dioxygen and reduction of the resulting 6-N-protected-2-hydroperoxomethylpyridine to the 2-hydroxymethylpyridine, O-tosylation and finally amination to the TPA (see below).

4.2.2. Synthesis of [6-(n-hexylureyl)-2-pyridylmethyl)-bis-(2-pyridylmethyl)]amine, L_{21}.

In 2007 a new method for the oxidation of 4-methyl heteroaryls with molecular oxygen was reported by Berlin et al[37] as part of a facile multigram synthesis of 2-[t-butoxycarbonyl)amino]-4-pyridinecarbaldehyde, a versatile pharmaceutical intermediate. This involved conversion of side chain methyl to hydroxymethyl. This, as an alternative to generating a bromomethyl substituent for the final amination step, seemed to be generally applicable to a wide variety of methyl heteroaryls and there was no reason to suppose that it would not proceed in good yield on a variety of 6-N-substituted amino-2-picolines. Following the same strategy, firstly 6-amino-2-picoline **1** is converted into the 6-N-boc and 6-N-n-hexylureyl derivatives with di-tert-butyl dicarbonate or hexyl isocyanate **2** respectively in dry THF. Both of these reactions proceed in good yield and are described briefly below for L_{21}, figure 4.8. The next step was the activation of the methyl group. This is carried out by firstly deprotonating it with butyl lithium at -78° C (3.3 equivalents in the case of the reaction for the N-hexylureyl but only 2.2 equivalents for N-Boc protected to ensure that all NH's are

deprotonated). The efficiency of the reaction at this point was tested by quenching the product with D_2O wherein ^1H NMR revealed evidence of the single deuteration of the methyl group in high yield. Pre-dried molecular oxygen was passed through the -78° C suspension of the trianion wherein the dark orange colour quickly changed to bright yellow.

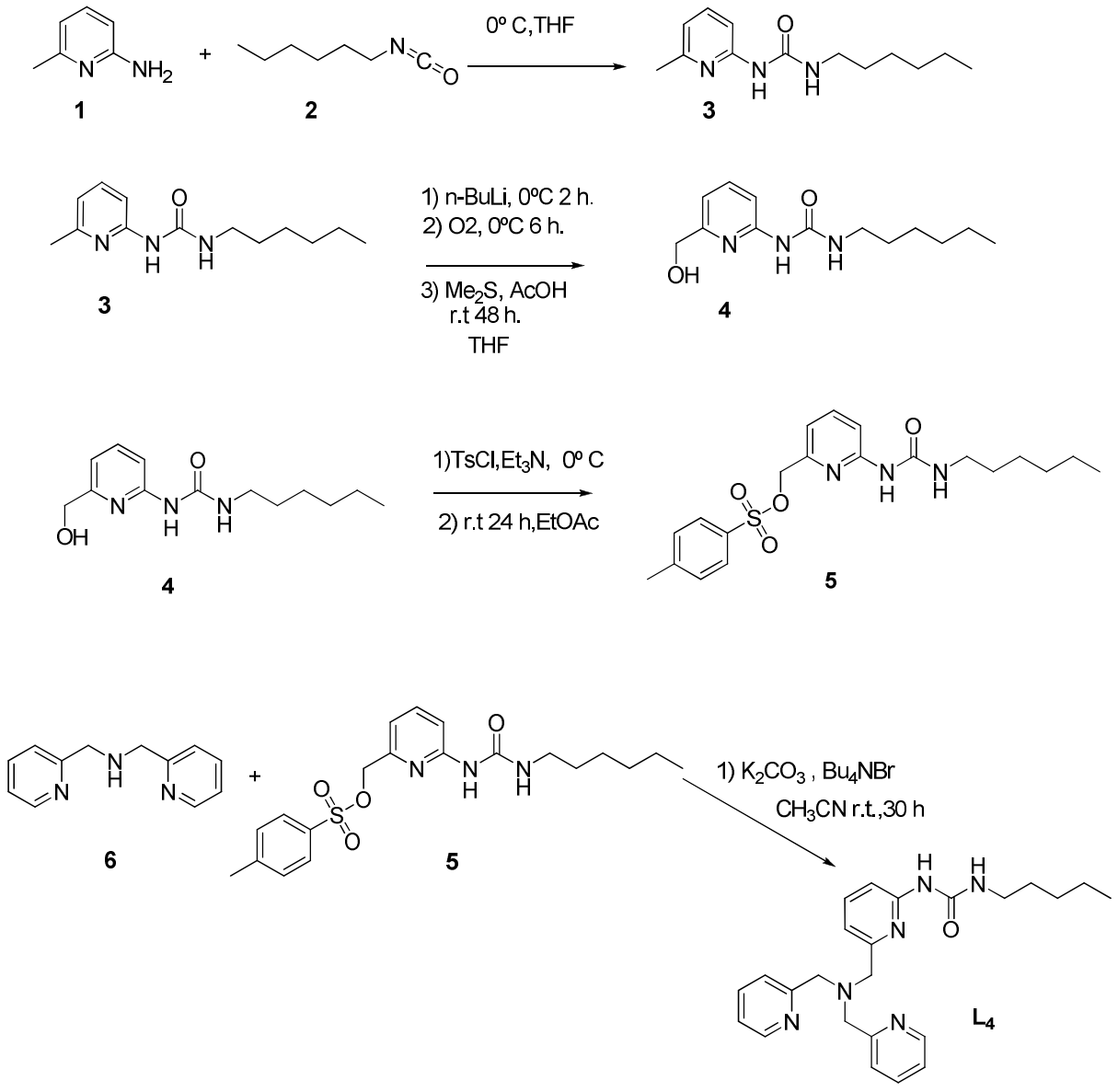

Figure 4.8: Synthesis of [6-(hexylureyl)-2-pyridylmethyl)-bis-(2-pyridylmethyl)]amine, $\mathbf{L_{21}}$

After several hours, the reaction mixture was quenched with two equivalents of acetic acid together with an excess of dimethyl sulfide. The crude mixture was stirred for an additional 48 hours at room temperature since it appeared from TLC that formation of the alcohol **4** via

3, presumed to occur via the hydroperoxide intermediate, was not very complete at this time. The desired alcohol **4** was subsequently isolated in 43 % yield. To activate the alcohol group, it was tosylated with p-toluenesulfonyl chloride in the presence of triethylamine to give **5**, yield 64%. Finally reaction of **5** with 1.1 equivalents of bis(2-picolyl)amine **6** using K_2CO_3 as a base and tetrabutylammonium bromide as a phase transfer agent[30] gave L_{21} as a colourless solid in 19% yield.

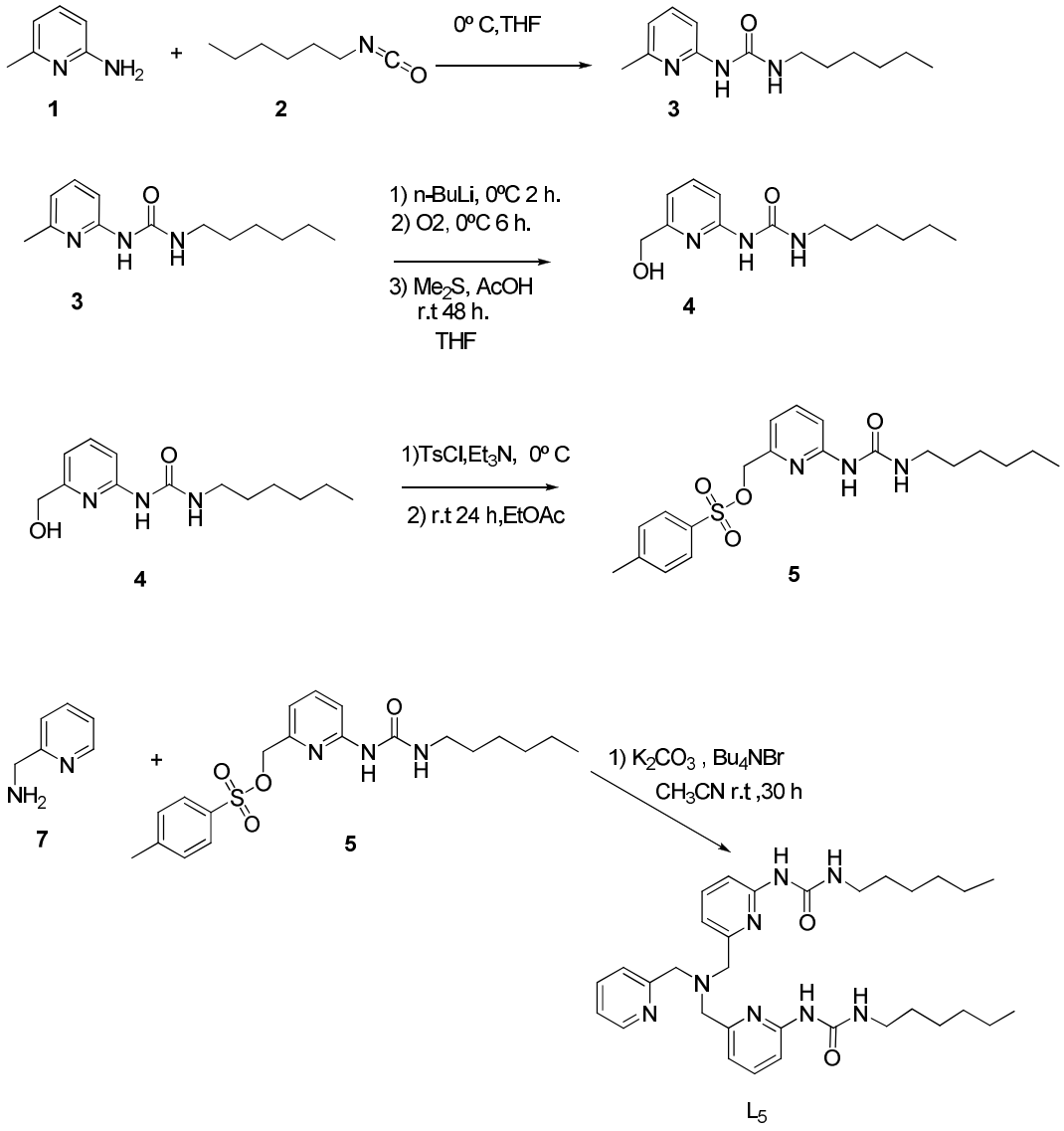

Figure 4.9: Synthesis of [Bis-(6-(hexylureyl)-2-pyridylmethyl)-2-pyridylmethyl]amine, $\mathbf{L_{22}}$

equivalents of **5** with 2-aminomethylpyridine **7** using K_2CO_3 as a base and tetrabutylammonium bromide as a phase transfer agent gave the desired ligand L_{22} as a colourless solid in an overall 48% yield.

4.2.4. Attempted synthesis of Tris-(6-(hexylureyl)-2-pyridylmethyl)amine, L_{23}.

The synthesis of L_6 was attempted before knowledge of Berreau's improved method for amination involving use of ammonia acetate and potassium carbonate with tetrabutylammonium bromide as phase transfer agent. Conversion of the tosylated alcohol **5** into the corresponding tripodal ligand L_6 was thus carried out using a Gabriel Synthesis[29], figure 4.10. Firstly, **5** was treated with potassium phthalimide to give **8**, and afterwards reaction with hydrazine in ethanol under reflux gives **9**. However, reaction between **9** and two equivalents of **5** did not occur probably because of the absence of tetrabutylammonium bromide which appeared to be crucial. Unfortunately, there was not sufficient time available to reinvestigate this reaction in the presence of tetrabutylammonium bromide. Nonetheless, the successful synthesis of L_4 and L_5 has allowed a detailed investigation of the influence of having one or more 6-N-hexylureyl-pyridine substituents on the subsequent properties and catalytic activity of the corresponding iron complexes.

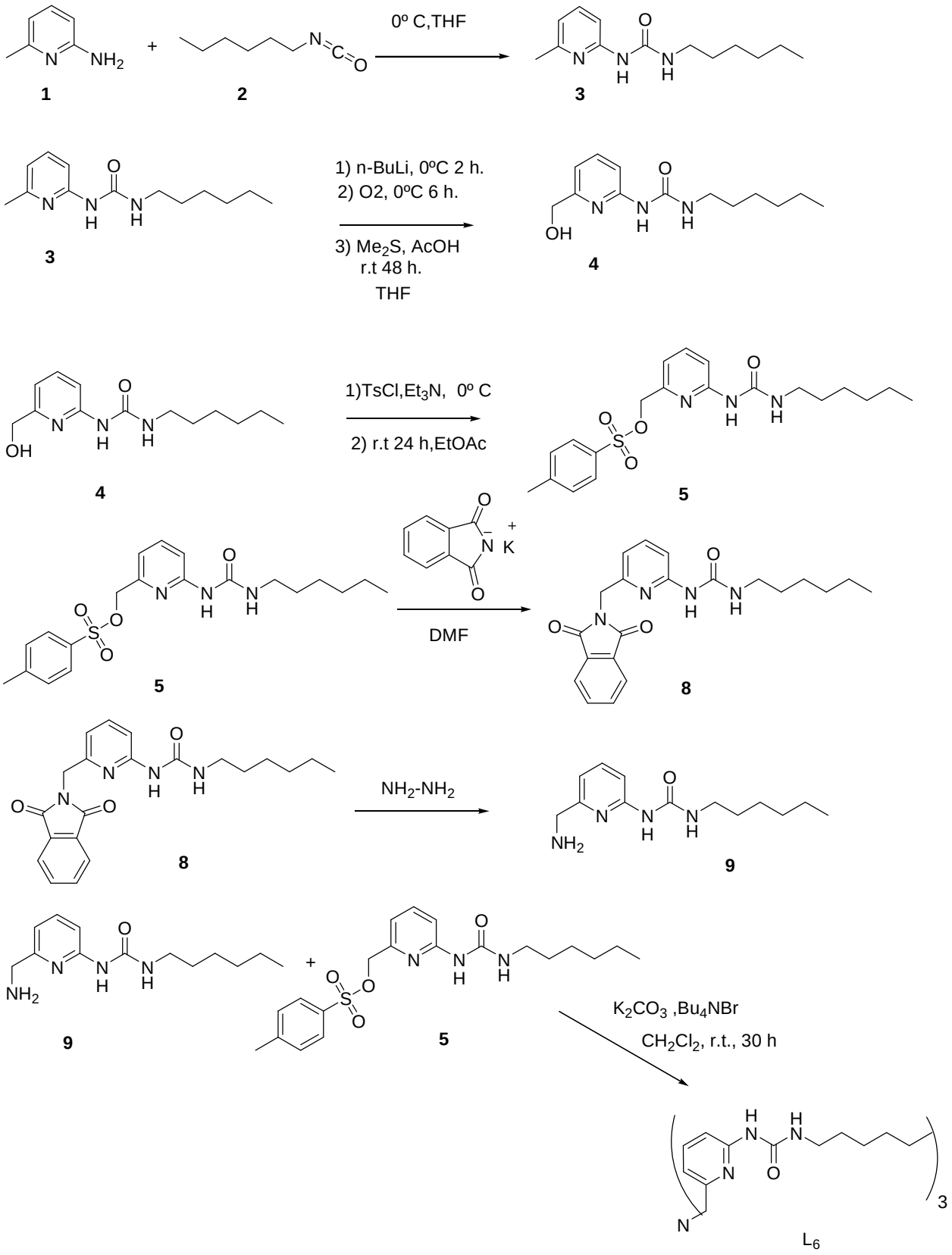

Figure 4.10: Synthetic route to tris-(6-(hexylureyl)-2-pyridylmethyl)amine **L_{23}**

4.3. Synthesis of Iron(II) complexes:

The 6-N-hexylureyl-TPA ligands, L_{21} and L_{22} were each reacted with 1 equivalent of the iron(II) salt; $[Fe(CH_3CN)_2(O_3SCF_3)_2]$ in CH_3CN solvent. The method of vapour diffusion using diethyl ether was employed to grow crystals suitable for X-ray diffraction as described in chapter 2. However only the crystals obtained from the reaction of $[Fe(CH_3CN)_2(O_3SCF_3)_2]$ with L_5 were suitable for X-ray determination.

4.3.1. Reaction of $[Fe(CH_3CN)_2(O_3SCF_3)_2]$ with L_{22}.

An X-ray structure investigation of the crystalline product revealed it to contain the iron(II) bistriflate salt $[Fe(L_{22})](O_2SCF_3)_2$, C_{21}, figure 4.11.

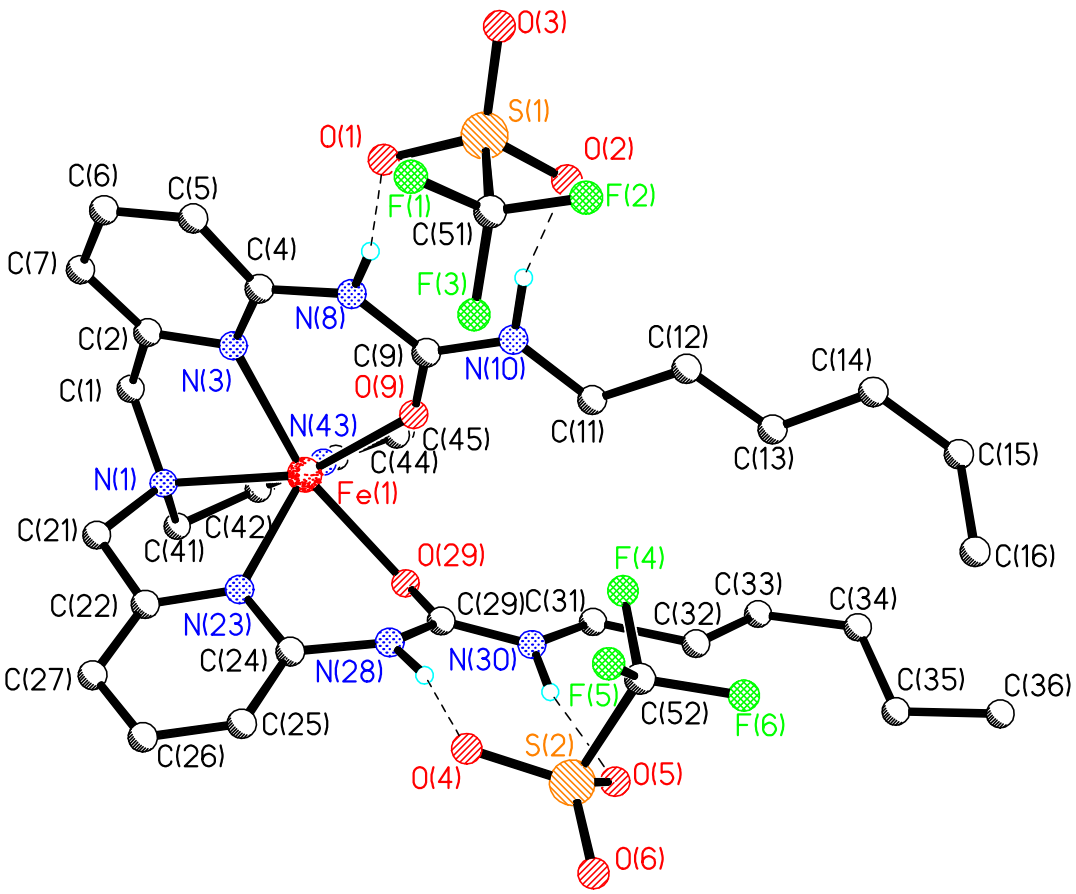

Figure 4.11: Molecular structure of $[Fe(L_{22})](O_3SCF_3)_2$, C_{21}

The iron(II) centre is in a distorted octahedral geometry coordinated to all four nitrogen donors of L_{22}, plus two carbonyl oxygens from the 6-N-hexylureyl substituent. As a result of coordination of the two urea carbonyls to iron(II) the n-hexyl substituents are orientated out on one side of the complex forming a hydrophobic channel adjacent to the iron coordination centre. Coordination of amide carbonyl oxygens is not unusual for iron(II) and indeed the structure of $[Fe(L_{22})](O_3SCF_3)_2$ is very similar to that of the iron(II) complex $[Fe(BPPA)]^{2+}$ reported by Masuda et al.[19] Selected bond lengths and angles are listed in table 4.1.

Table 4.1: Selected bond lengths (Å) and angles (°) for $[Fe(L_{22})](O_3SCF_3)_2$ (esds in parentheses).

Fe(1)-O(9)	2.018(4)	Fe(1)-O(29)	2.185(4)
Fe(1)-N(43)	2.127(5)	Fe(1)-N(1)	2.232(5)
Fe(1)-N(23)	2.139(5)	Fe(1)-N(3)	2.239(5)
O(9)-Fe(1)-O(43)	109.36(17)	O(9)-Fe(1)-N(43)	114.44(18)
N(9)-Fe(1)-O(23)	127.83(17)	O(9)-Fe(1)-O(29)	81.31(15)
N(43)-Fe(1)-O(29)	81.81(16)	N(23)-Fe(1)-O(29)	78.25(17)
O(9)-Fe(1-N(1)	155.98(17)	N(43)-Fe(1)-N(1)	76.27(17)
N(23)-Fe(1)-N(1)	75.20(18)	O(29)-Fe(1)-N(1)	122.69(16)
O(9)-Fe(1)-O(3)	80.28(16)	N(43)-Fe(1)-N(3)	109.14(18)
N(23)-Fe(1)-N(3)	104.95(17)	O(29)-Fe(1)-N(3)	160.91(16)
N(1)-Fe(1)-N(3)	75.88(17)	C(21)-Fe(1)-N(14)	112.2(4)

The octahedral geometry is highly distorted with distinctly different Fe-O bond lengths, 2.018(4) and 2.185(4) to the two-urea carbonyls. There was no evidence of the uniquely long Fe-N bond to the tertiary amine nitrogen that characterises seven coordinate iron(III)-TPA centres such as those present in $[Fe_3(L_{11})_2](ClO_4)_3$ (H_3L_{11} = tris(6-hydroxymethyl)-2-pyridylymethyl)amine (chapter 2). This is presumably as a result of binding to iron(II) in this case. Indeed the longest Fe-N bond is to a nitrogen atom of one of the pyridines carrying a 6-N-hexylureyl substituent. Finally, the two-urea N-H groups are in a hydrogen-bonded arrangement with the two trifluoromethanesulfonate anions. It is hoped that subsequent reaction with H_2O_2 to form peroxo-iron(III) complexes will lead to dissociation of urea oxygen facilitating the intended hydrogen-bonded interactions of urea N-H with the hydroperoxo groups, figure 4.4 rather than amide oxygen coordination as in $[Fe(BPPA)]^{2+}$ and $[Fe(BPPA)(O_2CBu^t)]^{2+}$, figure 4.5.[18] This is explored in the next chapter.

4.3.2. Characterisation of high spin $[Fe(L_{21})(CH_3CN)](O_3SCF_3)_2$ C_{20}, and $[Fe(L_{22})](O_3SCF_3)_2$ C_{21} in solution by ^1H NMR spectroscopy.

$[Fe(L_{22})](O_3SCF_3)_2$. Figure 4.12 shows a ^1H NMR spectrum of a solution of $[Fe(L_{22})](O_3SCF_3)_2$ in CD_3CN. The spectrum taken over a wide sweep from -5 to +100 ppm shows broad signals corresponding to a high spin iron(II) complex. The resonances at 110, 53.5 and 56 ppm are assigned to the α and β and β' protons respectively of the unsubstituted pyridine ring with its tertiary amine methylene assigned to the resonance at 99 ppm. The β and β' protons of the substituted pyridine ring appear at 40 and 46 ppm along with two resonances for tertiary amine methylene at 68 and 58 ppm. The upfield resonances at 32, 8.7, 3.8 and 2.5 ppm are assigned to the first and the subsequent methylenes of the n-hexyl chain. Finally, the upfield resonances at 0.8 and 1.1 ppm are assigned to the γ protons respectively on the two types of pyridine ring. These assignments, listed below in table 4.2, are based upon

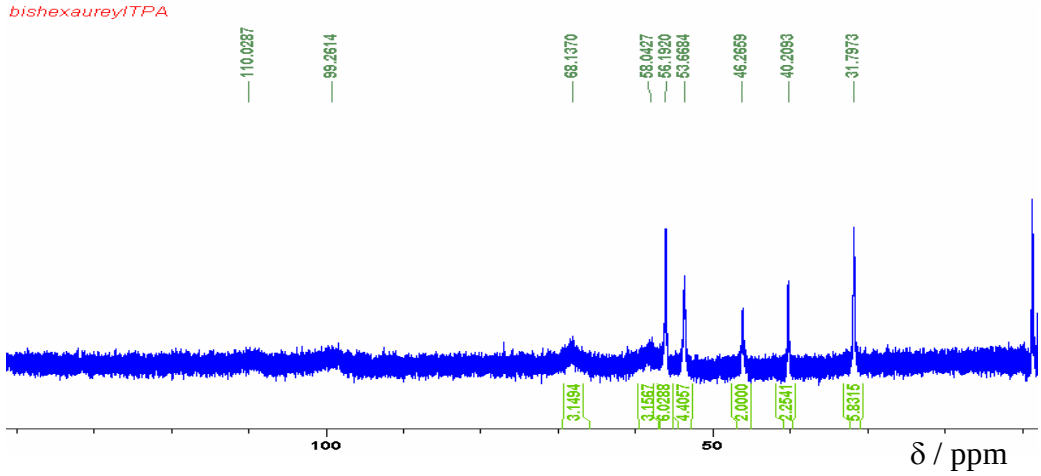

Figure 4.12: ^{1}H NMR spectrum of $[Fe(L_{22})](O_3SCF_3)_2$ in CD_3CN, C_{21}.

comparisons with the ^{1}H NMR spectrum of $[Fe(6\text{-}Me_2TPA)(CH_3CN)_2]^{2+}$.[18] Further confirmation would have required a ^{1}H COSY NMR experiment. However, this was not possible due to lack of material available and the poor quality noisy spectrum obtained.

$[Fe(L_{21})(CH_3CN)](O_3SCF_3)_2$.

Figure 4.13 shows a ^{1}H NMR spectrum of a solution of $[Fe(L_{21})(CH_3CN)](O_3SCF_3)_2$ recorded in CD_3CN. In the absence of further X-ray characterisation it has been assumed that one acetonitrile molecule remains coordinated to the iron(II) centre as L_{21} only contains one 6-N-n-hexylureyl substituent on one of the pyridine rings presumed coordinated through oxygen as in $[Fe(L_{22})](O_3SCF_3)_2$. The resonances at 131, 47 and 48 ppm are assigned to the α and the β and β' protons of the two unsubstituted pyridine rings with the tertiary amine methylene assigned at 72 ppm. The β and β' protons of the substituted pyridine ring appear at 23 and 35 ppm along with two resonances for tertiary amine methylene at 67 and 37 ppm. The resonances at 18.4 and 2.5 ppm are assigned to the first and subsequent methylenes of the n-hexyl chain; the rest presumed to be amongst the large solvent peaks around 2 ppm. Finally, the two highly upfield broad resonances around 0 and -1 ppm are assigned to the upfield shifted γ protons respectively on the two types of pyridine ring. These assignments, listed

below in table 4.2 are based upon comparisons with the ^{1}H NMR spectrum of [Fe(6-MeTPA)$(CH_3CN)_2]^{2+}$ [18] and would require a ^{1}H COSY experiment for confirmation. However, this was not possible due to lack of material available and the poor quality noisy spectra obtained.

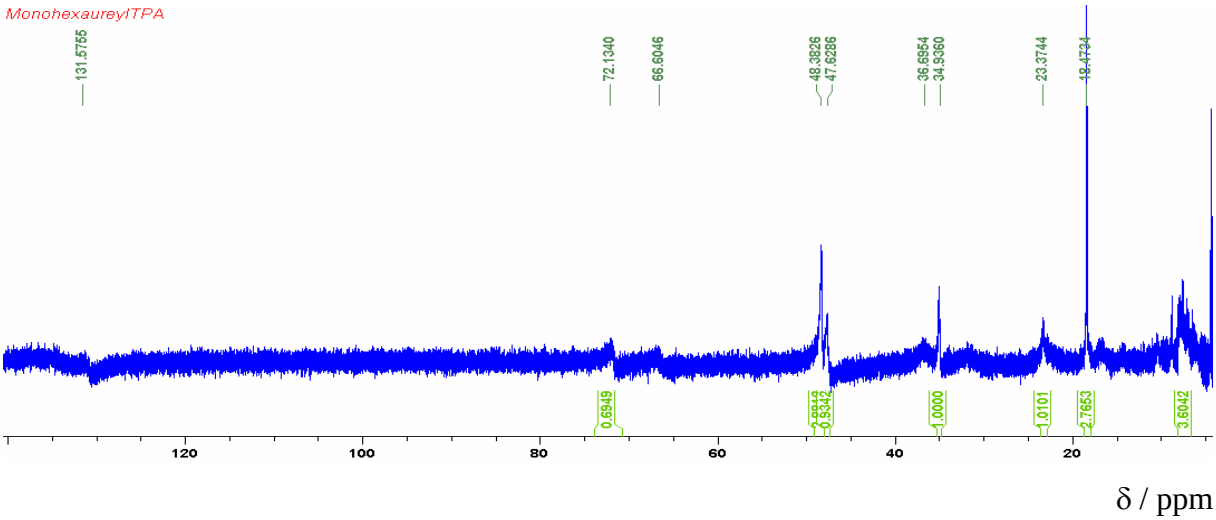

Figure 4.13: ^{1}H NMR spectrum of $[Fe(L_{21})(CH_3CN)](O_3SCF_3)_2$ in CD_3CN.

Table 4.2: ^{1}H NMR parameters (in CD_3CN) for high spin iron(II) complexes of L_{21} and L_{22} along with those for high spin $[Fe(6\text{-}MeTPA)(CH_3CN)_2]^{2+}$ and $[Fe(6\text{-}Me_2TPA)(CH_3CN)_2]^{2+}$.[9]

Complex	CH_2-N-	α-H	β,β'-H	γ-H	α-X
$[Fe(L_{21})(CH_3CN)]^{2+}$	72 67, 37	131 -	35, 23 47, 48	-1 0	18.5 (X = NHCONHC**H$_2$**C_5H_{11}-n)
$[Fe(6\text{-}MeTPA)(CH_3CN)_2]^{2+}$ *	88 82, 37	95 -	48, 52 50, 51	-7 -6	-24 (X = CH_3)
$[Fe(L_{22})]^{2+}$	99 68, 58	110 -	53.5, 56 40, 46	0.8 1.1	32 (X = NHCONHC**H$_2$**C_5H_{11}-n)
$[Fe(6\text{-}Me_2TPA)(CH_3CN)_2]^{2+}$ *	92 86, 75	106 -	56, 59 52, 57	-11 -6	-25 (X = CH_3)

4.4. Experimental:

4.4.1. Synthesis of tris(6-bromo-2-pyridylmethyl)amine and attempted synthesis of tris(6-amino-2-pyridylmethyl)amine via direct amination:

4.4.1.1. Synthesis of 2-bromo-6-hydroxymethylpyridine:

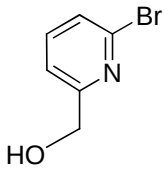

To a solution of n-BuLi (15.625 cm^3, 25 mmol, 1.6 mol dm^{-3} in hexane) in THF (30 cm^3) at -78ºC was added dropwise a solution of 2,6-dibromopyridine (5.925 g, 25 mmol) in THF (70 cm^3). The internal temperature was kept below -78ºC during the addition. After mixing the resulting green solution was stirred for additional 15 minutes then neat DMF (3.0 cm^3, 38.75 mmol) was added over a period of 30 s. The reaction was stirred at -78 for 15 min. followed by the addition of methanol (25 cm^3) and acetic acid (1.6 cm^3) and finally $NaBH_4$ (0.95 g, 25 mmol). The cooling bath was removed and the reaction solution carefully warmed up to room temperature. The reaction mixture was carefully quenched with a saturated aqueous solution of ammonium chloride (75 cm^3) and then extracted with ethyl acetate (100 cm^3 followed by 50 cm^3 respectively). The combined organic layers were washed with brine (50 cm^3) dried over Na_2SO_4, and concentrated giving 2-bromo-6-hydroxymethylpyridine as a pale-yellow oil (4.01 g, 85%).

^{1}H NMR ($CDCl_3$) 7.54 (t,1H), 7.36 (d,1H), 7.29 (d,1H), 4.73 (s,2H), 3.64 (br,1H)

4.4.1.2. Synthesis of 2-bromo-6-bromomethylpyridine:

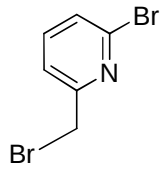

2-bromo-6-hydroxymethylpyridine (9.43 g. 50 mmol) was added to 100 cm^3 of 48% hydrobromic acid, and the reaction was heated at reflux for 12 h. The reaction solution was neutralized carefully with 1 mol dm^{-3} sodium hydroxide and then extracted with CH_2Cl_2. The combined organic layers were dried over Na_2SO_4 and evaporated. Flash chromatography (hexane/ethyl acetate; 4:1) and evaporation gave 2-bromo-6-bromomethylpyridine as a colourless solid (8.52 g, 67.85 %).

^{1}H NMR ($CDCl_3$) 7.58 (t,1H), 7.44 (d,2H), 4.53 (s,2H)

4.4.1.3. Synthesis of tris(6-bromo-2-pyridylmethyl)amine, L_{24}:

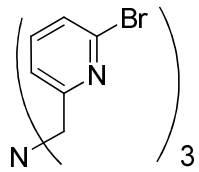

2-bromo-6-bromomethylpyridine (8.5 g, 33 mmol) was dissolved in dry CH_3CN (15 cm^3) and ammonium acetate (0.870, 11.29 mmol) and sodium carbonate (2.39g, 22.58 mmol) added under nitrogen gas and the reaction mixture stirred for 3 d at room temperature. The reaction was followed by TLC (DCM) and additional portion of sodium carbonate (1.12 g, 11.29 mmol) was added after three days. The mixture was filtered to remove the salts and the filtrate was dried under vacuum to give tris(6-bromo-2-pyridylmethyl)amine as a white solid. Recrystallisation was carried out by dissolving the compound in warm diethyl ether and storing the solution in the freezer, white needles of pure product were obtained (2.76 g, 46.37 %) ^{1}H NMR ($CDCl_3$) 7.58 (d,3H), 7.55 (t,3H), 7.38 (d,3H), 3.96 (s,6H) MS: ES+: m/z: 550.95 [$(M+Na)^+$ 100%]

4.4.1.4. Synthesis of tris(6-amino-2-pyridylmethyl)amine via direct amination of tris(6-bromo-2-pyridylmethyl)amine, L_{20}.

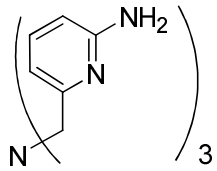

Method 1. Tris(6-bromo-2-pyridylmethyl)amine (200 mg, 0.38 mmol) was added to a solution of potassium amide prepared from (166.9 mg, 4.26 mmol) of metallic potassium in 100 cm^3 of NH_3 in a foil-wrapped flask. The mixture was then quenched after 15 min. with excess of ammonium bromide. Diethyl ether (100 cm^3) was added while the ammonia was evaporated. The ethereal mixture was filtered and the residual salts triturated with diethyl ether (4 x 50 cm^3). The combined ethereal extracts were concentrated to yield a brown solid (0.123 g) which was not soluble in any solvent.

Method 2. A 500 cm^3 pressure tested autoclave was charged with Cu_2O (1 mg), then a solution of tris(6-bromo-2-pyridylmethyl)amine (200 mg, 0.38 mmol) in ethylene glycol (5 cm^3). The mixture was cooled to 0ºC and liquid ammonia was added over a 30 min. period. The autoclave was then sealed and the reaction mixture heated at 80ºC for 16 h. at a pressure of ~ 50 psi. The reaction mixture cooled down to room temperature and drained into a beaker. The pH was adjusted to 10.5 with 2 mol dm^{-3} H_2SO_4 solution and the mixture extracted with EtOAc to give a brown solid (0.1271 g). The ^1H NMR spectrum shows only broad peaks which could match with the data reported in literature.[28] However, the MS does not match with the entitle compound.

^1H NMR ($CDCl_3$) 7.31 (br,3H), 6.73 (br,3H), 6.24 (br,3H), 5.77 (br,6H), 3.36 (br,50 H)

Method 3. In a screw-capped vial in a dry box under argon gas containing (0.527g, 1 mmol) of tris(6-bromo-2-pyridylmethyl)amine was placed tri(t-butyl)phosphine (10.116 mg, 0.05 mmol), $Pd(dba)_2$ (22.875 mg, 0.025 mmol) (dba = dibenzylideneacetone) and LiHMDS (0.1840 g, 1.1 mmol) (HMDS = hexamethyldisilazane, followed by toluene (2.5 cm^3). The vial was sealed with a cap that fitted a PTFE septum and removed from the dry box for heating at 70ºC. The crude mixture was diluted with diethyl ether (20 cm^3) and the silylamide deprotected by adding a drop of 1 mol dm^{-3} HCl. The mixture was transferred to a separating funnel with aqueous 1 mol dm^{-3} NaOH (20 cm^3). The organic layer was dried over anhydrous $MgSO_4$, filtered and then concentrated under reduced pressure. A brown solution was obtained from which a brown solid precipitated. The ^1H NMR spectrum in (d^6-DMSO) did not match with the literature values.

Method 4. Dry toluene (10 cm^3) was introduced into a 25 cm^3 Schlenk tube and the mixture was degassed, (vacuum/N_2 cycle, three times). Tris(6-bromo-2-pyridylmethyl)amine (0.572 g, 1 mmol), dppf (dppf = bis(diphenylphosphine) ferrocene) (83.15 mg, 0,15 mmol), sodium t-butoxide (0.37 g, 3.30 mmol), palladium(II) acetate (16.8 mg, 0.075 mmol) and benzophenone imine (0.609 g, 3.36 mmol) were then charged and the mixture heated at such rate that the inner temperature rose to 78-82 ºC within 30-60 min. The reaction mixture agitated for 1 h at 78-82 ºC and then allowed to cool to room temperature and stand for 10 min. Tri(n-butyl)phosphine (0.326 g, 1.611 mmol) was then added to the mixture which was allowed to stand at ambient temperature for a further 10 min. The toluene solution was poured for into 5 % aqueous solution of citric acid (100 cm^3) and allowed to stand for a further 30 min. at room temperature. The aqueous layer was then washed with ^iPrOAc (50 cm^3) and the organic layer discarded. The citric acid layer was washed with 5 mol dm^{-3} NaOH solution (10 cm^3) keeping the temperature between 15 - 20ºC. The aqueous layer contained a precipitate. A yellow solid (91 mg) was obtained upon evaporation of the solvent. The solid

was soluble in DMSO and $CDCl_3$. The ^1H NMR spectrum in (d^6-DMSO) did not match with the literature values.

4.4.2. Synthesis of [(6-(n-hexylureyl)-2-pyridylmethyl)-2-bis(pyridylmethyl)]amine, L_{21}, [bis-(6-(n-hexylureyl)-2-pyridylmethyl)-2-pyridylmethyl]amine, L_{22} and attempted synthesis of tris[(6-n-hexylureyl)-2-(pyridylmethyl)]amine, L_{23}:

4.4.2.1. Synthesis of 6-(n-hexylureyl)-2-methylpyridine:

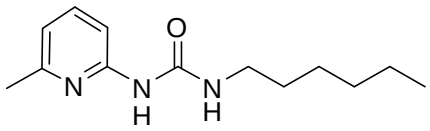

To a solution of 6-amino-2-methylpyridine (1.72 g, 15.7 mmol) in THF (15 cm^3) was added n-hexylisocyanate (2.00 g, 1.57 mmol). The reaction mixture was stirred overnight for 16 h at RT. The white product was removed by filtration, washed with THF, then with diethyl ether, before being dried under vacuum to give 6-(n-hexylureyl)-2-methylpyridine as a white powder (2.20 g, 59.4%).

^1H NMR (300.06 MHz, $CDCl_3$, 298 K): δ= 9.64 (1H, br, s, NH), 8.01 (1H, br, s, NH), 7.48 (1H, t, $^3J_{HH}$ = 7.4 Hz, 1H of C_5H_3N), 6.73 (1H, d, $^3J_{HH}$ = 7.5 Hz, 1H of C_5H_3N), 5.57, (1H, d, $^3J_{HH}$ = 8.01 Hz, 1H of C_5H_3N), 3.41 (2 H q, $^3J_{HH}$ = 5.63 Hz, CH_2), 2.47 (3 H s , CH_3), 1.64 (m , CH_2), 1.36 (m,3 CH_2), 0.92 (3H, t, $^3J_{HH}$ = 6.6 Hz, CH_3).

^{13}C-{^1H} NMR (75.45 MHz, $CDCl_3$, 298 K) δ_C= 14.48, 23.07, 24.49, 27.25, 30.18, 31.98, 40.18, 108.93, 116.18, 138,94, 153.24, 156.40, 157.49

MS: ES+: m/z: 258.16 [$(M+Na)^+$ 100%].

4.4.2.2. Synthesis of 6-(n-hexylureyl)-2-hydroxymethylpyridine:

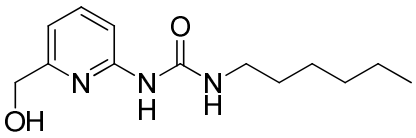

To a solution of 6-(n-hexylureyl)-2-methylpyridine (3 g, 12.75 mmol) in THF (150 cm^3) -78ºC (acetone/dry ice bath) was added a solution of n-butyl lithium (2.5 mol dm^{-3}) in hexane (19.13 cm^3, 48.84 mmol). The mixture was warmed up and stirred for 2 h at room temperature resulting in the formation of an orange solution. The mixture was cooled to -78ºC and pre-dried O_2 (passed through a Drierite column) was bubbled through the suspension for 6 h. The reaction was quenched by adding (6.48 cm^3, 34.4 mmol) of Me_2S at -78ºC, followed by glacial acetic acid (2.76 cm^3, 19.28 mmol). The reaction mixture was warmed and stirred for 48 h at RT. Dilution with water and extraction with ethyl acetate was followed by concentration and flash chromatography of the residue (dichloromethane/acetone; 6:1). Evaporation gave 6-(n-hexylureyl)-2-hydroxymethylpyridine as a pale yellow solid (1.07g, 43 %).

^{1}H NMR (300.06 MHz, $CDCl_3$, 298 K): δ= 9.30 (1H,br, s, NH), 8.98 (1H, br, s, NH), 7.57 (1H, t, $^3J_{HH}$ = 7.7 Hz, 1H of C_5H_3N), 6.98 (1H, d, $^3J_{HH}$ = 7.7 Hz, 1H of C_5H_3N), 6.68, (1H, d, $^3J_{HH}$ = 8.0 Hz, 1H of C_5H_3N), 4.70 (2H s , $HOCH_2$), 3.38 (2H q, $^3J_{HH}$ = 5.8 Hz, $^3J_{HH}$ = 7.7 Hz, CH_2), 3.00 (1H, br , OH), 1.64 (2H, m , CH_2), 1.36 (6H, m, 3 CH_2), 0.91 (3H, t, $^3J_{HH}$ = 6.6 Hz, CH_3).

^{13}C-{^{1}H} NMR (75.45 MHz, $CDCl_3$, 298 K) δ_C= 14.46, 23.02, 27.21, 30.13, 31.93, 31.93, 40.23, 65.61, 110.00, 113.57, 139.13, 153.21, 157.03, 157.75.

MS: ES+: m/z: 274.15 [$(M+Na)^+$ 100%].

4.4.2.3. Synthesis of 6-(n-hexylureyl)-2-(p-toluenesulfonoxymethyl)pyridine:

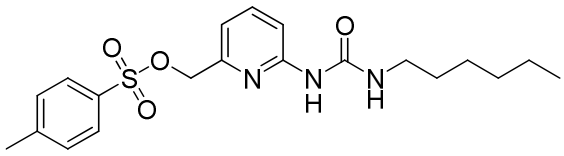

To a solution of 6-(n-hexylureyl)-2-hydroxymethylpyridine (261.18 mg, 1.04 mmol) and Et_3N (0.45ml, 3.24 mmol) in ethyl acetate (10 cm^3), was added p-toluenesulfonyl chloride (59.086 mg, 3.10 mmol) at 0 ºC. The mixture was warmed to room temperature and stirred for 24 h; then quenched by the addition of saturated aqueous $NaHCO_3$. The organic layer was separated, washed with H_2O and brine, dried (anhydrous $MgSO_4$) and evaporated. The crude residue was purified by flash chromatography (CH_2Cl_2/acetone; 4:1) to yield the pure tosylate product as a colourless solid (270 mg, 64 %).

^{1}H NMR (300.06 MHz, $CDCl_3$, 298 K): δ= 9.21 (1H,br, s, NH), 8.92 (1H, br, s, NH), 7.82 (1H, d, $^3J_{HH}$ = 8.3 Hz, 1H of C_6H_4), 7.56 (1H, t, $^3J_{HH}$ = 7.8 Hz, 1H of C_5H_3N), 7.35 (1H, d, $^3J_{HH}$ = 7.9 Hz, 1H of C_6H_4), 6.89 (1H, d, $^3J_{HH}$ = 7.5 Hz, 1H of C_5H_3N), 6.78, (1H, d, $^3J_{HH}$ = 8.7 Hz, 1H of C_5H_3N), 5.06 (2H s , $TsOCH_2$), 3.38 (2H q, $^3J_{HH}$ = 5.8 Hz, $^3J_{HH}$ = 6.6 Hz, CH_2), 2.46 (1H, s , CH_3), 1.62 (2H, m , CH_2), 1.36 (6H, m, 3 CH_2), 0.92 (3H, t, $^3J_{HH}$ = 6.6 Hz, CH_3).

^{13}C-{^{1}H} NMR (75.45 MHz, $CDCl_3$, 298 K) δ_C= 14.11, 21.66, 22.64, 26.79, 29.83, 31.54, 39.91, 71.04, 111.87, 114.86, 127.91, 129.87, 138.90, 145.06, 149.99, 153.20, 155.73, 155.95.

MS: ES+: m/z: 428.16 [$(M+Na)^+$ 100%].

4.4.2.4. Synthesis of 6-(n-hexylureyl)-2-pyridylmethyl-N-isoindole-1,3-dione:

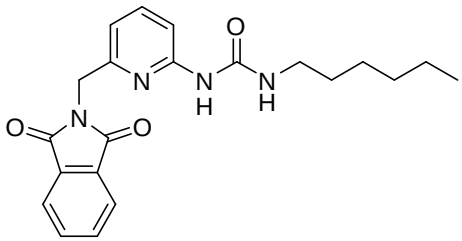

Potassium phthalimide (388.2 mg, 2.09 mmol) was suspended in a solution of 6-(n-hexylureyl)-2-(p-toluenesulfonoxymethyl)pyridine (850 mg, 2.09 mmol) in DMF (50 cm^3), and the mixture stirred at 80ºC overnight. Following evaporation of the DMF, water was added to precipitate the crude product. This was extracted with dichloromethane and dried over anhydrous $MgSO_4$. Following evaporation the resulting solid residue was washed with diethyl ether to give 6-(n-hexylureyl)-2-pyridylmethyl-N-isoindole-1,3-dione as a colourless solid (143.5mg 18.05 %).

^{1}H NMR (300.06 MHz, $CDCl_3$, 298 K): δ= 9.14 (1H,br, s, NH), 8.79 (1H, br, s, NH), 7.79 (1H, d, $^3J_{HH}$ = 2.4 Hz, $^3J_{HH}$ = 3 Hz 1H of C_6H_4), 7.66 (1H, d, $^3J_{HH}$ = 2.4 Hz, $^3J_{HH}$ = 3 Hz 1H of C_6H_4), 7.44 (1H, t, $^3J_{HH}$ = 7.8 Hz, 1H of C_5H_3N), 6.84 (1H, d, $^3J_{HH}$ = 7.5 Hz, 1H of C_5H_3N), 6.64, (1H, d, $^3J_{HH}$ = 8.7 Hz, 1H of C_5H_3N), 4.79 (2H s , NCH_2), 3.18 (2H q, $^3J_{HH}$ = 7 Hz, $^3J_{HH}$ = 6.6 Hz, CH_2), 1.45 (2H, m , CH_2), 1.22 (6H, m, 3 CH_2), 0.81 (3H, t, $^3J_{HH}$ = 6.6 Hz, CH_3).

^{13}C-{^{1}H} NMR (75.45 MHz, $CDCl_3$, 298 K): δ_C= 14.14, 22.65, 26.75, 30.25, 31.68, 39.96, 42.51, 111.24, 115.01, 123.16, 123.48, 132.03, 133.85, 134.18, 138.84, 153.53, 156.09, 167.93.

MS: ES+: m/z: 428.16 [$(M+Na)^+$ 100%].

4.4.2.5. Synthesis of 6-(n-hexylureyl)-2-aminomethylpyridine:

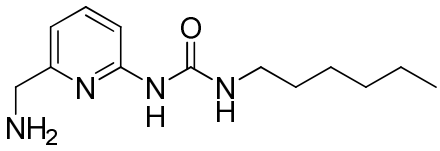

A mixture of 6-(n-hexylureyl)-2-pyridylmethyl-N-isoindole-1,3-dione (140 mg, 368 mmol) and hydrazine hydrate (17,9 cm^3, 368 µmol) in of ethanol (5 cm^3) was heated under reflux overnight. The white precipitate was removed by filtration and the filtrate evaporated. Recrystallization of the residue from ethanol gave 6-(n-hexylureyl)-2-aminomethylpyridine as a white solid (18.9 mg 20.5 %).

^{1}H NMR (300.06 MHz, $CDCl_3$, 298 K) δ= 9.18 (1H,br, s, NH), 7.37 (1H, t, $^3J_{HH}$ = 7.8 Hz, 1H of C_5H_3N), 6.75 (1H, br, s, NH), 6.70 (1H, d, $^3J_{HH}$ = 7.7 Hz, 1H of C_5H_3N), 6.32, (1H, d, $^3J_{HH}$ = 8.1 Hz, 1H of C_5H_3N), 4.70 (2H s , NH_2CH_2), 3.19 (2H q, $^3J_{HH}$ = 5.6 Hz, $^3J_{HH}$ = 7.2 Hz, CH_2), 1.40 (2H, m , CH_2), 1.14 (6H, m, 3 CH_2), 0.71 (3H, t, $^3J_{HH}$ = 6.6 Hz, CH_3)

MS: ES+: m/z: 251.19[$(M+Na)^+$ 100%].

^{13}C NMR (75 MHz, $CDCl_3$): δ = 28.29, 63.65, 80.89, 109.60, 115.67, 147.60, 152.66, 152.73, 152.91.

4.4.2.6. Synthesis of [bis(2-pyridylmethyl)-6-(n-hexylureyl)-2-pyridylmethyl)]amine, L_{21}:

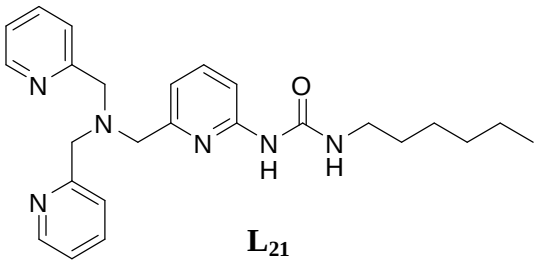

L_{21}

Bis(2-picolyl)amine (0.111 cm^3, 0.617 mmol) and 6-(n-hexylureyl)-2-(p-toluenesulfonoxy methyl)pyridine (0.250 g, 0.617 mmol) were dissolved in CH_3CN (25 cm^3) under N_2 gas. Following addition of Na_2CO_3 (0.327 g, 3.086 mmol) and 5 mg Bu_4NBr, the mixture was heated in a nitrogen atmosphere under reflux for 21 hours. The reaction mixture was cooled to

RT wherein 10 ml of distilled water and aqueous 1 mol dm^{-3} sodium hydroxide (1.6 cm^3) were added. Following extraction with CH_2Cl_2 (3 x 20 cm^3), the combined organic extracts were dried over anhydrous Na_2SO_4 and then evaporated under reduced pressure to give a yellow oil. The oil was dissolved in diethyl ether and after the addition of hexane was kept in the freezer for several days depositing L_4 as a white solid, yield 50 mg (19 %).

^{1}H NMR (300.06 MHz, $CDCl_3$, 298 K) δ= 9.48 (1H,br, s, NH), 8.45 (2H, d, $^3J_{HH}$ = 7.8 Hz, 1H of C_5H_3N), 8.15 (1H, br, s, NH), 7.6 (2H, t, $^3J_{HH}$ = 7.7 Hz, 1H of C_5H_3N), 7.48 (2H, t, $^3J_{HH}$ = 7.7 Hz, 1H of C_5H_3N), 7.42 (1H, d, $^3J_{HH}$ = 7.7 Hz, 1H of C_5H_3N), 7.10 (1H, d, $^3J_{HH}$ = 7.7? Hz, 1H of C_5H_3N), 7.05 (1H, d, $^3J_{HH}$ = 7.7? Hz, 1H of C_5H_3N), 6.5, (1H, d, $^3J_{HH}$ = 8.1 Hz, 1H of C_5H_3N), 3.80 (4H s , NH_2CH_2), 3.70 (2H s , NH_2CH_2), 3.3 (2H q, $^3J_{HH}$ = 5.6 Hz, $^3J_{HH}$ = 7.2 Hz, CH_2), 1.50 (2H, m , CH_2), 1.14 (6H, m, 3 CH_2), 0.80 (3H, t, $^3J_{HH}$ = 6.6 Hz, CH_3).

^{13}C NMR (75 MHz, $CDCl_3$): δ = 14,11, 22.63, 26.82, 30.00, 31.56, 39.40, 59.92, 60.35, 110.04, 115.48, 122.09, 122.78, 136.45, 138.64, 149.14, 152.93, 156.05, 159.30.

MS: ES+: m/z: 495.19[$(M+Na)^+$ 100%].

4.4.2.7. Synthesis of [Bis-(6-(hexylureyl)-2-pyridylmethyl)-2-pyridylmethyl]amine, L_{22}:

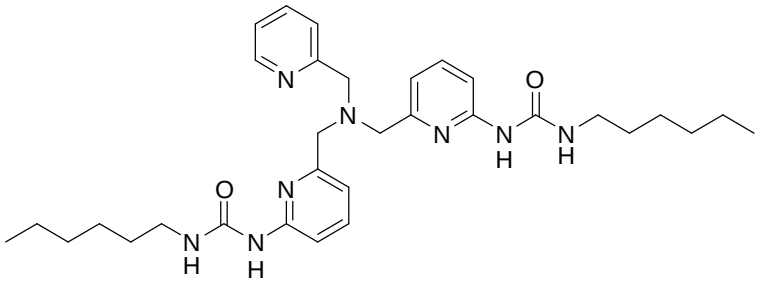

L_{22}

Under N_2 atmosphere 2-aminomethylpyridine (0.032 cm^3, 0.308 mmol) was mixed with 6-(n-hexylureyl)-2-(p-toluenesulfonoxymethyl)pyridine (0.250 g, 0.6128 mmol) in CH_3CN (25 cm^3). Following addition of Na_2CO_3 (0.654 mg, 6.17 mmol) and 5 mg of NBu_4Br, the reaction mixture was heated under reflux for 21 hours. The mixture was cooled to room temperature wherein 10 cm^3 of distilled water and aqueous 1 mol dm^{-3} sodium hydroxide (3.2

cm^3) were added. After extraction with dichloromethane and the combined organic extracts were dried over anhydrous Na_2SO_4 and evaporated to dryness under reduced pressure to yield an orange-brown oil, to which acetone was added. After storing at -18^oC for two days, L_5 was obtained as a white precipitate, yield 81 mg (48 %).

^1H NMR (300.06 MHz, $CDCl_3$, 298 K) δ= 9.48 (2H, br, s, NH), 8.45 (1H, d, $^3J_{HH}$ = 7.8 Hz, 1H of C_5H_3N), 8.15 (2H, br, s, NH), 7.6 (2H, t, $^3J_{HH}$ = 7.7 Hz, 1H of C_5H_3N), 7.48 (1H, t, $^3J_{HH}$ = 7.7 Hz, 1H of C_5H_3N), 7.42 (2H, d, $^3J_{HH}$ = 7.8 Hz, 1H of C_5H_3N), 7.10 (1H, t, $^3J_{HH}$ = 7.8 Hz, 1H of C_5H_3N), 7.05 (2H, d, $^3J_{HH}$ = 7.7 Hz, 1H of C_5H_3N), 6.5 (2H, d, $^3J_{HH}$ = 8.1 Hz, 1H of C_5H_3N), 3.80 (2H s , NH_2CH_2), 3.70 (4H s , NH_2CH_2), 3.3 (4H q, $^3J_{HH}$ = 5.6 Hz, $^3J_{HH}$ = 7.2 Hz, CH_2), 1.50 (4H, m , CH_2), 1.14 (12H, m, 3 CH_2), 0.80 (6H, t, $^3J_{HH}$ = 6.6 Hz, CH_3). MS:

^{13}C NMR (75 MHz, $CDCl_3$): δ = 14,10, 22.64, 26.82, 29.99, 31.55, 39.87, 60.05, 60.46, 110.14, 115.23, 122.19, 122.64, 136.50, 138.66, 149.16, 153.01, 156.05, 159.30.

ES+: m/z: 597.36 [$(M+Na)^+$ 100%]**.**

4.4.2.8. Attempted synthesis of tris-(6-(n-hexylureyl)-2-pyridylmethyl)amine, L_{23}:

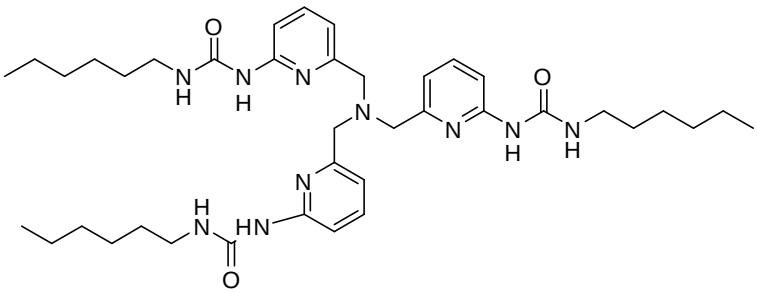

L_{23}

Under N_2 6-(n-hexylureyl)-2-aminomethylpyridine (19 mg, 7.59 μmol) was reacted with a 2 fold excess of 6-(n-hexylureyl)-2-(p-toluenesulfonoxymethyl)pyridine (67.6 mg, 0.167 mmol) in CH_2Cl_2 (10 cm^3) under reflux overnight at 40ºC. The solvent was evaporated and the ^1H NMR of the crude residue was recorded to look for evidence of the required TPA product. Three different species appeared to be present but none consistent with the presence of a TPA

derivative (no resonance for methylene between tertiary amine and pyridine observed around 4 ppm).

4.4.3. Synthesis of iron(II) complexes:

The iron(II) salt $[Fe(CH_3CN)_2(O_3SCF_3)_2]$ was utilised as the iron precursor in the preparation of the iron(II) complexes of L_{21} and L_{22}.

4.4.3.1. $[Fe(L_{21})(CH_3CN)](O_2SCF_3)_2$. To a solution of $[Fe(CH_3CN)_2(O_3SCF_3)_2]$ (4.36 mg, 0.01 mmol) in CH_3CN (4 cm^3) was added a solution of L_{21} (4.32 mg, 0.01 mmol) in CH_3CN (4 cm^3). The mixture was stirred in an open vial for 1 h. Diethyl ether was then mixed in slowly using vapour diffusion. After 2 days, orange crystals were obtained (2.1mg, 23.2 %) which were found to be unsuitable for X-ray diffraction.

4.4.3.2. $[Fe(L_{22})](O_3SCF_3)_2$. To a solution of $[Fe(CH_3CN)_2(O_3SCF_3)_2]$ (4.36 mg, 0.01 mmol) in CH_3CN (4 cm^3) was added a solution of L_{22} (5.74 mg, 0.01 mmol) in CH_3CN (4 cm^3). The mixture was stirred in an open vial for 1 h. Diethyl ether was then mixed in slowly using vapour diffusion. After two days, orange crystals were obtained (2.5mg, 14.85 %) which were found to be suitable for X-ray diffraction.

4.5. Summary and Conclusions.

A new synthetic route for the synthesis of 6-N-amino-TPA derivatives has been developed via lithiation of the methyl group of N-protected 6-amino-2-picoline followed by reaction with O_2 to generate the 2-hydroxymethylpyridine derivative under reducing work up conditions. This reaction goes in high yield, works on a variety of N-protected 6-amino-2-picolines and bastly superior in every way to radical bromination, which gives much, poorer yields and exhaustive chromatography due to preferential bromination on the pyridine ring. Tosylation of the hydroxymethyl group allows the TPA framework to be synthesised using the recently modified amine coupling method of Berreau in the presence of the mass transfer agent nBu_4NBr. As a result we have synthesized and fully characterised two new 6-substituted TPA ligand derivatives, L_{21} and L_{22} possessing respectively N-ureyl substituents at the 6-position on one and two of the pyridine moieties. Unfortunately due to lack of time and material the synthesis of L_{23} with all three pyridine rings substituted using Berreau's method was not achieved, the initial attempts without the presence of nBu_4NBr being unsuccessful. High spin iron(II) complexes of L_{21} and L_{22} have however been successfully isolated and suitable crystals for X-ray diffraction were obtained for the iron(II) triflate complex of L_{22}. The iron(II) centre is in a distorted octahedral environment coordinated to both urea carbonyl groups along with the four nitrogens of the TPA moiety. It represents the first such structurally characterised iron(II) complex coordinated to two urea amido-type carbonyl oxygens in this family of TPA derivatives. The activity of high spin $[Fe(L_{21})(CH_3CN)](O_3SCF_3)_2$ and $[Fe(L_{22})](O_3SCF_3)_2$ towards the catalysis of alkane oxygenation with H_2O_2 was evaluated and is reported in chapter 5. Along with a study of the reaction products of $[Fe(L_{21})(CH_3CN)](O_3SCF_3)_2$ and $[Fe(L_{22})](O_3SCF_3)_2$ with both H_2O_2 and t-BuOOH in CH_3CN solvent which were examined at low temperature (100K) by X-band EPR spectroscopy and at RT by UV-visible spectrophotometry.

4.6. References:

1. E. I. Solomon, T. C. Brunold, M. I. Davis, J. N. Kemsley, S.-K. Lee, N. Lehnert, F. Neese, A. J. Skulan, Y.-S. Yang and J. Zhou, *Chemical Reviews (Washington, D. C.)*, 2000, **100**, 235-349.
2. J. N. Siedow, *Annual Review of Plant Physiology and Plant Molecular Biology*, 1991, **42**, 145-188.
3. S. Yamamoto, *Biochimica et Biophysica Acta, Lipids and Lipid Metabolism*, 1992, **1128**, 117-131.
4. M. J. Nelson, B. A. Brennan, D. B. Chase, R. A. Cowling, G. N. Grove and R. C. Scarrow, *Biochemistry*, 1995, **34**, 15219-15229.
5. S. Ogo, S. Wada, Y. Watanabe, M. Iwase, A. Wada, M. Harata, K. Jitsukawa, H. Masuda and H. Einaga, *Angew. Chem., Int. Ed.*, 1998, **37**, 2102-2104.
6. S. K. Mandal and L. Que, Jr., *Inorg. Chem.*, 1997, **36**, 5424-5425.
7. R. T. Jonas and T. D. P. Stack, *J. Am. Chem. Soc.* 1997, **119**, 8566-8567.
8. Y. Dong, Y. Zang, K. Kauffmann, L. Shu, E. C. Wilkinson, E. Muenck and L. Que, Jr., *J. Am. Chem. Soc.*, 1997, **119**, 12683-12684.
9. Y. Zang, J. Kim, Y. Dong, E. C. Wilkinson, E. H. Appelman and L. Que, Jr., *J. Am. Chem. Soc.*, 1997, **119**, 4197-4205.
10. Y. Dong, H. Fujii, M. P. Hendrich, R. A. Leising, G. Pan, C. R. Randall, E. C. Wilkinson, Y. Zang, L. Que, Jr. and et al., *J. Am. Chem. Soc.*, 1995, **117**, 2778-2792.
11. Y. Zang, T. E. Elgren, Y. Dong and L. Que, Jr., *J. Am. Chem. Soc.*, 1993, **115**, 811-813.
12. M. J. Nelson, *Biochemistry*, 1988, **27**, 4273-4278.

13. Y. Zhang, Q.-F. Gan, E. G. Pavel, E. Sigal and E. I. Solomon, *J. Am. Chem. Soc.* 1995, **117**, 7422-7427.

14. J. C. Boyington, B. J. Gaffney and L. M. Amzel, *Science (Washington, DC, U. S.)*, 1993, **260**, 1482-1486.

15. S. A. Gillmor, A. Villasenor, R. Fletterick, E. Sigal and M. F. Browner, *Nat. Struct. Biol.* 1997, **4**, 1003-1009.

16. M. Costas, J.-U. Rohde, A. Stubna, R. Y. N. Ho, L. Quaroni, E. Muenck and L. Que, Jr., *J. Am. Chem. Soc.*, 2001, **123**, 12931-12932.

17. M. Harata, K. Jitsukawa, H. Masuda and H. Einaga, *Chem. Lett.*, 1996, 813-814.

18. A. Wada, M. Harata, K. Hasegawa, K. Jitsukawa, H. Masuda, M. Mukai, T. Kitagawa and H. Einaga, *Angew. Chem., Int. Ed.*, 1998, **37**, 798-799.

19. A. Wada, S. Ogo, Y. Watanabe, M. Mukai, T. Kitagawa, K. Jitsukawa, H. Masuda and H. Einaga, *Inorg. Chem.*, 1999, **38**, 3592-3593.

20. C. E. MacBeth, A. P. Golombek, V. G. Young, Jr., C. Yang, K. Kuczera, M. P. Hendrich and A. S. Borovik, *Science (Washington, D. C.)*, 2000, **289**, 938-941.

21. A. Wada, S. Ogo, S. Nagatomo, T. Kitagawa, Y. Watanabe, K. Jitsukawa and H. Masuda, *Inorg. Chem.*, 2002, **41**, 616-618.

22. M. Sono, M. P. Roach, E. D. Coulter and J. H. Dawson, *Chem. Rev. (Washington, DC, U. S.)*, 1996, **96**, 2841.

23. D. R. Doerge, N. M. Cooray and M. E. Brewster, *Biochemistry (Moscow, Russ. Fed.)*, 1991, **30**, 8960.

24. K. Machii, Y. Watanabe and I. Morishima, *J. Am. Chem. Soc.*, 1995, **117**, 6691.

25. *Cytochrome P-450: Structure, Mechanism and Biochemistry*, Plenum Press, New York, 1995.

26. C. Walling, *Acc. Chem. Res.*, 1975, **8**, 125.

27. G. A. Russell, *J. Am. Chem. Soc.*, 1957, **8**, 3871.

28. J. C. Mareque-Rivas, R. Torres Martin de Rosales and S. Parsons, *Chem. Commun. (Cambridge, U. K.)*, 2004, 610-611.

29. M. Harata, K. Jitsukawa, H. Masuda and H. Einaga, *Chem. Lett.*, 1995, 61-62.

30. L. M. Berreau, S. Mahapatra, J. A. Halfen, V. G. Young, Jr. and W. B. Tolman, *Inorg. Chem.* 1996, **35**, 6339-6342.

31. L. Metteau, S. Parsons and J. C. Mareque-Rivas, *Inorg. Chem.*, 2006, **45**, 6601-6603.

32. C.-L. Chuang, O. dos Santos, X. Xu and J. W. Canary, *Inorg. Chem.* 1997, **36**, 1967-1972.

33. M. P. Moon, A. P. Komin, J. F. Wolfe and G. F. Morris, *J. Org. Chem.* 1983, **48**, 2392-2399.

34. F. Lang, D. Zewge, I. N. Houpis and R. P. Volante, *Tetrahedron Lett.* 2001, **42**, 3251-3254.

35. J. P. Wolfe, J. Ahman, J. P. Sadighi, R. A. Singer and S. L. Buchwald, *Tetrahedron Lett.* 1997, **38**, 6367-6370.

36. S. Lee, M. Jorgensen and J. F. Hartwig, *Org. Lett.* 2001, **3**, 2729-2732.

37. M. Berlin, R. Aslanian, M. de Lera Ruiz and K. D. McCormick, *Synthesis*, 2007, 2529-2533.

Chapter Five

Catalysis of H_2O_2 oxygenation of cyclohexane by hydrophobic iron(II)-TPA derivative complexes in acetonitrile solvent. GC and time resolved EPR and UV-VIS studies.

5.1. Introduction

Hydrocarbons, especially saturated hydrocarbons, are the main constituents of oil and natural gases, the feedstocks for the chemical industry. Selective transformation of saturated hydrocarbons constitutes an extremely important field of contemporary chemistry from an economic point of view, since their oxidation products are versatile intermediates for the further synthesis of a wide range of chemicals.[1, 2] New selective routes from hydrocarbons to valuable products such as alcohols, ketones, acids and peroxides would be hugely beneficial to sustaining existing large scale chemical synthesis from the dwindling crude oil supply[3] but remains highly challenging as described in chapter 1. H_2O_2 and O_2 remain the desired oxidizing agents for large-scale industrial applications and the achievement of selective oxidation of hydrocarbons by these oxidants catalyzed by transition metal species remains the target of much contemporary research.[4, 5] Non-heme iron complexes of tetradentate pyridine-based ligands such as $[Fe(TPA)(CH_3CN)_2]^{2+}$ and $[Fe(BPMEN)(CH_3CN)_2]^{2+}$ have shown significant activity towards the H_2O_2 oxygenation of hydrocarbons in CH_3CN solvent principally from studies on cyclohexane.[6, 7, 8] These catalyst give significantly high A:K ratios compared to those based on radical intermediates implying the involvement of high valent metal-oxo based reactive species. Radical based processes give much lower A:K ratios which under certain conditions, like in Gif chemistry in pyridine, can fall well below unity favouring the ketone as product. $[Fe(BPMEN)(CH_3CN)_2]^{2+}$ is the most active and efficient of the polypyridine chelate-based non-heme iron catalysts investigated so far.[6] Catalysis of stereospecific hydroxylation has been observed with a prochiral substrate[9, 10] which has been

used as further evidence for metal-oxo based processes involving either iron(IV)-oxo or iron(V)-oxo species.[6] The existence of such high-valent iron-oxo species as intermediates is supported by recent crystallographic characterisation of two non-heme Fe(IV)=O complexes.[11, 12]

As a result of the successes with iron(II)-TPA and related complexes as providing a template for significant alkane oxygenation activity with H_2O_2 it was decided to structurally modify the properties of the TPA ligand with the aim of further enhancing the catalytic activity and selectivity. At the focus of this work were attempts to improve selectivity towards the 1-oxygenation of linear n-alkanes by restricting the approach of the internal CH_2 groups at the active iron centre. To achieve this, several TPA ligand derivatives were synthesized modified at the 6-position of the pyridine ring with alkyl chains. The aim was to create a narrow hydrophobic channel adjacent to the iron centre that might restrict access to the active oxo-iron centre of only the end CH_3 group of the n-alkane substrate. The synthesis and characterisation of a number of these derivatives (see figure 5.1 below) was reported in chapters 2, 3 and 4. In this chapter the results of a study of the catalytic activity of their iron(II) complexes towards the selective H_2O_2 oxygenation of cyclohexane is reported.

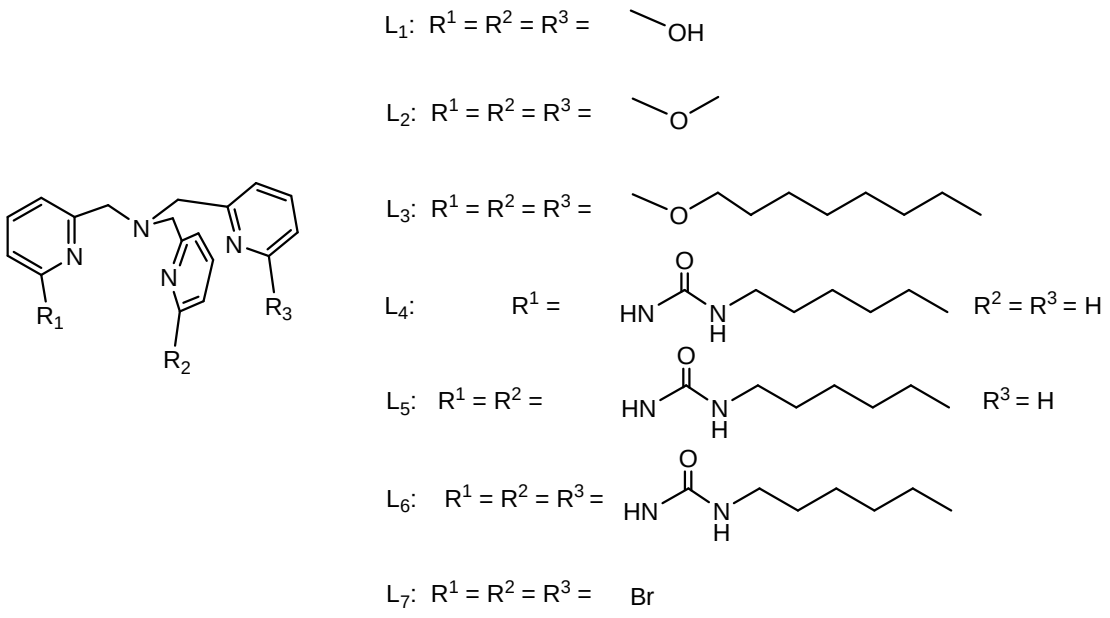

Figure 5.1: Modified 6-substituted TPA ligands used in the studies in this chapter

Cyclohexane was chosen as the initial substrate of study (rather than using a linear alkane from the outset) since the measurement of the A:K ratio offers a quick benchmark comparison with the behaviour of $[Fe(TPA)(CH_3CN)_2]^{2+}$ and $[Fe(BPMEN)(CH_3CN)_2]^{2+}$ under identical experimental conditions. Reactions of the iron(II) complexes; $[Fe(L)(CH_3CN)_x]^{2+}$ (L = $L_{15,16,21}$ – L_{23}) towards H_2O_2 and ^tBuOOH in CH_3CN solution have also been followed by X-band EPR spectroscopy at 110 K and time-resolved UV-VIS spectrophotometry. Low spin purple species such as Fe(III)-hydroperoxo Fe(III)-η^2-peroxo derived from the reaction of [(trispicMeen)FeCl]Cl (trispicMeen = *N*-methyl-*N´*, *N´*, *N´*-tris(pyridylmethyl)ethane-1,2-diamine)) with H_2O_2 have been studied in detail by Bill *et al* and characterized by EPR and Mössbauer spectropscopy.[13] A quantitative information about low spin [(TPA)LFe(III)-OOH] and [(TPA)LFe(III)-OO^{t}Bu] in terms of stability and reactivity were obtained from a study carried out by Talsi *et al*,(Talsi et al Reference) where the nature of the sixth ligand L could be determined by EPR.

A correlation between the observed catalytic activity and the nature of the Fe^{III}(L)-OOR intermediates generated has become apparent. As a result a number of important consequences for future directions of this research are discussed.

5.2 Results and Discussion

5.2.1 EPR studies of reactions of $[Fe(L)(CH_3CN)_x]^{2+}$ (L = $L_{15,16,21}$ – L_{23}) with H_2O_2 or ^{t}BuOOH. General procedure:

A 1 cm^3 stock solution (3 x 10^{-4} mol dm^{-3}) of each iron(II) complex in acetonitrile was prepared. A 0.3 cm^3 aliquot of this was then transferred to a quartz EPR tube, (12cm length x 0.4cm i.d.) which was then immersed in a Dewar of liquid nitrogen. The frozen iron(II) sample was then rapidly transferred to a cooled sample holder within the EPR spectrometer whose cavity was maintained at 110 K. The EPR spectrum was then acquired. Following data acquisition the tube was removed from the frozen sample holder of the spectrometer and kept

frozen in a separate dewar of liquid nitrogen. An aliquot of H_2O_2 or ^tBuOOH was then added from a small syringe to the frozen EPR tube of the iron(II) complex. The tube was then thawed enough so as to permit mixing of the two solutions over ~ 2 minutes before rapidly refreezing and re-introduced into the frozen cavity of the EPR spectrometer. The spectrum was then re-acquired. The aim was to observe the appearance and then decay of the reactive paramagnetic peroxo-iron(III) species for each ligand. The partial re-thawing (over 2 min intervals) and refreezing procedure were repeated at few times with the spectrum acquired. Finally the solution was allowed to warm up and stand for up to 1-5 hours depending upon the system before re-acquiring the spectrum of the final product of the reaction. The exact procedure followed varied slightly from sample to sample as required.

5.2.1.1 Reaction of $[Fe(L_{15})(CH_3CN)_x]^{2+}$ with H_2O_2

The frozen solution of $[Fe(L_{15})(CH_3CN)_x]^{2+}$ obtained via dissolution of $[Fe(L_{15})(CH_3CN)_2](O_3SCF_3)_2$ in CH_3CN, figure 5.2(a), was EPR silent as expected for a paramagnetic high spin iron(II) complex. An aliquot of aqueous H_2O_2 representing 170 equivalents was then added to the frozen iron(II) solution. Following partial hand thawing to allow some mixing a deep purple colouration was observed to form at the mixing interface of the two solutions. After 2 minutes had elapsed the mixture was quickly re-frozen and its EPR spectrum acquired, figure. 5.2(b)**.** A single isotropic high-spin g = 4.4 signal was present indicative of a high spin (S = 5/2) iron(III) complex in a rhombic environment, whose sharpness and intensity may result from an increase in molecular symmetry in the oxidized complex compared with that of $[Fe(L_{15})(CH_3CN)_x]^{2+}$ itself. A second 2 minute thawing – refreezing procedure resulted in an increase in the intensity of the purple colour paralleling a further growth in the intensity of the g = 4.4 signal, figure 5.2(c)**.** Finally the solution was re-thawed and allowed to stand for 5 hours at room temperature before being refrozen and the spectrum acquired for a final time. After this time the purple colour had long vanished and the

solution was now yellow-brown. The EPR spectrum, figure 5.2(d), had a noticeably smaller g = 4.4 feature signal which was considerably different in appearance to that characterising the purple intermediate in figure 5.2 (c), and (d) possessed two broad features either side of the main g = 4.4 line. It is believed that further reactions of the purple iron(III) species had given rise to two iron species, a new mononuclear high spin iron(III) complex accompanied by an EPR silent iron species. Clues as to the nature of these species resulted from the study of the corresponding reaction with ^{t}BuOOH.

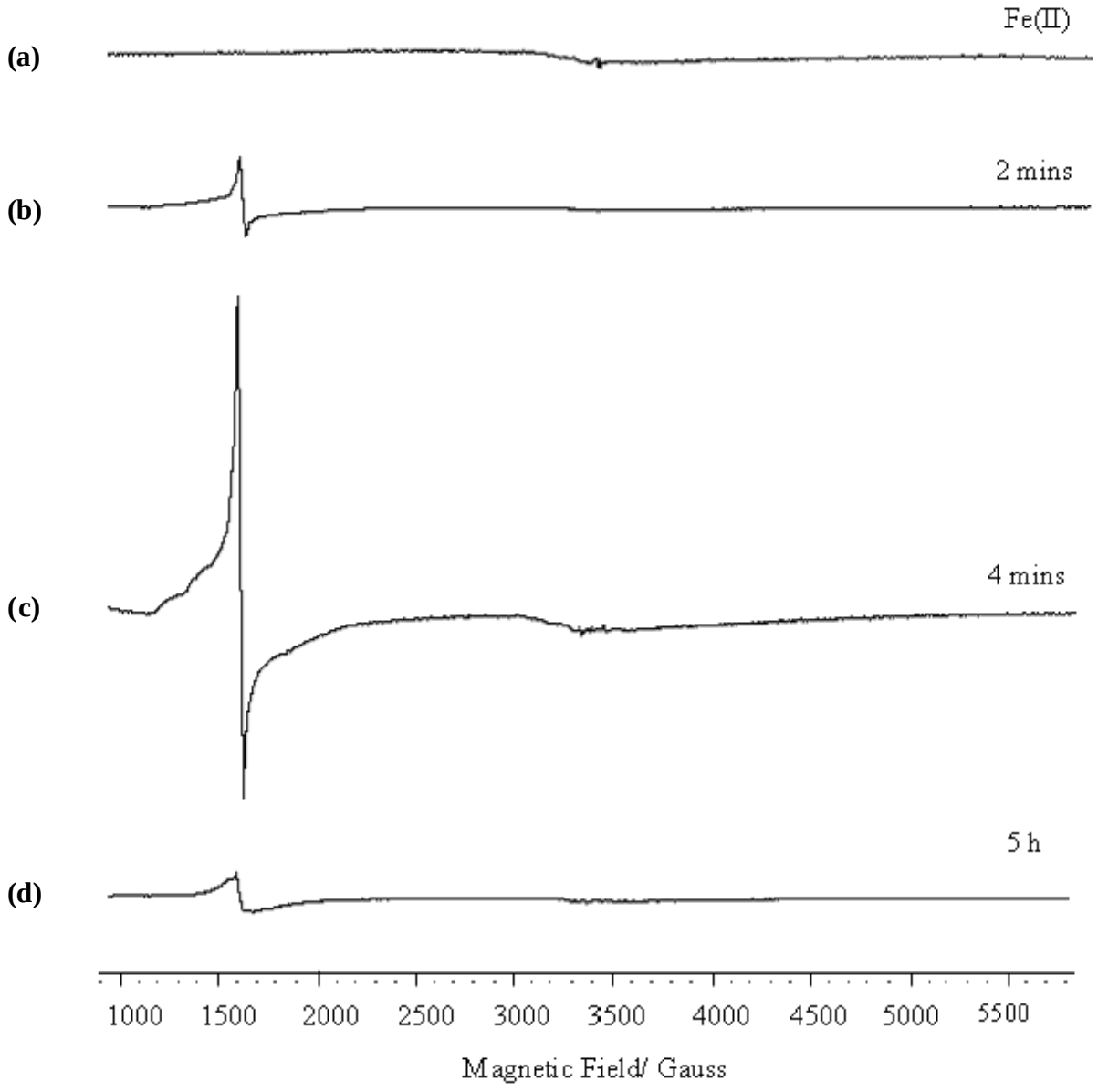

Figure 5.2: X-band EPR spectra at 110 K for a 3 x 10^{-4} mol dm^3 CH_3CN solution of (a) $[Fe(L_{15})(CH_3CN)_x]^{2+}$; (b) after thawing 2 mins/refreeze following addition of 170-fold excess

of H_2O_2 (purple colour at interface); (c) after further thawing 2 mins/refreeze (homogeneous purple colour) and (d) allowed to stand at room temperature for 5 hours and then refrozen (yellow- brown).

5.2.1.2 Reaction of $[Fe(L_{15})(CH_3CN)_x]^{2+}$ with ^tBuOOH.

The reaction of $[Fe(L_{15})(CH_3CN)_x]^{2+}$ with 170 equivalents of an aqueous solution of ^tBuOOH was carried out in an identical fashion to the study with H_2O_2. Following partial hand thawing to allow some mixing a deep purple colouration was again observed to form at the mixing interface of the two solutions. After 2 minutes had elapsed the mixture was quickly re-frozen and its EPR spectrum acquired. As with H_2O_2 a distinct low field EPR signal appeared upon development of the purple colour but it was noticeably different in appearance to that obtained from the H_2O_2 generated purple species, this time having three distinct features around g = 7.5, 5.0 and 4.4, figure 5.3 (b). The sample was again removed from the spectrometer, thawed for 2 min and then refrozen and the spectrum re-acquired. After this process the solution was homogeneously purple in colour. In this case several thawing-refreezing cycles up to ~ 20 mins total incubation, resulted in the same EPR features for the resulting purple solution, figure 5.2(c). The three low field EPR features seen in figure 5.2(b) were again observed but this time accompanied by a strong sharp resonance at ~ g = 2 which is assigned to the $^tBuOO^{\bullet}$ radical.[14-16] The $^tBuOO^{\bullet}$ radical has a half life of ~1 hour below 40^oC and so is trappable under these conditions unlike $HOO^{\bullet}$ which may have formed similarly in the reaction with H_2O_2. The $^tBuOO^{\bullet}$ signal accompanied a decrease in intensity of the high spin iron(III) low field EPR features and is attributed to steps (5.1) and (5.2) involving initial formation of a high spin t-butylperoxoiron(III) complex $[Fe(L_{15})(CH_3CN)_x(OOBu^t)]^{2+}$ followed by homolytic Fe-O cleavage giving $^tBuOO^{\bullet}$ and a new EPR silent iron(II) species.

$$[Fe^{II}(L_{15})(CH_3CN)_x]^{2+} + {}^tBuOOH \longrightarrow [Fe^{III}(L_{15})(OOBu^t)]^{2+} \text{ (purple)} \quad (5.1)$$

$$[Fe^{III}(L_{15})(OOBu^t)]^{2+} \longrightarrow {}^tBuOO\cdot + [Fe^{II}(L_{15})(X)]^{2+} \quad (5.2)$$

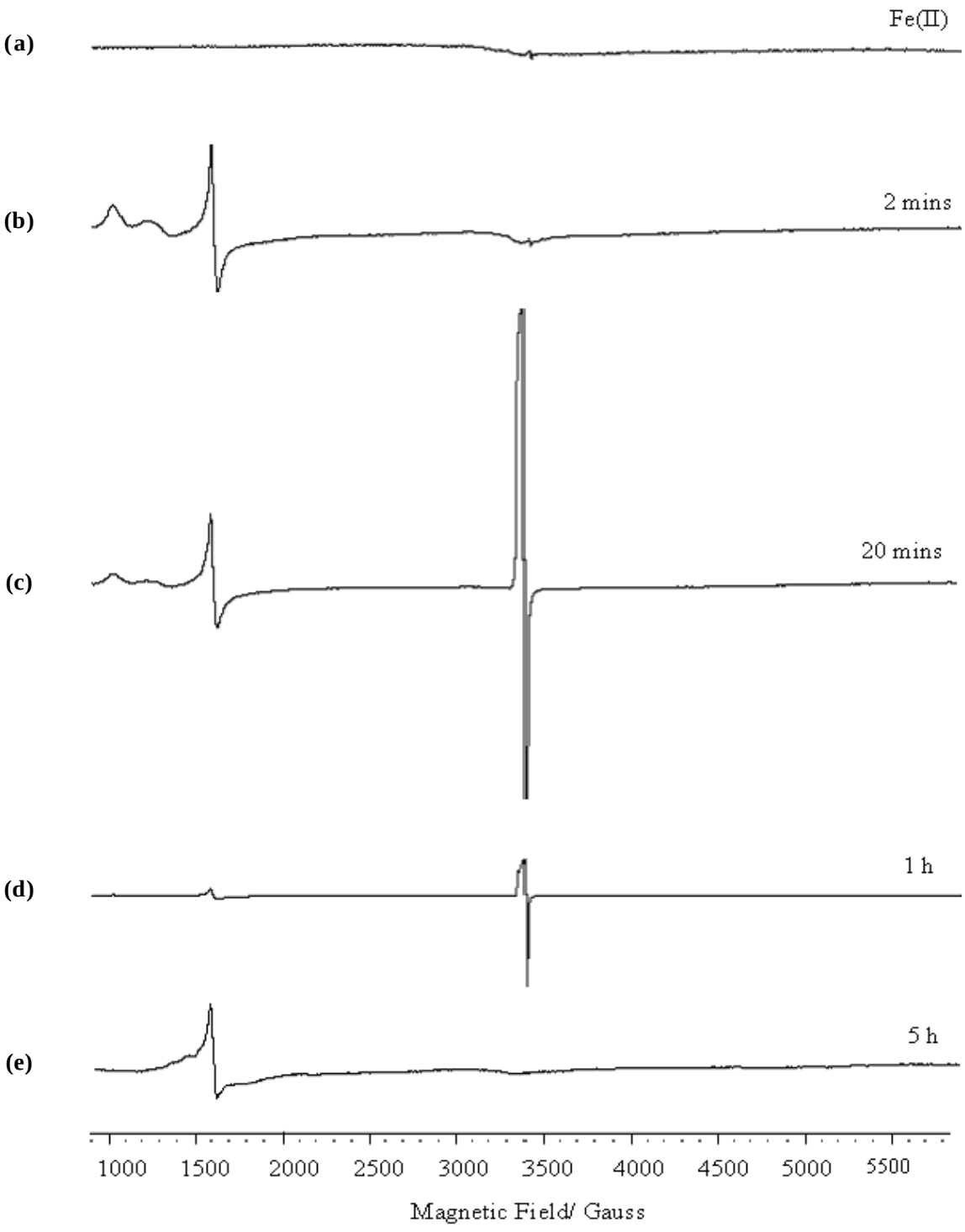

Figure 5.3: X-band EPR spectra at 110 K for a 3 x 10^{-4} mol dm^3 CH_3CN solution of (a) $[Fe(L_{15})(CH_3CN)_x]^{2+}$; (b), (a) with 170-fold excess of ^tBuOOH after 2 minutes (purple colour

at interface); (c), (b) warmed to RT for 20 minutes and refrozen (purple); (d), (c) after standing at RT for 1 hour then refrozen (yellow) and (e), (d) after standing at RT for 5 hours then refrozen (yellow –brown).

The presence of steps (5.1) and (5.2) was further confirmed by thawing and then refreezing after 1 hour incubation wherein only the residual signal of ^{t}BuOO$^{\cdot}$ remained, figure 5.3(d) which will slowly decompose via Russel-type reaction. Further standing at room temperature for 5 hours and then refreezing resulted in the EPR spectrum shown in figure 5.3(e). The signal for ^{t}BuOO$^{\bullet}$ was now absent and the only signal which is present corresponds to the high spin iron(III) signal around g = 4.4, probably obtained from the oxidation of iron (II) oxidadized by the oxygen present in the solution originated in the decomposition of ^{t}BuOO$^{\bullet}$. This signal was identical to the final yellow-brown product obtained in the reaction with H_2O_2, Figure 5.2(d) possessing two broad features either side of the main g = 4.4 line. It is known from previous work in our own laboratory[17] and the work of Que[18] and others[19] that high spin ^{t}BuOOFe(III) complexes are susceptible to homolytic Fe-O cleavage. However, further proofs are needed to rule out whether it is Fe-O cleavage or O-O cleavage. Scheme 5.1 attempts to explain the sequence of reactions resulting from reaction of $[Fe(L_{15})(CH_3CN)_2]^{2+}$ with the two hydroperoxides. The similarity of the EPR features of the purple ^{t}BuOOFe(III) intermediate here to the distinctly rhombic signals characterising the seven-coordinated iron(III) complexes; $[Fe(BPPA)(OOBu^{t})]^{2+}$ and $[Fe(BPPA)(OOCBu^{t})]^{2+}$, obtained by Masuda et al (chapter 4, figure 4.5)[20] suggests assignment to a similar low symmetry seven-coordinate high spin iron(III) species with two of the ether oxygen donors coordinated, figure 5.4**.**

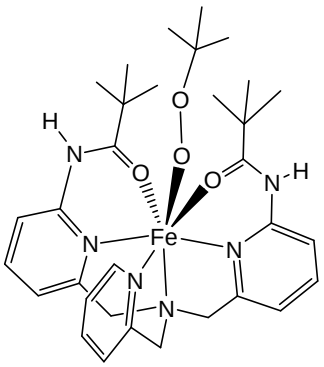

[Fe(BPPA)(OOBu^t)]$^{2+}$ [20]

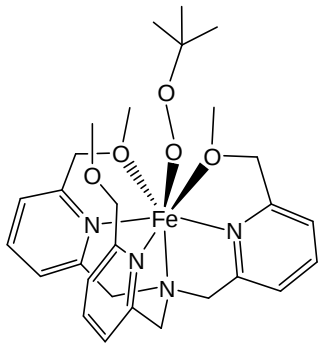

[Fe(L_{15})(OOBu^t)]$^{2+}$ (this work)

Figure 5.4: Structures of high spin seven-coordinated t-butylperoxoiron(III) intermediates of 6-substituted TPA ligands deduced from X-band EPR studies at 110K.

This then undergoes homolytic Fe-O cleavage to generate a different iron(II) complex to that initially present which is then slowly oxidised by the excess ^{t}BuOOH or by oxygen (air) to give the final (stable) high spin iron(III) species.

The nature of this final iron(III) product has not thus far been ascertained. However the lower intensity of its EPR signal compared to that from the purple peroxoiron(III) intermediate, particularly apparent in the H_2O_2 reaction, figures 5.2(c) and (d), and the fact that once formed further treatment with ^{t}BuOOH fails to restore the purple colour, suggests assignment to an unreactive stable high spin iron(III) product possibly a hydroxo(aqua) complex involved in an equilibrium to form an unreactive μ-oxo dimer, scheme 5.1**.**

The reason why the purple alkylperoxo or hydroperoxo iron(III) [Fe(L_{15})(OOR)]$^{3+}$ intermediate deriving from H_2O_2 (R = H) is different (more symmetric) that for R = Bu^t is not obvious. One idea is that the slightly

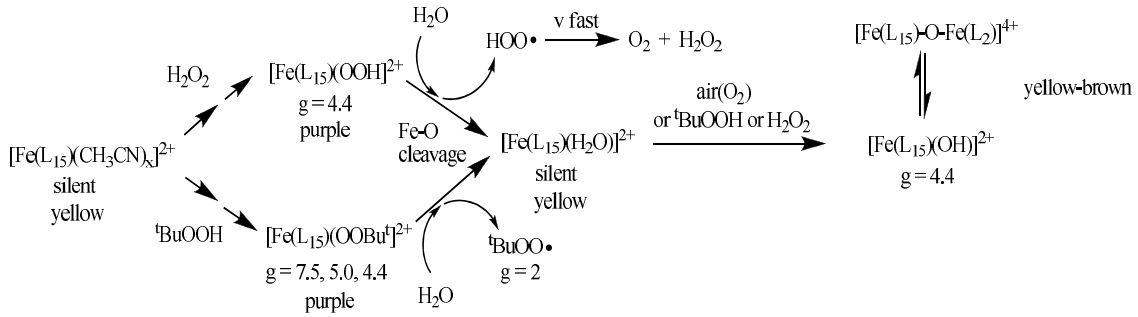

Scheme 5.1

more hydrophobic nature of ^{t}BuOOH may lead to a greater interaction with the methyl groups of the MeO substituents hence favouring the seven coordinated alkylperoxo iron(III) intermediate with two of the ether groups coordinated whereas the presence of proton on the OOH group may lead to hydrogen bonding with the ether oxygen thus leading to a more symmetric 6-coordinated hydroperoxoiron(III) species, figure 5.5, with coordination of only one ether oxygen to iron(III).

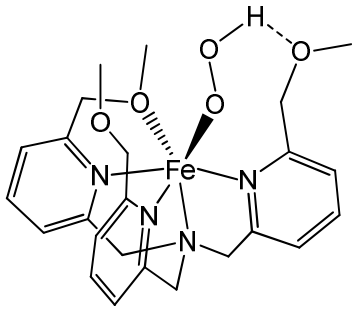

Figure 5.5: Possible hydrogen-bonding interaction from OOH leading to a more symmetric 6- coordinated complex for putative purple $[Fe(L_{15})(OOH)]^{2+}$ having only one ether oxygen coordinated to iron(III).

5.2.1.3 Reaction of $[Fe(L_{16})(CH_3CN)_x]^{2+}$ with H_2O_2

The reaction of the octyloxymethyl TPA derivative complex $[Fe(L_{16})(CH_3CN)_x]^{2+}$ with 170 equivalents of H_2O_2 in CH_3CN was carried out in an identical fashion to the study of the reaction of $[Fe(L_{16})(CH_3CN)_x]^{2+}$. The frozen solution of $[Fe(L_{16})(CH_3CN)_x]^{2+}$ in CH_3CN, figure 5.6(a), was EPR silent as expected for a paramagnetic high spin iron(II) complex. An

aliquot of aqueous H_2O_2 representing 170 equivalents was then added to the frozen iron(II) solution. Following partial hand thawing to allow some mixing a deep purple colouration was observed to form at the mixing interface of the two solutions. After 2 minutes had elapsed the mixture was quickly re-frozen and its EPR spectrum acquired, figure 5.6(b)**.** A single isotropic high-spin g = 4.4 signal was present similar to that formed with $[Fe(L_{15})(CH_3CN)_x]^{2+}$ indicative of a high spin (S = 5/2) iron(III) complex in a high symmetry rhombic environment. A second 2 minute thawing – refreezing procedure resulted in an increase in the intensity of the purple colour paralleling a further growth in the intensity of the g = 4.4 signal, not shown.

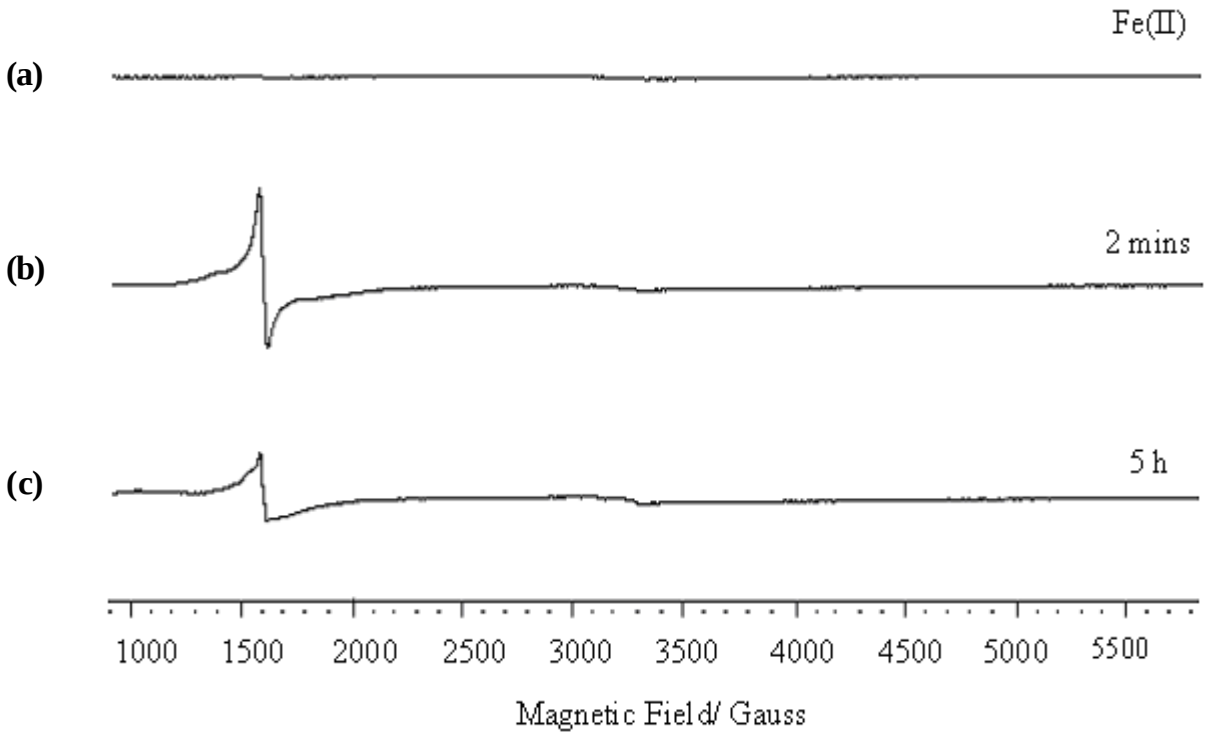

Figure 5.6: X-band EPR spectra at 110 K for a 3 x 10^{-4} mol dm^3 CH_3CN solution of (a) $[Fe(L_{16})(CH_3CN)_x]^{2+}$; (b) following addition of 170-fold excess of H_2O_2 after 2 minutes (purple colour at interface); (c) allowed to stand at room temperature for 5 hours and then refrozen (yellow-brown).

Finally the solution was re-thawed and allowed to stand for 5 hours at room temperature before being refrozen and the spectrum acquired for a final time. After this time the purple colour had long vanished and the solution was now yellow-brown. The EPR spectrum, figure 5.6(c), was virtually identical to that obtained from reaction with $[Fe(L_{15})(CH_3CN)_x]^{2+}$ with H_2O_2 after 5 h with a noticeably smaller g = 4.4 feature signal considerably different in appearance (more rhombic) to that characterising the purple intermediate, figure 5.2(b), possessing two broad feature either side of the main g = 4.4 line. It is believed that further reactions of the purple iron(III) species had given rise to two iron species, a new mononuclear high spin iron(III) complex accompanied by an EPR silent iron species. Clues as to the nature of these species again resulted from the study of the corresponding reaction of $[Fe(L_{16})(CH_3CN)_x]^{2+}$ with ^tBuOOH.

5.2.1.4 Reaction of $[Fe(L_{16})(CH_3CN)_x]^{2+}$ with ^tBuOOH

The reaction of $[Fe(L_{16})(CH_3CN)_x]^{2+}$ with 170 equivalents of an aqueous solution of ^tBuOOH was carried out in an identical fashion to the reaction of $[Fe(L_{15})(CH_3CN)_x]^{2+}$. In this case, however, the solution of $[Fe(L_{16})(CH_3CN)_x]^{2+}$ already possessed a weak g = 4 signal, figure 5.7(a). Following partial hand thawing to allow some mixing a deep purple colouration was again observed to form at the mixing interface of the two solutions. After 2 minutes had elapsed the mixture was quickly re-frozen and its EPR spectrum acquired. As with H_2O_2 a distinct low field EPR signal appeared upon development of the purple colour which was noticeably different in appearance to that obtained from the H_2O_2 generated purple species and as with $[Fe(L_{15})(CH_3CN)_x]^{2+}$ possessed three distinct low field features around g = 7.5, 5.0 and 4.4, figure 5.7(b). The sample was again removed from the spectrometer, thawed for 15 min and then refrozen and the spectrum re-acquired. After this process the solution was homogeneously purple in colour. The three low field EPR features seen in figure 5.7(b) were again observed, figure 5.7(c), but this time lower in intensity accompanied by a strong sharp

resonance at ~ g = 2 assigned to the ^{t}BuOO$^{\bullet}$ radical. It is believed that steps (5.1) and (5.2) take place as for the methoxymethyl L^1 derivative involving initial formation of the high spin iron(III) complex $[Fe(L_{16})(OOBu^{t})]^{2+}$ followed by homolytic Fe-O cleavage giving ^{t}BuOO$^{\bullet}$ and a new EPR silent iron(II) species.

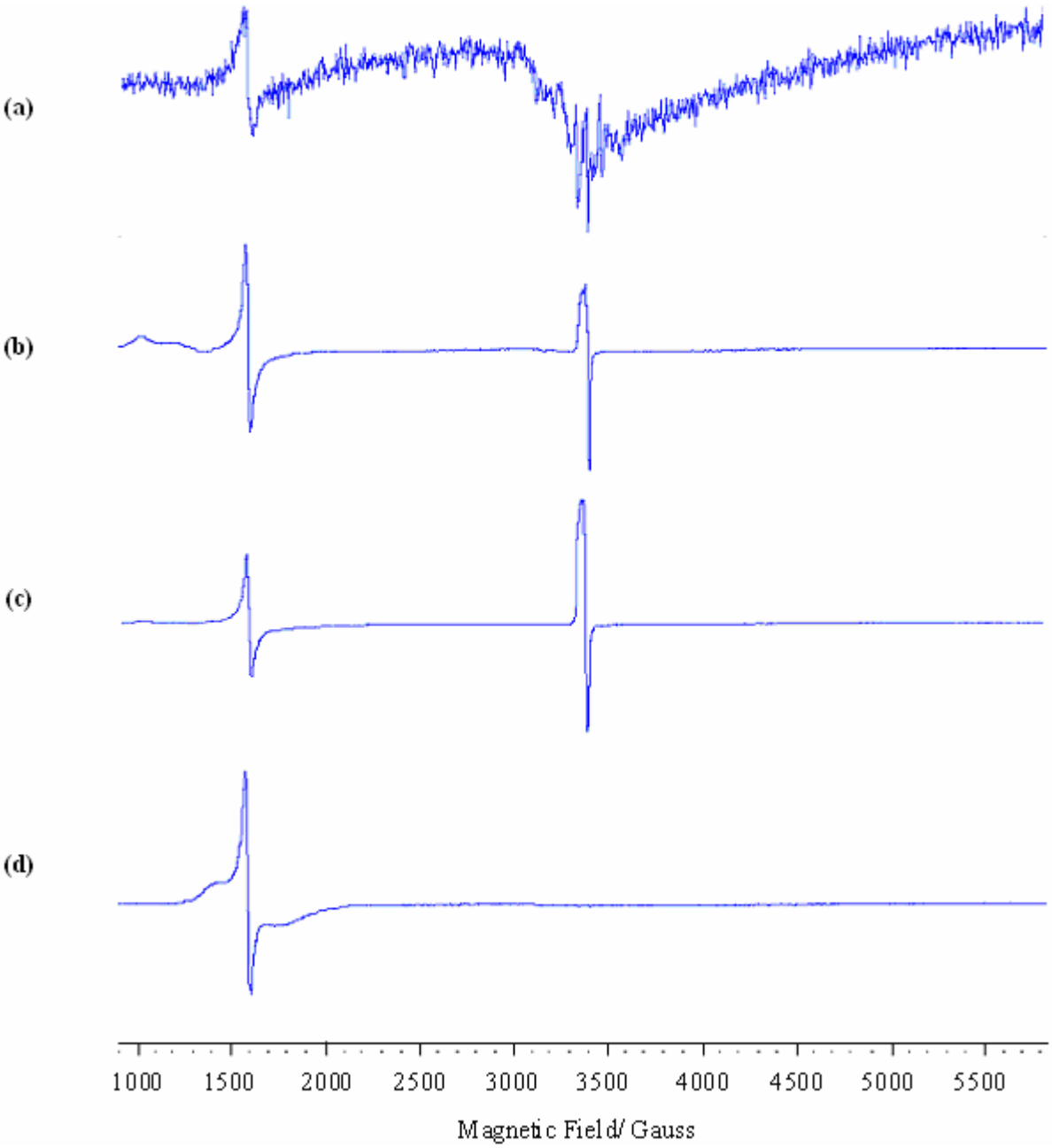

Figure 5.7: X-band EPR spectra at 110 K for a 3 x 10^{-4} mol dm^3 CH_3CN solution of (a) $[Fe(L_{16})(CH_3CN)_x]^{2+}$; (b), (a) with 170-fold excess of ^{t}BuOOH after 2 minutes (purple colour

at interface); (c), (b) warmed to RT for 15 mins and the refrozen (purple); (d), (c) after standing at RT for 5 hours then refrozen (yellow–brown).

Further standing at room temperature for 5 hours and then refreezing resulted in the EPR spectrum shown in figure 5.7(d). The signal of $^{t}BuOO^{\bullet}$ had now vanished and was replaced by a new narrower rhombic high spin iron(III) signal around g = 4.4 with distinct broad features either side of the main g = 4.4. line. The spectrum was identical to that obtained from the reaction of $[Fe(L_{15})(CH_3CN)_x]^{2+}$ with $^{t}BuOOH$ after 5 h, figure 5.3(e). The behaviour overall paralleled that observed with the methoxymethyl derivative L^2 suggesting that introduction of the longer n-octyl groups did not have a significant effect on the overall scheme of reactions of the iron(II) complexes with either hydroperoxide.

The detection of largely Haber-Weiss-Fenton behaviour in the reactions of both $[Fe(L_{15})(CH_3CN)_x]^{2+}$ and $[Fe(L_{16})(CH_3CN)_x]^{2+}$ with H_2O_2 and $^{t}BuOOH$, as has been observed previously with e.g. trispicolinatoiron(III) in pyridine,[17] with little evidence of high valent iron intermediates, was a little disappointing. The reactivity pathways are believed to reflect the high spin nature of the peroxoiron(III) intermediates favouring Fe-O, rather than O-O, cleavage pathways. As a result interest turned to corresponding experiments with the iron(II) complexes of the n-hexylurea-substituted TPA ligands; L_{21} and L_{22}. The synthesis and characterisation of the iron(II) complexes of these ligands was reported in chapter 4. Here the reactivity of $[Fe(L_{21})(CH_3CN)_x]^{2+}$ and $[Fe(L_{22})(CH_3CN)_x]^{2+}$ with H_2O_2 and $^{t}BuOOH$ in CH_3CN solvent is explored by X-band EPR accompanied in this case by time-resolved UV-VIS studies.

5.2.1.5 Reaction of $[Fe(L_{21})(CH_3CN)_x]^{2+}$ with H_2O_2

The reactivity of the iron(II) complex of L_{21}, carrying only one 6-n-hexylurea substituent, is of interest in that reaction of peroxides with $[Fe(6\text{-MeTPA})(CH_3CN)_2]^{2+}$ (only one 6-Me substituent) form predominantly low spin peroxoiron(III) complexes albeit in equilibrium

with small quantities of high spin forms.[21, 22] Low spin peroxoiron(III) intermediate are more likely than high spin forms at promoting O-O rather than Fe-O cleavage reactions and are thus more likely to give rise to the desirable high

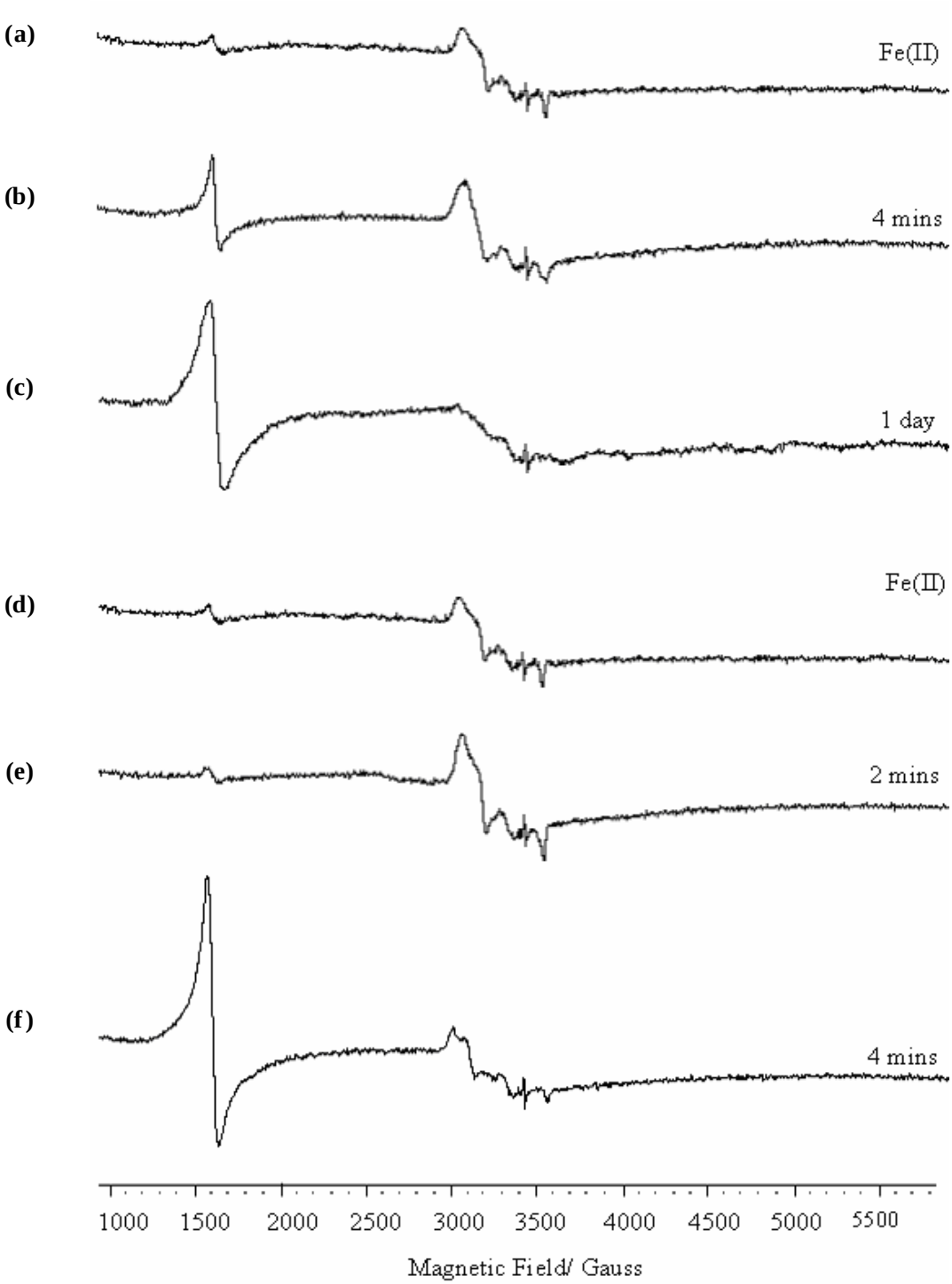

Figure 5.8: X-band EPR spectra at 110 K for a 3 x 10^{-4} mol dm^3 CH_3CN solution of (a) $[Fe(L_{21})(CH_3CN)_x]^{2+}$; (b) following addition of 170-fold excess of H_2O_2, thaw/refreeze after 4 minutes (pinkish-brown colour at interface) and (c) allowed to stand at room temperature for

1 hour and then refreeze (yellow-brown). Runs (d) – (e) are for a repeat experiment with fresh $[Fe(L_{21})(CH_3CN)_x]^{2+}$.

valent iron intermediate oxidants. The X-band EPR study of the reaction of H_2O_2 with $[Fe(L_{21})(CH_3CN)_x]^{2+}$ was carried out in identical fashion to that for $[Fe(L_{15})(CH_3CN)_x]^{2+}$ and $[Fe(L_{16})(CH_3CN)_x]^{2+}$. The results are shown in figure 5.8. $[Fe(L_{21})(CH_3CN)_x]^{2+}$ differed from $[Fe(L_{15})(CH_3CN)_x]^{2+}$ and $[Fe(L_{16})(CH_3CN)_x]^{2+}$ in being noticeably air-sensitive. Despite attempts to make up the iron(II) solutions under air-free conditions, fresh frozen yellow solutions of $[Fe(L_{21})(CH_3CN)_x]^{2+}$ in CH_3CN always showed a weak rhombic signal in the region around g = 2 attributable to a low spin iron(III) species in equilibrium with a very small amount of a high spin species (weak g = 4.5 signal), figure 5.8(a) and (d)**.** Following addition of 170 equivalents of aqueous H_2O_2 to the CH_3CN solution of $[Fe(L_{21})(CH_3CN)_x]^{2+}$ with partial thawing to mix and then refreezing after 2-4 minutes incubation the solution did not exhibit a distinct purple colour this time at the interface but revealed a faint pinkish-brown colour which turned brownish with time. The acquired EPR spectrum showed an increase in the rhombic low spin feature followed by its collapse (4 mins) to reveal a growing low field signal at g = 4.5 attributable to a high spin iron(III) species. When the solution was allowed to stand for 1 hour and then re-frozen the pinkish brown colour persisted as did the low spin feature around g = 2 only slowly fading away over a period of 1 day to leave behind the low field high spin iron(III) signal. In order to understand what was being formed here it was decided to following the corresponding reaction of $[Fe(L_{21})(CH_3CN)_x]^{2+}$ with ^tBuOOH.

5.2.1.6 Reaction of $[Fe(L_{21})(CH_3CN)_x]^{2+}$ with ^tBuOOH.

A yellow CH_3CN solution of $[Fe(L_{21})(CH_3CN)_x]^{2+}$ was frozen and into this was syringed a small aliquot representing 170 equivalents of aqueous ^tBuOOH. Following partial hand thawing to allow solution mixing a deep blue colouration was observed to form at the mixing interface of the two solutions.

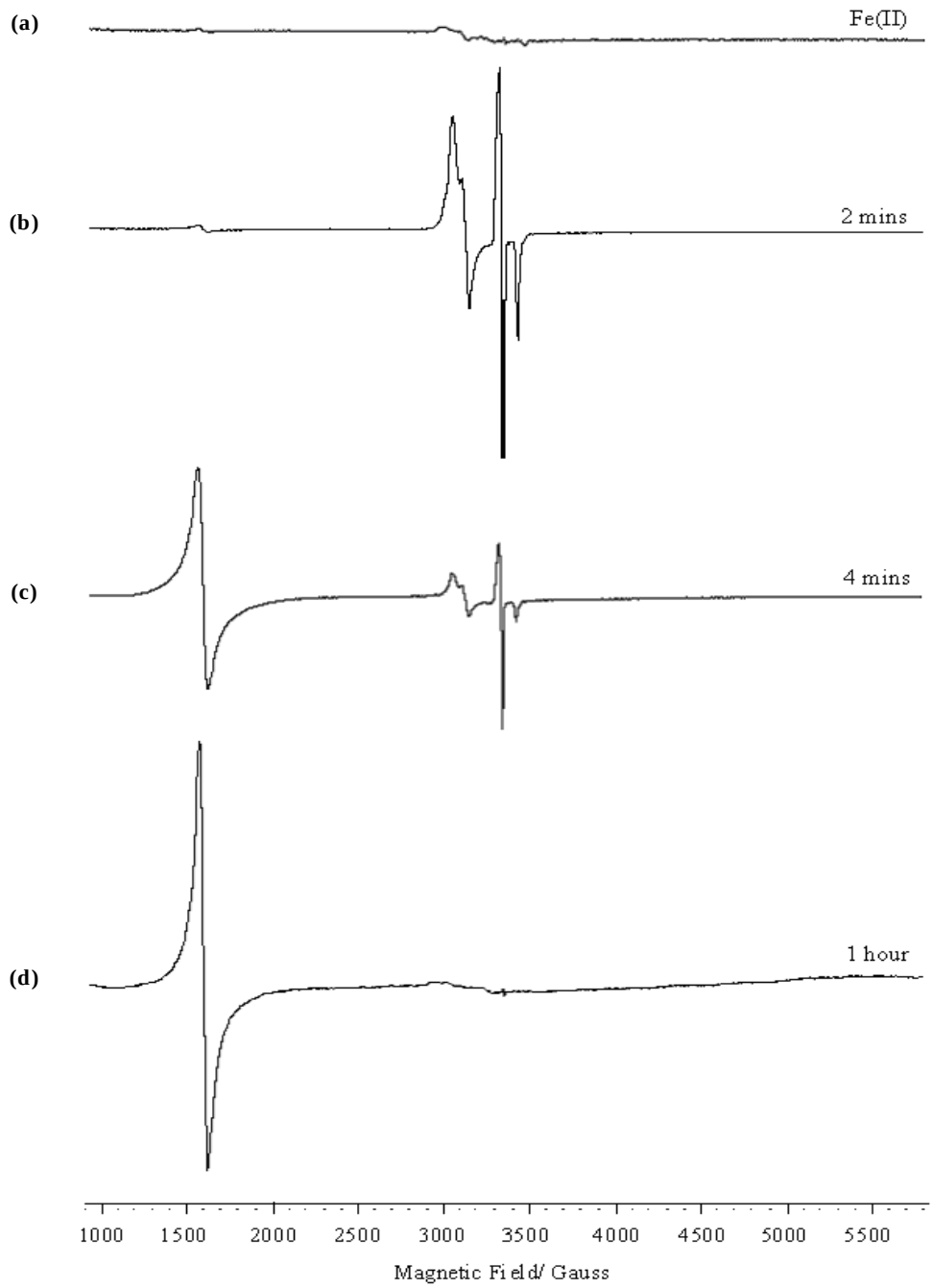

Figure 5.9: X-band EPR spectra at 110 K for a 3 x 10^{-4} mol dm^3 CH_3CN solution of (a) $[Fe(L_{21})(CH_3CN)_x]^{2+}$; (b), (a) with 170-fold excess of ^{t}BuOOH after 2 minutes (deep blue colour at interface); (c), (b) warmed to RT for 2 mins and the refrozen (homogeneous deep blue); (d), (c) after standing at RT for 1 hour then refrozen (yellow–brown).

After 2 minutes had elapsed the mixture was quickly re-frozen and its EPR spectrum acquired. Unlike the reaction with H_2O_2, above here the changes were more distinct. A distinct rhombic low spin iron(III) signal appeared in the g = 2 region accompanied by a strong sharp feature around g = 2 corresponding to the ^{t}BuOO$^{\bullet}$ radical, figure 5.9 (b). There was little change in the high spin region apart from the presence of a small residual g = 4.5 signal. The sample was again removed from the spectrometer, thawed for another 2 min and then refrozen and the spectrum re-acquired. After this process the solution was homogeneously deep-blue in colour. The resulting EPR spectrum, figure 5.9(c), showed a decrease in the intensity of both the rhombic low spin iron(III) feature and the g = 2 signal for ^{t}BuOO$^{\bullet}$ accompanied by the appearance of a strong isotropic high spin signal at ~ g = 4.4. Warming for 1 hour then refreezing completely removed both of the features in the ~g = 2 region with the only feature remaining being the now quite intense isotropic g = 4.4 signal attributable to a high spin iron(III) centre in a fairly high symmetry environment, figure 5.9(d).

The big difference between $[Fe(L_{21})(CH_3CN)_x]^{2+}$ and both $[Fe(L_{15})(CH_3CN)_x]^{2+}$ and $[Fe(L_{16})(CH_3CN)_x]^{2+}$, which have all three py rings 6-substituted, is the formation of a deep blue low spin t-butylperoxo-iron(III) intermediate even if the final product again is a yellow-brown high spin iron(III) species. The formation of the low spin peroxoiron(III) complexes with L_{21} is attributed to the maintenance of a reasonably strong ligand field around the iron centre as a result of the presence of only one 6-alkyl-py substituent. Similar behaviour has been observed with the monomethylated TPA complex; $[Fe(6\text{-MeTPA})(CH_3CN)_2]^{2+}$. Low spin t-butylperoxoiron(III) complex tend to react on via O-O cleavage processes which if so would generate the putative EPR silent high valent intermediate complex $[Fe^{IV}(L_{21})(O)(CH_3CN)_x]^{2+}$ and ^{t}BuO$^{\bullet}$ radical **(5.3)**. The formation here of some ^{t}BuOO$^{\bullet}$ could then be as a result of rapid C-H abstraction on the excess ^{t}BuOOH by ^{t}BuO$^{\bullet}$ radical **(5.4)**.

$$[Fe^{III}(L_{21})(OOBu^t)]^{2+} \longrightarrow {}^tBuO\cdot + [Fe^{IV}(L_{21})(O)]^{2+} \quad (5.3)$$

$${}^tBuO\cdot + {}^tBuOOH \longrightarrow {}^tBuOO\cdot + {}^tBuOH \quad (5.4)$$

So the observation here of some $^tBuOO^{\bullet}$ radical is not necessarily an indication of the operation of Haber-Weiss Fe-O cleavage as far as low spin peroxoiron(III) complexes are concerned although further independant proof of the O-O cleavage reaction **(5.3)** is required. Formation of the final iron(III) product could be as a result of further oxidative reactions involving reduction of putative $[Fe^{IV}(L_{21})(O)(CH_3CN)_x]^{2+}$ or via oxidation (via O_2, ^tBuOOH or $Fe^{IV}O$) of the iron(II) species generated via Haber-Weiss Fe-O cleavage as for L_{15} and L_{16}.

5.2.1.7 Reaction of $[Fe(L_{22})(CH_3CN)_x]^{2+}$ with H_2O_2.

The reaction of the bis(6-n-hexylurea substituted TPA complex; $[Fe(L_{22})(CH_3CN)_x]^{2+}$ with 170 equivalents of H_2O_2 in CH_3CN was carried out in an identical fashion to the study of the reaction of $[Fe(L_{21})(CH_3CN)_x]^{2+}$. The frozen solution of $[Fe(L_{22})(CH_3CN)_x]^{2+}$ in CH_3CN, Figure 5.10 (a), was EPR silent as expected for a paramagnetic high spin iron(II) complex. An aliquot of aqueous H_2O_2 representing 170 equivalents was then added to the frozen iron(II) solution. Following partial hand thawing to allow some mixing a faint purple-brown colouration was observed to form at the mixing interface of the two solutions. After 2 minutes had elapsed the mixture was quickly re-frozen and its EPR spectrum acquired, figure 5.10 (b). A very weak isotropic high-spin g = 4.4 signal was now present in the spectrum. A second 2 minute thawing – refreezing procedure resulted in bleaching of the purple-brown colour to give a yellow solution which paralleled the appearance now of an intense isotropic signal at g = 4.4, figure 5.10 (c), similar to that formed with $[Fe(L_{15})(CH_3CN)_x]^{2+}$ and indicative of a high spin (S = 5/2) iron(III) complex in a high symmetry environment. The spectrum obtained was unchanged on further standing at RT for 1 hour. Clues as to the nature of the species being generated came from a study of the corresponding reaction of $[Fe(L_{22})(CH_3CN)_x]^{2+}$ with ^tBuOOH.

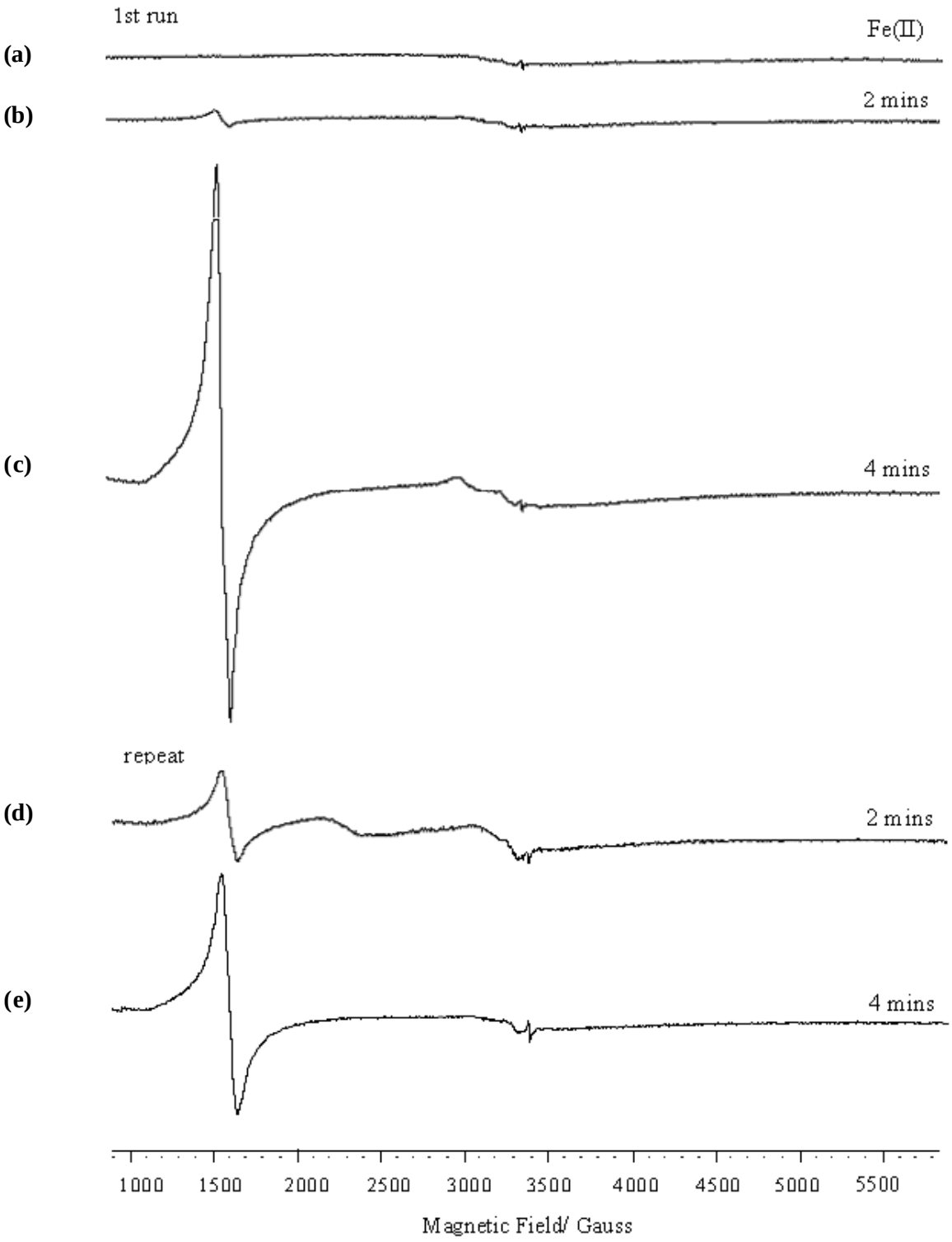

Figure 5.10: X-band EPR spectra at 110 K for a 3 x 10^{-4} mol dm^3 CH_3CN solution of (a) $[Fe(L_{22})(CH_3CN)_x]^{2+}$; (b) thawing 2 mins/refreeze following addition of 170-fold excess of H_2O_2 (pale-purple colour at interface); (c) (b) after thawing 2 mins/refreeze (yellow). (d) and (e) are from a repeat experiment.

5.2.1.8 Reaction of $[Fe(L_{22})(CH_3CN)_x]^{2+}$ with ^tBuOOH

The reaction of $[Fe(L_{22})(CH_3CN)_x]^{2+}$ with 170 equivalents of an aqueous solution of ^tBuOOH was carried out in an identical fashion to the study with H_2O_2. An aliquot of aqueous ^tBuOOH representing 170 equivalents was added to the frozen yellow iron(II) solution. Following partial hand thawing to allow some mixing a deep blue colouration was observed to form at the mixing interface of the two solutions. After 2 minutes had elapsed the mixture was quickly re-frozen and its EPR spectrum acquired. As with H_2O_2 a distinct low field EPR signal appeared upon development of the blue colour but it was noticeably different in appearance to that obtained from reaction with H_2O_2. A highly asymmetric rhombic high spin signal was obtained reminiscent of that obtained with $[Fe(L_{15})(CH_3CN)_x]^{2+}$ and $[Fe(L_{16})(CH_3CN)_x]^{2+}$. Three distinct rhombic features were observed at g = 8.5, 6.0 and 4.4, figure 5.10(b), along with a weak g = 2 signal for $^tBuOO^{\bullet}$. The sample was again removed from the spectrometer, thawed for 2 min and then refrozen and the spectrum re-acquired. After this process the solution was homogeneously deep blue in colour. The spectrum, figure 5.11 (c), was similar to that in Figure 5.11(b) except for an increase in all the observed features. A further thaw for 5 minutes and refreeze resulted in a slight drop in the intensity of the low field signals at the expense of an increase in the intensity of the g = 2 signal of $^tBuOO^{\bullet}$. After warming to RT and standing for 1 hour remarkably the solution was still deep blue in colour. The acquired EPR spectrum upon freezing still showed that the low field features were very slowly disappearing while the g = 2 signal of $^tBuOO^{\bullet}$ was still in evidence. This is the longest time after standing at RT that some $^tBuOO^{\bullet}$ could still be detectable in these Fe(II)(L)/^{t}BuOOH mixtures by EPR indicating that it must be being continuously produced via the slow collapsed of the species responsible for the low field EPR features and the intense blue colour, the high spin t-butylperoxoiron(III) species, $[Fe(L_{22})(OOBu^t)]^{2+}$. $[Fe(L_{22})(OOBu^t)]^{2+}$ is by far the longest lived of all the t-butylperoxoiron(III) complexes

studied in this work with its mode of decay being an incredibly slow (Haber-Weiss) Fe-O cleavage process generating a steady flux of ^{t}BuOO$^{\bullet}$ radical.

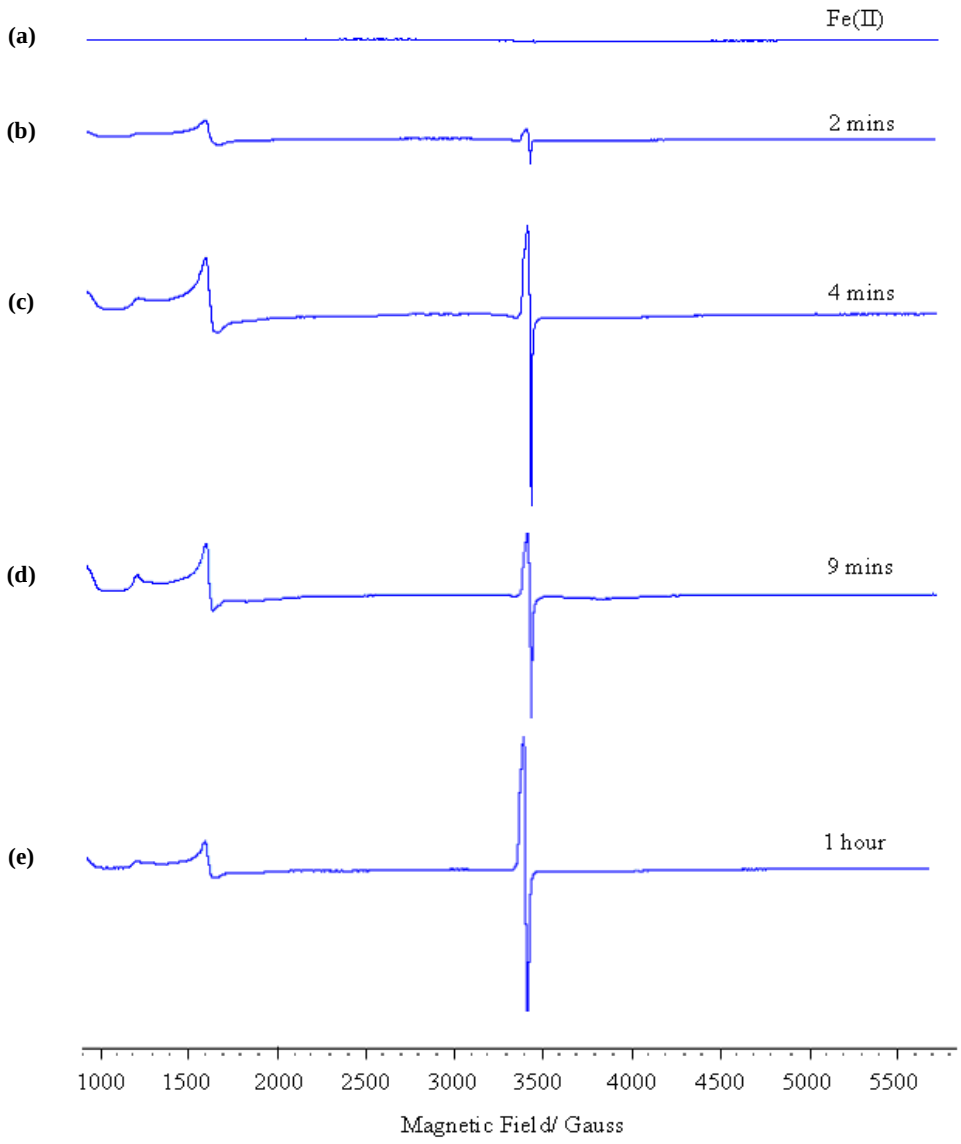

Figure 5.11: X-band EPR spectra at 110 K for a 3 x 10^{-4} mol dm^3 CH_3CN solution of (a) $[Fe(L_{22})(CH_3CN)_x]^{2+}$; (b), (a) with 170-fold excess of ^{t}BuOOH after 2 minutes (deep purple colour at interface); (c), (b) thaw 2 minutes/refreeze (homogeneous deep purple); (d), (c) thaw 5 minutes/refreeze (homogeneous deep purple); (e) (d) warm to RT for 1 hour then refreeze (still purple!!).

This prompted a time-resolved UV-VIS spectrophotometric study at 25°C of the decay of both $[Fe(L_{21})(OOBu^t)]^{2+}$ and $[Fe(L_{22})(OOBu^t)]^{2+}$ in CH_3CN solution under different conditions for comparisons with other known ROOFe(III)(L) species reported in the literature.

5.2.2. Time-resolved UV-VIS spectrophotometric studies of the reactions of $[Fe(L)(CH_3CN)_x]^{2+}$ species with H_2O_2 and ^tBuOOH in CH_3CN solvent at 25°C.

5.2.2.1 Reaction of $[Fe(L_{21})(CH_3CN)_x]^{2+}$ with H_2O_2.

Figure 5.12 shows a UV-visible spectrum for a 2.5 x 10^{-3} mol dm^{-3} solution of $[Fe(L_{21})(CH_3CN)_x]^{2+}$ in CH_3CN following the addition of 100 fold excess of H_2O_2 at 25°C (spectrum A) and after completion of the reaction (spectrum B). Spectrum A corresponds to the maximum amount of the hydroperoxoiron(III) complex; $[Fe(L_{21})(OOH)]^{2+}$ (λ_{sh} = 530 nm) generated under these conditions.

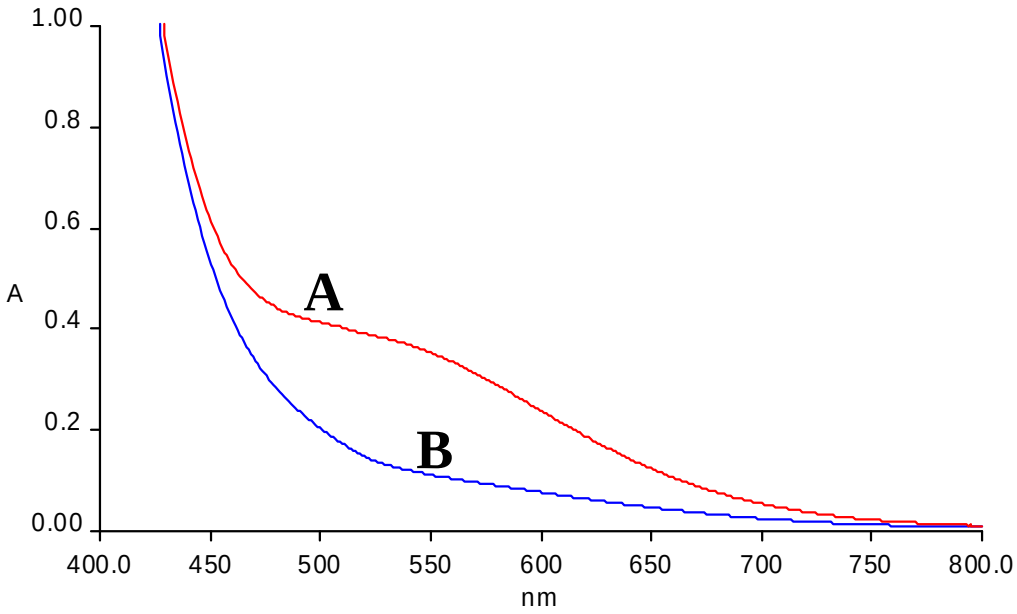

Figure 5.12: UV-VIS spectra in CH_3CN following the addition of a 100 fold excess of H_2O_2 to a solution of $[Fe(L_{21})(CH_3CN)_x]^{2+}$ (2.5 x 10^{-3} mol dm^{-3}) at 25°C (spectrum A) and at the completion of the decay (spectrum B).

Figure 5.13 shows a plot of the decay in the absorbance of the hydroperoxoiron(III) complex at 530 nm versus time at 25°C. Each data point was taken at 5 minute intervals. The data was fitted successfully to a single exponential decay corresponding to a rate constant of (3.80 ± 0.02) x 10^{-2} min^{-1}. It cannot be ascertained from the UV-VIS data whether the decay of $[Fe(L_{21})(OOH)]^{2+}$ is due to homolytic Fe-O or O-O cleavage since if formed in the latter process the putative oxoiron(IV) species; $[Fe(L_{21})(O)(CH_3CN)_x]^{2+}$ would decay rapidly at

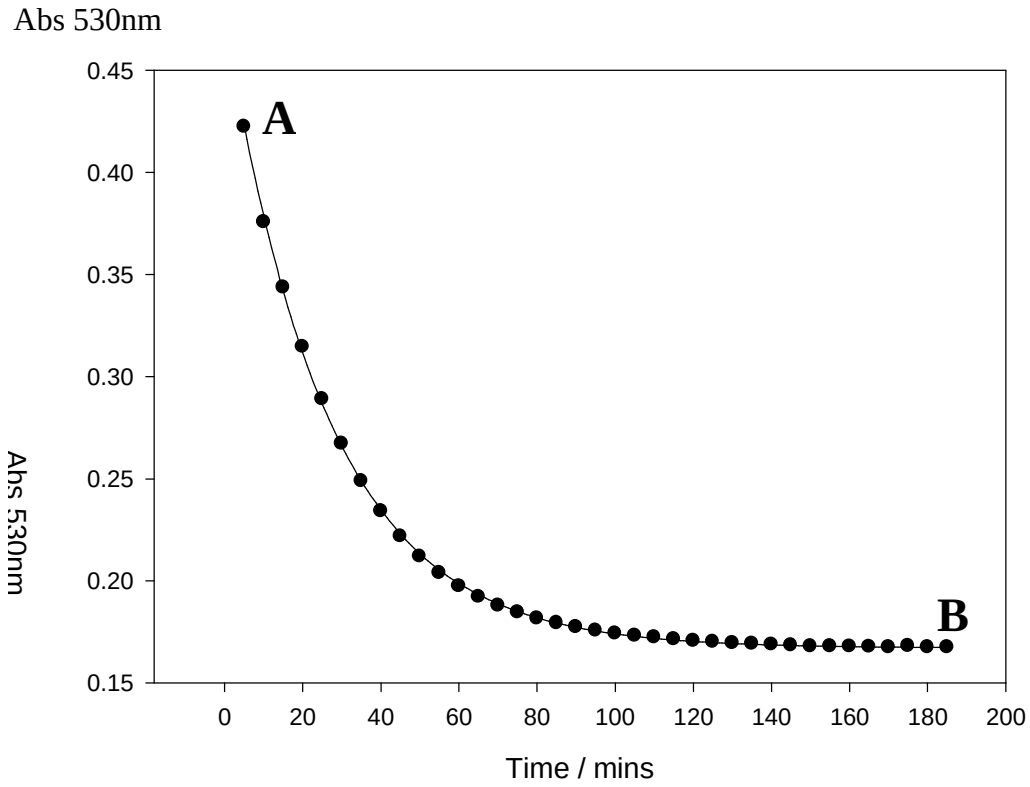

Figure 5.13: Plot of the decay in the absorbance at 530nm (data at 5 minute intervals) following the addition of a 100 fold excess of H_2O_2 to a solution of $[Fe(L_{21})(CH_3CN)_x]^{2+}$ (2.5 x 10^{-3} mol dm^{-3}) in CH_3CN at 25°C. The solid line is a least square fit to a single exponential decay.

temperatures ~ 25°C as observed from the reactions of H_2O_2 with $[Fe(TPA)(CH_3CN)_2]^{2+}$ and $[Fe(6\text{-}MeTPA)(CH_3CN)_2]^{2+}$ [8] Here the oxoiron(IV) species $[Fe(L)(O)(CH_3CN)_x]^{2+}$ can only be trapped in CH_3CN at temperatures below -40°C. Indications as to which process may be

responsible for the absorbance changes in figure 5.13 however are apparent from studies of the catalysis by $[Fe(L_{21})(CH_3CN)_x]^{2+}$ of H_2O_2 oxygenation on cyclohexane reported at the end of this chapter, section 5.3.

5.2.2.2 Reaction of $[Fe(L_{21})(CH_3CN)_x]^{2+}$ with ^{t}BuOOH

Initial investigations at 25^{o}C showed that the putative blue t-butylperoxoiron(III) complex $[Fe(L_{21})OOBu^t]^{2+}$ decayed away too rapidly for a kinetic study to be undertaken since it was not available a low temperature cryostatic kinetic capability. Nonetheless the observed rate of decay was reminiscent of the reactions of ^{t}BuOOH with $[Fe(TPA)(CH_3CN)_2]^{2+}$ and $[Fe(6\text{-}MeTPA)(CH_3CN)_2]^{2+}$ wherein temperatures of at least -40^{o}C are required to detect the blue t-butylperoxoiron(III) intermediate and observe its decay. In this regard the much slower decay of the $[Fe(L_{21})(OOH)]^{2+}$ is interesting and may be as a result of a hydrogen-bonded stabilisation via the single n-hexylurea substituent group, figure 5.14. Such hydrogen–bonding will be absent in the corresponding t-butylperoxoiron(III) intermediate.

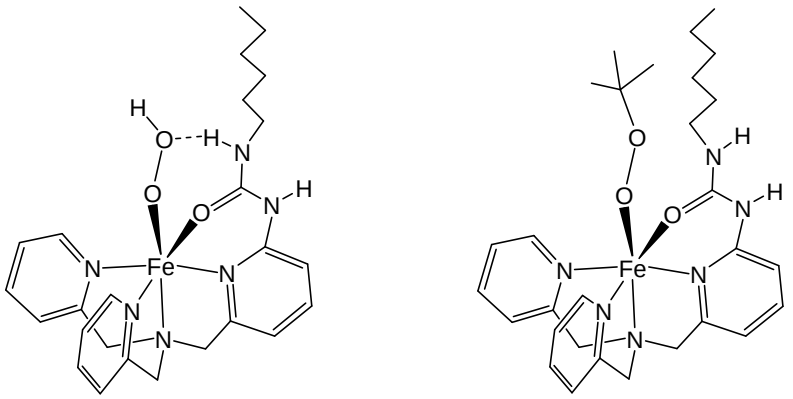

A **B**

Figure 5.14: Structures of putative peroxoiron(III) intermediates deriving from reaction of $[Fe(L_{21})(CH_3CN)_x]^{2+}$ in CH_3CN with H_2O_2 (**A**) and ^{t}BuOOH (**B**).

5.2.2.3 Reaction of $[Fe(L_{22})(CH_3CN)_x]^{2+}$ with H_2O_2

Initial investigations at 25°C showed that the purple-brown hydroperoxoiron(III) intermediate $[Fe(L_{22})OOH]^{2+}$ seen in the low temperature EPR experiments decayed away too rapidly for a kinetic study to be undertaken since it was not available a low temperature cryostatic kinetic capability. Nonetheless the observed rate of decay was reminiscent of the reactions of H_2O_2 with $[Fe(TPA)(CH_3CN)_2]^{2+}$ wherein temperatures of at <-40°C are required to follow the appearance and decay of the corresponding purple hydroperoxoiron(III) intermediate.

5.2.2.4 Reaction of $[Fe(L_{22})(CH_3CN)_x]^{2+}$ with ^{t}BuOOH

Figure 5.15 shows a UV-visible spectrum for (a) 7 x 10^{-4} mol dm^{-3} $[Fe(L_{22})(CH_3CN)_x]^{2+}$ in CH_3CN (spectrum A); (b) following

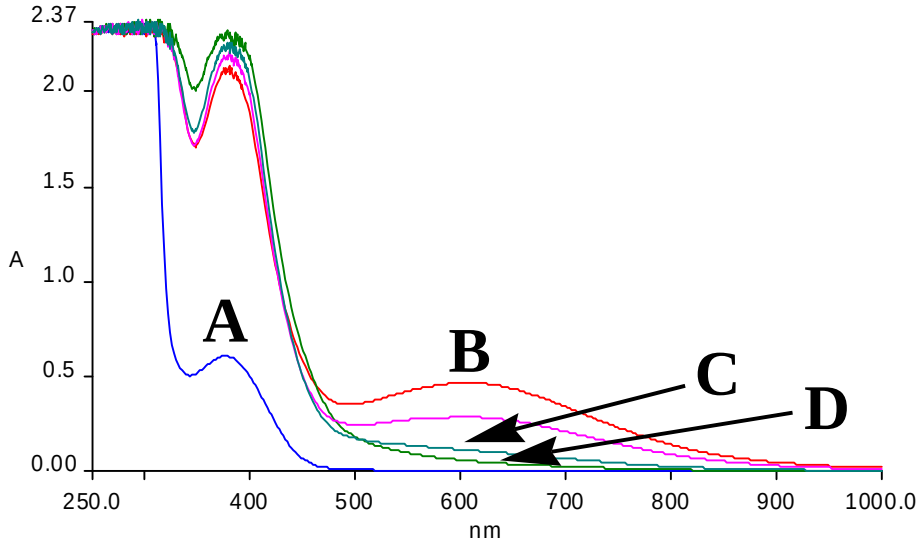

Figure 5.15: UV-VIS spectra for $[Fe(L_{22})(CH_3CN)_x]^{2+}$ (7 x 10^{-4} mol dm^{-3}) in CH_3CN (spectrum A); (b) following the addition of an 18 fold excess of ^{t}BuOOH in CH_3CN at 25°C, $[Fe(L_{22})(OOBu^t)]^{2+}$ (spectrum B); (c) after completion of the first stage (spectrum C) and (d) at the completion of the second stage (spectrum D).

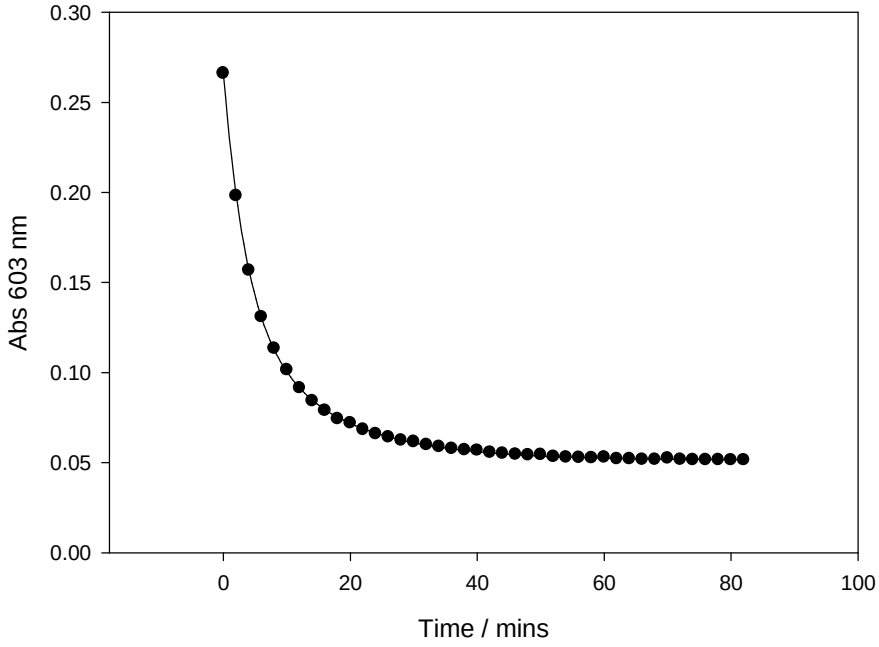

Figure 5.16: Plot of the decay in the absorbance at the 603 nm peak maximum versus time (2 min intervals) following the reaction of $[Fe(L_{22})(CH_3CN)_x]^{2+}$ (7×10^{-4} mol dm^{-3}) with an 18 fold excess of $^{t}BuOOH$ in CH_3CN at 25^{o}C (the solid line represents a non-linear least squares fit to two exponential decays, B→C and C→D).

the addition of an 18 fold excess of $^{t}BuOOH$ in CH_3CN at 25^{o}C, the t-butylperoxoiron(III) intermediate (spectrum B); (c) after completion of the first stage (spectrum C) and (d) at the end of the final second stage of the reaction (spectrum D). Spectrum B corresponds to the amount of $[Fe(L_{22})(OOBu^{t})]^{2+}$ (λ_{max} = 603 nm) generated at its maximum. Figure 5.16 shows a plot of the decay in the absorbance at the 603 nm peak maximum versus time at 25^{o}C. Each data point was taken at 2 minute intervals. The data was fitted to two successive exponential decays corresponding to rate constants k_1 (B→C) and k_2 (C→D) with values respectively; $k_1 = (2.80 \pm 0.06) \times 10^{-1}$ min^{-1} and $k_2 = (7.28 \pm 0.02) \times 10^{-2}$ min^{-1}.

The reaction was then repeated but this time with a much larger 350 fold excess of $^{t}BuOOH$. The UV-VIS spectra for this experiment are shown in figure 5.17. As before spectrum

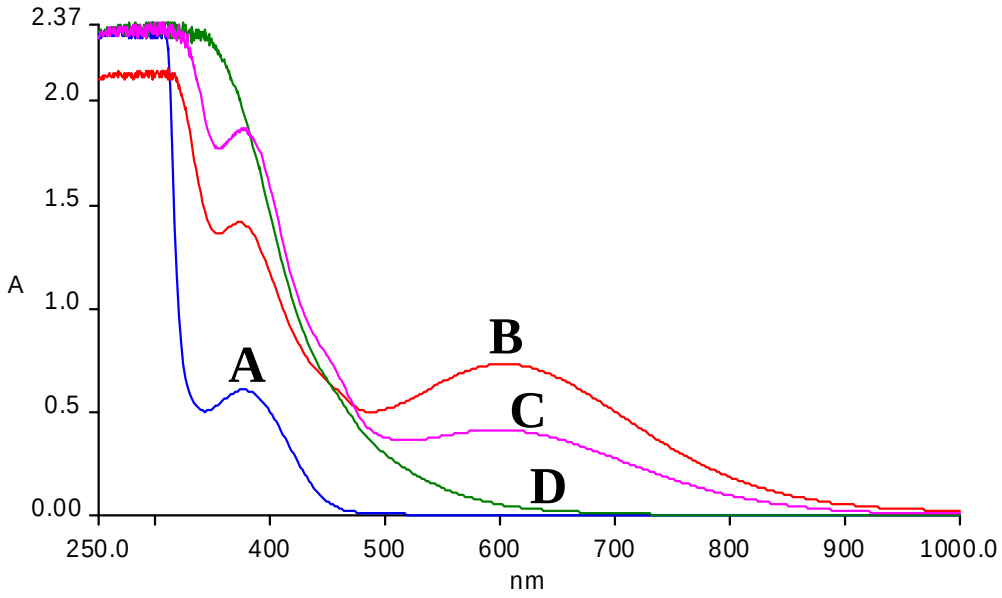

Figure 5.17: UV-VIS spectra for $[Fe(L_{22})(CH_3CN)_x]^{2+}$ (7 x 10^{-4} mol dm^{-3}) in CH_3CN (spectrum A); (b) following the addition of an 350 fold excess of ^tBuOOH in CH_3CN at 25^{o}C, $[Fe(L_{22})(OOBu^t)]^{2+}$ (spectrum B); (c) after completion of the first stage (spectrum C) and (d) at the completion of the second stage (spectrum D).

A corresponds to $[Fe(L_{22})(CH_3CN)_x]^{2+}$ before peroxide addition. Spectrum B corresponds to $[Fe(L_{22})(OOBu^t)]^{2+}$ at its maximum absorbance with its subsequent decay characterised by two distinct stages to spectrum C and finally to spectrum D. The biphasic nature of the decay is clearly apparent in a plot of absorbance at the 603 nm peak maximum, figure 5.18, as a function of time. Each data point was this time taken at 10 min intervals. An initial fast stage, complete in less that 100 minutes, is followed by a very slow decay taking place over 14 hours. A least squares fit to two exponentials k_3 (B→C) and k_4 (C→D) with values respectively; k_3 = (6.84 ± 0.16) x 10^{-2} min^{-1} and k_4 = (2.4 ± 0.1) x 10^{-3} min^{-1}. It is noted that the value of k_3 is identical

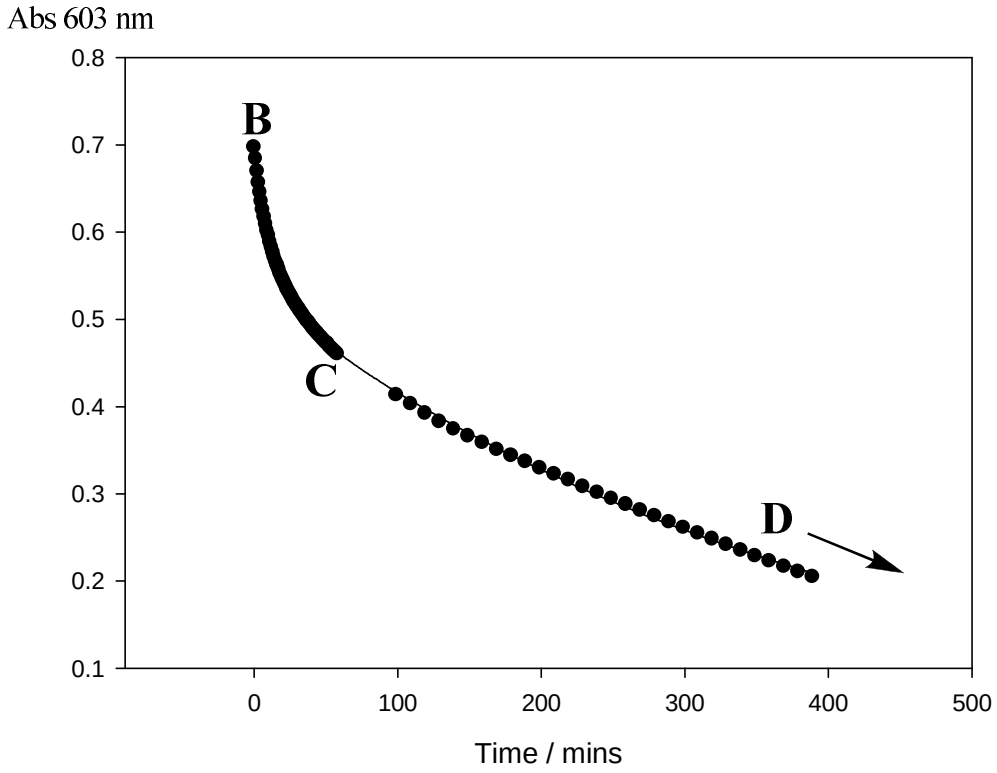

Figure 5.18: Plot of the decay in the absorbance at the 603 nm peak maximum versus time (10 min intervals) following the reaction of $[Fe(L_{22})(CH_3CN)_x]^{2+}$ (7×10^{-4} mol dm^{-3}) with an 350 fold excess of ^{t}BuOOH in CH_3CN at 25^{o}C (the solid line represents a non-linear least squares fit to two exponential decays, B→C and C→D).

within experimental error to that of k_2 (the second stage when using only an 18 fold excess of ^{t}BuOOH). No new species is detectable in the spectral changes with time and it appears that the decay behaviour is due to different processes affecting the observed rate of decay of the same species namely $[Fe(L_{22})(OOBu^{t})]^{2+}$ to the final iron(III) product. The persistence of both the blue $[Fe(L_{22})(OOBu^{t})]^{2+}$ intermediate and its decay product ^{t}BuOO$^{\cdot}$ in these solutions over some considerable time when a large excess (>100 fold) of ^{t}BuOOH is explained here by the slow rate of the second stage process here ($k_4 = (2.4 \pm 0.1) \times 10^{-3}$ min^{-1}) the conditions of which are quite close to those used for the EPR experiments. The observation of this very slow rate of decay when a large excess of ^{t}BuOOH is present suggests that there are rate defined processes involving ^{t}BuOOH that are competing to replenish $[Fe(L_{22})(OOBu^{t})]^{2+}$

while it decays. Unlike in the case of high spin $[Fe(L_{16})(OOBu^t)]^{2+}$ and $[Fe(L_{21})(OOBu^t)]^{2+}$ and the reaction of $[Fe(L_{22})(CH_3CN)_x]^{2+}$ with H_2O_2 it appears that the iron(II) product formed via the Fe-O homolytic decay process on $[Fe(L_{22})(OOBu^t)]^{2+}$ behaves like $[Fe(L_{22})(CH_3CN)_x]^{2+}$ reacting with excess ^{t}BuOOH to regenerate $[Fe(L_{22})(OOBu^t)]^{2+}$ leading to a steady flux of ^{t}BuOO· radical. These competing replenishing reactions are less efficient at lower excesses of ^{t}BuOOH so the observed rate of decay of $[Fe(L_{22})(OOBu^t)]^{2+}$ is faster. Steps 5.5 – 5.9 attempt to explain the sequence of reactions taking place.

$$[Fe^{III}(L_{22})OOBu^t)]^{2+} \xrightarrow{\text{slow}} [Fe^{II}(L_{22})]^{2+} + {}^t\text{BuOO}\bullet \qquad (5.5)$$

$$[Fe^{II}(L_{22})]^{2+} + {}^t\text{BuOOH} \longrightarrow [Fe^{II}(L_{22})OOBu^t)]^{+} + H^{+} \qquad (5.6)$$

$$[Fe^{II}(L_{22})OOBu^t)]^{+} + H^{+} \longrightarrow [Fe^{III}(L_{22})OH]^{2+} + {}^t\text{BuO}\bullet \qquad (5.7)$$

$${}^t\text{BuO}\bullet + {}^t\text{BuOOH} \xrightarrow{\text{fast}} {}^t\text{BuOH} + {}^t\text{BuOO}\bullet \qquad (5.8)$$

$$[Fe^{III}(L_{22})OH]^{2+} + {}^t\text{BuOOH} \longrightarrow [Fe^{III}(L_{22})OOBu^t)]^{2+} + H_2O \qquad (5.9)$$

$$\text{overall:} \quad 3\ {}^t\text{BuOOH} \longrightarrow 2\ {}^t\text{BuOO}\bullet + {}^t\text{BuOH} + H_2O \qquad (5.10)$$

The basic process is catalysis of the reaction of three equivalents of ^{t}BuOOH to give two equivalents of ^{t}BuOO· radical, ^{t}BuOH and water (5.10). The faster observed rate of decay of $[Fe(L_{22})(OOBu^t)]^{2+}$ under lower concentrations of ^{t}BuOOH suggests that the replenishing steps 5.6 – 5.9, involving consumption of three equivalents of ^{t}BuOOH, are not rapid processes and are therefore rate determining to some extent dependant upon (the order of) [^{t}BuOOH]. Thus we assign the fastest process governed by k_1 (2.80 ± 0.06) x 10^{-1} min^{-1}) as representing step 5.5 the intrinsic rate of decay of $[Fe(L_{22})(OOBu^t)]^{2+}$. This decay process is never observed using larger (350 fold) equivalents of tBuOOH since steps 5.6 – 5.9 are now efficient at replenishing the t-butylperoxo complex as it decays.

Masuda reported a relatively slow decay ($t_{1/2}$ ~ 30 mins at 25^{o}C) for the t-butylperoxo complex of BPPA[23] similar to that observed for $[Fe(L_{22})(OOBu^t)]^{2+}$. Since the X-ray structural study on $[Fe(L_{22})](O_3SCF_3)_2$ (chapter 4) showed coordination of both urea carbonyl

oxygen donors it is likely that similar urea carbonyl oxygen coordination will occur at the relatively harder iron(III) centre in $[Fe(L_{22})(OOBu^t)]^{2+}$. Moreover the EPR study reveals evidence of a very low symmetry rhombic environment for high spin iron(III) centre in $[Fe(L_{22})(OOBu^t)]^{2+}$ similar to that observed for $[Fe(L_{15})(OOBu^t)]^{2+}$ (coordination by two ether oxygens) and hepta coordinated $[Fe(BPPA)(OOBu^t)]^{2+}$ and $[Fe(BPPA)(O_2CBu^t)]^{2+}$ (coordinated by two amide oxygens). Thus as for $[Fe(L_{15})(OOBu^t)]^{2+}$ we assign the hepta coordinated structure in figure. 5.19

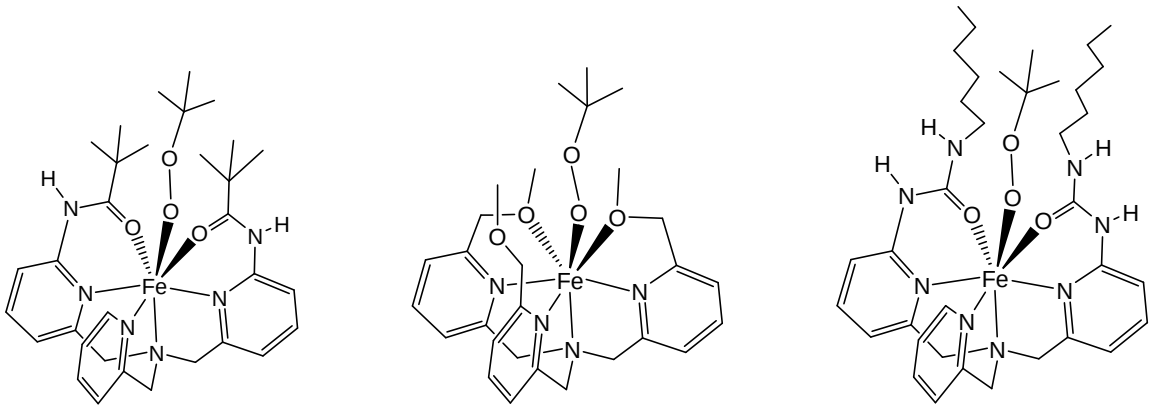

L = BPPA [23] L = L_{15} (this work) L = L_{22} (this work)

Figure 5.19: Structures of hepta coordinated $Fe^{III}(L)OOBu^t)]^{2+}$ complexes

to $[Fe(L_{22})(OOBu^t)]^{2+}$ with its slow decay due to sterically-restricted dissociation of the $^tBuOO^{\cdot}$ radical moiety. Interestingly this is the first evidence of an influence on the properties these iron-TPA derivatives by the introduction of a long alkyl chain.

5.2.3. Study of the catalysis of H_2O_2 oxygenation on alkanes by $[Fe(L)(CH_3CN)_x]^{2+}$ (L = $L_{11,15,16,21,22}$ and L_{24})

Since cyclohexane is a benchmark substrate for investigations of metal-oxo versus radical based oxygenation process with H_2O_2 it was decided to investigate catalysis of cyclohexane oxygenation, figure 5.20, by $[Fe(L)(CH_3CN)_x]^{2+}$ (L = $L_{11,15,16,21,22}$ and L_{24}) as a first screening of any enhanced activity versus those of TPA and other related derivatives. The results are compared with the catalytic behaviour of a range of iron polypyridine systems

towards the H_2O_2 and m-chloro-perbenzoic acid (mCPBA) oxygenation of both cyclohexane and adamanatane. Some definitive conclusions have been reached.

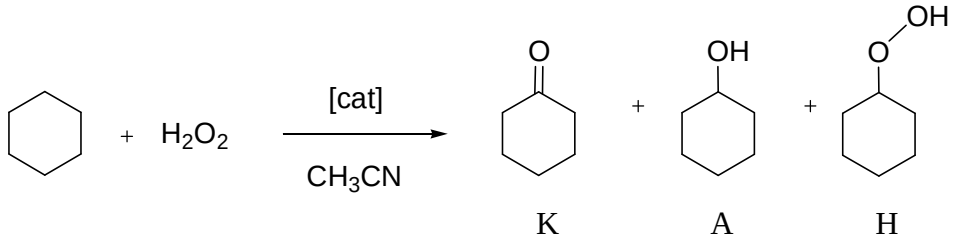

Figure 5.20: Products of cyclohexane oxygenation.

The preparation of iron(II) complexes of the 6-py substituted TPA ligands; $L_{11,\ 15,16,21}$ and L_{22} has been described in chapters 2, 3 and 4. The formation and decay of peroxoiron(III) derivatives with $L_{15,16,21}$ and L_{22} has been discussed earlier in this chapter. Each of the iron(II) complexes has been prepared using $[Fe(O_3SCF_3)_2(CH_3CN)_2]$ which is air stable, can be easily made anhydrous, contains a weakly coordinating anion, and is a safe substitute for perchlorate salts.[24]

.

5.2.3.1 Methodology

The oxygenation reactions were carried out in acetonitrile as the solvent at room temperature under air. Aqueous solutions of 30% w/w hydrogen peroxide were standardised by titration with potassium permanganate as described in Vogel.[25] To start the reaction the hydrogen peroxide solution (70 mM, 10 equiv or 700 mM, 100 equiv) was added by means of a syringe pump over a 30 min period at 25°C to an acetonitrile solution containing the iron(II) catalyst (2.1 µmol, 1 equiv) and cyclohexane (2.1 mmol, 1000 equiv). A large excess of substrate was used in order to minimize over-oxidation of cyclohexanol (A) to cyclohexanone (K). Use of the syringe pump ensured that decomposition of H_2O_2 was minimised. After syringe pump addition the solution was stirred for another 5 min before work up. The iron(II) catalyst was removed by passing the solution through silica gel followed by elution with 3 ml of CH_3CN.[10] An internal standard (toluene) was added at this point, and the solution was subjected to GC

analysis. The organic products were identified by GC-MS comparison with authentic compounds. All reactions were run at least in duplicate, and the data reported was the average of two runs. The yields were based on the amount of oxidant (H_2O_2) converted into oxygenated products. Two series of catalytic experiments were carried out initially, using both 10 and 100 equivalents of H_2O_2 following the methodology previously reported by Que[9,26] and Britovsek.[27]

5.2.3.2 Catalysis by the iron(II) complexes of $L_{11,15,16,21,22}$ and, L_{24}

Table 5.5 summarizes the results of catalytic H_2O_2 oxygenations on cyclohexane by the iron(II) complexes of $L_{11,15,16,21,22}$ and L_{24}.

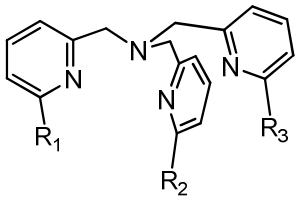

L_{11}: $R^1 = R^2 = R^3 =$ OH

L_{15}: $R^1 = R^2 = R^3 =$ O

L_{16}: $R^1 = R^2 = R^3 =$ O

L_{21}: $R^1 =$ HN N H $R^2 = R^3 = H$

L_{22}: $R^1 = R^2 =$ HN N H $R^3 = H$

L_{23}: $R^1 = R^2 = R^3 =$ HN N H

L_{24}: $R^1 = R^2 = R^3 =$ Br

The main observations are as follows:

(i) The catalytic efficiency (moles oxidation products/mole of oxidant) decreases as the amount of H_2O_2 used is increased from 10 equivalents to 100 equivalents. Even using 10 equivalents of H_2O_2 none of the six iron catalysts achieves an efficiency of greater than 7%.

(ii) The A/K (cyclohexanol/cyclohexanone) ratio increases when the equivalents of H_2O_2 used are increased from 10 to 100 fold.

(iii) Only the complexes $[Fe(L_{21})(CH_3CN)_x]^{2+}$, $[Fe(L_{22})(CH_3CN)_x]^{2+}$ and $[Fe(L_{24})(CH_3CN)_2]^{2+}$ give rise to an A/K ratio >2 when using 100 equivalents of H_2O_2. Only those for $[Fe(L_{22})(CH_3CN)_x]^{2+}$ and $[Fe(L_{24})(CH_3CN)_2]^{2+}$ are above 3.0. The higher the A/K ratio the more likely metal oxo species may be involved in the cyclohexane oxygenation.

(iv) The highest turnover number (moles of oxidised products/mol catalyst - relevant for the runs using 100 equivalents of H_2O_2) was 4.6 for the 35 minute incubation time using the 6-Br_3-TPA derivative complex, $[Fe(L_{24})(CH_3CN)_2]^{2+}$.

These findings show that these iron-TPA derivative complexes show somewhat disappointing activity compared to that shown by the parent TPA complex; $[Fe(TPA)(CH_3CN)_2]^{2+}$ and also $[Fe(BPMEN)(CH_3CN)_2]^{2+}$.[28] The A/K ratios are similar to those obtained using the 6-Me substituted complexes; $[Fe(6\text{-}Me_2TPA)(CH_3CN)_2]^{2+}$ and $[Fe(6\text{-}Me_3TPA)(CH_3CN)_2]^{2+}$ both of which generate high spin peroxo intermediates. These results indicate products stemming largely from OH radical based processes. It is particularly noticable how inferior the mono-6-hexylurea TPA derivative complex $[Fe(L_{21})(CH_3CN)_x]^{2+}$ is compared with the mono-6-methylated TPA complex $[Fe(6\text{-}MeTPA)(CH_3CN)_2]^{2+}$ despite the fact that low spin peroxo intermediates are formed in both cases. Here it is believed that the low activity of $[Fe(L_{21})(CH_3CN)_x]^{2+}$ stems from the presence of only one vacant site in the iron complexes due to likely coordination of the urea carbonyl oxygen in the hydroperoxo complex $[Fe^{III}(L_{21})OOH]^{2+}$. Thus L_{21} effectively behaves as a pentadentate ligand (x = 1), figure 5.14, like N4py in the complex $[Fe(N4py)(CH_3CN)]^{2+}$.[28] $[Fe(N4py)(CH_3CN)]^{2+}$, which despite forming low spin peroxo intermediates, shows poor activity in the air towards H_2O_2 oxygenation of cyclohexane (at 10 equivalents) with a turnover number of only 3.1 and an A/K ratio of 1.4 implying products deriving from OH radical based processes. The urea groups were introduced in the hope of triggering hydrogen bonding from N-H to the bound

OOH group on the hydroperoxoiron(III) complex to hopefully promote heterolytic cleavage of the O-O bond to generate the powerful iron(V) oxidant. However, it appears in these systems that coordination of the urea carbonyl rather occurs limiting the number of available coordination sites for reactivity. The low activity of Masuda's pivaloylamido complexes such as, [Fe(BPPA)(OOBu^t], figure 5.4, towards catalysis of alkane oxygenation is believed to be the result of similar amido oxygen coordination.[20] Finally, the expected strong coordination of the hydroxymethyl groups to iron(III) in the complex of H_3L_{11} (chapter 2) results in saturation of the coordination sphere so that a hydroperoxo complex intermediate is unable to form. The result is a complete shut down of the catalytic oxygenation activity, table 5.1. These findings provide strong support to Que's assertion[22] that the presence of both a low spin iron centre and of two labile and available *cis* sites are required for the facilitation of selective metal-oxo based processes in alkane oxygenation catalysts by these families of non-heme iron polypyridine systems.

Table 5.1: Results of catalytic H_2O_2 oxygenations on cyclohexane by iron(II) complexes of L_1 – L_5 and L_7

-

Oxidations with H_2O_2	Eq.H_2O_2	Eq. C_6H_{10}	Eff	TN.	A:K	KIE	3°:2°	Ref.
$[Fe(H_3L_{11})(CH_3CN)_x]^{2+}$	100	1000	nr	nr	nr	-	-	*
$[Fe(L_{15})(CH_3CN)_x]^{2+}$	10	1000	6.4	0.6	1.6	-	-	*
$[Fe(L_{15})(CH_3CN)_x]^{2+}$	100	1000	1.8	1.8	1.6	-	-	*
$[Fe(L_{16})(CH_3CN)_x]^{2+}$	100	1000	3.0	3.0	1.2	-	-	*
$[Fe(L_{21})(CH_3CN)_x]^{2+}$	10	1000	5.1	0.5	0.8	-	-	*
$[Fe(L_{21})(CH_3CN)_x]^{2+}$	100	1000	2.3	2.3	2.1	-	-	*
$[Fe(L_{22})(CH_3CN)_x]^{2+}$	100	1000	1.4	1.4	3.3	-	-	*
$[Fe(L_{24})(CH_3CN)_2]^{2+}$	100	1000	4.6	4.6	3.1	-	-	*
$[Fe(6\text{-}Me_2TPA)(CH_3CN)_2]^{2+}$	10	1000	29	2.9	2.0	4.0	33	10, 29
$[Fe(6\text{-}Me_3TPA)(CH_3CN)_2]^{2+}$	10	1000	14	1.4	1.0	3.3	15	10, 29
$[Fe(6\text{-}MeTPA)(CH_3CN)_2]^{2+}$	10	1000	40	4.0	7.0	3.6	30	10, 29
Simple Fe salts								
$[Fe(CH_3CN)_4]^{2+}$	10	1000	10	1.0	1.0	1.8	-	30
$Fe(ClO_4)_3$	10	1000	37	3.7	1.9	1.5	3.3	31
Free $OH^{\cdot}$ radical	10	1000	1.0		1-2	2	2.0	32-35

Conditions: Iron catalyst:H_2O_2:alkane = 1:10:1000 (cyclohexane), 1:100:1000 (cyclohexane), and 1:10:10 (adamantane).
Solvent – acetonitrile H_2O_2 added by syringe pump in the air at 25°C over 30mins, total incubation time 35 mins before work up.
Eff. (cyclohexanol+cyclohexanone):H_2O_2/100 in the oxidation of cyclohexane.
TN - mols oxidised products:mols cat. in the oxidation of cyclohexane
A:K - cyclohexanol:cyclohexanone in the oxidation of cyclohexane.
KIE - kinetic isotope effect of cyclohexanol formation in the oxidation of cyclohexane and cyclohexane-*d*12
3°:2° - 1-adamantanol:(2-adamantanol+2-adamantanone) in the oxidation of adamantane taking into account of the correction for a number of C-H bonds in a group.
nr – no products detected.
*This work

5.2.3.3 Survey of H_2O_2 and mCPBA oxygenations on cyclohexane and adamantane by iron(II) polypyridine complexes

It order to draw detailed conclusions of how the iron(II) complexes of ligands $L_{11,15,16,21,22}$ and L_{24} compare to the range of other reported iron catalysts it was decided to review the literature data available on iron polypyridine complex catalysis of H_2O_2 oxygenation of cyclohexane and adamantane in CH_3CN solvent to see if any patterns in activity with ligand type and design were emerging and what lessons could be learnt. A number of systems using m-chloroperbenzoic acid (mCPBA) as the oxidant will also be commented on for comparison. The survey is broken down into two classes of ligand; TPA-like and BPMEN-like and whether the starting iron(II) complexes are low spin or high spin. Figure 5.21 shows the range of literature polypyridine-based ligands employed in the various studies reviewed.

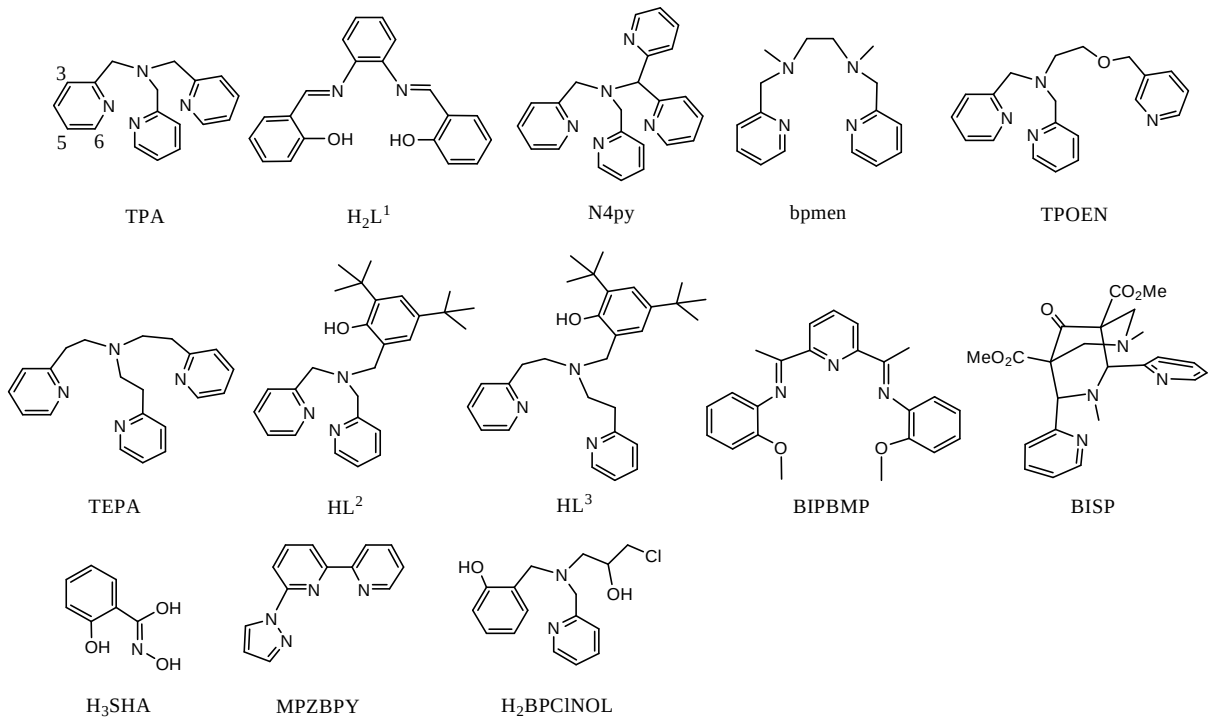

Figure 5.21: TPA and related polypyridine-based ligands used in the iron catalysis of H_2O_2 oxygenations on cyclohexane and adamantane in CH_3CN solvent.

Based upon A/K ratios and KIE values for oxygenations on cyclohexane and $3^o/2^o$ ratios for oxygenations on adamantane (where available) an attempt has been made to come up with a

set of completely empirical and subjective criteria for deciding on the nature of the active ROO-Fe^{III} derived oxidant for ROOH oxidations of alkanes, table 5.2, based on a survey of the behaviour of the literature systems. The criteria are based on the three ways that a hydro(alkyl)peroxo-iron(III) complex can subsequently react, see discussion in chapter 1, (i) via Fe-O bond homolysis – generating iron(II) and $OH^{\bullet}$ radical; (ii), via O-O bond homolysis generating a high valent Fe^{IV}=O species and $OH^{\bullet}$ radical and finally (iii) via O-O bond heterolysis generating Fe^{V}=O (or Fe^{IV}-$O^{\cdot}$) and OH^{-}.

Table 5.2: Criteria for deciding on the active ROO-Fe^{III}-derived oxidant for ROOH oxidations on cycloalkanes (R = H, ^{t}Bu, m-$ClC_6H_4C(=O)$)

cyclohexane		adamantane	ROO-Fe^{III} cleavage process	proposed active oxidant
A/K	KIE	$3^o/2^o$		
≤2.4	(≤2)	(<10)	Fe-O homolysis	$OH^{\cdot}$
≤2.4	(2<4)	-	O-O homolysis	Fe^{IV}=O, $OH^{\cdot}$
≤2.4	(2<4)	(≥10)	O-O homolysis	Fe^{IV}=O, $OH^{\cdot}$
>4	(>3)	(>4)	O-O heterolysis	Fe^{V}=O (Fe^{IV}-$O^{\cdot}$)

Tables 5.3 and 5.4 summarize data for the catalysis of H_2O_2 oxygenation on cyclohexane and adamantane catalysed respectively by high spin and low spin iron(II) polypyridine (TPA-like) complexes along with data for simple high spin iron salts; $[Fe(CH_3CN)_4]^{2+}$, $Fe(ClO_4)_{2/3}$, $Fe(OPPh_3)_4]^{2+}$ and $[Fe(bipy)_2]^{2+}$. Based on the criteria proposed in table 5.2 virtually all the high spin iron(II) catalysts in table 5.3 fall into the category suggesting that the primary reaction of the hydroperoxoiron(III) intermediate is Fe-O homolysis to generate $OH^{\cdot}$ radicals as the active oxidant. All have A/K ratios <2.4 with KIE values (where available) also <2. The exceptions are $[Fe(6\text{-}Me_2TPA)(CH_3CN)_2]^{2+}$ and $[Fe(6\text{-}Me_3TPA)(CH_3CN)_2]^{2+}$ which exhibit KIE values of >3 and $[Fe(HBPClNOL)Cl_2]$ which has an A/K ratio >2.4. $[Fe(BIPBMP)(CH_3CN)_n]^{2+}$ is a highly efficient catalyst but the small A/K ratio (close to unity) suggests $OH^{\cdot}$ radical based processes. $[Fe(6\text{-}Me_2TPA)(CH_3CN)_2]^{2+}$ stands out as having

a high $3^o/2^o$ ratio (33) for adamantane oxygenation whilst satisfying the other criteria for homolytic O-O cleavage suggesting that a high valent oxo species (possibly $LFe^{IV}=O$?) is formed and may be active in the subsequent oxygenation chemistry. For the ultra high valent oxidant $Fe^V=O$ (or Fe^{IV}-$O^{\cdot}$) to be proposed as an active species however a set of extreme criteria must be satisfied comprising an A/K ratio of >4 coupled with a KIE value of >4 and a $3^o/2^o$ ratio (adamantane) of >4. None of the high spin iron(II) catalysts listed in table 5.3 come anywhere near satisfying all of these empirical criteria for proposal of an active $Fe^V=O$ oxidant.

The situation for low spin iron(II) catalysts, table 5.4, is however somewhat different. Here there is tentative evidence under the empirical criteria for the involvement of high valent $Fe^V=O$ centres. Indeed all the low spin TPA derivatives satisfy the criteria for a $Fe^V=O$ oxidant being involved via O-O bond heterolysis of the hydroperoxoiron(III) precursor. Only the BISP complexes of Comba et al,[36] Feringa's $[Fe(N4py)(CH_3CN)]^{2+}$ complex[37,38] and $[Fe^{III}_2(\mu\text{-}O)(TPOEN)_2]^{4+}$ [39] fail to satisfy all the criteria with the low A/K ratios and KIE values (both <2) implying OH radical based processes (Fe-O homolysis). The latter dimer complex is moreover anomalously termed 'low spin' because of antiferromagnetic coupling between two high spin Fe^{III} centres.

Table 5.5 shows data for corresponding catalytic oxygenations using a number of the iron-polypyridine (TPA-like) catalysts with the oxidant mCPBA. In the reactions with mCPBA even some high spin iron complexes satisfy the criteria for the proposal of a high valent iron oxidant being involved. Both high spin $[Fe(TPOEN)Cl]^+$ and $[Fe(TPOEN)Cl_3]$ exhibit A/K ratios of >3 with a $3^o/2^o$ ratio (adamantane) of ~19 implying O-O bond homolysis to give $LFe^{IV}=O$ and m-chlorobenzoyloxo radical ($mCBPO^{\cdot}$). $[Fe(N4py)(CH_3CN)]^{2+}$,[37,38] $[Fe(TPA)(OAc)(H_2O)]^+$ [40] and $[Fe^{III}_2(\mu\text{-}O)(L^1)_2]$ (H_2L^1 shown in figure 5.21), (each under N_2 or Ar gas) exhibit A/K ratios of >4 (in the case of $[Fe^{III}_2(\mu\text{-}O)(L^1)_2]$ a value of >12 and a $3^o/2^o$ of 5.3) and for $[Fe(N4py)(CH_3CN)]^{2+}$ a KIE of 4.5 satisfying the criteria for heterolytic O-O

cleavage of the hydroperoxo species. However what is significant is when the catalysis by $[Fe(N4py)(CH_3CN)]^{2+}$ is carried out in the air wherein the A/K ratio drops sharply to 1.3 and the efficiency reduces by a third. Unfortuntely no KIE data is available but the above data suggests that a dominant radical based pathway is now involved. Finally the runs with the acetato-TPA complex; $[Fe(TPA)(OAc)(H_2O)]^{+}$ are of interest in that quenching with PPh_3 was performed prior to GC analysis to reduce out any cyclohexylhydroperoxide (H) present to cyclohexanol (A). $[Fe(TPA)(OAc)(H_2O)]^{+}$ is a highly efficient catalyst towards mCPBA oxygenation (Eff 46%, 460 turnovers/hr) although data on $[Fe(TPA)(CH_3CN)_2]^{2+}$ under the same conditions are not available for comparison. The A/K ratio following PPh_3 quenching is 6.4. The possible promoting effect of acetate was discussed in chapter 1.

Quenching the final product solution with PPh_3 is standard practice for many reported studies of iron-heme based alkane oxygenation catalysts such as $[Fe(F_{20}TPP)Cl]$.[41] This treatment can have the effect of increasing quite dramatically the apparent A/K ratio if a significant amount of H is formed as a co-product. Thus the efficient catalysis (91% based on oxidant) of mCPBA oxygenation of cyclohexane by $[Fe^{III}(F_{20}TPP)Cl]$ in 1:1 acetonitrile:CH_2Cl_2 exhibits an A/K ratio of 44.5 with a KIE of 5.2. [41]

Catalytic cycloalkane oxygenations carried out with mCPBA generally give significantly higher A/K ratios and higher efficiencies for a particular catalyst than those observed with H_2O_2 or ^{t}BuOOH (even for cases where PPh_3 quenching has not been employed). This implies an increased tendency towards heterolytic O-O cleavage for m-Cl-$C_6H_4C(O)OOFe(III)$ intermediates. This phenomenon has been reviewed and discussed by Que et al[42] and may simply be a reflection of m-Cl-$C_6H_4C(O)O^{-}$ being a better leaving group than either OH^{-} or $tBuO^{-}$ rather than any virtuous property of the iron-ligand system. Unfortunately mCPBA is a somewhat exotic oxidant and although good for mechanistic study it is not a viable reagent for commercial scale reaction which remains the domain of H_2O_2 or better still

Table 5.3 A Survey of H_2O_2 oxygenation on alkanes catalysed in CH_3CN by high spin iron-TPA and TPA-like complexes.

Catalyst	eq. H_2O_2	eq. C_6H_{10}	Eff.	TN.	A:K	KIE	3°:2°	cleavage process	oxidising species	Ref.
$Fe(ClO_4)_3$	10	1000	37	3.7	1.9	1.5	3.3	Fe-O homolysis	O	31
$Fe(ClO_4)_3$ * £	150	1000	37	63	2.3	-	-	Fe-O homolysis	$OH^{\cdot}$	31
$Fe(ClO_4)_3$ * $	150	1000	78	99	0.6	-	-	Fe-O homolysis	$OH^{\cdot}$	31
$Fe(ClO_4)_2$ * “	150	1000	87	100	0.5	-	-	Fe-O homolysis	$OH^{\cdot}$	31
$Fe(ClO_4)_2$ * “”	150	1000	87	100	1.1	-	-	Fe-O homolysis	$OH^{\cdot}$	31
$Fe(ClO_4)_2$ * %	150	1000	37	37	0.1	-	-	Fe-O homolysis	$OH^{\cdot}$	31
$[Fe(OPPh_3)_4]^{2+}$	10	1000	13	1.3	1.2	1.9	-	Fe-O homolysis	$OH^{\cdot}$	30
$[Fe(CH_3CN)_4]^{2+}$	10	1000	10	1.0	1.0	1.8	-	Fe-O homolysis	$OH^{\cdot}$	30
$[Fe(bpy)_2]^{2+}$	10	1000	9	0.9	0.8	1.4	-	Fe-O homolysis	$OH^{\cdot}$	30
$[Fe(6\text{-}Me_2TPA)(CH_3CN)_2]^{2+}$	10	1000	29	2.9	2.0	4.0	33	O-O homolysis	Fe^{IV}=O, $OH^{\cdot}$	10, 29
$[Fe(6\text{-}Me_3TPA)(CH_3CN)_2]^{2+}$	10	1000	14	1.4	1.0	3.3	15	O-O homolysis	Fe^{IV}=O, $OH^{\cdot}$	10, 29
$[Fe(BIPBMP)(CH_3CN)_n]^{2+}$ *	150	100	51	100	0.3	-	-	Fe-O homolysis	$OH^{\cdot}$ (Gif-like)	43
$[Fe(BIPBMP)(CH_3CN)_n]^{2+}$ *	150	100	99	100	1.1^{+}	-	-	Fe-O homolysis	$OH^{\cdot}$	43
$[Fe(BIPBMP)(CH_3CN)_n]^{2+}$ *	150	100	81	100	0.8^{++}	-	-	Fe-O homolysis	$OH^{\cdot}$	43
$[Fe(HBPClNOL)Cl_2]$ **	1000	1000	2.2	140	2.7	-	-	O-O homolysis	Fe^{IV}=O, $OH^{\cdot}$	44
$[Fe(HBPClNOL)Cl_2]$ ** +	1000	1000	6.0	269	3.0	-	-	O-O homolysis	Fe^{IV}=O, $OH^{\cdot}$	44
$[Fe(TPOEN)Cl]^{+}$ ***	200	1000	12.2	24.4	2.4	-	3.2	Fe-O homolysis	$OH^{\cdot}$	39
$[Fe(TPOEN)Cl_3]$ ***	200	1000	18.1	36.1	2.3	-	3.0	Fe-O homolysis	$OH^{\cdot}$	39
$[Fe(MPZPBY)(CH_3CN)_3]^{2+}$ ******	100	1000	2.9	2.9	1.6			Fe-O homolysis	$OH^{\cdot}$	45

Conditions: Iron catalyst:H_2O_2:alkane = 1:10:1000 (cyclohexane) and 1:10:10 (adamantane). H_2O_2 added by syringe pump in air, 25°C, 30mins, total time 35 mins.
Eff. - (cyclohexanol+cyclohexanone):H_2O_2/100 in the oxidation of cyclohexane.
TN - mols total oxidised products:mols cat. in the oxidation of cyclohexane.
A:K - cyclohexanol:cyclohexanone in the oxidation of cyclohexane. KIE - kinetic isotope effect of cyclohexanol formation in the oxidation of C_6H_{12} and C_6D_{12}.
3°:2° - 1-adamantanol:(2-adamantanol+2-adamantanone) in the oxidation of adamantane correcting for the number of C-H bonds in a group.
*Conditions: Iron catalyst:H_2O_2:alkane = 1:150:100 (cyclohexane), 50°C, 3h in air. + after 7h, ++ after 23h. £ 25°C for 18h in air $ 22h in air. “ 23h in air, “” 2h under Ar, % 19h in acetone.
** Conditions: iron catalysts:H_2O_2:alkane = 1:1000:1000 (cyclohexane), 25°C 24h, + 50°C 24h
****** Conditions: Iron catalyst:H_2O_2:alkane = 1:100:500 (cyclohexane) in acetonitrile 25°C, 3h under N_2.
*** Conditions: Iron catalyst:H_2O_2:alkane = 1:200:1000 in acetonitrile 20°C, 90mins under N_2.

Table 5.4: A Survey of H_2O_2 oxygenation on alkanes catalysed in CH_3CN by low spin iron-TPA and TPA-like complexes**.**

Catalyst	eq.H_2O_2	eq. C_6H_{10}	Eff.	TN.	A:K	KIE	3°:2°	cleavage process	oxidising species	Ref.
$[Fe(TPA)(CH_3CN)_2]^{2+}$	10	1000	37	3.7	5.0	3.5	17	O-O heterolysis	$Fe^V=O$	46
$[Fe(3\text{-}Me_3TPA)(CH_3CN)_2]^{2+}$	10	1000	45	4.5	14	3.7	27	O-O heterolysis	$Fe^V=O$	10, 29
$[Fe(5\text{-}(Me)_2TPA)(CH_3CN)_2]^{2+}$	10	1000	23	2.3	19	3.7	15	O-O heterolysis	$Fe^V=O$	10, 29
$[Fe(5\text{-}Me_3TPA)(CH_3CN)_2]^{2+}$	10	1000	40	4.0	9.0	3.8	21	O-O heterolysis	$Fe^V=O$	10, 29
$[Fe(6\text{-}MeTPA)(CH_3CN)_2]^{2+}$	10	1000	40	4.0	7.0	3.6	30	O-O heterolysis	$Fe^V=O$	10, 29
$[Fe(BISP)(CH_3CN)_2]^{2+}$ *****	400	1000	34	34	1.4			Fe-O homolysis	$OH^{\cdot}$	36
$[Fe(BISP)(CH_3CN)_2]^{2+}$ ***** +	100	1000	25	25	1.1			Fe-O homolysis	$OH^{\cdot}$	36
$[Fe(N4py)(CH_3CN)]^{2+}$	10	1000	31	3.1	1.4	1.5	3.3	Fe-O homolysis	$OH^{\cdot}$	37,38
$[Fe^{III}_2(\mu\text{-}O)(TPOEN)_2]^{4+}$ ****	400	1000	6	24	1.9	-	3.1	Fe-O homolysis	$OH^{\cdot}$	39
Free $OH^{\cdot}$ radical	10	1000	1.0		1-2	2	2.0		$OH^{\cdot}$	22

Conditions: Iron catalyst:H_2O_2:alkane = 1:10:1000 (cyclohexane) and 1:10:10 (adamantane).
H_2O_2 added by syringe pump in the air at 25°C over 30mins, total incubation time 35 mins before work up.

Eff. - (cyclohexanol+cyclohexanone):H_2O_2/100 in the oxidation of cyclohexane.
TN - mols total oxidised products:mols cat. in the oxidation of cyclohexane
A:K - cyclohexanol:cyclohexanone in the oxidation of cyclohexane.
KIE - kinetic isotope effect of cyclohexanol formation in the oxidation of cyclohexane and cyclohexane-*d*12.
3°:2° - 1-adamantanol:(2-adamantanol+2-adamantanone) in the oxidation of adamantane correcting for the number of C-H bonds in a group.
****Conditions: Iron catalyst:H_2O_2:alkane = 1:400:1000 in acetonitrile 20°C, 90mins under N_2.
***** Conditions: Iron catalyst:H_2O_2:alkane = 1:100:1000 (cyclohexane) in acetonitrile 25°C, 35mins under N_2. $^+$ in the air
5-$(ME)_2$TPA = bis(5-methoxycarbonyl-2-pyridylmethyl)-2'-pyridylmethylamine, 6-MeTPA = 6-methyl-2-pyridylmethyl-bis(2'-pyridylmethyl)amine
5-Me_3TPA = tris(5-methyl-2-pyridylmethyl)amine; 3-Me_3TPA = tris(3-methyl-2-pyridylmethyl)amine;

Table 5.5: A Survey of mCPBA oxygenation on alkanes catalysed in CH_3CN by low spin iron-TPA and TPA-like complexes

Catalysts	eq.mCPBA	eq. C_6H_{10}	Eff.	TN.	A:K	KIE	3°:2°	cleavage process	oxidising species	Ref.
High spin Fe species										
$[Fe(TPOEN)Cl]^{+}$ **	200	1000	24.9	49.7	3.2		18.5	O-O homolysis	Fe^{IV}=O, mCPBO·	39
$[Fe(TPOEN)Cl_3]$ **	200	1000	36.2	72.4	3.0		19.4	O-O homolysis	Fe^{IV}=O, mCPBO·	39
Low spin Fe species										
$[Fe(N4py)(CH_3CN)]^{2+}$ a	100	1000	33	33	5.6	4.5	-	O-O heterolysis	Fe^{V}=O	47
$[Fe(N4py)(CH_3CN)]^{2+}$ b	100	1000	9.6	9.6	1.3	-	-	Fe-O homolysis	mCPBO·	47
$[Fe(TPA)(OAc)(H_2O)]^{+}$ c	1000	7576	45.8	458	6.4	-		O-O heterolysis	Fe^{V}=O	40
$[Fe^{III}(L^1)Cl]$ d	500	2000	5.6	27.8	1.7	-	2.2	Fe-O homolysis	mCPBO·	48
$[Fe^{III}_2(\mu\text{-}O)(L^1)_2]$ d	500	2000	2.6	13.2	12.2	-	5.3	O-O heterolysis	Fe^{V}=O	48
$[Fe^{III}_2(\mu\text{-}O)(TPOEN)_2]^{4+}$ ***	400	1000	26	104	2.9		30.3	O-O homolysis	Fe^{IV}=O, mCPBO·	39
Free OH· radical	10	1000	1.0		1-2	2	2.0		OH·	22

a - Conditions: Iron catalyst:mCPBA:alkane = 1:100:1000 under N_2 at 25°C, total incubation time 1h before work up. b – in air.
Eff. - 100 x (cyclohexanol+cyclohexanone):mCPBA in the oxidation of cyclohexane.
TN - mols oxidised products:mols cat. in the oxidation of cyclohexane
A:K - cyclohexanol:cyclohexanone in the oxidation of cyclohexane
KIE - kinetic isotope effect of cyclohexanol formation in the oxidation of cyclohexane and cyclohexane-*d*12.
c - Conditions: Iron catalyst:mCPBA:alkane = 1:1000:7576 (cyclohexane) in CH_2Cl_2-CH_3CN 3:1 at 25°C for 1h under Ar. PPh_3 used to quench
Eff. - 100 x (cyclohexanol+cyclohexanone):mCPBA in the oxidation of cyclohexane.
TN - mols oxidised products:mols cat. in the oxidation of cyclohexane
A:K - cyclohexanol:cyclohexanone in the oxidation of cyclohexane.
3°:2° - 1-adamantanol:(2-adamantanol+2-adamantanone) in the oxidation of adamantane correcting for the number of C-H bonds in a group.
**Conditions: Iron catalyst:mCPBA:alkane = 1:200:1000 in acetonitrile 20°C, 90mins under N_2.
***Conditions: Iron catalyst: mCPBA:alkane = 1:400:1000 in acetonitrile 20°C, 90mins under N_2.
d – Conditions: Iron catalyst:mCPBA:alkane = 1:500:2000 in acetonitrile, total incubation time 6h at 25°C under N_2.

O_2. Therfore catalytic systems employing H_2O_2 and/or O_2 remain the benchmark for exploitable study.

The final series of iron polypyridine complexes that have received detailed study towards the catalytic H_2O_2 oxygenations on cyclohexane and adamantane are those employing the family of tetradentate BPMEN and related ligands. The $[Fe(BPMEN)(CH_3CN)_2]^{2+}/H_2O_2$ catalytic system reported by Que et al[6] and Britovsek[26, 49, 50] is so far the most active and selective catalyst using H_2O_2 as the oxygen source. Britovsek *et al* have carried out a detailed study of various BPMEN derivatives looking at the ligand topology.[26, 49, 50] These are summarized in figure 5.22. table 5.6 summarizes the results of catalytic studies obtained with BPMEN and ligands L_{25} – L_{31}.

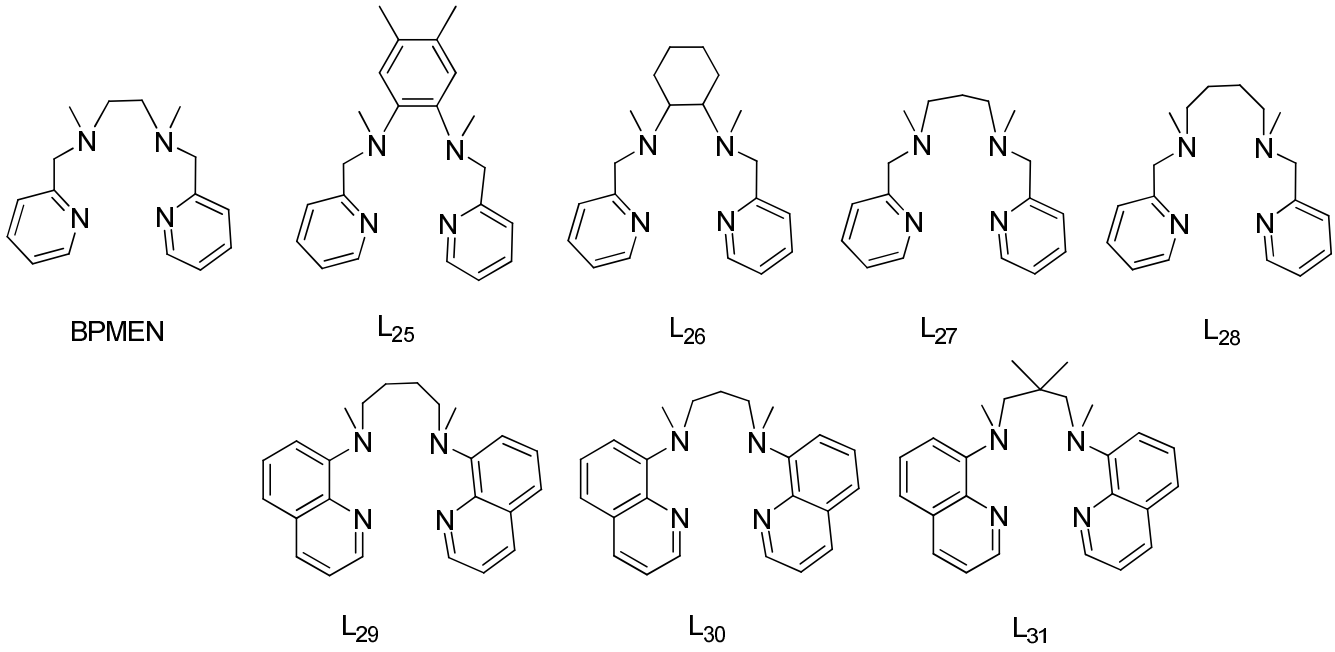

Figure 5.22: BPMEN and related tetradentate ligands.[26, 49, 50]

The most active ligands were BPMEN itself, L_{29} and L_{30}. Each of these systems satisfied the criteria for O-O heterolysis to generate an active Fe^{V}=O catalyst when using 10 equivalents of H_2O_2 and each was unique in exhibiting an A/K ratio of >4. However using the larger 100 fold excess of H_2O_2 the A/K ratio dropped in all cases to values <3 implying products

deriving from homolytic O-O cleavage of the hydroperoxoiron(III) intermediate. Under all conditions the systems exhibited KIE values in the range 2.5 – 4.5 with $3^o/2^o$ values of between 10 and 16, each supportive of O-O bond breaking processes, and for BPMEN, L[29]

Table 5.6: A Survey of H_2O_2 oxygenation on alkanes catalysed in CH_3CN by the family of iron-BPMEN complexes

Catalyst	eq.H_2O_2	eq. C_6H_{10}	Eff.	TN.	A:K	KIE	3°:2°	cleavage process	oxidising species	Ref.
$[Fe(BPMEN)(CH_3CN)_2]^{2+}$	10	1000	65	6.5	9.5	2.5 – 4.5	10-16	O-O heterolysis	$Fe^{V}=O$	16, 51
$[Fe(BPMEN)(CH_3CN)_2]^{2+\,f}$	100	1000	48	48	2.5	"	"	O-O homolysis	$Fe^{IV}=O$, $OH^{\cdot}$	16, 27
$[Fe(L_{25})(CH_3CN)_2]^{2+}$	10	1000	62	6.2	2.4	"	"	O-O homolysis	$Fe^{IV}=O$, $OH^{\cdot}$	52
$[Fe(L_{25})(CH_3CN)_2]^{2+\,f}$	100	1000	23	23	2.2	"	"	O-O homolysis	$Fe^{IV}=O$, $OH^{\cdot}$	52
$[Fe(L_{26})(CH_3CN)_2]^{2+}$	10	1000	18	1.8	1.2	"	"	Fe-O homolysis	$OH^{\cdot}$	50
$[Fe(L_{26})(CH_3CN)_2]^{2+\,f}$	100	1000	6	6	2.3	"	"	O-O homolysis	$Fe^{IV}=O$, $OH^{\cdot}$	50
$[Fe(L_{27})(CH_3CN)_2]^{2+}$	10	1000	42	4.2	1.4	"	"	Fe-O homolysis	$OH^{\cdot}$	50
$[Fe(L_{27})(CH_3CN)_2]^{2+\,f}$	100	1000	6	6	1.4	"	"	Fe-O homolysis	$OH^{\cdot}$	50
$[Fe(L_{28})(CH_3CN)_2]^{2+}$	10	1000	n r	n r	n r	"	"	-	-	50
$[Fe(L_{28})(CH_3CN)_2]^{2+\,f}$	100	1000	0.9	0.9	1.1	"	"	Fe-O homolysis	$OH^{\cdot}$	50
$[Fe(L_{29})(CH_3CN)_2]^{2+}$	10	1000	51	5.1	5.0	"	"	O-O heterolysis	$Fe^{V}=O$	49
$[Fe(L_{29})(CH_3CN)_2]^{2+\,f}$	100	1000	30	30	2.3	"	"	O-O homolysis	$Fe^{IV}=O$, $OH^{\cdot}$	49
$[Fe(L_{30})(CH_3CN)_2]^{2+}$	10	1000	49	4.9	4.4	"	"	O-O heterolysis	$Fe^{V}=O$	49
$[Fe(L_{30})(CH_3CN)_2]^{2+\,f}$	100	1000	15	15	2.9	"	"	O-O homolysis	$Fe^{IV}=O$, $OH^{\cdot}$	49
$[Fe(L_{31})(CH_3CN)_2]^{2+}$	10	1000	34	3.4	2.1	"	"	O-O homolysis	$Fe^{IV}=O$, $OH^{\cdot}$	49
$[Fe(L_{31})(CH_3CN)_2]^{2+\,f}$	100	1000	9	9	1.8	"	"	Fe-O homolysis	$OH^{\cdot}$	49
Simple Fe salts										
$[Fe(CH_3CN)_4]^{2+}$	10	1000	10	1	1.0	1.8	-	Fe-O homolysis	$OH^{\cdot}$	30
$Fe(ClO_4)_3$	10	1000	37	3.7	1.9	1.5	3.3	Fe-O homolysis	$OH^{\cdot}$	31
Free $OH^{\cdot}$ radical	10	1000	1.0		1-2	2	2.0		$OH^{\cdot}$	22

Conditions: Iron catalyst:H_2O_2:alkane = 1:10:1000 (cyclohexane) and 1:10:10 (adamantane). H_2O_2 added by syringe pump, air at 25°C, 25mins, total time 40 mins. av. of 2 runs.
Eff. - (cyclohexanol+cyclohexanone):H_2O_2/100 in the oxidation of cyclohexane. TN - mols oxidised products:mols cat. in the oxidation of cyclohexane.
A:K - cyclohexanol:cyclohexanone in the oxidation of cyclohexane. KIE -kinetic isotope effect of cyclohexanol formation in the oxidation of cyclohexane and cyclohexane-*d*12.
3°:2° - 1-adamantanol:(2-adamantanol+2-adamantanone) in the oxidation of adamantane taking into account of the correction for a number of C-H bonds in a group.

and L^{30} evidence of heterolytic O-O cleavage when using 10 equivalents of H_2O_2. Those ligands showing the poorest activity and selectivity to alcohol were L^{27} and L^{28} with A/K ratios close to unity which for L^{27} was even apparent when using 10 equivalents of H_2O_2.

5.2.3.4 Conclusions on the activity of the catalysts; $[Fe(L)(CH_3CN)_x]^{2+}$ (L = $L_{11,15,16,21,22}$ and L_{24}) On basis of the A/K ratios it is concluded that none of the iron(II) complexes of **$L_{11,15,16,21,22}$ and L_{24}** are particularly effective in catalysing cyclohexane oxygenation by H_2O_2 certainly when compared to the established literature systems; $[Fe(TPA)(CH_3CN)_2]^{2+}$ and $Fe(BPMEN)(CH_3CN)_2]^{2+}$. Even so within the reactivity patterns seen the 6-n-hexylurea-substituted TPA complexes; $[Fe(L_{21})(CH_3CN)_2]^{2+}$ and $[Fe(L_{22})(CH_3CN)_2]^{2+}$ are slightly more active (A/K = 2.1 – 3.3; 100 equivalents of H_2O_2) compared to the alkyl-ether linked 6-py TPA derivative complexes; $[Fe(L_{15})(CH_3CN)_2]^{2+}$ (CH_3OCH_2-substituent) and $[Fe(L_{16})(CH_3CN)_2]^{2+}$ ($C_8H_{15}OCH_2$-substituent (A/K = 0.8 – 1.6) although $[Fe(L_{15})(CH_3CN)_2]^{2+}$ showed the highest efficiency (6.4% based on H_2O_2 at 10 equivalents). The bis-6-n-hexylurea-substituted TPA complex $[Fe(L_{22})(CH_3CN)_2]^{2+}$ exhibited the highest A/K of all the complexes studied (3.3). However the most active catalyst based on a balance between efficiency, turnover and A/K ratio was that using the 6-Br_3-TPA ligand; $[Fe(L_{24})(CH_3CN)_2]^{2+}$. 6-Br_3-TPA was only synthesised as a possible precursor to making 6-$(NH_2)_3$-TPA (chapter 4) but it was decided to screen it nonetheless. Given the relative poor reactivity of all of the complexes and their high spin nature (with the exception of the peroxoiron(III) derivatives with L_{21} which are low spin) it would be premature to make judgments on the virtue of L_{24}. It could be proposed that the electron donating Br groups are active in pushing e-density onto the O-O group of the bound peroxide so facilitating O-O cleavage rather than Fe-O cleavage in the same way as seen on the introduction of e-donating co-ligands on the iron like py^+O^-, acetate and RS^-.[53-55] However the principal reason for the poor reactivity of $[Fe(L)(CH_3CN)_x]^{2+}$ (L = $L_{11,15,16,21,22}$ and L_{24}) lies in the predominantly high

spin nature of the iron(II) and resulting peroxoiron(III) complexes. This is believed to be as a result of a weakening in the ligand field due to the steric effect of the 6-substituent. Que has observed that the introduction of two or more 6-substituents on the py groups of TPA induces a spin change of the iron complex from low spin for $[Fe(TPA)(CH_3CN)_2]^{2+}$ and $[Fe(6\text{-}MeTPA)(CH_3CN)_2]^{2+}$ to high spin for $[Fe(6\text{-}Me_2TPA)(CH_3CN)_2]^{2+}$ and $[Fe(6\text{-}Me_3\text{-}TPA)(CH_3CN)_2]^{2+}$.[22] This is found to strongly influence the catalytic activity shown by the complexes with the high spin complexes showing evidence of radical based processes (low A/K ratios) whereas the low spin complexes exhibit evidence of a high valent iron-oxo based oxidants (high A/K, KIE and $3^o/2^o$ ratios). However, provided the 6-substituent position on the py ring is avoided so maintaining the low spin configuration, some positive (enhancing) substituent effects have interestingly been observed, Table 5.2, in the catalysis of alkane oxygenation by H_2O_2. Firstly, low spin $[Fe(5\text{-}Me_3TPA)(CH_3CN)_2]^{2+}$ and $[Fe(3\text{-}Me_3TPA)(CH_3CN)_2]^{2+}$ show enhanced activity (A/K ratios of 9 and 14 respectively) compared to that found for $[Fe(TPA)(CH_3CN)_2]^{2+}$ itself (5) (the KIEs are fairly constant for all at between 3.5 – 3.8 with $3^o/2^o$ values in the range 15-21. [10, 29] Furthermore $[Fe(5\text{-}Me_3TPA)(CH_3CN)_2]^{2+}$ and $[Fe(3\text{-}Me_3TPA)(CH_3CN)_2]^{2+}$ are, if anything, slightly more efficient (Eff 40% based on 10 equivalents H_2O_2) compared to $[Fe(TPA)(CH_3CN)_2]^{2+}$ (37%). Secondly, the single 6-Me-substituted low spin complex $[Fe(6\text{-}MeTPA)(CH_3CN)_2]^{2+}$ exhibits a higher $3^o/2^o$ ratio (30) for adamantane oxygenation compared to that found using $[Fe(TPA)(CH_3CN)_2]^{2+}$ (17).[56]

5.3. Suggestions for further work

The focus of this project was to synthesize a number of 6-substituted peralkylated TPA ligand derivatives aimed ultimately at enhancing the activity of their subsequent iron complexes towards the 1-(terminal) oxygenation by H_2O_2 on linear n-alkanes as providing new catalytic routes to valuable C-1 oxygenates. The focus was also on the incorporation of a urea spacer group (ligands L_{21} and L_{22}) in the hope that it might hydrogen-bond to bound OOH in the hydroperoxoiron(III) precursor so facilitating heterolytic O-O cleavage (via facilitated OH^- dissociation) to generate the putative powerful oxo-iron oxidant $LFe^{V}=O$ encapsulated within the hydrophobic channel. However the findings of the catalytic studies have shown that any beneficial (enhancing) effect that might have arisen from the presence of the hydrogen – bonding and the hydrophobic channel created via the 6-peralkylurea substituents was largely outweighed by the shift to high spin peroxoiron(III) intermediates that cleave homolytically at the Fe-O bond leading to OH radical based products. However as discussed above, studies with iron complexes of certain methylated-TPA ligands have shown that, provided the 6-substituent position on the py ring is avoided so maintaining the low spin configuration at the iron, some positive (enhancing) substituent effects on the catalytic properties are observed, table 5.2. Thus future work could shift to the utilisation of the 5-py position for attaching enhancing peralkyl or supramolecular substituents to enhance selective substrate binding. Molecular modelling shows that the 5-position could also be used to create a range of potentially supramolecular iron-TPA derivatives such as those shown in figure 5.23 for methane binding and activation towards oxygenation to methanol.

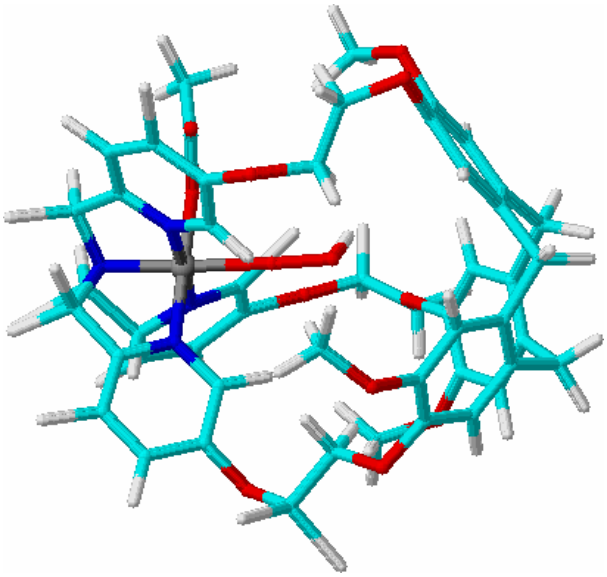

Figure 5.23: Geometry optimised model of a hydroperoxoiron(III) complex of a putative 5-py-substituted hydrophobic TPA-cryptophane based on an ether-attached cyclotriveratrylene to promote methane binding and selective oxygenation (to methanol).

The promoting effect of acetate in enhancing the tendency towards heterolytic O-O cleavage of the hydro(alkyl)peroxoiron(III) precursors also needs further study in order to understand fully the effects. $[Fe(TPA)(OAc)(H_2O)]^+$ remains one of the most efficient and active non-heme catalysts known, albeit towards mCPBA oxygenation of cycloalkanes, so further work in regard to catalysis of H_2O_2 and or O_2 oxygenations by this and related complexes is required.

Finally, studies to synthesise ligands that incorporate a carboxylate donor group into the polypyridine ligand backbone are of interest. An attempt to synthesise one such ligand; a derivative of BPMEN with a pendant carboxylate moiety, shown in figure 5.24, is described in chapter 6 using a copper(II)-templating method.

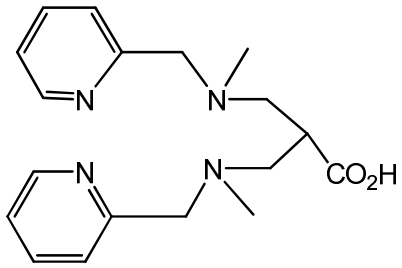

Figure 5.24: A putative carboxylate-pendent BPMPN ligand (see chapter 6)

5.4. Experimental section

GC analysis was carried out on Agilent 6890A chromatograph with HP-5 column (30 m x 0.25 mm, film thickness 0.25 μm) Toluene was used as a standard for quantitative analysis. UV-vis spectra were recorded at 25 ºC in acetonitrile solution on a Perkin-Elmer Lambda 2 spectrometer. EPR experiments were recorded on Bruker EMX 10/12 spectrometer operating at 9.5 GHz with 100 kHz modulation. The sample was transferred to a quartz EPR tube, (12cm length x 0.4cm i.d.) which was then immersed in a Dewar of liquid nitrogen, and transferred to a cooled sample holder within the EPR spectrometer whose cavity was maintained at 110 K

5.4.1 Materials

Reagents and solvents used were of commercially available reagent quality unless otherwise stated. Deoxygenation of solvents was effected by bubbling N_2 directly through the solutions. Preparation and handling of air-sensitive materials were performed under an inert atmosphere of Argon in a glove box. The synthesis of $[Fe(SO_3CF_3)_2(CH_3CN)_2]$ was described in chapter 3.

5.4.2 Characterisation of peroxoiron(III) complexes by X-band EPR

The reaction intermediates were obtained by adding ^{t}BuOOH or H_2O_2 to samples of the iron(II)(L) (L = L_2-L_5) complexes prepared *in situ* from the ligand and $[Fe(SO_3CF_3)_2(CH_3CN)_2]$. The CH_3CN solutions of the iron(II) complexes were prepared as follows:

5.4.2.1 $[Fe(L_{15})(CH_3CN)_x](O_3SCF_3)_2$:

A solution of L_{15} (0.025 g, 0.0349 mmol) in CD_3CN (3.5 cm^3) was added to a pale yellow solution of $[Fe(SO_3CF_3)_2(CH_3CN)_2]$ (0.01522 g, 0.0349 mmol) in CD_3CN (3.5 cm^3) under N_2 atmosphere to yield a reddish-orange solution. The final stock solution concentration was 5 x 10^{-3} mol dm^{-3}. For each EPR experiment a 0.3 cm^3 aliquot was transferred to the quartz EPR sample tube.

5.4.2.2 $[Fe(L_{16})(CH_3CN)_x](O_3SCF_3)_2$:

A solution of L_{16} (0.0147 g, 0.0349 mmol) in CD_3CN (3.5 cm^3) was added to a pale yellow solution of $[Fe(SO_3CF_3)_2(CH_3CN)_2]$ (0.01522 g, 0.0349 mmol) in CD_3CN (3.5 cm^3) under N_2 atmosphere to yield a reddish-orange solution. The final stock solution concentration was 5 x 10^{-3} mol dm^{-3}. For each EPR experiment a 0.3 cm^3 aliquot was transferred to the quartz EPR sample tube.

5.4.2.3 $[Fe(L_{21})(CH_3CN)_x](O_3SCF_3)_2$: A solution of L_{21} (0.0043g, 0.01 mmol) in CD_3CN (2 cm^3) was added to a pale yellow solution of $[Fe(SO_3CF_3)_2(CH_3CN)_2]$ (0.0044 g, 0.01 mmol) in CD_3CN (2 cm^3) under N_2 atmosphere to yield a reddish-orange solution. The final stock solution concentration was 2.5 x 10^{-3} mol dm^{-3}. For each EPR experiment a 0.3 cm^3 aliquot was transferred to the quartz EPR sample tube.

5.4.2.4 $[Fe(L_{22})(CH_3CN)_x](O_3SCF_3)_2$:

A solution of L_{22} (0.0057g, 0.01 mmol) in CD_3CN (2 cm^3) was added to a pale yellow solution of $[Fe(SO_3CF_3)_2(CH_3CN)_2]$ (0.0044 g, 0.01 mmol) in CD_3CN (2 cm^3) under N_2 atmosphere to yield a reddish-orange solution. The final stock solution concentration was 2.5 x 10^{-3} mol dm^{-3}. For each EPR experiment a 0.3 cm^3 aliquot was transferred to the quartz EPR sample tube.

5.4.3 Time-resolved UV-VIS spectrophotometric studies of the reactions of $[Fe(L)(CH_3CN)_x]^{2+}$ species with H_2O_2 and ^tBuOOH in CH_3CN solvent at 25^oC

5. 4.3.1 Reaction of $[Fe(L_{21})(CH_3CN)_x]^{2+}$ with H_2O_2.

A solution of L_{21} (0.0043g, 0.01 mmol) in CD_3CN (2 cm^3) was added to a pale yellow solution of $[Fe(SO_3CF_3)_2(CH_3CN)_2]$ (0.0044 g, 0.01 mmol) in CD_3CN (2 cm^3) under N_2 atmosphere to yield a reddish-orange solution. The final stock solution concentration was 2.5 x 10^{-3} mol dm^{-3}. For each UV/Vis experiment a 1 cm^3 aliquot was transferred to the quartz UV/Vis cubette and 100 fold excess of H_2O_2 at 25^oC

5. 4.3.2. Reaction of $[Fe(L_{21})(CH_3CN)_x]^{2+}$ with ^tBuOOH.

A solution of L_{21} (0.0043g, 0.01 mmol) in CD_3CN (2 cm^3) was added to a pale yellow solution of $[Fe(SO_3CF_3)_2(CH_3CN)_2]$ (0.0044 g, 0.01 mmol) in CD_3CN (2 cm^3) under N_2 atmosphere to yield a reddish-orange solution. The final stock solution concentration was 2.5 x 10^{-3} mol dm^{-3}. For each UV/Vis experiment a 1 cm^3 aliquot was transferred to the quartz UV/Vis cubette and 100 fold excess of ^tBuOOH at 25^oC

5. 4.3.3 Reaction of $[Fe(L_{22})(CH_3CN)_x]^{2+}$ with 18 fold excess ^tBuOOH.

A solution of L_{22} (0.0043g, 0.0078 mmol) in CD_3CN (5 cm^3) was added to a pale yellow solution of $[Fe(SO_3CF_3)_2(CH_3CN)_2]$ (0.0034 g, 0.0078 mmol) in CD_3CN (5 cm^3) under N_2 atmosphere to yield a reddish-orange solution. The final stock solution concentration was 7 x 10^{-4} mol dm^{-3}. For each UV/Vis experiment a 1 cm^3 aliquot was transferred to the quartz UV/Vis cubette and 18 fold excess of ^tBuOOH at 25^oC

5. 4.3.4 Reaction of $[Fe(L_{22})(CH_3CN)_x]^{2+}$ with 350 fold excess ^tBuOOH.

A solution of L_{22} (0.0043g, 0.0078 mmol) in CD_3CN (5 cm^3) was added to a pale yellow solution of $[Fe(SO_3CF_3)_2(CH_3CN)_2]$ (0.0034 g, 0.0078 mmol) in CD_3CN (5 cm^3) under N_2 atmosphere to yield a reddish-orange solution. The final stock solution concentration was 7 x 10^{-4} mol dm^{-3}. For each UV/Vis experiment a 1 cm^3 aliquot was transferred to the quartz UV/Vis cubette and 350 fold excess of ^tBuOOH at 25^oC.

5.5 References

1. U. Schuchardt, D. Cardoso, R. Sercheli, R. Pereira, R. S. da Cruz, M. C. Guerreiro, D. Mandelli, E. V. Spinace and E. L. Pires, *Appl. Catal A*, 2001, **211**, 1-17.
2. J. M. Thomas, R. Raja, G. Sankar and R. G. Bell, *Acc. Chem. Res.*, 2001, **34**, 191-200.
3. S. Tanase, C. Foltz, R. de Gelder, R. Hage, E. Bouwman and J. Reedijk, *J. Mol. Catal. A: Chem.* 2005, **225**, 161-167.
4. M. Costas, K. Chen and L. Que, *Coord. Chem. Rev.* 2000, **200-202**, 517-544.
5. M. Costas, M. P. Mehn, M. P. Jensen and L. Que, Jr., *Chem. Rev. (Washington, DC, U. S.)*, 2004, **104**, 939-986.
6. K. Chen and L. Que, Jr., *Chemical Communications (Cambridge)*, 1999, 1375-1376.
7. J. Kim, R. G. Harrison, C. Kim and L. Que, Jr., *J. Am. Chem. Soc.*, 1996, **118**, 4373-4379.
8. H. Lim Mi, J.-U. Rohde, A. Stubna, R. Bukowski Michael, M. Costas, Y. N. Ho Raymond, E. Munck, W. Nam and L. Que, Jr., *Proc Natl Acad Sci U S A* 2003, **100**, 3665-3670.
9. C. Kim, K. Chen, J. Kim and L. Que, Jr., *J. Am. Chem. Soc.*, 1997, **119**, 5964-5965.
10. K. Chen and L. Que, Jr., *J. Am. Chem. Soc.*, 2001, **123**, 6327-6337.
11. J.-U. Rohde, J.-H. In, M. H. Lim, W. W. Brennessel, M. R. Bukowski, A. Stubna, E. Muenck, W. Nam and L. Que, Jr., *Science (Washington, DC, U. S.)*, 2003, **299**, 1037-1039.
12. E. J. Klinker, J. Kaizer, W. W. Brennessel, N. L. Woodrum, C. J. Cramer and L. Que, Jr., *Angew. Chem., Int. Ed.*, 2005, **44**, 3690-3694.
13. A. J. Simaan, F. Banse, J.-J. Girerd, K. Wieghardt and E. Bill, *Inorg. Chem.* 2001, **40**, 6538-6540.
14. K. U. Ingold and J. R. Morton, *J. Am. Chem. Soc.* 1964, **86**, 3400-3402.
15. W. J. Maguire and R. C. Pink, *Trans. Faraday Soc.* 1967, **63**, 1097-1105.

16. M. V. Lobanova, K. P. Bryliakov, E. A. Duban and E. P. Talsi, *Mendeleev Commun.* 2003, 175-177.

17. D. T. Richens, S. L. Jain and A. C. Gale, *Inorg. React. Mech. (Philadelphia, PA, U. S.)*, 2007, **6**, 169-183.

18. M. P. Jensen, S. J. Lange, M. P. Mehn, E. L. Que and L. Que, Jr., *J. Am. Chem. Soc.*, 2003, **125**, 2113-2128.

19. C. Nguyen, R. J. Guajardo and P. K. Mascharak, *Inorg.* 1996, **35**, 6273-6281.

20. A. Wada, S. Ogo, S. Nagatomo, T. Kitagawa, Y. Watanabe, K. Jitsukawa and H. Masuda, *Inorg. Chem.*, 2002, **41**, 616-618.

21. Y. Zang, J. Kim, Y. Dong, E. C. Wilkinson, E. H. Appelman and L. Que, Jr., *J. Am. Chem. Soc.*, 1997, **119**, 4197-4205.

22. K. Chen, M. Costas and L. Que, Jr., *Journal of the Chemical Society, Dalton Transactions*, 2002, 672-679.

23. A. Wada, S. Ogo, Y. Watanabe, M. Mukai, T. Kitagawa, K. Jitsukawa, H. Masuda and H. Einaga, *Inorg. Chem.*, 1999, **38**, 3592-3593.

24. A. Diebold and K. S. Hagen, *Inorg. Chem.* 1998, **37**, 215-223.

25. *Vogel´s Textbook of Quantitaive Inorganic Analysis*, Longmann, London and New York, 1978.

26. G. J. P. Britovsek, J. England and A. J. P. White, *Inorg. Chem.* 2005, **44**, 8125-8134.

27. M. Costas, A. K. Tipton, K. Chen, D.-H. Jo and L. Que, Jr., *J. Am. Chem. Soc.*, 2001, **123**, 6722-6723.

28. J. Kaizer, E. J. Klinker, N. Y. Oh, J.-U. Rohde, W. J. Song, A. Stubna, J. Kim, E. Muenck, W. Nam and L. Que, Jr., *J. Am. Chem. Soc.*, 2004, **126**, 472-473.

29. K. Chen, M. Costas, J. Kim, K. Tipton Adrianne and L. Que, Jr., *J Am Chem Soc* 2002, **124**, 3026-3035.

30. H. C. Tung, C. Kang and D. T. Sawyer, *J. Am. Chem. Soc.* 1992, **114**, 3445-3455.

31. R. H. Fish, M. S. Konings, K. J. Oberhausen, R. H. Fong, W. M. Yu, G. Christou, J. B. Vincent, D. K. Coggin and R. M. Buchanan, *Inorg. Chem.* 1991, **30**, 3002-3006.

32. C. Walling, *Acc. Chem. Res.* 1975, **8**, 125-131.

33. G. V. Buxton, C. L. Greenstock, W. P. Helman and A. B. Ross, *J. Phys. Chem. Ref. Data*, 1988, **17**, 513-886.

34. S. Miyajima and O. Simamura, *Bull. Chem. Soc. Jpn.*, 1975, **48**, 533-535.

35. A. F. Trotman-Dickenson, *Adv. Free-Radical Chem.* 1965, **1**, 1-38.

36. R. Bukowski Michael, P. Comba, C. Limberg, M. Merz, L. Que, Jr. and T. Wistuba, *Angew Chem Int Ed Engl*, 2004, **43**, 1283-1287.

37. K. Chen and L. Que, Jr., *Angew. Chem., Int. Ed.*, 1999, **38**, 2227-2229.

38. G. Roelfes, M. Lubben, R. Hage, L. Que, Jr. and B. L. Feringa, *Chem.--Eur. J.*, 2000, **6**, 2152-2159.

39. F. Li, M. Wang, C. Ma, A. Gao, H. Chen and L. Sun, *Dalton Trans.* 2006, 2427-2434.

40. R. A. Leising, R. E. Norman and L. Que, Jr., *Inorg. Chem.*, 1990, **29**, 2553-2555.

41. K. A. Lee and W. Nam, *J. Am. Chem. Soc.* 1997, **119**, 1916-1922.

42. K. Ray, S. M. Lee and L. Que, Jr., *Inorg. Chim. Acta*, 2008, **361**, 1066-1069.

43. J. Tang, P. Gamez and J. Reedijk, *Dalton Trans.* 2007, 4644-4646.

44. A. Horn, I. Vencato, A. J. Bortoluzzi, R. Hoerner, R. A. N. Silva, B. Spoganicz, V. Drago, H. Terenzi, M. C. B. de Oliveira, R. Werner, W. Haase and A. Neves, *Inorg. Chim. Acta*, 2005, **358**, 339-351.

45. T. Ayers, R. Turk, C. Lane, J. Goins, D. Jameson and S. J. Slattery, *Inorg. Chim. Acta*, 2004, **357**, 202-206.

46. J. Kim, Y. Zang, M. Costas, R. G. Harrison, E. C. Wilkinson and L. Que, Jr., *JBIC, J. Biol. Inorg. Chem.*, 2001, **6**, 275-284.

47. T. A. van den Berg, J. W. de Boer, W. R. Browne, G. Roelfes and B. L. Feringa, *Chem. Commun. (Cambridge, U. K.)*, 2004, 2550-2551.

48. M. R. Maurya, S. J. J. Titinchi, S. Chand and I. M. Mishra, *J. Mol. Catal. A: Chem.*, 2002, **180**, 201-209.

49. J. England, G. J. P. Britovsek, N. Rabadia and A. J. P. White, *Inorg. Chem. (Washington, DC, U. S.)*, 2007, **46**, 3752-3767.

50. G. J. P. Britovsek, J. England and A. J. P. White, *Dalton Trans.* 2006, 1399-1408.

51. M. C. White, A. G. Doyle and E. N. Jacobsen, *J. Am. Chem. Soc.* 2001, **123**, 7194-7195.

52. J. England, C. R. Davies, M. Banaru, A. J. P. White and G. J. P. Britovsek, *Adv. Synth. Catal.* 2008, **350**, 883-897.

53. J. Kaizer, M. Costas and L. Que, Jr., *Angew. Chem., Int. Ed.*, 2003, **42**, 3671-3673.

54. C. V. Sastri, M. J. Park, T. Ohta, T. A. Jackson, A. Stubna, M. S. Seo, J. Lee, J. Kim, T. Kitagawa, E. Muenck, L. Que, Jr. and W. Nam, *J. Am. Chem. Soc.*, 2005, **127**, 12494-12495.

55. J.-U. Rohde and L. Que, Jr., *Angew. Chem., Int. Ed.*, 2005, **44**, 2255-2258.

56. M. Costas and L. Que, Jr., *Angew. Chem., Int. Ed.*, 2002, **41**, 2179-2181.

Chapter Six

Synthesis of some new ligands for low temperature bleaching applications

6.1. Attempted synthesis of N,N'-bis(pyridylmethyl)-1,3-diamino propane-2-carboxylic acid, (L_{25}) and crystallographic characterization of 1, 3-diaminopropane-2-carboxylic acid. 2HCl.

6.1.1. Introduction

The search for better and more effective low temperature metal based oxidation (bleaching) catalysts continues to be very important for the viewpoint of reducing energy costs in the use of domestic and industrial detergents.[1] As outlined in chapter 1, a range of biomimetic iron complexes of ligand containing pyridines and tetracoordinated amines have been investigated for their ability to catalyse the efficient catalytic air oxidation of various organic substrates. Popular target substrates for benchmark studies of catalytic activity have been cyclic hydrocarbons such cyclohexane or adamantane which are oxidised to the corresponding alcohol or ketone under ambient conditions.[2-4] Iron complexes showing some of the highest activity so far seen include those of the ligands containing; TPA (tris(pyridylmethyl)amine) and BPMEN (N,N'-dimethyl-N,N'-bis(2-pyridylmethyl)ethane-1,2-diamine). Moreover the high relative yields of alcohol versus ketone (cycloalkanes)[5] and the stereoselective epoxidation[6] and cis-dihydroxylation[7, 8] of alkenes by H_2O_2 observed using $[Fe^{II}(BPMEN)(CH_3CN)_2]^{2+}$ and $[Fe^{II}(TPA)(CH_3CN)_2]^{2+}$ provided strong evidence for the participation of a high-valent iron-oxo species.[9] Since complexes of BPMEN show the highest activity there is continuing interest in the studying the behaviour of metal complexes with related ligands of similar structure in the hope of discovering even higher activity. Here the attempted synthesis of a BPMEN analogue; N,N'-bis(pyridylmethyl)-1,3-diaminopropane-2-

carboxylic acid, L_{25} is reported. L_{25} shares common structural features with BPMEN; e.g. two pyridyl and two amino nitrogens but has an additional pendent carboxylate group, see figure 6.1. The availability of a additional carboxylate donor group in BPMEN-type ligands is of interest since Que and co-workers have shown that acetate/acetic acid enhances alkene epoxidation activity by both $[Fe^{II}(BPMEN)(CH_3CN)_2]^{2+}$ and $[Fe^{II}(TPA)(CH_3CN)_2]^{2+}$ attributed to significant accessing of the formally perferryl Fe^{V}=O state. This highly oxidising metal-based oxo species is also believed to be responsible for preferential alcohol product formation (versus ketone formation) in catalytic oxidation reactions on cycloalkanes.[10]

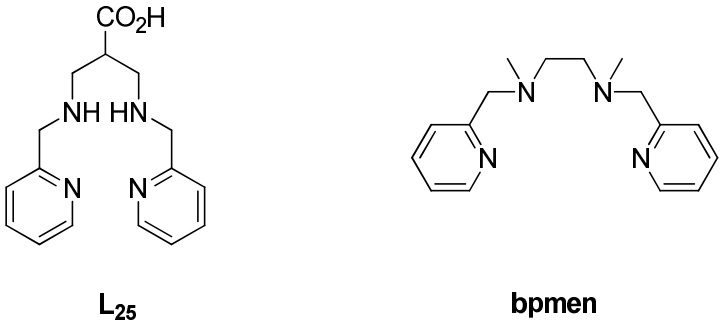

L_{25} bpmen

Figure 6.1: Schematic representation of **L_{25}** and BPMEN.

The synthesis of L_{25} derives from the reported template synthesis of N,N'-bis(2-pyridylmethylene)-1,3-diamino-2,2-dicarboxyethyl propane, L_{26}**,** in the form of its copper complex $[Cu(L_{26})(H_2O)](ClO_4)_2$, see figure 6.6.[11] Decarboxylation of $[Cu(L_{26})](ClO_4)_2$ with base followed by demetallation via reduction with zinc powder/HCl_{aq} to give L_{25} was however unreported despite being similar to the method used to make a number of carboxylated polyamine and macrocyclic amine ligands.[12-18] These reactions offer the convenient synthetic routes to a range of macrocyclic and open chain polychelate metal complexes, many of which can not be synthesised easily by others methods, the template effect may arise from the stereochemistry imposed by metal ion coordination of some of the reactants, promoting a series of controlled steps.[19-21] A wide variety of template reactions

involving metal-promoted condensation of primary amine functionalities with formaldehyde and either nitrogen or carbon acid in the presence of a base has been reported.[12, 18, 22, 23] Among the variety of metal centred templates that have been used in these reactions, the most common ones are Ni(II) and Cu(II), although other more recent examples use a "bisaminal route",[15] where no metal is required. These reactions can be designed to incorporate additional pendant donors, such as those from primary amino[24, 25] and carboxylate[12, 24, 26] functionalities, into the resulting ligand systems.

In 1985 Comba et al reported the structural characterisation of N,N'-bis(2-pyridyl methyl)-1,3-diamino-2-methyl-2-nitropropanecopper(II) perchlorate; $[Cu(L_{27})]^{2+}$ below, figure 6.2, via the reaction of copper(II) nitrate trihydrate in methanol with 2-aminomethyl pyridine, formaldehyde and nitroethane in the presence of ethanolamine as a non-coordinating base.[13]

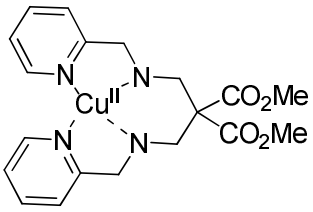

$[Cu(L_{26})]^{2+}$

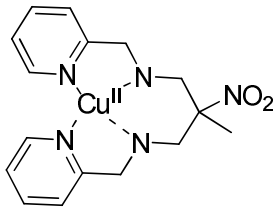

$[Cu(L_{27})]^{2+}$

Figure 6.2: Schematic representation of $[Cu(\mathbf{L_{26}})]^{2+}$ and $[Cu(L_{27})]^{2+}$

Later Lawrance et al [24, 27, 28] reported preliminary details of the synthesis of $[Cu(L_{26})]^{2+}$ via the corresponding reaction using diethylmalonate as the carboxylic acid in the presence of ethanolamine. The crystal structure of $[Cu(L_{26})(H_2O)](ClO_4)_2.H_2O$; L_{26} = N,N'-bis (2-pyridylmethylene)-1,3-diamino-2,2-dicarboxylethylpropane, was reported in 2002 by our group revealing a penta-coordinated copper(II) centre, in a distorted square-pyramidal geometry with a weakly bonded axial water molecule.[11] The behaviour of the complex in acid

media has been studied by kinetics as a function of $[H^+]$.[11] The study showed that $[Cu(L_{26})(H_2O)]^{2+}$ rapidly decomposes via protonation of L_{10} to give back a mixture of $[Cu(pyCH_2NH_2)_2]^{2+}$, diethylmalonate and formaldehyde. Base hydrolysis to give L_{25} however looked more promising. Base-promoted decarboxylation of related copper(II) macrocyclic complexes such as $[Cu(dimest)]^{2+}$ (L_{28}, dimest = *trans*-6,13-bis(methoxycarbonyl)-1,4,8,11-tetraazacyclotetradecane), figure 6.3, deriving from condensations of $[Cu(en)_2]^{2+}$ (en = ethane-1,2-diamine) with diethylmalonate yield the macrocyclic amino acid trans-1,4,8,11-tetraazacyclotetradecane-6,13-dicarboxylic acid ($diacH_2$),[26] followed by Zn/HCl demetallation has successfully afforded a number of chelating amine ligands with single pendant carboxylates.[24, 27, 29]

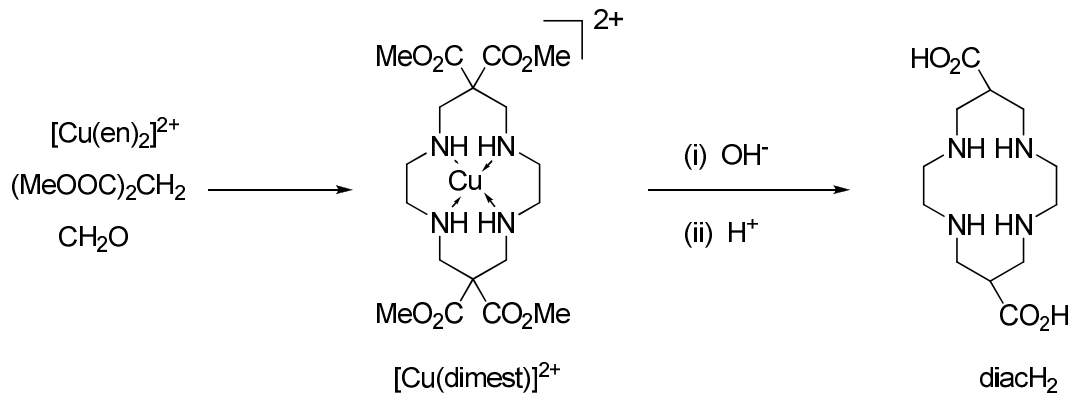

Figure 6.3: Base-promoted decarboxylation of the copper(II) macrocyclic complex $[Cu(dimest)]^{2+}$ to yield ligand $diacH_2$

Therefore it was conceivable that the same base-catalysed decarboxylation/demetallation could be carried out on $[Cu(L_{26})(H_2O)]$ $(ClO_4)_2.H_2O$ as a route to putative L_{25}. However, when the demetallation of $[Cu(L_{25})](ClO_4)$ was attempted using zinc powder and aqueous hydrochloric acid to release free L_{25} the only product isolated was a hydrolysis product of L_{25}, the new amino acid; 1,3-diaminopropane-2-carboxylic acid isolated as its hydrochloride salt.

6.1.2. Results and Discussion

6.1.2.1 Synthesis of N,N'-bis(2-pyridylmethyl)-1,3-diaminopropane-2-carboxylato copper(II) perchlorate; $[Cu(L_{25})](ClO_4)$.

Using the method described by Lawrance et al[27], figure 6.4, the pH of a solution of $[Cu(L_{26})](H_2O)](ClO_4)_2$ in water was raised to 10 with the addition of aqueous NaOH and stirred at ca. 70°C for 12 h. The solution was then evaporated to dryness to give a green powder, the IR spectrum of which showed the expected band for a coordinated carboxylate group at 1644 cm^{-1}, figure 6.6.[27] Comparison with the corresponding spectrum for $[Cu(\mathbf{L}_{26})(H_2O)](ClO_4)_2.H_2O$, figure 6.5, shows that the decarboxylation step had been achieved successfully. It was decided at this stage however not to isolate and further characterise $[Cu(L_{25})]^{2+}$ but to proceed on with the demetallation step below.

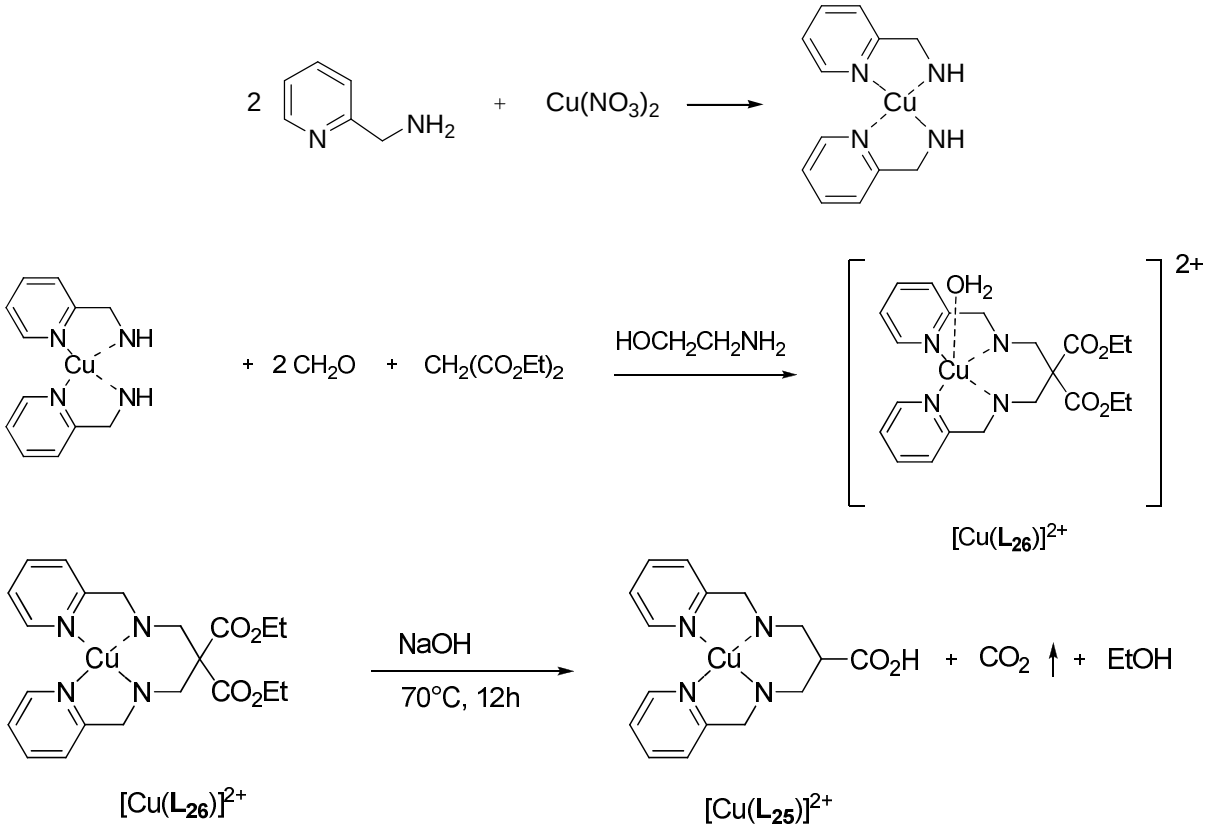

Figure 6.4: Schematic representation of the synthetic route to $[Cu(L_{25})]^{2+}$

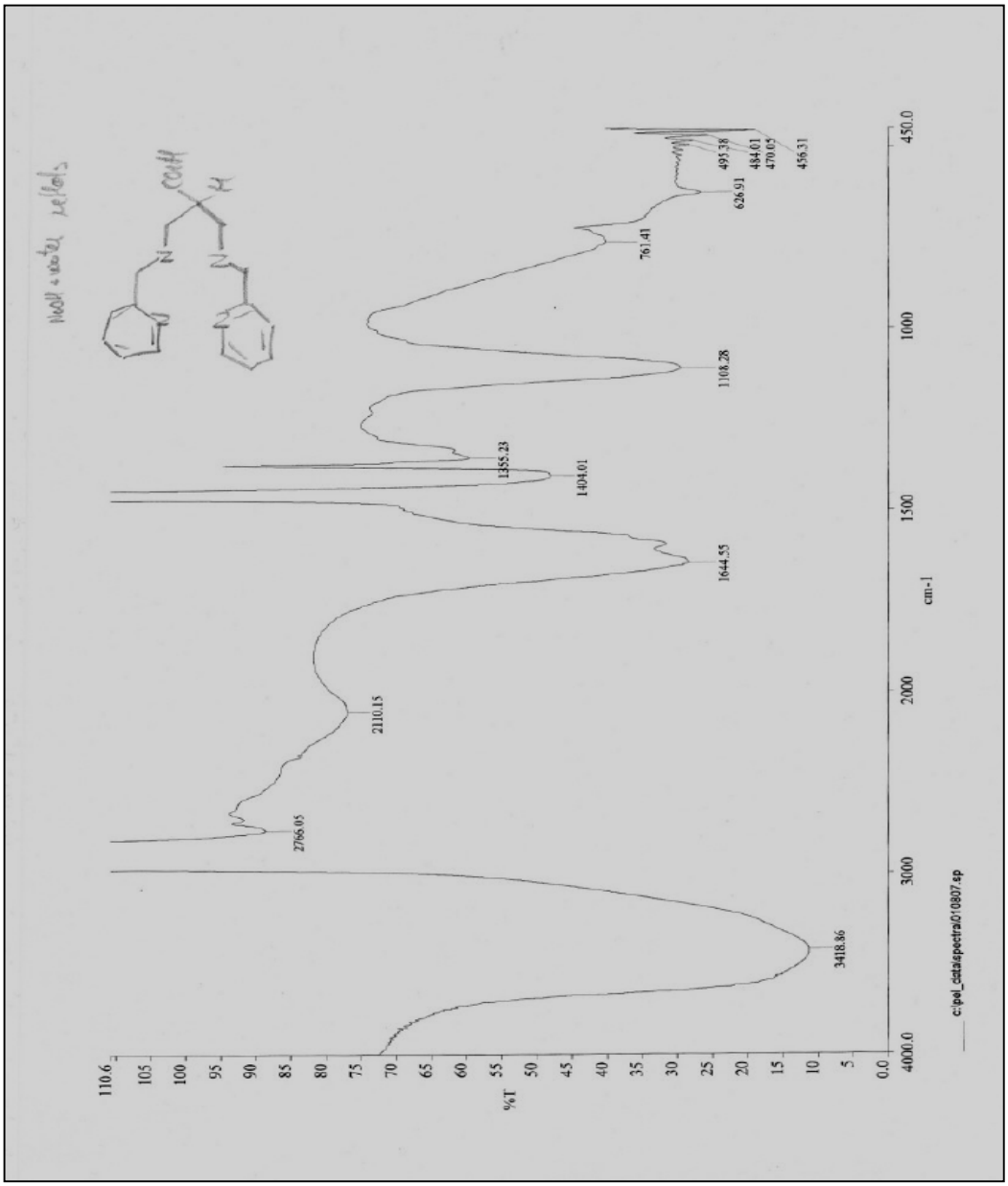

Figure 6.5: IR spectrum of the green solid obtained following treatment of $[Cu(\mathbf{L_{25}})](H_2O)](ClO_4)_2$ with aqueous NaOH.

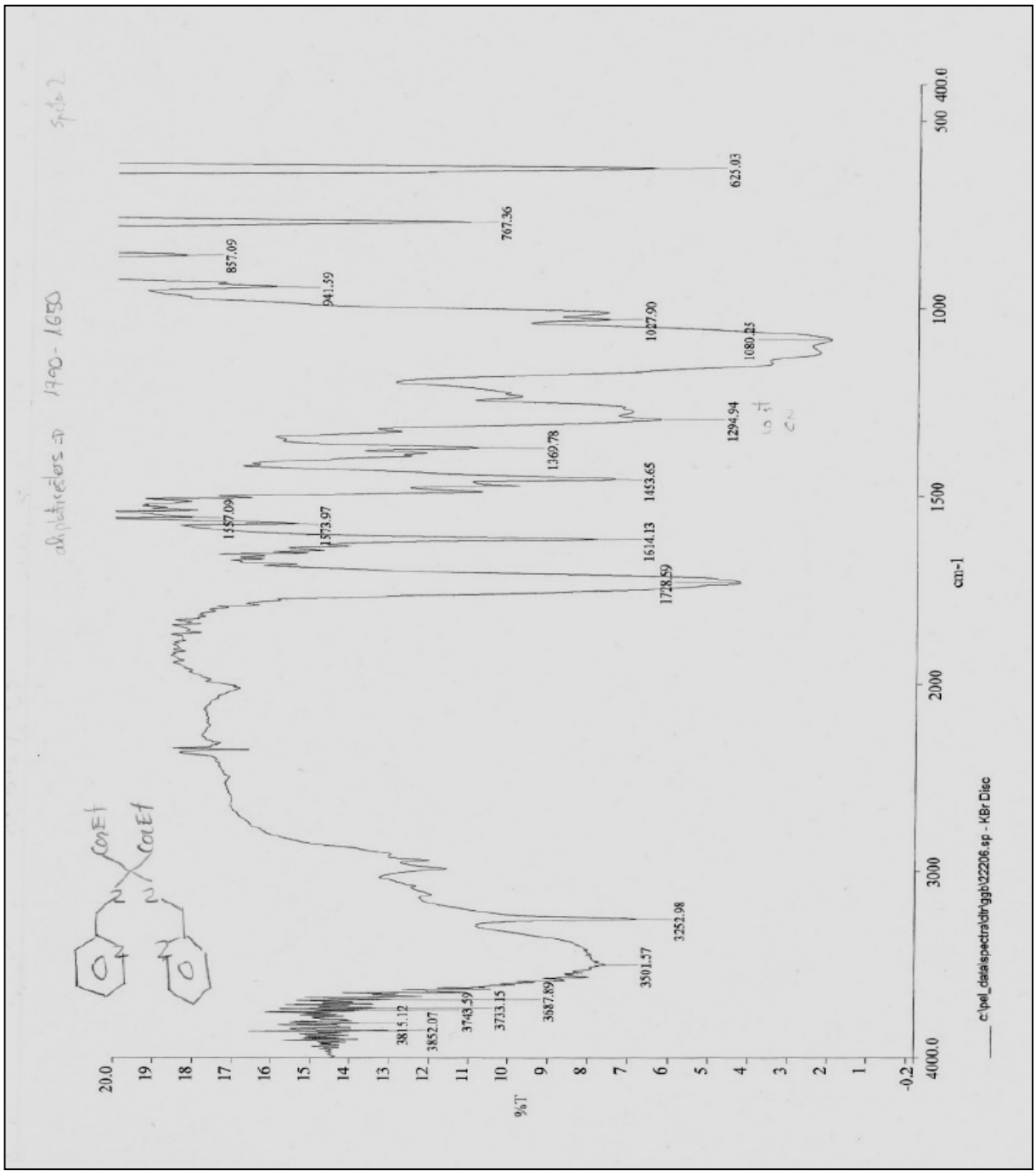

Figure 6.6: IR spectrum of $[Cu(\mathbf{L_{26}})](H_2O)](ClO_4)_2$.

The crystallographic characterisation of 1,3-diaminopropane-2-carboxylic acid is reported below. The mechanism for the hydrolysis of L_8 during the zinc/HCl demetallation step is discussed below along with suggestions of possible future alternative routes to the synthesis of L_{25} and its analogues.

6.1.2.2 The attempted synthesis of N,N'-bis(2-pyridylmethyl)-1,3-diaminopropane-2-carboxylic acid, L_{25}.

Using the method reported by Lawrance et al [27] a solution of the green solid above and a solution of hydrochloric acid were added dropwise from different dropping funnels into a flask containing zinc powder over a 1 h period. The solution was stirred for a further 0.5 h at 60°C and then filtered to remove metallic copper and any remaining zinc powder. The solution was then diluted with water and loaded onto a 5 cm x 40 cm column of Dowex 50W X2 cation-exchange resin (H^+ form). The column was washed with 1.0 mol dm^{-3} HCl to remove Zn^{2+} ions until no further evidence was found (i.e. failure to give a white precipitate (zinc hydroxide) on the addition of base). The desired amino acid ligand product was then eluted with 3.0 mol dm^{-3} HCl, testing fractions obtained for the presence of free L_{25} via the development of a green colour on the addition of a base to neutrality and then aqueous Cu^{2+}, see figure 6.7.

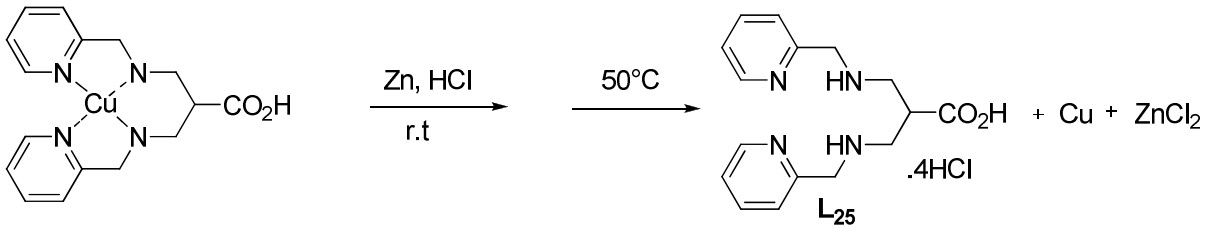

Figure 6.7: Synthetic route to obtain to obtain free **L_{25}** from its Cu^{2+} complex

Each fraction believed to contain L_{25}.4HCl was then evaporated to dryness. The residue was then taken up in water and reloaded onto the cation-exchange column charged again in its H^+ form. This time elution was carried out with different concentrations of hydrochloric acid; 0.5, 1.0 and 1.5 mol dm^{-3}. In each case the fractions were evaporated to dryness and the ^1H and ^{13}C NMR spectra recorded in D_2O. These are shown in figures 6.8 (for elution with 0.5

mol dm^{-3} [H^+]), figure 6.9 (1.0 mol dm^{-3}) and figures 6.10 (1.5 mol dm^{-3}). The ^1H NMR of the 1.5 mol cm^{-3} eluate, figure 6.10, displays the expected resonances in the aliphatic

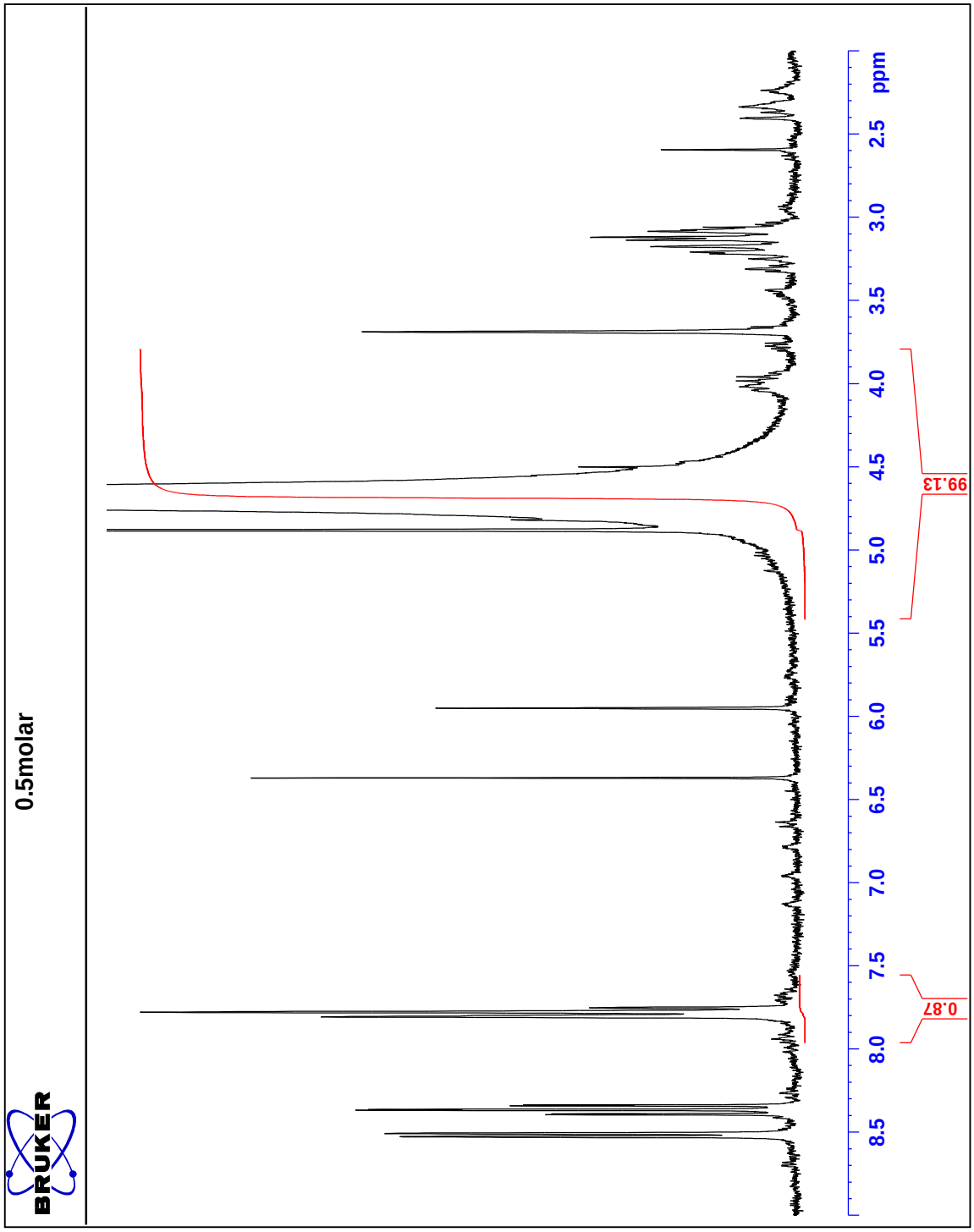

Figure 6.8: ^1H NMR spectrum in D_2O corresponding to the evaporated fraction eluted with 0.5 mol dm^{-3} HCl.

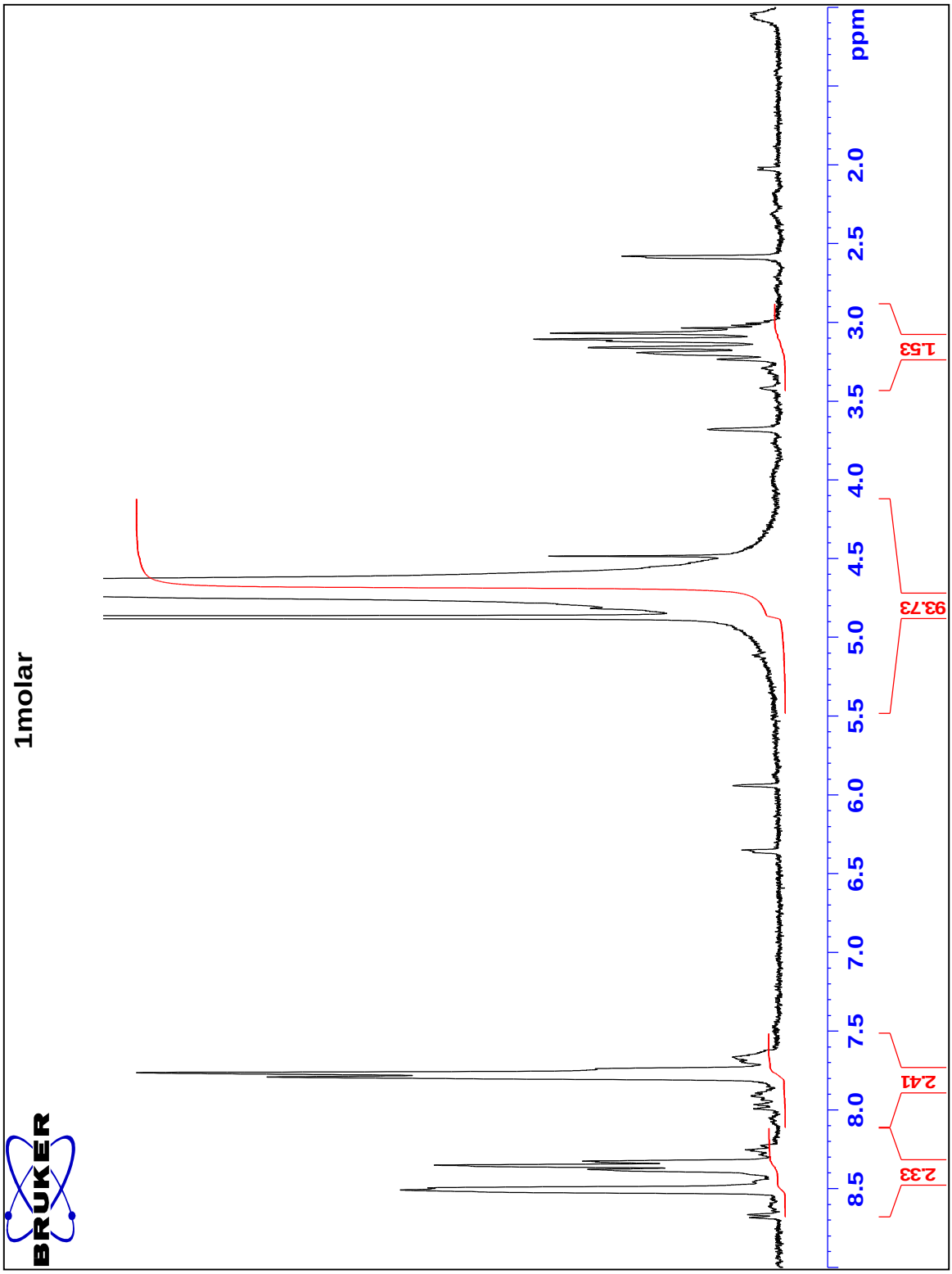

Figure 6.9: ^{1}H NMR spectrum in D_2O corresponding to the evaporated fraction eluted with 1.0 mol dm^{-3} HCl.

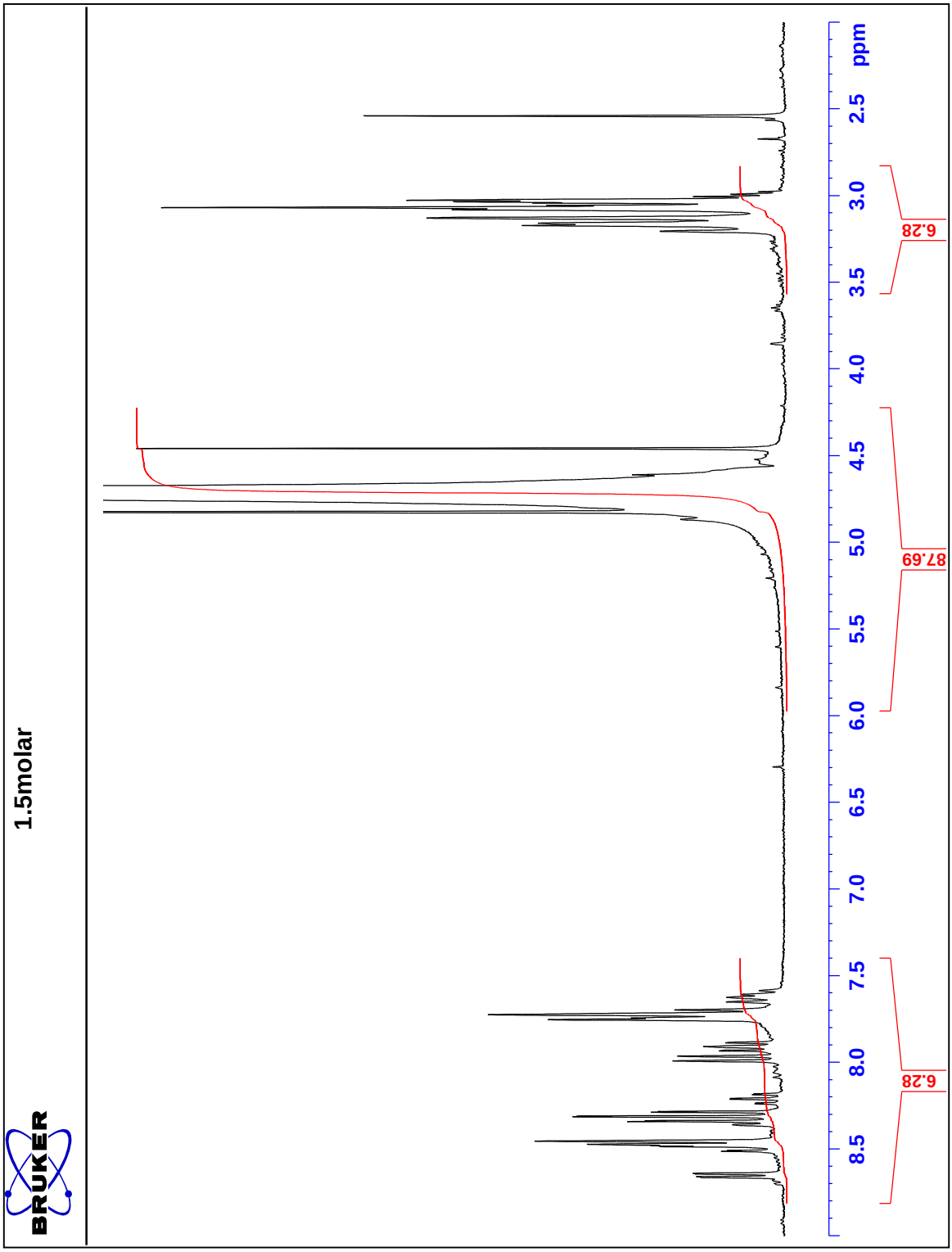

Figure 6.10: ^{1}H NMR spectrum in D_2O corresponding to the evaporated fraction eluted with 1.5 mol dm^{-3} HCl.

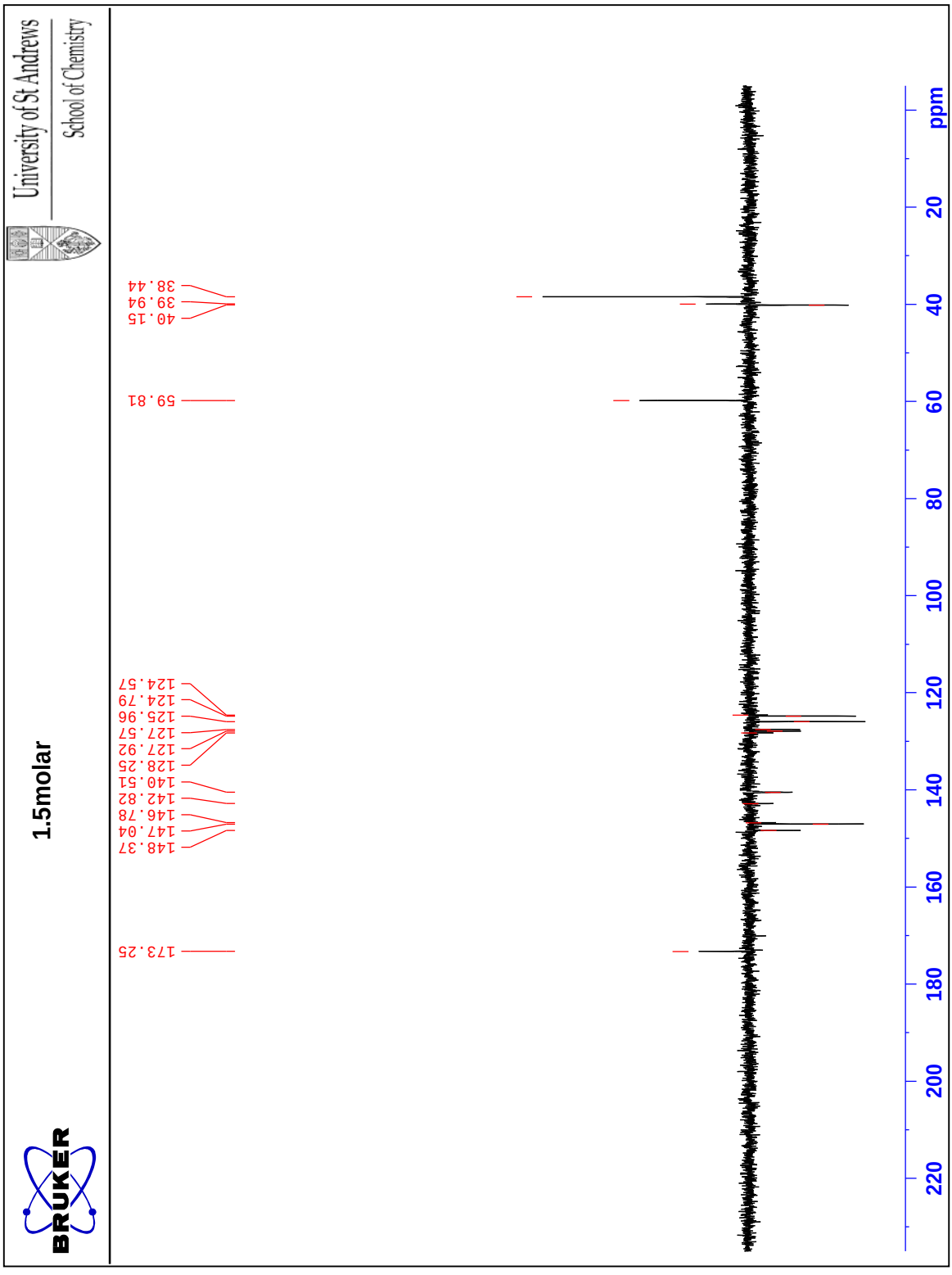

Figure 6.11: DEPT ^{13}C NMR spectrum in D_2O corresponding to the evaporated fraction eluted with 1.5 mol dm^{-3} HCl.

and aromatic regions for the protons of L_{25}. However closer analysis showed that the integration did not fit. This became further apparent when the spectra from the earlier fractions were analysed showing highly variable peak integrations even though resonances appeared in the regions expected for L_{25}. The ^{13}C NMR spectra, figure 6.11, of the 1.5 mol cm^{-3} eluant showed the presence of the carboxylate group (172 ppm) but no resonance for the expected methylene. It was quickly concluded that ligand fragmentation must have occurred during the Zn/HCl treatment to give aliphatic amine and pyridine moieties eluting as separate species from the various acid treatments. Ultimately colourless crystals suitable for X ray analysis were obtained from the 1.5 mol cm^{-3} fractions following slow evaporation in the air. The X-ray structure corresponded not to L_8 as suspected but to the aliphatic amino acid; 1,3-diaminopropane-2-carboxylic acid.2HCl. The structure of this new amino acid, shown below in figure 6.12, has not been described before, although interestingly traces of it have been found in several meteorites,[30] and its methyl ester has been described as an ntermediate in the synthesis of tripeptides which are used as protein tyrosine phosphatase inhibitors.[31]

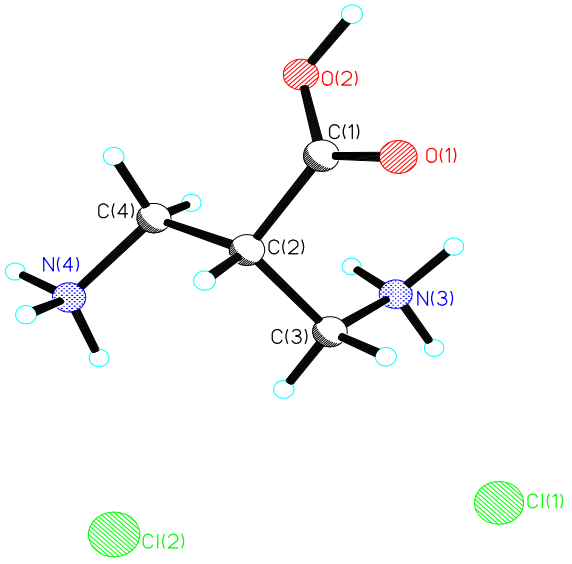

Figure 6.12: Molecular structure of 1,3-diaminopropane-2-carboxylic acid.2HCl.

Table 6.1: Selected bond lengths (Å) and angles (°) for 1,3-diaminopropane-2-carboxylic acid.2HCl.

O(1)-C(1)	1.2088(16)	C(3)-N(3)	1.5004(17)
C(1)-O(2)	1.3280(16)	N(3)-H(3NA)	0.9798(11)
C(1)-C(2)	1.5255(18)	C(4)-N(4)	1.4932(17)
O(2)-H(2O)	0.9798(11)	N(4)-H(4NA)	0.9798(11)
O(1)-C(1)-O(2)	124.04(12)	H(3NA)-N(3)-H(3NB)	106.3(15)
O(1)-C(1)-C(2)	123.11(11)	C(3)-N(3)-H(3NC)	112.7(11)
O(2)-C(1)-C(2)	112.83(11)	H(3NA)-N(3)-H(3NC)	107.4(15)
C(1)-O(2)-H(2O)	111.9(12)	H(3NB)-N(3)-H(3NC)	105.9(15)
C(1)-C(2)-C(4)	111.56(10)	N(4)-C(4)-C(2)	111.86(10)
C(1)-C(2)-C(3)	108.78(10)	C(4)-N(4)-H(4NA)	108.4(12)
C(4)-C(2)-C(3)	114.99(11)	C(4)-N(4)-H(4NC)	116.4(12)
N(3)-C(3)-C(2)	113.13(10)		

Table 6.2: Hydrogen bond distances (A) and angles (°) for 1,3-diaminopropane-2-carboxylic acid.2HCl. The hydrogen bond donor atoms are denoted as *D* and the acceptors as *A*

	D-H	H...A	D...A	DHA
O(2)-H(2O)...Cl(1)#1	0.9798(11)	1.981(3)	2.9543(11)	172.0(19)
N(3)-H(3NA)...Cl(1)#2	0.9798(11)	2.542(10)	3.3904(12)	144.8(14)
N(3)-H(3NA)...Cl(2)#3	0.9798(11)	2.592(15)	3.2028(13)	120.5(12)
N(3)-H(3NB)...Cl(1)	0.9798(11)	2.299(9)	3.1846(12)	149.9(14)
N(3)-H(3NB)...O(1)#4	0.9798(11)	2.525(16)	3.0055(15)	110.1(12)
N(3)-H(3NC)...Cl(2)#5	0.9798(11)	2.269(5)	3.2167(13)	162.4(14)
N(4)-H(4NA)...Cl(1)#6	0.9798(11)	2.293(9)	3.1888(13)	151.6(15)
N(4)-H(4NB)...Cl(2)#2	0.9799(11)	2.354(9)	3.2125(12)	145.9(13)
N(4)-H(4NB)...Cl(1)#3	0.9799(11)	2.885(14)	3.5030(13)	121.9(12)
N(4)-H(4NC)...Cl(2)	0.9798(11)	2.461(14)	3.2380(12)	135.9(15)
N(4)-H(4NC)...Cl(2)#3	0.9798(11)	2.701(17)	3.3554(13)	124.5(14)

iSelected interatomic distances and bond angles are given in table 6.1, and hydrogen bonding parameters appear in table 6.2. In the (3) the carboxyl group has hydrogen bonds with the amine protons. The C=O and C-O(H) distances respectively are 1.209 and 1.328 Å. No solvent inclusion occurred in structure.

6.1.3. Experimental

6.1.3.1. Materials:

All reagents/ solvents were of reagent grade quality unless specified. Sodium chloride, sodium perchlorate and hydrochloric acid (all Aldrich AR grade) were used as supplied.

6.1.3.2. X-ray crystallography

Data were collected on a Rigaku AFC7S diffractometer using graphite monochromated Mo-KA radiation (L= 0.71013 A). the data were corrected for Lorenz and polarisation effect. Hydrogen atoms were inserted in calculated positions but not refined. No decay or absorption corrections were applied.

6.1.3.3. Synthesis of N,N'-bis(2-pyridylmethyl)-1,3-diamino-2,2-dicarboxyethylpropane copper(II) perchlorate, $[Cu(L_9)(H_2O)](ClO_4)_2$.

The synthesis of $[Cu(L_{27})](ClO_4)_2$ was carried out as reported by Richens et al.[11] The Copper(II) nitrate trihydrate (2.5g, 0.01 mols) was dissolved in methanol (380 cm^3) and to this solution was added 2-aminomethylpyridine (2.1 cm^3, 0.02 mols). To the resultant bluish-purple suspension of bis(2-aminomethylpyridine)-copper(II) nitrate was added diethylmalonate (1.5 cm^3, 0.012 mols), formaldehyde (2.5 cm^3 0.09 mols) and ethanolamine (0.61 g, 0.6027 cm^3, 4 mmol) in order and the mixture stirred at ~50 °C for 4 hours. After this time water (170 cm^3) was added, resulting in dissolution of the suspension, followed by

further quantities of diethylmalonate (10 cm³, 0.06 mols) and formaldehyde (12.5 cm³, 0.45 mols) and the mixture stirred at 50 °C for a further 3 hours. The volume of solution was reduced to 400 cm³ and cooled in ice bath during the addition of a saturated (3.5 mol/ cm³) solution of sodium perchlorate (100 cm³). The resulting lilac coloured precipitate was removed by filtration and the air dried, yield 3.34 g. Analysis showed that the title complex was contaminated with 0.8 equivalent of sodium perchlorate. Recrystallisation from methanol however yielded purple crystals of the title complex, yield 2.84 g (41.3 %). Analysis: calculated for $C_{21}H_{28}N_4O_{12}Cl_2Cu$, C 39.9, H 4.2, N 8.4%; found C 38.3, H 4.16, N 8.51%; IR (cm^{-1}) (KBr pellet) 3251s (υ NH), 1718 s(υ C=O, ester), 1105s, 624 (ClO_4^-); λ max (H_2O) 594 nm (ε =125 M^{-1} cm^{-1}).

6.1.3.4. Synthesis of N,N'-bis-(2-pyridylmethyl)-1,3-diaminopropane-2-carboxylato) copper(II) perchorate, [Cu(L_{25})](ClO_4).

Using a method based upon that used by Lawrence et al.[27] The pH of a solution containing (2 g. 4.3 mmols of [Cu**(**L_{26})(H_2O)](ClO_4)$_2$ was raised to ca. 10 with 2.5 mol dm^{-3} aqueous NaOH and it was stirred at ca. 70°C for 12h. The green solution was evaporated to dryness in vacuum to leave a green residue of [Cu(L_{25})](ClO_4): IR (cm^{-1}) (nujol) 2995s (υ NH), 1644 s (υ C=O, carboxylate). The coordination of the carboxylate is confirmed by the low frequency C=O shift; cf. 1720 (COOH) to ~1620 cm^{-1} (COO^-).[8]

6.1.3.5. The attempted synthesis of N,N'bis(2-pyridylmethyl)-1,3-diaminopropane-2-carboxylic acid, L_{25}.

Following the method reported by Lawrence.[27] The green solid obtained above was dissolved in water and this solution along with hydrochloric acid (3 mol dm^{-3}, 10 cm^3) were added from separated funnels dropwise over 1 h to a 100 cm^3 flask containing zinc powder (1.5 g) while stirring. The solution was stirred for a further 0.5 h. at 60° C, and then filtered to remove

copper metal and any remaining zinc. The solution was diluted to 5 cm³ with water and then absorbed onto a Dowex 50W X2 resin (H^+ form, 2cm x 30cm). The column was washed with 1 mol dm^{-3} HCl until no further evidence of Zn^{2+} ions were detected (formation of zinc hydroxide on addition of base) and then eluted successively with 1.5, 2.0 and 3.0 mol dm^{-3} HCl. The combined eluates were then taken to dryness on a rotary evaporator and dried in vacuum. The residue was then dissolved in water and reloaded onto the column in the H^+ form. It was eluted successively with 0.5, 1.0 and 1.5 mol dm-3 HCl solution and following evaporation to dryness the fractions were analysed by ^1H and ^{13}C NMR in D_2O. Crystals suitable for X-ray crystallography were obtained from the 1.5 mol dm^{-3} HCl fraction via slow air evaporation.

6.1.4. Conclusions:

Structural characterisation of the new amino acid 1,3-diaminopropane-2-carboxylic acid.2HCl has been reported. This species was obtained as a consequence of our attempted synthesis of the free BPMEN ligand analogue; N,N'-bis(2-pyridylmethyl)-1,3-diaminopropane-2-carboxylic acid, L_{25}, via Zn/HCl demetallation of its Cu(II) complex. The first step, decarboxylation of the gem diester amine complex $[Cu(L_{26})(H_2O)](ClO_4)_2$ was carried out successfully. However ligand fragmentation is believed to have occurred during the final treatment of $[Cu(L_{26})](ClO_4)$ with Zn/HCl in the attempt to remove the Cu(II) ions via reduction to copper metal. This step has been carried out successfully in the case of related aliphatic polyamine ligands.[27] However it is believed that the acute sensitivity of L_{26} to acid stems from the electrophilic reactivity of the benzylic methylene groups adjacent to the pyridine upon protonation of the secondary amine groups, figure 6.13 below. A mixture of 2-hydroxymethylpyridine and 2-picoline is suspected as responsible for the pyridine resonances seen in the fractions eluted along with and contaminating samples of the crystals of 1,3-diaminopropane-2-carboxylic acid.2HCl.

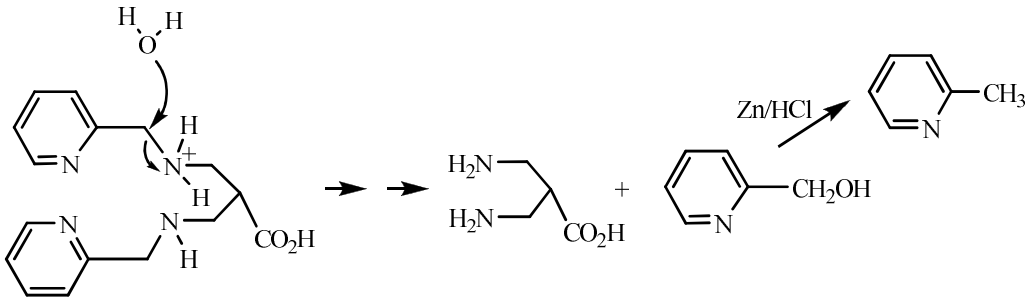

Figure 6.13: Mechanistic scheme for the acid catalysed hydrolysis of L_{25} to 1,3-diaminopropane-2-carboxylic acid.

A number of alternative synthetic routes to L_{25} or close analogues of it are proposed below based on the reaction of 3,3'-dichloropivalic acid with 1,2 diaminoethane, figure 6.14, according to the method of Bernhardt et al.[16]

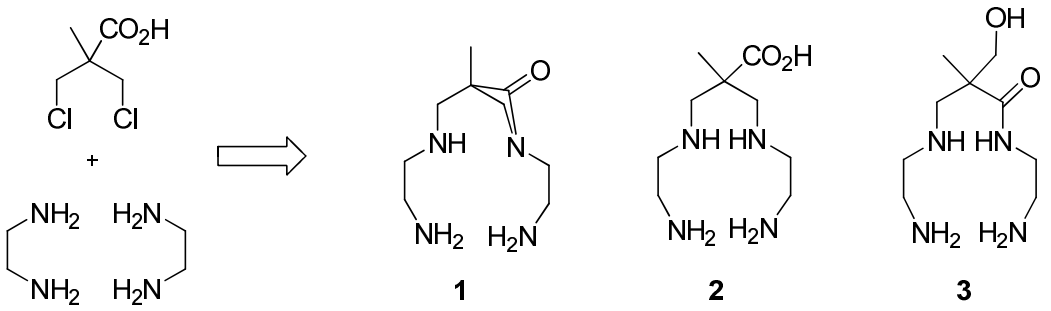

Figure 6.14: A possible synthetic route to the synthesis of analogues of L_{25} using 3,3'-dichloropivalic acid.

A similar alternative route could use a 3,3'-dichloropivalic acid derivative 3-bromo-2-(bromomethyl) propanoic acid reacting with 2-aminomethylpyridine. In the first example, **2**, figure 6.15, the pendant carboxylate is not found to coordinate when using copper(II) as the metal centre. This was explained by the greater rigidity imposed by the adjacent methyl group.[16] However this may be overcome by using 3-bromo-2-(bromomethyl)propanoic acid. Finally another possible alternative involves starting from methyl 3-bromo-2-(bromomethyl)propanoate, transforming it to methyl 3-amino-2-(aminomethyl)propanoate[31] and then reacting with pyridine-2-carbaldehyde.[32]

6.2. Convenient 'One-Pot' Synthesis of the Benzene-1,3,5-Tricarboxamide of L-Histidine Methyl ester L_{28}

6.2.1. Introduction:

The imidazole group of l-histidine is a commonly found binding ligand for metal centres in a variety of metalloproteins and enzymes. As many as four imidazole N donors have been found coordinated to one metal centre, an example being the copper(II) site of the bovine form of superoxide dismutase.[33-35] Many more examples have three histidine imidazole groups attached to the metal; these include zinc(II) in human carbonic anhydrase[36, 37] and in the T and R states of 2-Zn-insulin hexamer,[38-40] iron(III) in soybean lipoxygenase-1[41], iron(II),(III) in marine hemyrithrin,[42] Cu(I),(II) in arthropoda and mollusca hemocyanin[43, 44] and bacterial tyrosinase[45, 46], the type 2 copper(II) site of the blue oxidases; laccase[47], ascorbate oxidase[48, 49], ceruloplasmin[47] and amine oxidase[50], the Cu_B site of cytochrome oxidase[51], the copper site of nitrite reductase[52] and iron and manganese superoxide dismutase.[53, 54] Despite the importance of histidine imidazole coordination there are few, if any, examples of coordinating ligands that containing two or more histidine imidazole moieties; most biomimetic studies preferring over the years to simulate imidazole coordination using other N-heterocycles such as pyrazole, pyrazine, pyridine and benzimidazole. Even more surprising are the few reported examples of single molecule ligands containing three or more imidazole groups. A few recent examples of tripodal imidazole-containing ligands are the Schiff-base condensation products of 1-phenyl(methyl)-2-imidazolecarboxaldehyde[55, 56] and 4-methyl-5-imidazole carboxaldehyde [57-59] with tris(2-aminoethyl)amine (tren), and tris(3-aminopropyl)amine (trpn), L_{29} and L_{30}, figure 6.15, and the reduced Schiff-base condensation product of histamine with two equivalents of 4-methyl-5-imidazolecarboxaldehyde, L_{31}.[60] Reaction of bis(imidazol-2-yl)nitromethane with histamine gives the tripodal ligand L_{32}.[61]

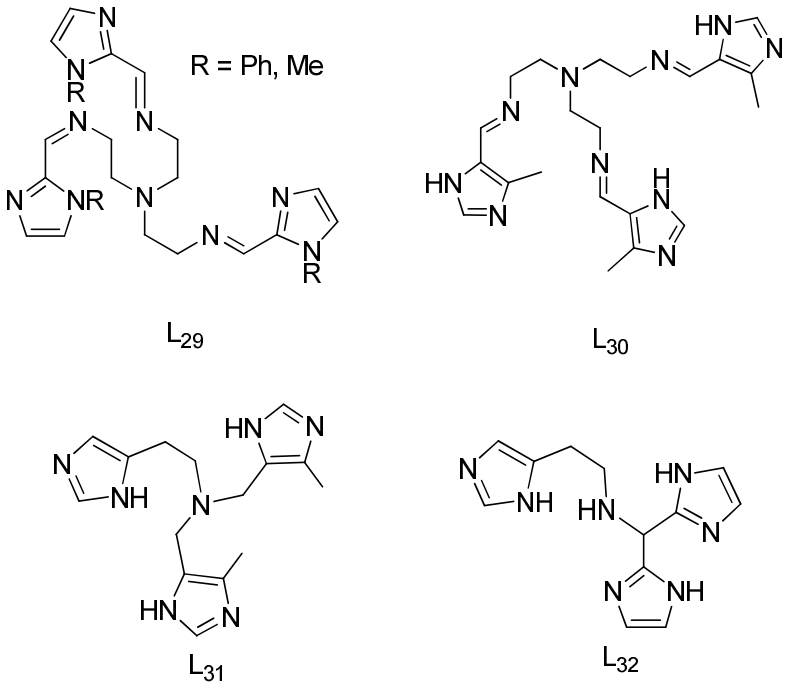

Figure 6.15: Schematic representation of tripodal imidazole ligands **L_{29}- L_{32}**

The hexaimidazole ligand L_{33} has been obtained via dual metallation (potassium diisopropylamide) at C5 of the N-protected imidazoles in 1,3-bis(2-imidazolyl)benzene, Geometry optimised structure followed by condensation with bis(N-methylimidazolyl)ketone, methylation of the resulting diol and deprotection,[62] see figure 6.16.

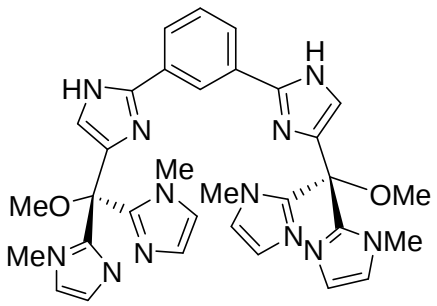

Figure 6.16: Schematic representation of **L_{33}**

Binuclear copper(II) complexes containing L_{32}[61] and L_{33}[63] have been structurally characterised in efforts to model the type 3 binuclear copper site of hemocyanin. Fewer, if

any, examples of such ligands deriving from L-histidine moieties themselves have been reported.[64] The benzene-1,3,5-tricarbonyl moiety has been recently used to prepare synthetic tripodal dentritic analogues for iron-binding siderophores[65, 66] as well as an expanding range of dentritic carboxamides with various peptides some of which have interesting globular structures.[67 68]

Here the successful one pot synthesis of the benzene-1,3,5-tricarboxamide of l-histidine methyl ester is reported in a pure state in 37% yield. A preliminary investigation of its copper coordination chemistry is also described.

6.2.2. Results and Discussion:

6.2.2.1 Synthesis of L_{28}.

Initial attempts at synthesizing L_{28} involved liberation of the free base of l-histidine methyl ester from the dihydrochloride using sodium methoxide in methanol followed by reaction with the acid chloride. However the difficulty of completely removing methanol from the free base solutions led to competing methanolysis and isolation of mixed carboxamide/ carboxymethyl ester products. Karle et al recently reported reaction of 2,2-dithiodibenzoylchloride with l-histidine methyl ester dihydrochloride producing the required carboxamide in 56% yield using dichloromethane as solvent and triethylamine as base.[67] We have adapted this procedure herein to report the successful 'one pot' synthesis of the benzene-1,3,5-tricarboxamide of l-histidine methyl ester L_{28} from benzene-1,3,5-tricarbonyl chloride, l-histidine methyl ester dihydrochloride and an excess of dry triethylamine in dry dichloromethane, figure. 6.17.

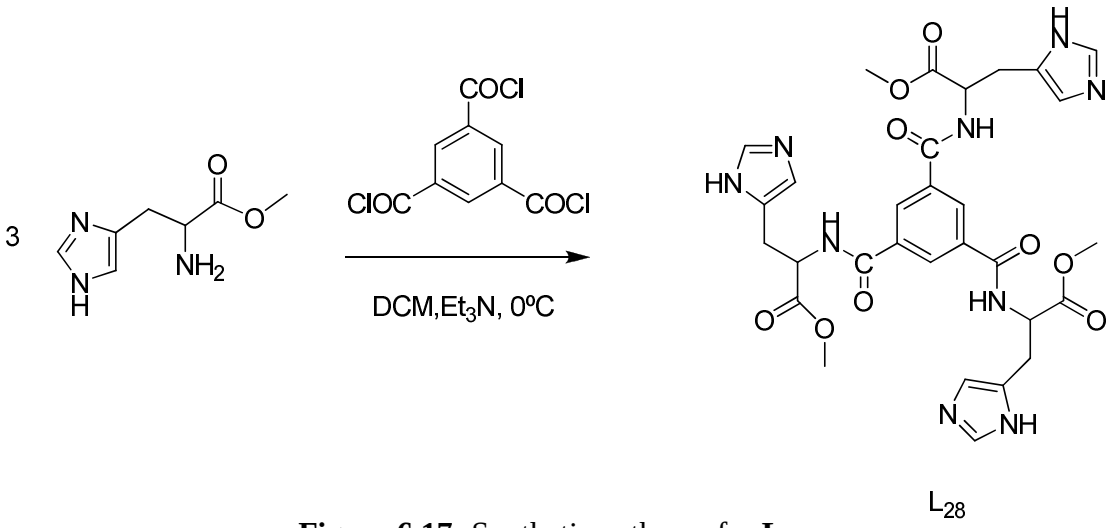

Figure 6.17: Synthetic pathway for **L_{28}**.

After stirring the above mixture for 48 hours at RT it was transferred to a separating funnel and washed with three 20cm^3 portions of aqueous $NaHCO_3$ and water, before separating the dichloromethane layer and drying over anhydrous $MgSO_4$. Based on the reported amide coupling reaction of l-histidine methyl ester free base with 2,2-dithiodibenzoylchloride[26] the dichloromethane layer was expected to contain the carboxamide product but in this case following gentle water pump evaporation only a small amount of unreacted triethylamine was found (^{1}H NMR). A colourless sticky solid was, however, observed to have deposited on the walls of the separating funnel following the aqueous washings. This solid subsequently dissolved in methanol which, upon evaporation and drying at the vacuum pump, yielded 0.93g.

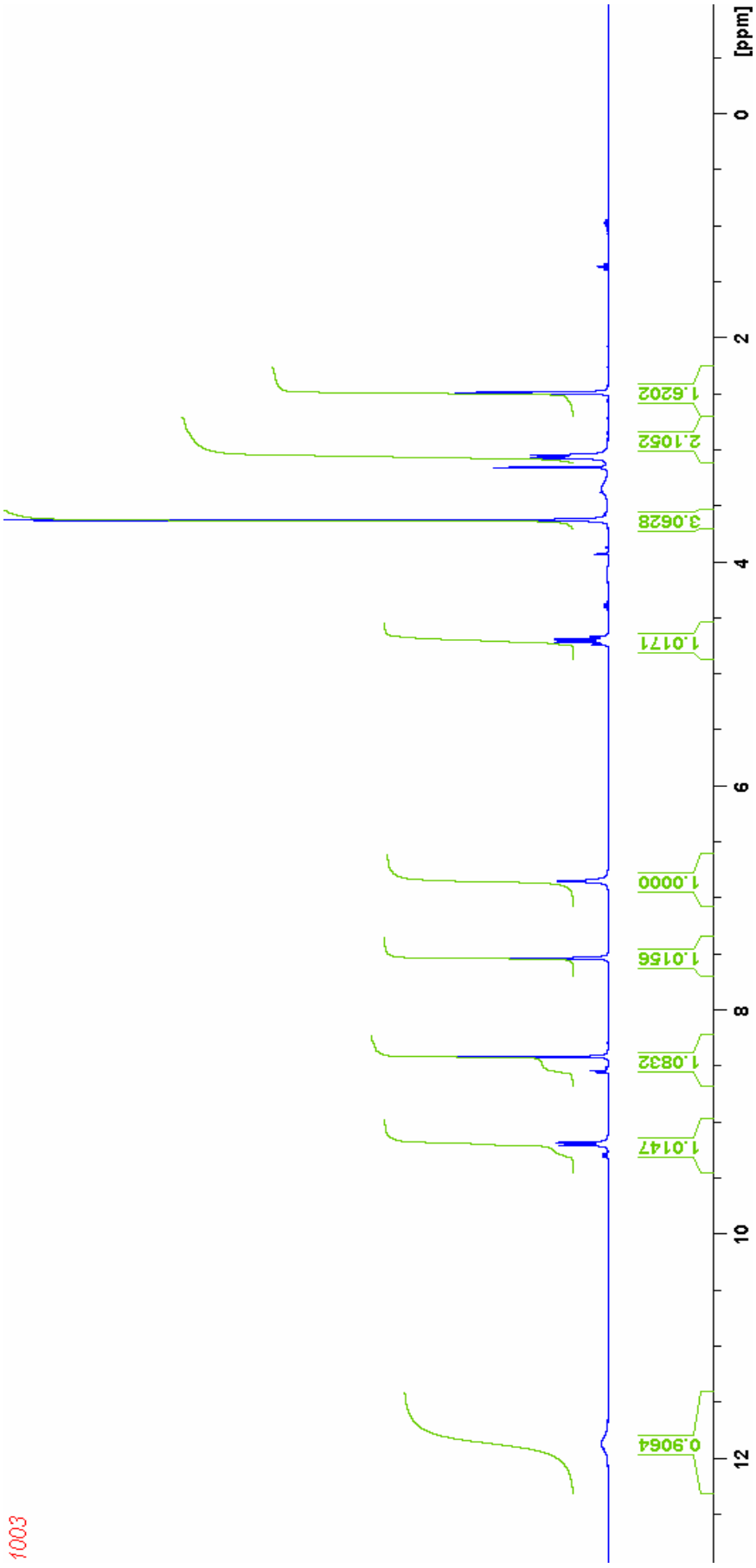

Figure 6.18: ^{1}H NMR spectrum of $\mathbf{L_{28}}$ in d^{6}-DMSO

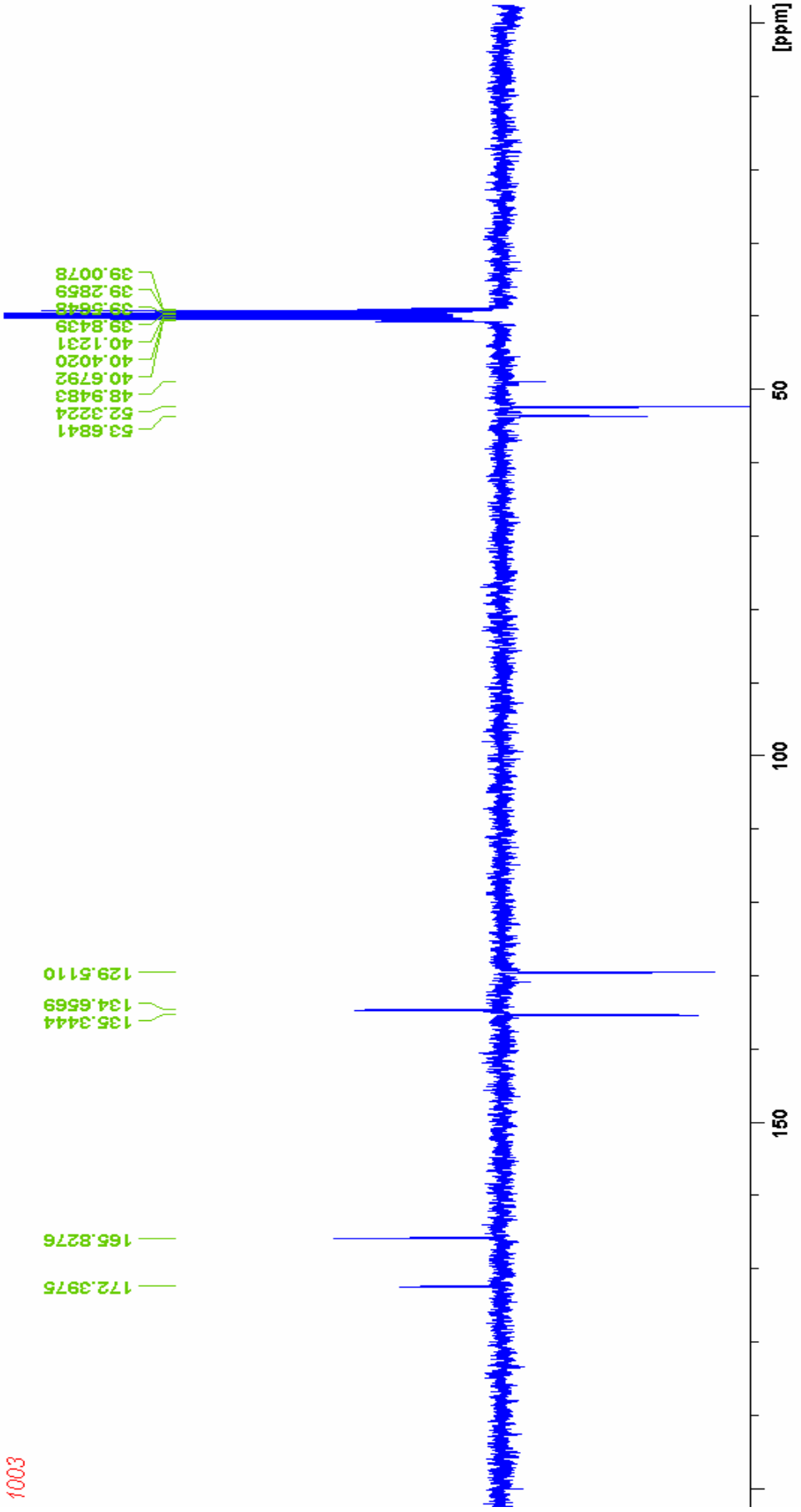

Figure 6.19: ^{13}C DEPT NMR spectrum of **L_{28}** in d^6-DMSO

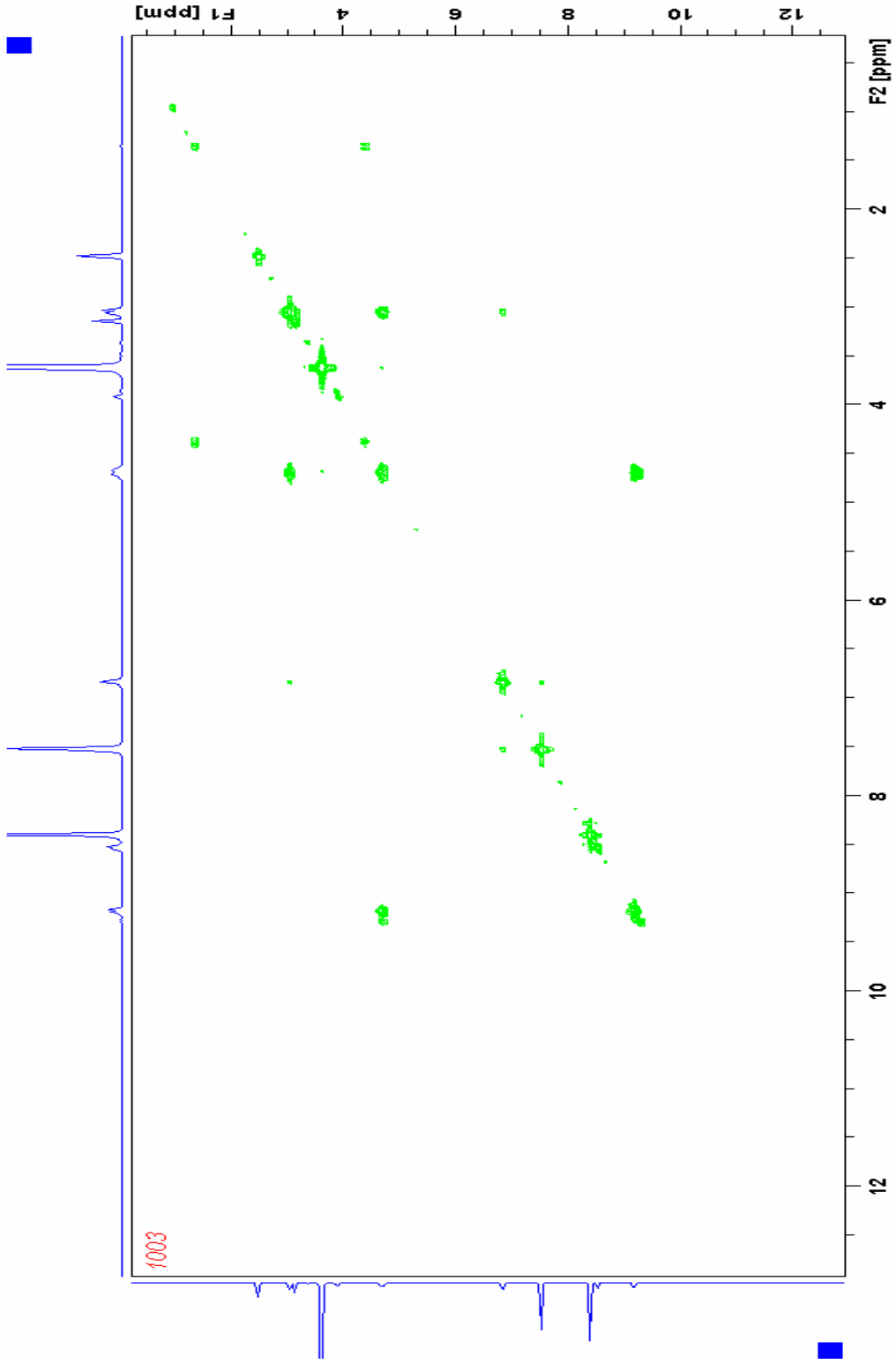

Figure 6.20: ^{1}H COSY NMR spectrum of L_{28} in d^{6}-DMSO shows coupling of the L-histidine CH proton at 4.75ppm to the adjacent CH_2 (3.05ppm) and amide NH (9.2ppm).

of a white solid. A ^{1}H NMR spectrum, figure 6.18, together with a ^{13}C DEPT NMR, figure 6.19, from the dissolved solid in d^{6}-DMSO together with a high resolution TOF-ES+ mass spectrum and low resolution TOF-ES- of the white solid were consistent with the presence of the pure benzene-1,3,5-tricarboxamide L_{28}, yield 37%.[27] The ^{1}H and ^{13}C NMR assignments were confirmed in standard 2D ^{1}H COSY and ^{1}H-^{13}C HNQC and HMBC NMR experiments. The ^{1}H COSY spectrum, figure 6.20, shows coupling of the L-histidine CH proton at 4.75ppm to the adjacent CH_2 (3.05ppm) and amide NH (9.2ppm). The somewhat disappointing yield was offset by the convenience of the 'one pot' method and the purity of the isolated product. Moreover the method readily lends itself to the synthesis of benzene-1,3,5-tricarboxamides of a range of L-amino acid esters from their hydrochloride salts.

The coordination chemistry of L_{28} and its tricarboxylate anion analogue with Cu(II) was investigated. Simple molecular modelling of putative derivatives with Cu(I) and Cu(II), Figures 6.21 and 6.22 illustrate the huge potential of L_{28} as a fascinating biomimetic co-ordinating ligand.

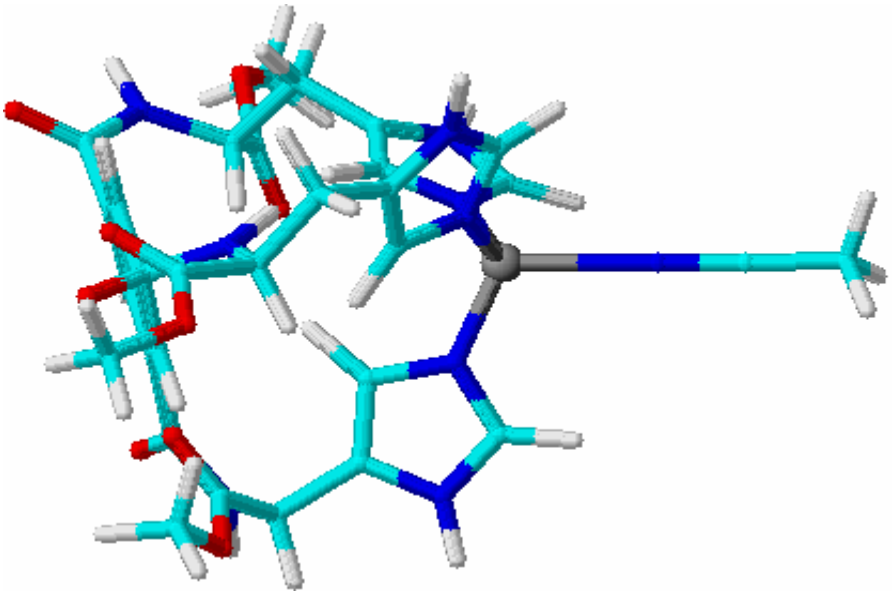

Figure 6.21: A geometry optimised structure for putative $[Cu^{I}(\mathbf{L_{28}})(NCCH_3)]^{+}$

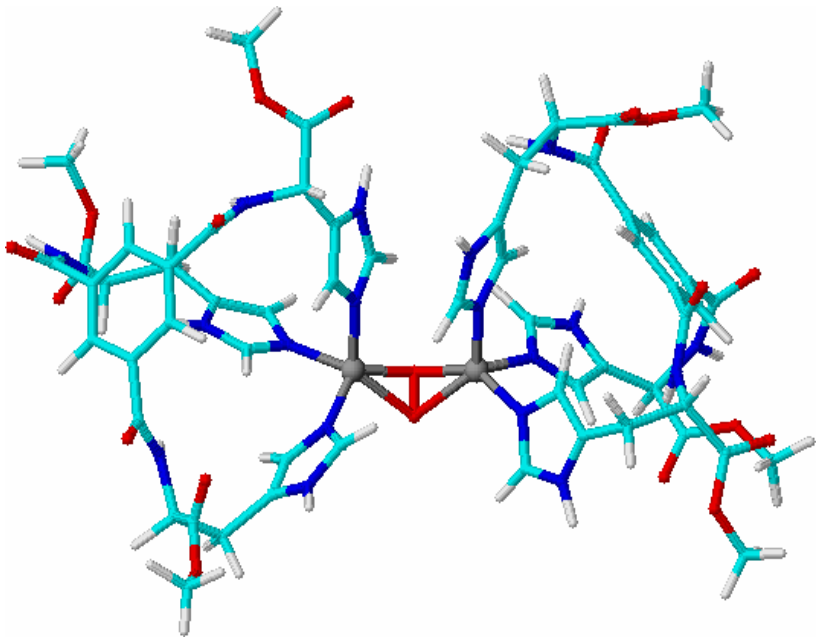

Figure 6.22: A geometry optimised structure of [(**L$_{28}$**)Cu^{II}(O$_2$)Cu^{II}(**L$_{28}$**)]**, a** putative model for oxyhemocyanin and oxytyrosinase.

6.2.2.2. Reaction of L_{28} with $[Cu^{I}(CH_3CN)_4](ClO_4)$.

The synthesis of $[Cu^{I}(L_{28})(CH_3CN)_x]^+$ was carried out by mixing equimolecular amounts of $[Cu^{I}(CH_3CN)_4](ClO_4)$ and L_{28} in dry CH_3CN ar room temperature overnight. Immediately a pale-bluish solid precipitated which was found to be insoluble in all solvents. A polynuclear structure was concluded. Attempts to grow crystals suitable for X-ray analysis were not successful due to the insolubility. Vahrenkamp et al have reported the synthesis of the corresponding ethyl ester derivative L_{34},[69] figure 6.23. Reaction between L_{34} and zinc(II) salts was studied yielding similar insoluble precipitates under preparative conditions whose composition could not be ascertained. Potentiometric titration experiments under more diluted conditions resulted in formulation of the simplest species as $L_{34}ZnOH^+$, figure 6.23.[69] This

metal complex models the active site of the zinc enzyme carbonic anhydrase[70] as well as a large group of matrix metalloproteases.[71, 72]

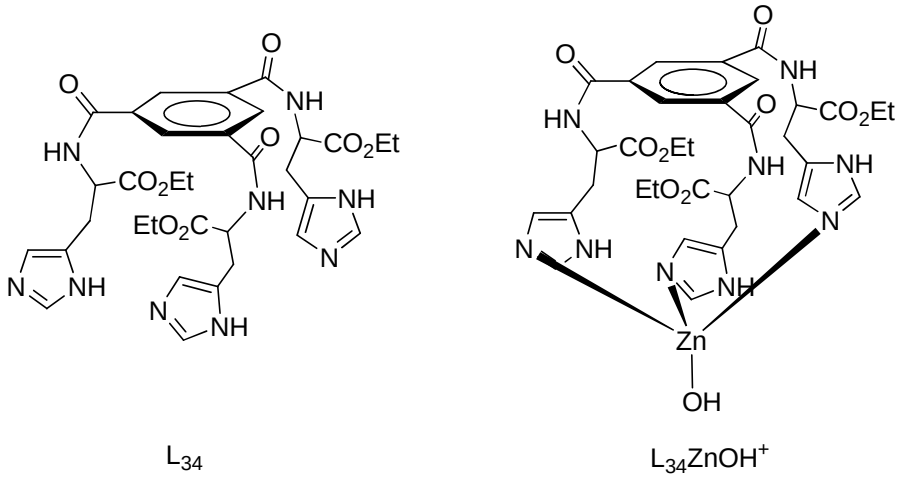

L_{34} $L_{34}ZnOH^+$

Figure 6.23: Schematic representation of L_{34} and $L_{34}ZnOH^+$

6.2.3 Experimental:

6.2.3.1. Materials:

Benzene-1,3,5-tricarbonyl chloride, l-histidine methyl ester dihydrochloride, sodium bicarbonate and methanol were used as supplied. Triethylamine and dichloromethane were freshly distilled from calcium hydride under nitrogen prior to use. Distilled water was used for all aqueous washings.

6.2.3.2. Synthesis of Benzene-1,3,5-Tricarboxamide of L-Histidine Methyl ester L_{28}:

The experimental operations were performed under ambient conditions unless indicated. Benzene-1,3,5-tricarbonyl chloride (1.032g, 3.88 mmol) in 50 cm^3 of dry dichloromethane was added dropwise to an ice-cooled and stirred mixture of the free base of l-histidine methyl ester (generated in-situ by the addition of dry triethylamine (5.75 cm^3, 41.04 mmol) to an ice cooled and stirred suspension of the dihydrochloride (3.11 g, 12.33 mmol) in 120 cm^3 of dry dichloromethane). Since the reaction is highly exothermic, care was taken not to add the acid

chloride all at once too quickly. The resulting creamy suspension was stirred under nitrogen for 48 hours after which it was transferred to a standard 100 cm^3 separating funnel. The organic mixture was washed thoroughly with a cold saturated aqueous solution of sodium bicarbonate (3 x 20 cm^3), followed by distilled water (2 x 20 cm^3). The organic phase was then removed to a 50 cm^3 conical flask leaving a colourless sticky solid on the walls of the funnel. This solid was found to be extractable with methanol (3 x 30 cm^3). Evaporation of the methanol extract under vacuum (10^{-2} torr) gave L_{28} as a colourless solid, yield 0.93g (37%). Mp 80.1°C.

FT-IR (nujol mull) (cm^{-1}): 3400 (s, br, amide N-H), 3250 (s, br, imidaz N-H), 1738 (s, ester C=O), 1654 (s, amide C=O), 1535 (s, amide δN-H), 1460, 1376, 1217 (s, ester C-O).

^{1}H NMR: (DMSO-d^6), 300 MHz, 298 K, ppm from TMS): δ 11.87 (s, br, 3H, N-H imid); 9.20 (d, 3H, N-H amide); 8.40 (s, 3H, C_6H_3); 7.52 (s, 3H, 2-imidCH); 6.85 (s, 3H, 4-imidCH); 4.75 (q, 3H, CH); 3.75 (s, 9H, CO_2CH_3); 3.05 (d, 6H, CH_2).

^{13}C NOESY NMR: (DMSO-d^6), MHz, 298K, ppm from TMS): δ 172.4 (**C**O_2CH_3); 165.8 (CONH); 135.3, (2-imid CH); 134.6 (imid quat), 130.8 (2,4,6-benz CH); 129.5 (4-imid CH), 53.7 (**C**HCH_2), 52.3 (CH**C**H_2); 39 (CO_2**C**H_3); not observable: 1,3,5-benz quat.

MS: LCTOF ES- 662.17 (M-H); TOF ES+ 664.27 (M+H), 686.24 (M+Na)

Single Mass Analysis for M+Na: found 686.2291 (calc for $C_{30}H_{33}N_9O_9Na$ = 686.2299).

6.2.3.3. Synthesis of $[Cu(CH_3CN)_4](ClO_4)$.

$Cu(ClO_4)_2 \cdot 6H_2O$ (2.925g, 7.865 mmol) was dissolved in a mixture of dry acetonitrile and dry methanol (20-30 cm^3) and reduced with an excess of copper powder electrochemically prepared. The suspension was stirred for 30 min and then filtered via cannula, the clear solution was transferred to another schlenk. A colourless solid was obtained after evaporation of the solvent. Yield. 2.1 g (95.03 %).

6.2.3.4. Reaction of L_{28} with $[Cu^{I}(CH_3CN)_4](ClO_4)$: attempted synthesis of $[Cu^{I}(L_{28})(CH_3CN)](ClO_4)$.

A solution of $[Cu^{I}(CH_3CN)_4](ClO_4)$ (0.1g, 0.36 mmol) and **L_{28}** (0.24g, 0.36 mmol) both in dry CH_3CN were mixed at room temperature under an N_2 atmosphere and stirred overnight. A pale-bluish solid precipitated immediately which was eventually isolated by filtration. The solid failed to dissolve in any solvent and its composition was concluded to be polymeric. Attempts to grow crystals of the complex suitable for X-ray analysis were not successful due to insolubility.

6.2.4. Conclusions:

A novel biomimetic benzene 1,3,5, tricarboximide of l-histidine methyl ester L_{28} has been obtained pure in 37% yield via a one pot reaction of benzene-1,3,5-tricarbonyl chloride with three equivalents of free base l-histidine methyl ester generated in situ under anhydrous conditions via the dihydrochloride salt and an excess of triethylamine. An attempt was made to prepare a copper(I) complex of L_8 under air-free conditions using $[Cu^{I}(CH_3CN)_4](ClO_4)$. However the complex (presumed to be a copper(II) species from its bluish colour) could not be fully characterised due to its insolubility in all solvents and it was concluded to consist of an intractable polymeric species. This seems to be general phenomenon from the reaction of divalent metal ions with tripodal amino acid ligands of this type and it is wondered whether spontaneous hydrolysis of the ester groups takes place upon metal ion coordination (bearing in mind the excellent Lewis acid properties of Zn(II) and Cu(II)) giving a multidentate ligand system that favours polynuclear complexation. Further work will be required to confirm.

6.2.5. References:

1. R. Hage and A. Lienke, *Angew. Chem., Int. Ed.* 2006, **45**, 206-222.
2. D. H. R. Barton, *Chem. Soc. Rev.* 1996, **25**, 237-239.
3. D. H. R. Barton and D. Doller, *Acc. Chem. Res.*, 1992, **25**, 504-512.
4. D. H. R. Barton, S. D. Beviere, W. Chavasiri, E. Csuhai, D. Doller and W. G. Liu, *J. Am. Chem. Soc.* 1992, **114**, 2147-2156.
5. K. Chen and L. Que, Jr., *Book of Abstracts, 219th ACS National Meeting, San Francisco, CA, March 26-30, 2000*, 2000, INOR-557.
6. K. Chen, M. Costas, J. Kim, A. K. Tipton and L. Que, Jr., *J. Am. Chem. Soc.*, 2002, **124**, 3026-3035.
7. M. Fujita, M. Costas and L. Que, Jr., *J. Am. Chem. Soc.*, 2003, **125**, 9912-9913.
8. K. Chen and L. Que, Jr., *Angew. Chem., Int. Ed.*, 1999, **38**, 2227-2229.
9. K. Chen and L. Que, Jr., *Chemical Communications (Cambridge)*, 1999, 1375-1376.
10. M. Fujita and L. Que, Jr., *Adv. Synth. Catal.*, 2004, **346**, 190-194.
11. A. McConnell, P. Lightfoot and D. T. Richens, *Inorg. Chim. Acta*, 2002, **331**, 143-150.
12. P. Comba, N. F. Curtis, G. A. Lawrance, A. M. Sargeson, B. W. Skelton and A. H. White, *Inorg. Chem.* 1986, **25**, 4260-4267.
13. P. Comba, T. W. Hambley and G. A. Lawrance, *Helv. Chim. Acta*, 1985, **68**, 2332-2341.
14. M. van den Heuvel, T. A. van den Berg, R. M. Kellogg, C. T. Choma and B. L. Feringa, *J. Org. Chem.*, 2004, **69**, 250-262.
15. F. Boschetti, F. Denat, E. Espinosa, J.-M. Lagrange and R. Guilard, *Chem. Commun. (Cambridge, U. K.)*, 2004, 588-589.

16. J. M. Harrowfield, Y. Kim, G. A. Koutsantonis, Y. H. Lee and P. Thuery, *Inorg. Chem.* 2004, **43**, 1689-1696.

17. M. Mitsuya, K. Kobayashi, K. Kawakami, A. Satoh, Y. Ogino, T. Kakikawa, N. Ohtake, T. Kimura, H. Hirose, A. Sato, T. Numazawa, T. Hasegawa, K. Noguchi and T. Mase, *J. Med. Chem.*, 2000, **43**, 5017-5029.

18. L. Fabbrizzi, M. Licchelli, A. M. Manotti Lanfredi, O. Vassalli and F. Ugozzoli, *Inorg. Chem.* 1996, **35**, 1582-1589.

19. E. L. Blinn and D. H. Busch, *Inorg. Chem.* 1968, **7**, 820-824.

20. C. Thompson and D. H. Busch, *J. Am. Chem. Soc.*, 1964, **86**, 213-217.

21. M. C. Thompson and D. H. Busch, *J. Am. Chem. Soc.* 1962, **84**, 1762-1763.

22. O. Costisor and W. Linert, *Rev. Inorg. Chem.* 2000, **20**, 63-127.

23. H. A. Boucher, G. A. Lawrance, P. A. Lay, A. M. Sargeson, A. M. Bond, D. F. Sangster and J. C. Sullivan, *J. Am. Chem. Soc.*, 1983, **105**, 4652-4661.

24. Y. Baran, G. A. Lawrance and E. N. Wilkes, *Polyhedron*, 1996, **16**, 599-602.

25. G. A. Lawrance, T. M. Manning, M. Maeder, M. Martinez, M. A. O'Leary, W. C. Patalinghug, B. W. Skelton and A. H. White, *J. Chem. Soc., Dalton Trans.*, 1992, 1635-1641.

26. N. F. Curtis, L. Xin and D. C. Weatherburn, *Inorg. Chem.*, 1993, **32**, 5838-5843.

27. T. W. Hambley, G. A. Lawrance, M. Maeder and E. N. Wilkes, *Inorg. Chim. Acta* 1996, **246**, 65-71.

28. G. A. Lawrance, M. Maeder, M. A. O'Leary, B. W. Skelton and A. H. White, *Aust. J. Chem.* 1991, **44**, 1227-1236.

29. P. V. Bernhardt, G. A. Lawrance, B. W. Skelton and A. H. White, *Aust. J. Chem.* 1990, **43**, 399-404.

30. G. M. Munoz Caro, U. J. Meierhenrich, W. A. Schutte, B. Barbler, A. A. Segovia, H. Rosenbauer, W. H. P. Thiemann, A. Brack and J. M. Greenberg, *Nature (London, U. K.)*, 2002, **416**, 403-406.

31. K. Lee, S. K. Boovanahalli, K.-Y. Nam, S.-U. Kang, M. Lee, J. Phan, L. Wu, D. S. Waugh, Z.-Y. Zhang, K. T. No, J. J. Lee and T. R. Burke, *Bioorg. Med. Chem. Lett.*, 2005, **15**, 4037-4042.

32. A. Antoniadou-Vyzas, G. B. Foscolos and A. Chytiroglou-Ladas, *Eur. J. Med. Chem.--Chim. Ther.* 1986, **21**, 73-74.

33. L. Banci, I. Bertini, B. Bruni, P. Carloni, C. Luchinat, S. Mangani, P. L. Orioli, M. Piccioli, W. Ripniewski and K. S. Wilson, *Biochem. Biophys. Res. Commun.* 1994, **202**, 1088-1095.

34. J. A. Tainer, E. D. Getzoff, J. S. Richardson and D. C. Richardson, *Nature (London)*, 1983, **306**, 284-287.

35. J. A. Tainer, E. D. Getzoff, K. M. Beem, J. S. Richardson and D. C. Richardson, *J Mol Biol*, 1982, **160**, 181-217.

36. A. E. Eriksson, T. A. Jones and A. Liljas, *Proteins* 1988, **4**, 274-282.

37. K. K. Kannan, B. Notstrand, K. Fridborg, S. Lovgren, A. Ohlsson and M. Petef, *Proc. Natl. Acad. Sci. U. S. A.* 1975, **72**, 51-55.

38. J. Bordas, G. G. Dodson, H. Grewe, M. H. J. Koch, B. Krebs and J. Randall, *Proc. R. Soc. London, [Ser.] B*, 1983, **219**, 21-39.

39. G. D. Smith, D. C. Swenson, E. J. Dodson, G. G. Dodson and C. D. Reynolds, *Proc. Natl. Acad. Sci. U. S. A.*, 1984, **81**, 7093-7097.

40. J. M. Sowadski, M. D. Handschumacher, H. M. Murthy, B. A. Foster and H. W. Wyckoff, *J Mol Biol*, 1985, **186**, 417-433.

41. J. C. Boyington, B. J. Gaffney and L. M. Amzel, *Science (Washington, DC, U. S.)*, 1993, **260**, 1482-1486.

42. M. A. Holmes, I. Le Trong, S. Turley, L. C. Sieker and R. E. Stenkamp, *J Mol Biol*, 1991, **218**, 583-593.

43. K. A. Magnus, B. Hazes, H. Ton-That, C. Bonaventura, J. Bonaventura and W. G. Hol, *Proteins*, 1994, **19**, 302-309.

44. B. Hazes, K. A. Magnus, C. Bonaventura, J. Bonaventura, Z. Dauter, K. H. Kalk and W. G. Hol, *Protein Sci*, 1993, **2**, 597-619.

45. Y. Matoba, T. Kumagai, A. Yamamoto, H. Yoshitsu and M. Sugiyama, *J. Biol. Chem.*, 2006, **281**, 8981-8990.

46. H. Decker, T. Schweikardt and F. Tuczek, *Angew Chem Int Ed Engl*, 2006, **45**, 4546-4550.

47. A. V. Lyashenko, N. E. Zhukhlistova, E. V. Stepanova, K. Schirwiz, Y. N. Zhukova, O. V. Koroleva, V. S. Lamzin, V. N. Zaitsev, A. G. Gabdulkhakov and A. M. Mikhailov, *Crystallogr. Rep.* 2006, **51**, 278-285.

48. A. Messerschmidt, R. Ladenstein, R. Huber, M. Bolognesi, L. Avigliano, R. Petruzzelli, A. Rossi and A. Finazzi-Agro, *J. Mol. Biol.* 1992, **224**, 179-205.

49. A. Messerschmidt, H. Luecke and R. Huber, *J Mol Biol*, 1993, **230**, 997-1014.

50. M. R. Parsons, M. A. Convery, C. M. Wilmot, K. D. S. Yadav, V. Blakeley, A. S. Corner, S. E. V. Phillips, M. J. McPherson and P. F. Knowles, *Structure (London)*, 1995, **3**, 1171-1184.

51. T. Tsukihara, H. Aoyama, E. Yamashita, T. Tomizaki, H. Yamaguchi, K. Shinzawa-Itoh, R. Nakashima, R. Yaono and S. Yoshikawa, *Science*, 1995, **269**, 1069-1074.

52. M. E. P. Murphy, S. Turley, M. Kukimoto, M. Nishiyama, S. Horinouchi, H. Sasaki, M. Tanokura and E. T. Adman, *Biochemistry*, 1995, **34**, 12107-12117.

53. M. S. Lah, M. M. Dixon, K. A. Pattridge, W. C. Stallings, J. A. Fee and M. L. Ludwig, *Biochemistry*,1995, **34**, 1646-1660.

54. M. L. Ludwig, A. L. Metzger, K. A. Pattridge and W. C. Stallings, *J Mol Biol*, 1991, **219**, 335-358.

55. C. Brewer, G. Brewer, J. Butcher Ray, E. Carpenter Everett, L. Cuenca, M. Schmiedekamp Ann and C. Viragh, *Dalton Trans*, 2005, 3617-3619.

56. I. Katsuki, N. Matsumoto and M. Kojima, *Inorg Chem*, 2000, **39**, 3350-3354.

57. C. Brewer, G. Brewer, J. Butcher Ray, E. Carpenter Everett, L. Cuenca, C. Noll Bruce, W. R. Scheidt, C. Viragh, Y. Zavalij Peter and D. Zielaski, *Dalton Trans*, 2006, 1009-1019.

58. C. Brewer, G. Brewer, G. Patil, Y. Sun, C. Viragh and R. J. Butcher, *Inorg. Chim. Acta*, 2005, **358**, 3441-3448.

59. C. Brewer, G. Brewer, C. Luckett, S. Marbury Gwen, C. Viragh, M. Beatty Alicia and W. R. Scheidt, *Inorg Chem*, 2004, **43**, 2402-2415.

60. A. Jancso, I. Toeroek, L. Korecz, A. Rockenbauer and T. Gajda, *J. Chem. Soc., Dalton Trans.*, 2002, 2601-2607.

61. G. J. A. A. Koolhaas, W. L. Driessen, J. Reedijk, H. Kooijman and A. L. Spek, *J. Chem. Soc., Chem. Commun.* 1995, 517-518.

62. W. B. Tolman, R. L. Rardin and S. J. Lippard, *J. Am. Chem. Soc.* 1989, **111**, 4532-4533.

63. C. M. Hartshorn and P. J. Steel, *Angew. Chem., Int. Ed. Engl.*, 1996, **35**, 2655-2657.

64. Y. Yuan, R. Xiao, G. Gao, X.-Y. Su, H. Yu, J. You and R.-G. Xie, *J. Chem. Res., Synop.* 2002, 267-269.

65. E. C. Berndt Ursula, T. Zhou, C. Hider Robert, D. Liu Zu and H. Neubert, *J Mass Spectrom*, 2005, **40**, 1203-1214.

66. T. Zhou, Z. D. Liu, H. Neubert, X. L. Kong, Y. M. Ma and R. C. Hider, *Bioorg. Med. Chem. Lett.*, 2005, **15**, 5007-5011.

67. I. L. Karle and D. Ranganathan, *J Pept Res*, 2005, **65**, 65-70.

68. C. Koellner, B. Pugin and A. Togni, *J. Am. Chem. Soc.*, 1998, **120**, 10274-10275.

69. M. Gelinsky, R. Vogler and H. Vahrenkamp, *Inorg. Chem.* 2002, **41**, 2560-2564.

70. F. Botre, G. Gros, B. T. Storey and Editors, *Carbonic Anhydrase: From Biochemistry and Genetics to Physiology and Clinical Medicine. Proceedings of the International Workshop on Carbonic Anhydrase, held in Spoleto, Italy in March 1990*, 1991.

71. D. W. Christianson, *Adv. Protein Chem.* 1991, **42**, 281-355.

72. B. L. Vallee and D. S. Auld, *Acc. Chem. Res.* 1993, **26**, 543-551.